2019

Molecularly imprinted nanoparticles (MINPs) for recognition and sensing of bioactive drug molecules

Likun Duan
Iowa State University

Molecularly imprinted nanoparticles (MINPs) for recognition and sensing of bioactive drug molecules

by

Likun Duan

A dissertation submitted to the graduate faculty

in partial fulfillment of the requirements for the degree of

DOCTOR OF PHILOSOPHY

Major: Chemistry

Program of Study Committee:
Yan Zhao, Major Professor
Levi Stanley
Wenyu Huang
Brett VanVeller
Arthur Winter

The student author, whose presentation of the scholarship herein was approved by the program of study committee, is solely responsible for the content of this dissertation. The Graduate College will ensure this dissertation is globally accessible and will not permit alterations after a degree is conferred

Iowa State University

Ames, Iowa

2019

TABLE OF CONTENTS

ACKNOWLEDGEMENTS

I would like to thank my advisor, Professor Yan Zhao, for his valuable guidance and support throughout my Ph.D. study. Writing this dissertation would not have been possible without his mentorship. He taught me the fundamentals of conducting scientific research in the area of molecular recognition at the academic level. Under his supervision, I learned how to identify a research problem, find suitable solutions, and eventually publish the results. He also influenced me on a personal level with his hard-working and passion for science. To sum up, I'd give most of the credit to Professor Zhao to become the kind of scientist I am today.

In addition, I would like to thank Professors Levi Stanley, Wenyu Huang, Brett VanVeller, and Arthur Winter for serving as my committee members. They used their precious time to provide professional guidance during my study.

I would also like to thank the department of chemistry, Iowa State University, the National Science Foundation (NSF), the National Institute of General Medical Sciences (NIGMS), for providing financial support for the research/course work that I have completed. I'm grateful to the members of the chemical instrumentation facility including Dr. Sarah Cady, Dr. Shu Xu, Dr. Kamel Harrata, and Mr. Steve Veysey for their training and technical assistance to my research.

Many thanks also go to my group members for providing an encouraging and helpful working environment in the research laboratory.

Nobody has been more important to me than my family members. Special appreciation to my family, whose love, comfort, and support are always with me.

ABSTRACT

Bioactive drugs are small molecules that can bind therapeutic targets like enzymes, proteins, and receptors and modulate their biological activities. Effective binding between bioactive drugs and receptors in vivo or in vitro is key to constructing useful tools in biomedical research and diagnosis. Molecular imprinting within surface/core cross-linked micelles was shown to afford water-soluble nanoparticle receptors for bioactive drugs. The molecularly imprinted nanoparticles obtained resembled proteins in size and were easy to prepare and very stable in adverse temperature or pH conditions. Strong imprinting effects were consistently observed for different bioactive molecules including alkaloids, folic acid, nonsteroidal anti-inflammatory drugs (NSAIDs), and catecholamines, in comparison to nonimprinted nanoparticles without the templates during the preparation. Fluorescent molecularly imprinted nanoparticles were also used as sensors for NSAIDs and catecholamines.

CHAPTER 1. GENERAL INTRODUCTION

Dissertation Organization

This dissertation consists of 6 chapters, focusing on investigations of molecularly imprinted nanoparticles (MINPs) for recognition and sensing of bioactive drug molecules. Chapter 1 is a review of molecular recognition, molecularly imprinted polymers (MIPs) and the latter's applications as artificial receptors. Chapter 2 was published in *the Journal of Organic Chemistry* in 2019. In this manuscript, molecularly imprinting nanoparticle receptors were prepared for alkaloids with strong imprinting effects in comparison to nonimprinted nanoparticles prepared without the templates. The ionic nature of the cross-linkable surfactant was found to strongly affect the imprinting and recognition process. Chapter 3 was published in *Bioconjugate Chemistry* in 2018. In this manuscript, MINPs were prepared for folic acid and its derivatives. It was found that MINP could be used to reveal the relative contributions of different functional groups toward the binding, by comparing structural analogues during the binding processes. Chapter 4 was submitted for publication in 2019. In this manuscript, a thiourea-containing fluorescent functional monomer was employed to MINP sensors for NSAIDs including Indomethacin and Tolmetin. Micromolar binding affinities were obtained, with binding selectivity comparable to those by polyclonal antibodies. Chapter 5 was submitted for publication in 2019. A phenylboronic acid- and anthracene-containing fluorescent functional monomer was developed to construct MINP sensors for important catecholamines including dopamine and adrenaline. Chapter 6 is a summary of this dissertation.

Literature Reviews

Molecular recognition is a fundamental step in biological processes such as enzymatic catalysis, protein crowding, molecular transport, cellular signaling, protein-protein association, and non-covalent binding of a ligand molecule by its receptor. All those biological processes involve the recognition of two or more molecular binding partners, leading either to their binding or to their dissociation.[1] Numerous biological receptors are found in cells, with each receptor binding its intended target molecules. However, applications of biological receptors are limited by the high cost and delicate nature of proteins. Noncovalent interactions such as hydrogen bonding, electrostatic interactions, hydrophobic effect, π-π interactions are generally utilized in the study of molecular recognition.[2] Because individual noncovalent interactions are normally weak, they are used together to obtain sufficient binding strength. Chemists have used these tools over the past several decades to create small organic molecules receptors, primarily in organic solvents.[3-4] These synthetic receptors should have a highly complementary binding motif for the guest to achieve high affinity and selectivity. Many synthetic receptors have been developed for various applications, such as macrocycles, whose concave structures have appropriate size and functionality for the guest molecule. Recently, foldamers with the benefit of using guest-triggered conformational changes to amplify the guest binding have been reported.[5-11] In general, the synthetic receptors are prepared by step-by-step synthesize to construct the binding motif complementary to their guest molecules. As the complexity of the guest molecule increases, the design and synthesis will also become more and more challenging.

Molecular imprinting technology has provided a very unique solution to the construction of artificial receptors.[12-22] The method of molecular imprinting includes the

polymerization of cross-linker molecules and functional monomers around a template molecule. First, a complex is formed between the selected template molecule and a functional monomer via various covalent or noncovalent interactions, with the exact configuration of the complex different for different types of molecular imprinting techniques.[23] A polymerization reaction is then carried out around the complex in the presence of cross-linking molecules, and the subsequent removal of some or all of the template molecules is required to provide recognition sites in the polymer network. The recognition sites usually have a three-dimensional geometry complementary to the functional groups of the template molecule. In comparison to the synthesis of molecular receptors, molecular imprinting enables easy and convenient preparation of recognition sites for target molecules which are large or complex. This is partly the reason why molecularly imprinted polymer (MIPs) have been developed by researchers from various backgrounds for applications including separation, purification, enzyme-mimetic catalysis, and sensing.[24-28] However, traditional MIP polymers face multiple challenges. Over the past decades, many different techniques have been used to improve the properties of traditional MIPs by developing different systems to improve the solubility, number of binding sites, and binding selectivity.[27-42] Those systems include but are not limited to molecularly imprinting nanoparticles,[43-49] micro/nanogels,[37-42] and imprinting within dendrimers.[27-28]

Bioactive drugs are normally small in size compared to their biological targets, but can modulate the activities of biological molecules like proteins, receptors, and enzymes by binding to them. For example, non-steroidal anti-inflammatory drugs, also known as NSAIDs, are one the most commonly prescribed pain-relieving drugs. These drugs relieve the pain by binding to and inhibiting Cyclooxygenases (COXs) enzymes, which are rate-determining enzymes for

prostaglandins and other prostanoids synthesis, such as thromboxanes.[50] Vinblastine, a vinca alkaloid, inhibits the assembly of microtubules by binding to tubulin, a protein that polymerizes into long chains or filaments that form microtubules.[51] Thus, the development of artificial receptors toward these molecules is very significant, as it would provide useful tools in biomedical research and diagnosis. Various drug-binding systems have been reported. For example, different artificial folate receptors were developed in order to achieve highly selective binding toward folic acid.[52-54] However, compared with natural receptors, most of those reported artificial receptors bind folic acid with very low affinities in aqueous solution, not to mention those water-insoluble receptors.[55-59] The main challenges come from the size and complexity of the drug molecule, the selective recognition among close relatives which differ subtly from the target drug molecule, and the reduced recognition effect in aqueous conditions.

All these challenges encouraged us to develop synthetic receptors for bioactive drugs. In 2013, our research group reported a new molecular imprinting technique by forming molecularly imprinted nanoparticles (MINPs) with surface/core doubly cross-linking. After template removal, a hydrophobic pocket complementary to the template will be formed in the MINP. The MINP material is already used to develop receptors for bile salt derivatives, aromatic carboxylates, sulfonates, nonsteroidal anti-inflammatory drugs (NSAIDs), peptides and carbohydrates.[43-48, 60] Besides, MINP is fully water-soluble and mimics enzymes in size. In this dissertation, we report MINP receptors for selective binding of different bioactive species, including alkaloids and folic acid. We also report MINP sensors for the selective binding and sensing of NSAIDs and catecholamine derivatives.

References

1. Baron, R.; McCammon, J. A., Molecular Recognition and Ligand Association. *Annu. Rev. Phys. Chem.* **2013,** *64* (1), 151-175.

2. Schug, K. A.; Lindner, W., Noncovalent Binding between Guanidinium and Anionic Groups: Focus on Biological- and Synthetic-Based Arginine/Guanidinium Interactions with Phosph[on]ate and Sulf[on]ate Residues. *Chem. Rev. (Washington, DC, U. S.)* **2005,** *105* (1), 67-114.

3. Atwood, J. L.; Lehn, J. M., *Comprehensive Supramolecular Chemistry*. Pergamon: New York, 1996.

4. Steed, J. W.; Gale, P. A., *Supramolecular Chemistry: From Molecules to Nanomaterials*. Wiley: Weinheim, 2012.

5. Juwarker, H.; Suk, J. M.; Jeong, K. S., Foldamers with helical cavities for binding complementary guests. *Chem. Soc. Rev.* **2009,** *38* (12), 3316-3325.

6. Hua, Y.; Liu, Y.; Chen, C.-H.; Flood, A. H., Hydrophobic Collapse of Foldamer Capsules Drives Picomolar-Level Chloride Binding in Aqueous Acetonitrile Solutions. *J. Am. Chem. Soc.* **2013,** *135* (38), 14401-14412.

7. Gan, Q. A.; Ferrand, Y.; Bao, C. Y.; Kauffmann, B.; Grelard, A.; Jiang, H.; Huc, I., Helix-Rod Host-Guest Complexes with Shuttling Rates Much Faster than Disassembly. *Science* **2011,** *331* (6021), 1172-1175.

8. Zhao, Y.; Zhong, Z., Tuning the sensitivity of a foldamer-based mercury sensor by its folding energy. *J. Am. Chem. Soc.* **2006,** *128* (31), 9988-9.

9. Hou, J. L.; Shao, X. B.; Chen, G. J.; Zhou, Y. X.; Jiang, X. K.; Li, Z. T., Hydrogen bonded oligohydrazide foldamers and their recognition for saccharides. *J. Am. Chem. Soc.* **2004,** *126* (39), 12386-94.

10. Zhong, Z.; Li, X.; Zhao, Y., Enhancing Binding Affinity by the Cooperativity between Host Conformation and Host–Guest Interactions. *J. Am. Chem. Soc.* **2011,** *133* (23), 8862-8865.

11. Zhao, Y., Cooperatively Enhanced Receptors for Biomimetic Molecular Recognition. *ChemPhysChem* **2013,** *14* (17), 3878-3885.

12. Wulff, G., Molecular Imprinting in Cross-Linked Materials with the Aid of Molecular Templates— A Way towards Artificial Antibodies. *Angew. Chem. Int. Ed. Engl.* **1995,** *34* (17), 1812-1832.

13. Wulff, G., Enzyme-like Catalysis by Molecularly Imprinted Polymers. *Chem. Rev.* **2001,** *102* (1), 1-28.

14. Haupt, K.; Mosbach, K., Molecularly Imprinted Polymers and Their Use in Biomimetic Sensors. *Chem. Rev.* **2000,** *100* (7), 2495-2504.

15. Ye, L.; Mosbach, K., Molecular Imprinting: Synthetic Materials As Substitutes for Biological Antibodies and Receptors. *Chem. Mater.* **2008,** *20* (3), 859-868.

16. Shea, K. J., Molecular imprinting of synthetic network polymers: the de novo synthesis of macromolecular binding and catalytic sites. *Trends Polym. Sci.* **1994,** *2*, 166-173.

17. Sellergren, B., *Molecularly imprinted polymers: man-made mimics of antibodies and their applications in analytical chemistry*. Elsevier: Amsterdam, 2001.

18. Komiyama, M., *Molecular imprinting: from fundamentals to applications*. Wiley-VCH: Weinheim, 2003.

19. Yan, M.; Ramström, O., *Molecularly imprinted materials: science and technology*. Marcel Dekker: New York, 2005.

20. Alexander, C.; Andersson, H. S.; Andersson, L. I.; Ansell, R. J.; Kirsch, N.; Nicholls, I. A.; O'Mahony, J.; Whitcombe, M. J., Molecular imprinting science and technology: a survey of the literature for the years up to and including 2003. *J. Mol. Recognit.* **2006,** *19* (2), 106-180.

21. Sellergren, B.; Hall, A. J., Molecularly Imprinted Polymers. In *Supramolecular Chemistry: From Molecules to Nanomaterials*, Steed, J. W.; Gale, P. A., Eds. Wiley: Online, 2012.

22. Haupt, K., *Molecular Imprinting*. Springer: Heidelberg ; New York, 2012.

23. Chen, L.; Wang, X.; Lu, W.; Wu, X.; Li, J., Molecular imprinting: perspectives and applications. *Chem. Soc. Rev.* **2016,** *45* (8), 2137-2211.

24. Zhang, Z.; Zhang, X.; Liu, B.; Liu, J., Molecular Imprinting on Inorganic Nanozymes for Hundred-fold Enzyme Specificity. *J. Am. Chem. Soc.* **2017,** *139* (15), 5412-5419.

25. Bie, Z.; Xing, R.; He, X.; Ma, Y.; Chen, Y.; Liu, Z., Precision Imprinting of Glycopeptides for Facile Preparation of Glycan-Specific Artificial Antibodies. *Anal. Chem.* **2018,** *90* (16), 9845-9852.

26. Li, D.; Chen, Y.; Liu, Z., Boronate affinity materials for separation and molecular recognition: structure, properties and applications. *Chem. Soc. Rev.* **2015,** *44* (22), 8097-8123.

27. Zimmerman, S. C.; Wendland, M. S.; Rakow, N. A.; Zharov, I.; Suslick, K. S., Synthetic hosts by monomolecular imprinting inside dendrimers. *Nature* **2002,** *418* (6896), 399-403.

28. Zimmerman, S. C.; Zharov, I.; Wendland, M. S.; Rakow, N. A.; Suslick, K. S., Molecular Imprinting Inside Dendrimers. *J. Am. Chem. Soc.* **2003,** *125* (44), 13504-13518.

29. Li, Z.; Ding, J.; Day, M.; Tao, Y., Molecularly Imprinted Polymeric Nanospheres by Diblock Copolymer Self-Assembly. *Macromolecules* **2006,** *39* (7), 2629-2636.

30. Hoshino, Y.; Kodama, T.; Okahata, Y.; Shea, K. J., Peptide Imprinted Polymer Nanoparticles: A Plastic Antibody. *J. Am. Chem. Soc.* **2008,** *130* (46), 15242-15243.

31. Priego-Capote, F.; Ye, L.; Shakil, S.; Shamsi, S. A.; Nilsson, S., Monoclonal Behavior of Molecularly Imprinted Polymer Nanoparticles in Capillary Electrochromatography. *Anal. Chem.* **2008,** *80* (8), 2881-2887.

32. Cutivet, A.; Schembri, C.; Kovensky, J.; Haupt, K., Molecularly Imprinted Microgels as Enzyme Inhibitors. *J. Am. Chem. Soc.* **2009,** *131* (41), 14699-14702.

33. Yang, K. G.; Berg, M. M.; Zhao, C. S.; Ye, L., One-Pot Synthesis of Hydrophilic Molecularly Imprinted Nanoparticles. *Macromolecules* **2009,** *42* (22), 8739-8746.

34. Zeng, Z. Y.; Patel, J.; Lee, S. H.; McCallum, M.; Tyagi, A.; Yan, M. D.; Shea, K. J., Synthetic Polymer Nanoparticle-Polysaccharide interactions: A Systematic Study. *J. Am. Chem. Soc.* **2012,** *134* (5), 2681-2690.

35. Ma, Y.; Pan, G. Q.; Zhang, Y.; Guo, X. Z.; Zhang, H. Q., Narrowly Dispersed Hydrophilic Molecularly Imprinted Polymer Nanoparticles for Efficient Molecular Recognition in Real Aqueous Samples Including River Water, Milk, and Bovine Serum. *Angew. Chem. Int. Ed.* **2013,** *52* (5), 1511-1514.

36. Zhang, Y.; Deng, C.; Liu, S.; Wu, J.; Chen, Z.; Li, C.; Lu, W., Active Targeting of Tumors through Conformational Epitope Imprinting. *Angew. Chem. Int. Ed.* **2015,** *54* (17), 5157-5160.

37. Biffis, A.; Graham, N. B.; Siedlaczek, G.; Stalberg, S.; Wulff, G., The synthesis, characterization and molecular recognition properties of imprinted microgels. *Macromol. Chem. Phys.* **2001,** *202* (1), 163-171.

38. Maddock, S. C.; Pasetto, P.; Resmini, M., Novel imprinted soluble microgels with hydrolytic catalytic activity. *Chem. Commun.* **2004,** (5), 536-537.

39. Wulff, G.; Chong, B. O.; Kolb, U., Soluble single-molecule nanogels of controlled structure as a matrix for efficient artificial enzymes. *Angew. Chem. Int. Ed.* **2006,** *45* (18), 2955-2958.

40. Carboni, D.; Flavin, K.; Servant, A.; Gouverneur, V.; Resmini, M., The First Example of Molecularly Imprinted Nanogels with Aldolase Type I Activity. *Chem. -Eur. J.* **2008,** *14* (23), 7059-7065.

41. Servant, A.; Haupt, K.; Resmini, M., Tuning Molecular Recognition in Water-Soluble Nanogels with Enzyme-Like Activity for the Kemp Elimination. *Chem.-Eur. J.* **2011,** *17* (39), 11052-11059.

42. Çakir, P.; Cutivet, A.; Resmini, M.; Bui, B. T.; Haupt, K., Protein-size molecularly imprinted polymer nanogels as synthetic antibodies, by localized polymerization with multi-initiators. *Adv. Mater.* **2013,** *25* (7), 1048-51.

43. Awino, J. K.; Hu, L.; Zhao, Y., Molecularly Responsive Binding through Co-occupation of Binding Space: A Lock–Key Story. *Org. Lett.* **2016,** *18* (7), 1650-1653.

44. Awino, J. K.; Gunasekara, R. W.; Zhao, Y., Selective Recognition of d-Aldohexoses in Water by Boronic Acid-Functionalized, Molecularly Imprinted Cross-Linked Micelles. *J. Am. Chem. Soc.* **2016,** *138* (31), 9759-9762.

45. Awino, J. K.; Zhao, Y., Polymeric Nanoparticle Receptors as Synthetic Antibodies for Nonsteroidal Anti-Inflammatory Drugs (NSAIDs). *ACS Biomaterials Science & Engineering* **2015,** *1* (6), 425-430.

46. Awino, J. K.; Zhao, Y., Water-Soluble Molecularly Imprinted Nanoparticles (MINPs) with Tailored, Functionalized, Modifiable Binding Pockets. *Chemistry – A European Journal* **2015,** *21* (2), 655-661.

47. Awino, J. K.; Zhao, Y., Molecularly imprinted nanoparticles as tailor-made sensors for small fluorescent molecules. *Chem. Commun. (Cambridge, U. K.)* **2014,** *50* (43), 5752-5755.

48. Awino, J. K.; Zhao, Y., Rigidity versus amphiphilicity in transmembrane nanopore formation by cholate-based macrocycles. *Supramol. Chem.* **2014,** *26* (3-4), 302-311.

49. Awino, J. K.; Zhao, Y., Protein-Mimetic, Molecularly Imprinted Nanoparticles for Selective Binding of Bile Salt Derivatives in Water. *J. Am. Chem. Soc.* **2013,** *135* (34), 12552-12555.

50. Harirforoosh, S.; Asghar, W.; Jamali, F., Adverse effects of nonsteroidal antiinflammatory drugs: an update of gastrointestinal, cardiovascular and renal complications. *Journal of Pharmacy & Pharmaceutical Sciences* **2014,** *16* (5), 821-847.

51. Dhamodharan, R.; Jordan, M. A.; Thrower, D.; Wilson, L.; Wadsworth, P., Vinblastine suppresses dynamics of individual microtubules in living interphase cells. *Mol. Biol. Cell* **1995,** *6* (9), 1215-1229.

52. Quiñonero, D.; López, K. A.; Deyà, P. M.; Piña, M. N.; Morey, J., Synthetic Tripodal Squaramido-Based Receptors for the Complexation of Antineoplastic Folates in Water. *Eur. J. Org. Chem.* **2011,** *2011* (31), 6187-6194.

53. Low, P. S.; Henne, W. A.; Doorneweerd, D. D., Discovery and Development of Folic-Acid-Based Receptor Targeting for Imaging and Therapy of Cancer and Inflammatory Diseases. *Acc. Chem. Res.* **2008,** *41* (1), 120-129.

54. Quaglia, M.; Chenon, K.; Hall, A. J.; De Lorenzi, E.; Sellergren, B., Target Analogue Imprinted Polymers with Affinity for Folic Acid and Related Compounds. *J. Am. Chem. Soc.* **2001,** *123* (10), 2146-2154.

55. Quaglia, M.; Chenon, K.; Hall, A. J.; De Lorenzi, E.; Sellergren, B., Target Analogue Imprinted Polymers with Affinity for Folic Acid and Related Compounds. *J. Am. Chem. Soc.* **2001,** *123* (10), 2146-2154.

56. Hall, A. J.; Quaglia, M.; Manesiotis, P.; De Lorenzi, E.; Sellergren, B., Polymeric Receptors for the Recognition of Folic Acid and Related Compounds via Substructure Imprinting. *Anal. Chem.* **2006,** *78* (24), 8362-8367.

57. Prasad, B. B.; Tiwari, M. P.; Madhuri, R.; Sharma, P. S., Development of a highly sensitive and selective hyphenated technique (molecularly imprinted micro-solid phase extraction fiber–molecularly imprinted polymer fiber sensor) for ultratrace analysis of folic acid. *Anal. Chim. Acta* **2010,** *662* (1), 14-22.

58. Quiñonero, D.; López, K. A.; Deyà, P. M.; Piña, M. N.; Morey, J., Synthetic Tripodal Squaramido-Based Receptors for the Complexation of Antineoplastic Folates in Water (Eur. J. Org. Chem. 31/2011). *Eur J Org Chem* **2011,** *2011* (31), n/a-n/a.

59. de Oliveira, F. M.; Segatelli, M. G.; Tarley, C. R. T., Evaluation of a new water-compatible hybrid molecularly imprinted polymer combined with restricted access for the selective recognition of folic acid in binding assays. *J. Appl. Polym. Sci* **2016,** *133* (21), n/a-n/a.

60. Fa, S.; Zhao, Y., General Method for Peptide Recognition in Water through Bioinspired Complementarity. *Chem. Mater.* **2019,** *31* (13), 4889-4896.

CHAPTER 2. ZWITTERIONIC MOLECULARLY IMPRINTED CROSS-LINKED MICELLES FOR ALKALOID RECOGNITION IN WATER

Modified from a paper published in *JOC*, **2019**, *84*, 13457.

Likun Duan[1], Yan Zhao[1]*

[1]Department of chemistry, Iowa State University, Ames, Iowa, 50011 United States

* Corresponding Authors

Abstract

Molecular imprinting within surface/core doubly cross-linked micelles afforded water-soluble nanoparticle receptors for their template molecules. Extremely strong imprinting effects were consistently observed, with the imprinting factor >100:1 in comparison to nonimprinted nanoparticles prepared without the templates. The ionic nature of the cross-linkable surfactant strongly impacted the imprinting and binding process. Imprinted receptors prepared with a zwitterionic cross-linkable surfactant (**4**) outperformed a similar cationic one (**1**) when the template was zwitterionic or cationic, and preferred their templates over structural analogues regardless of their ionic characteristics. Electrostatic interactions, however, dominated the receptors made with the cationic surfactant. The same micellar imprinting applied to simple as well as complex alkaloids. Imprinted receptors from **4** were also shown to categorize their alkaloid guests according to their structural similarity.

Introduction

Molecular recognition is the basis of nearly every biological process including receptor–ligand binding, enzymatic catalysis, and transport of molecules across membranes. In order for a supramolecular host to bind its guest strongly and selectively, the two must have a complementary interface where multiple noncovalent interactions engage. When the guest is small and symmetrical, a complementary host can be constructed relatively easily using an organic framework such as a macrocycle. When the guest becomes more complex in shape and functionality, as with most bioactive molecules, design and synthesis of a complementary host become much more challenging. The difficulty increases further with additional requirements such as preorganization of the host's conformation for guest-binding, solubility in water, and ability to function under competitive aqueous environments. High specificity in binding also becomes a must for biomolecular recognition, since closely related biomolecules tend to have drastically different biological properties.

All these demands make traditional stepwise total synthesis of supramolecular hosts impractical for biomolecular recognition. In this regard, molecular imprinting is an attractive alternative for building receptors for complex molecules.[1,2] The method involves first formation of a template–functional monomer (FM) complex, either spontaneously through noncovalent interactions or chemically through reversible covalent bonds. The complex is then polymerized with a large amount of a cross-linker. Removal of the template from the resulting macroporous polymer network affords template-complementary binding sites in size, shape, and distribution of functional groups. Molecular imprinting can be applied readily to different-sized molecules[1,2] and even large entities including viruses and bacteria.[3-8] Its simplicity continues to attract many researchers' interest for their applications in a wide range of areas.[9-20]

Instead of using a macroporous polymeric network, our group found that micelles of doubly cross-linkable surfactant **1** could serve as an excellent platform for molecular imprinting (Scheme 1).[21] The process involves a two-stage cross-linking, first on the surface of the micelle using diazide **2** via the click reaction and then in the micellar core using divinylbenzene (DVB) via free-radical polymerization. The cross-linked micelles are typically functionalized on the surface using monoazide **3** by another round of click reaction for increased hydrophilicity and facile purification. Micellar imprinting can be done directly in water, thanks to the ability of micelles to strengthen hydrogen bonds in their nonpolar core.[22,23] The number of binding sites per cross-linked micelle is controlled by the surfactant/template ratio.[21] The so-called molecularly imprinted nanoparticles (MINPs) are ~5 nm in diameter, and resemble proteins in their nanosize, hydrophilic exterior, and hydrophobic core. They mimic protein receptors in their binding of common biological guests such as peptides,[24] carbohydrates,[25] and can be converted into highly selective catalysts similar to enzymes.[26]

The cross-linkable surfactant in micellar imprinting is the most important component for the synthesis. Not only does it set the boundary for imprinting by its self-assembled micelle, it also acts as the functional monomer and cross-linker to interact with the template through hydrophobic,[21] electrostatic,[21] and hydrogen-bonds.[27] Cationic surfactant **1** was used in the majority of our micellar imprinting. Although it has allowed a wide range of biologically interesting molecules to be imprinted, its cationic nature may not always be desirable for biological applications. Because biological entities (proteins, nucleic acids, and lipids) vary in charge, we need to be able to tune the charge of our materials for specific applications.

In this work, we designed and synthesized a new cross-linkable surfactant. Its zwitterionic headgroup was inspired by natural phosphatidylcholine and was found to strongly impact the

imprinting and binding of charged template molecules. In comparison to our original **1**, the new surfactant allowed MINPs to differentiate closely related natural products with varying ionic charges. It also enabled facile preparation of synthetic receptors for alkaloids, a highly important class of biomolecules with broad pharmaceutical applications.[28,29]

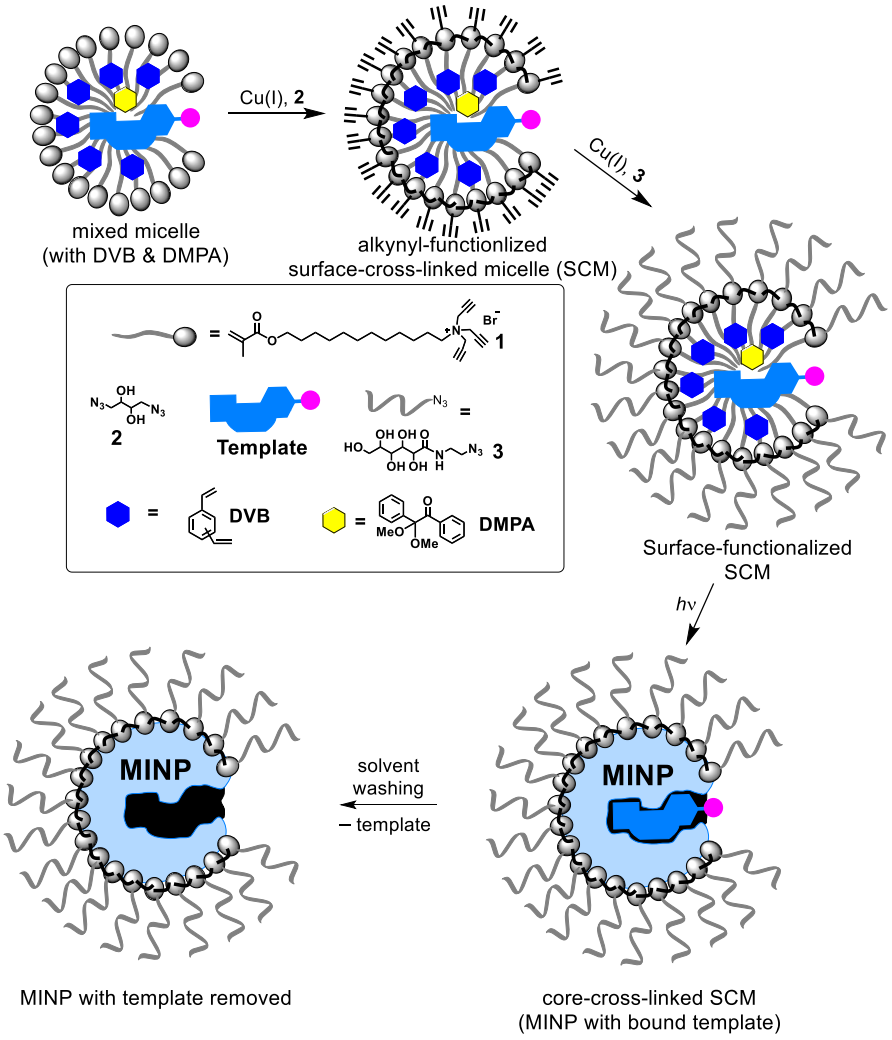

Scheme 1. Preparation of MINP by surface–core double cross-linking of template-containing micelle of **1**.

Results and Discussion

Synthesis and Characterization of Zwitterionic Cross-Linkable Surfactant. Phosphatidylcholine is a major component of biological membranes.[30,31] Its zwitterionic headgroup is connected via a glycerol to two fatty acid chains (Scheme 2). The headgroup is strongly solvated by water and provides a neutral background for a membrane to interact with its components including proteins and other lipids. It is known to cause low structural perturbation to associated water molecules. Related to this property, phosphatidylcholine-containing amphiphilic polymers have strong abilities to resist biofouling, due to their low tendencies to trigger conformational changes of adsorbed proteins.[32-35]

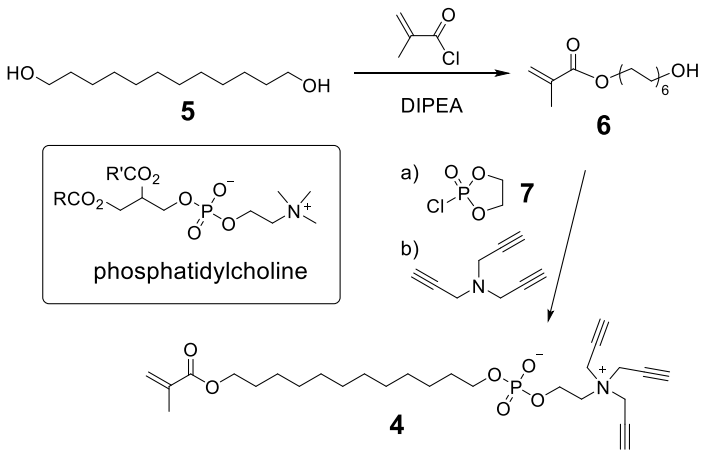

Scheme 2. Syntheses of cross-linkable surfactants **4**.

Synthesis of our phosphatidylcholine-like cross-linkable surfactant **4**, 12-(methacryloyloxy)dodecyl (2-(tri(prop-2-yn-1-yl)ammonio)ethyl) phosphate, is shown in Scheme 2. 1,12-Dodacanediol **5** is mono-methacrylated to afford **6**. This step is the same as that in the synthesis of **1**.[21] The mono alcohol is then phosphorylated with ethylene glycol chlorophosphate **7**, and the resulting cyclic phosphate is ring-opened by commercially available tripropargylamine to afford **4**, following reported literature procedures.[36] The surfactant is

similar to **1** in many aspects—a C12 carbon chain, a tripropargylammonium group for surface cross-linking, and a methacrylate at the end of the hydrocarbon tail for core-cross-linking. The compound was fully characterized by ^{1}H NMR spectroscopy, ^{13}C NMR spectroscopy, and high-resolution mass spectrometry.

An extremely important property of a surfactant is its critical micelle concentration (CMC), above which micelles start to form spontaneously in water. There are many ways to determine the CMC of a surfactant.[37] A method of choice utilizes an environmentally sensitive hydrophobic probe such as pyrene.[38] The method requires very little amounts of materials and, in our hands, afforded similar CMC values as those determined from the reduction of surface tension for analogous surfactants.[39] Typically, a series of surfactant solutions of varying concentrations are prepared using an aqueous solution containing 0.1 μM pyrene. The emission of pyrene has five vibronic bands, with the first band (I_1) near 372 nm becoming stronger in a more polar environment and the third (I_3) near 384 nm staying nearly constant. The I_3/I_1 ratio thus increases with decreasing environmental polarity.

Figure 1 plots the I_3/I_1 ratio of pyrene against the concentration of **4** in Millipore water. The ratio stayed unchanged at low surfactant concentration, around 0.80. Apparently, the hydrophobic probe stayed in the aqueous phase under such conditions, even though the solution contained some surfactant molecules. As the concentration of **4** increased beyond a certain point, the I_3/I_1 ratio began to rise sharply, with almost a linear dependence on the surfactant's concentration beyond the inflection point. The result was consistent with the formation of an increasing number of micelles at higher concentrations above the CMC, leading to a higher partition of the hydrophobic probe into the nonpolar region of the micelle. The inflection point of the curve is normally considered the CMC of the surfactant, and was 0.20 mM for **4**. This

number was lower than the 0.55 mM for the cationic surfactant **1**.[21] The result was reasonable, given the strong repulsion among the cationic headgroups in the micelle of **1** and the overall neutral charge of **4**.

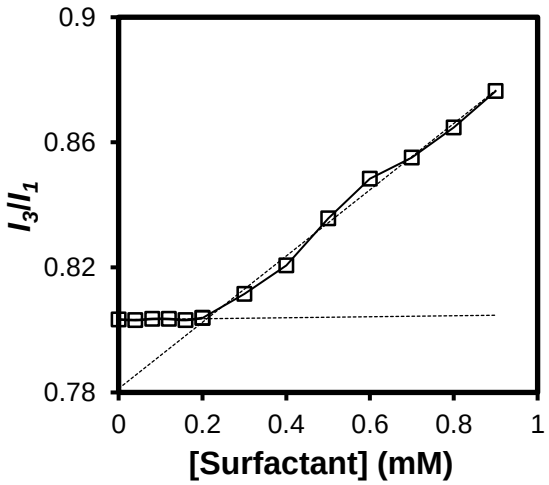

Figure 1. Pyrene I_3/I_1 ratio as a function of [**4**]. [pyrene] = 0.1 μM.

Binding Properties of Zwitterionic and Cationic MINPs. To understand how different headgroups impact micellar imprinting, we chose to study three model templates **8**–**10**, all of biological origin. 3-Indolepropionic acid **8** is a natural product with potential therapeutic benefits for Alzheimer's diease.[40] Tryptophan **9** is a natural aromatic amino acid. Tryptamine **10** is a monoamine alkaloid, able to bind human trace amine-associated receptors (hTAARs) in the central nervous system.[41] The three compounds share the same hydrophobe (i.e., indole) but have different ionic characteristics. These features make them particularly suitable for probing relative contributions of hydrophobic and electrostatic interactions in the imprinting and binding of MINPs.

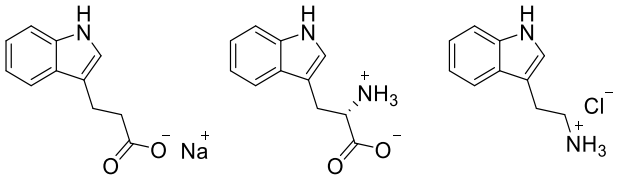

8 **9** **10**

Preparation of the MINPs is reported in the Experimental Section. The surface- and core-cross-linking of the micelle was monitored by ^{1}H NMR spectroscopy. The surface-cross-linking chemistry had been confirmed independently by mass spectrometry after the surface-cross-linkages were cleaved by periodate.[42] Dynamic light scattering (DLS) allowed us to follow the change of size for the micelles during the surface-cross-linking, surface-functionalization, and core-cross-linking. The DLS size had been confirmed by transmission electron microscopy (TEM).[43,44] Since a key different between surfactants **1** ad **4** was their ionic nature, we also determined the zeta potential of the corresponding MINPs. MINP$_1$, i.e., MINP prepared with **1** as the cross-linkable surfactant, afforded a zeta potential of 60.5 mV and MINP with **4** as the surfactant -14.4 mV (Figures S4 and S8).

One benefit of using indole-derived compounds is that their binding could be studied conveniently by fluorescence titration. Figure 2a shows the emission spectra of 2.0 μM **8** in 50 mM Tris buffer (pH = 7.4) upon the addition of 0–7.0 μM MINP$_4$(**8**), i.e., MINP prepared with **4** as the cross-linkable surfactant and **8** as the template. The higher concentration of the MINP caused a decrease of the main emission band at 363 nm. Two isoemissive points were observed at ca. 336 and 426 nm, suggesting a continuous transition from the free to the bound **8** during titration. A blank titration experiment showed that the MINP contributed negligibly to the observed fluorescence (Figure S18). The emission intensity at 363 nm fit nearly perfectly to a 1:1 binding isotherm (Figure 2b). Nonlinear least squares fitting afforded a binding constant (K_a) of (6.56 ± 0.90) × 10^5 M^{-1}. When the guest was titrated with nonimprinted nanoparticles

(i.e., NINP$_4$), the binding was much weaker, with an estimated binding constant of 0.06 × 10^5 M^{-1} (Figure S19). The imprinting factor (IF), thus, was >100:1, indicating an extremely strong imprinting effect.

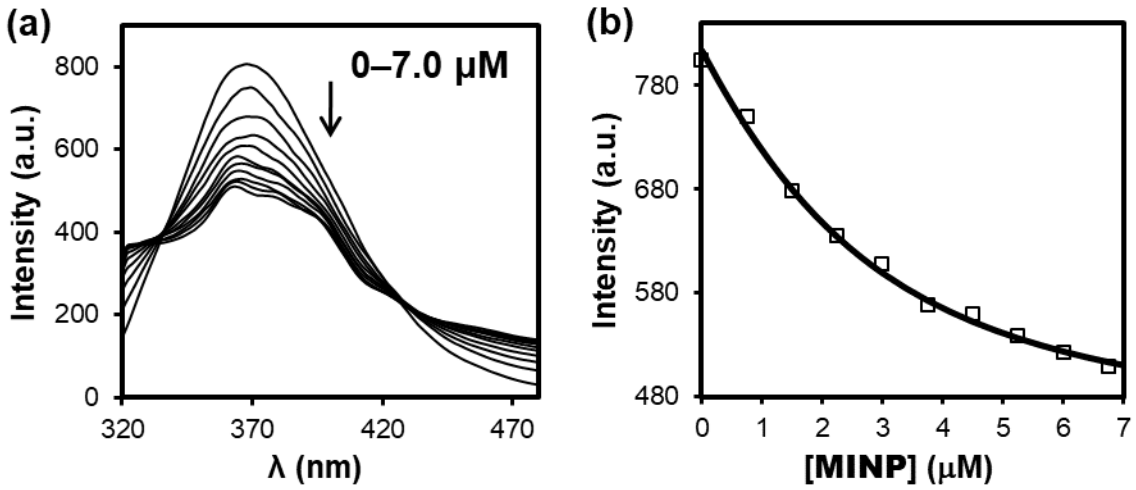

Figure 2. (a) Emission spectra of **8** (λ_{ex} = 300 nm) upon the addition of different concentrations of MINP$_4$(**8**) in 50 mM Tris buffer (pH = 7.4). [**8**] = 2.0 μM. The concentration of MINP was calculated based on a M.W. of 50,000 g/mol determined by DLS. (b) Nonlinear least squares fitting of the emission intensity of **8** at 363 nm to a 1:1 binding isotherm.

Figure 3a,b shows the emission spectra of **8** titrated by MINP$_1$(**8**) and the corresponding data fit to the 1:1 binding model, which yielded a K_a value of (13.2 ± 0.3) × 10^5 M^{-1}. The guest continued to show weak binding toward nonimprinted nanoparticles (i.e., NINP$_1$), with $K_a \approx$ 0.09 × 10^5 M^{-1} (Figure S20). The imprinting factor (IF) hence was also >100:1, indicating a strong imprinting effect with the cationic micelle as well.

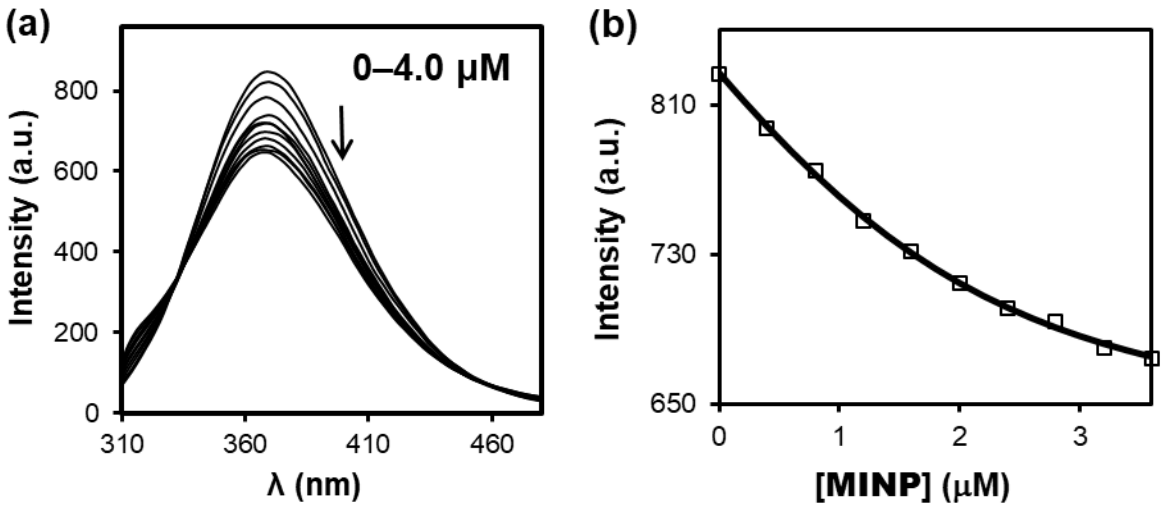

Figure 3. (a) Emission spectra of **8** (λ_{ex} = 300 nm) upon the addition of different concentrations of MINP$_1$(**8**) in 50 mM Tris buffer (pH = 7.4). [**8**] = 2.0 μM. The concentration of MINP was calculated based on a M.W. of 50,000 g/mol determined by DLS. (b) Nonlinear least squares fitting of the emission intensity of **8** at 363 nm to a 1:1 binding isotherm.

In addition to different binding constants, the emission spectra of the guest differed significantly in shape in the titrations with the two MINPs (Figures 2a and 3a). Whereas the cationic MINP$_1$(**8**) caused a quenching effect of the broad emission band of the indole ring, multiple vibronic bands appeared for **8** in the presence of the zwitterionic MINP$_4$(**8**). Indole derivatives have two over lapping electronic transitions, ^1L_a and ^1L_b.[45-47] The ^1L_a band is broad and sensitive to environmental polarity including hydrogen bonding interactions to the indole nitrogen and charged groups nearby.[48] The ^1L_b band, on the other hand, tends to have vibronic structures and meanwhile is less sensitive to the environment.[49] The relative contribution of ^1L_b band is known to increase in a hydrophobic microenvironment.[50] Although the complexity of indole fluorescence and its sensitivity to multiple factors make it difficult to pinpoint the exact cause of different spectra shapes in Figures 2a and 3a, the consistency in the difference (Figures

S21–36) suggests a common origin, most likely the stronger hydrophobicity of the zwitterionic micelle (vide infra).

Given the complexity of the indole fluorescence, we also confirmed the bindings by isothermal titration calorimetry (ITC). This method measures the heat change during titration, and is able to afford a number of parameters including the binding enthalpy (ΔH) and number of binding sites per nanoparticle (N), in addition to the binding constant. After background subtraction to account for the dilution effect, ITC showed that the number of binding sites per nanoparticle was 1.14 ± 0.13 for **8** by $MINP_4$(**8**), consistent with the 1:1 binding suggested by the fluorescence titration (Figure 4). Because typical MINPs contain ~50 cross-linked surfactants per particle as estimated by DLS, the 1:1 binding was expected when a 50:1 surfactant/template ratio was used in the preparation.[21] The K_a value obtained was (6.78 ± 0.31) × 10^5 M^{-1}, very similar to that from the fluorescence titration ((6.56 ± 0.90) × 10^5 M^{-1}). For the binding of **8** by $MINP_1$(**8**), ITC afforded a binding constant of (13.9 ± 0.5) × 10^5 M^{-1} (Figure S41), also in excellent agreement with what was obtained from the fluorescence titration. Since it was much quicker to perform fluorescence titration, we used this method whenever the template or guest molecule was fluorescent.

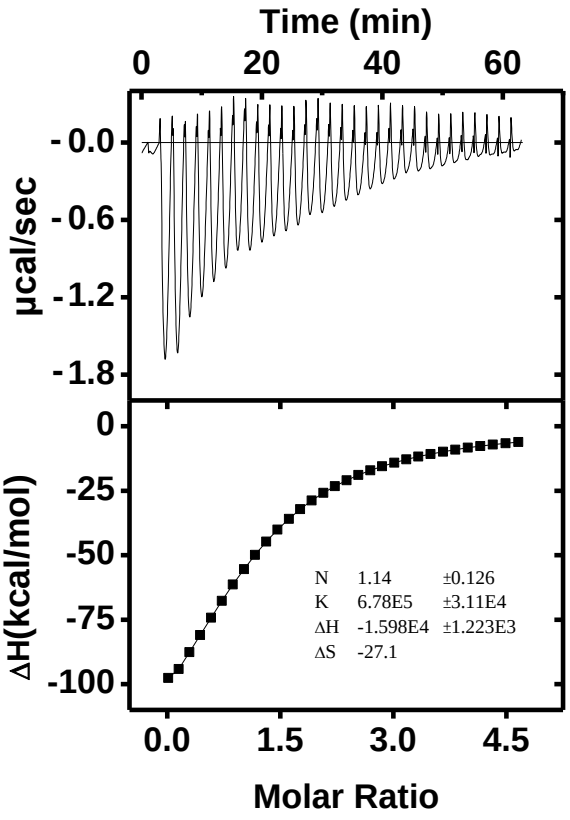

Figure 4. ITC curve obtained at 298.15 K from titration of MINP$_4$(**8**) with **8** in 50 mM Tris buffer (pH = 7.4). MINP$_4$(**8**) = 10 µM in the cell. The concentration of **8** in the syringe was 0.20 mM.

Table 1 summarizes the binding constants obtained in this study. Since surfactant **1** was good to at imprinting anionic guests, we studied the binding of **8** first. In our hands, MINP$_1$(**8**) bound the anionic template more strongly than MINP$_4$(**8**) prepared with the same template (Table 1, entry 1). Although the result was fully expected from the favorable electrostatic interactions between the cationic micelle and anionic template, the 2-fold increase in binding represented a very modest effect. Our previous work showed that electrostatic interactions played important

roles in the MINP binding of anionic guests when **1** was the cross-linkable surfactant.[21] It is

Table 1. Binding constants and selectivity for MINPs imprinted against **8**–**10**.[a]

Entry	Template	Guest	K_a ($\times 10^5$ M^{-1})		CRR[b]	
			MINP$_4$	MINP$_1$	MINP$_4$	MINP$_1$
1	**8**	**8**	6.56 ± 0.90 (6.78 ± 0.31)	13.2 ± 0.3 (13.9 ± 0.5)	1	1
2	**8**	**9**	3.84 ± 0.51	0.91 ± 0.31	0.59	0.07
3	**8**	**10**	4.08 ± 0.47	0.43 ± 0.10	0.62	0.03
4	**9**	**8**	2.95 ± 0.43	11.9 ± 3.7	0.38	13.4
5	**9**	**9**	7.75 ± 0.87	0.89 ± 0.10	1	1
6	**9**	**10**	3.38 ± 0.45	0.42 ± 0.02	0.44	0.47
7	**10**	**8**	3.80 ± 0.43	9.84 ± 2.25	0.51	15.9
8	**10**	**9**	3.77 ± 0.65	0.67 ± 0.13	0.50	1.08
9	**10**	**10**	7.52 ± 0.72	0.62 ± 0.14	1	1
10	none	**8**	0.06[c]	0.09[c]	-	-
11	none	**9**	0.05[c]	0.04[c]	-	-
12	none	**10**	0.05[c]	0.01[c]	-	-

[a] The binding constants were obtained from fluorescence titrations performed in duplicates in 50 mM Tris buffer (pH = 7.4). The binding constants in parentheses were obtained from ITC. [b] CRR is the cross-reactivity ratio, defined as the binding constant of a guest relative to that of the template for a particular MINP. [c] Binding was between the guest and nonimprinted nanoparticles (NINP$_4$ or NINP$_1$) prepared without any templates. The binding was very weak and the binding constants were estimated from fluorescence titrations (SI).

known that zwitterionic surfactants tend to pack more tightly than ionic ones during micellization due to reduced hydration of their headgroups.[51] This suggest that the micelle of **4** is more hydrophobic in the nonpolar interior than that of **1**. The effect would strengthen the hydrophobic interactions between MINP$_4$(**8**) and its template and most likely partly offset the loss of favorable electrostatic interactions between MINP$_1$(**8**) and **8**.

When zwitterionic **9** was used as the template, MINP$_4$(**9**) was able to bind the template with a K_a of 7.75 × 10^5 M^{-1} in Tris buffer (Table 1, entry 5). In contrast, MINP$_1$(**9**) showed a much weaker binding for the same template, with a K_a of 0.89 × 10^5 M^{-1}. The binding was nearly 9 time weaker, corresponding to a 1.28 kcal/mol difference in binding free energy ($\Delta\Delta G$). One possible reason for the stronger ability of **4** to imprint **9** could be the zwitterionic nature of both compounds. Essentially, both the positively and negatively charged groups of the template could find suitable groups on the micelle to ion-pair during imprinting in case of **4**, whereas only the negatively charged carboxylate of the template could enjoy favorable interactions with the surfactant if **1** is used to prepare MINP. Another possible reason is the "tighter and more hydrophobic micelle" of **4** mentioned above, which could help the imprinting and binding of any hydrophobic molecules.

The benefit of the zwitterionic over cationic surfactant was also evident in the imprinting of the cationic template (**10**). Entry 9 of Table 1 shows that the binding constant for the template was 7.52 and 0.62 × 10^5 M^{-1} by **MINP$_4$(10)** and MINP$_1$(**10**), respectively. Since these numbers do not differ much from those for the zwitterionic template **9** (entry 5), the double ion-pairing reason mentioned above must be minor in micellar imprinting, otherwise eliminating the factor should weaken the binding of **10** by MINP$_4$(**10**) relative to that of **9** by MINP$_4$(**9**) significantly.

On the other hand, the "tighter and more hydrophobic micelle" of **4**, would still help the imprinting and binding of any hydrophobic template, including the cationic **10**.

Another interesting observation was that the binding constants for **9** by MINP$_1$(**9**) and **10** by MINP$_1$(**10**) were quite similar, 0.89 and 0.62 × 10^5 M^{-1}, respectively (entries 5 and 9). This might appear quite strange, as the cationic MINP should repel the cationic template (**10**) but at least be able to "tolerate" the zwitterionic one (**9**). The assumption for this prediction, however, was that **10** stayed protonated during binding. The pK_a of a primary ammonium group is ~10. At pH 7.4 under our titration conditions, it should be largely protonated indeed, at least in solution. Nonetheless, a protonated amine can shift its pK_a dramatically in different environments. When Isom et al. prepared 25 variants of staphylococcal nuclease with lysine residues at varying positions, for example, 19 of the (protonated) lysine residues have depressed pK_a values, some as low as 5.3, due to a strong environmental effect on the acid–base equilibrium.[52] Essentially, when located in a hydrophobic microenvironment instead of an aqueous solution, the pK_a of an ammonium group is much lower because the protonated, positively charged ammonium is poorly solvated and unstable, relative to the neutral amine. The same could happen when the ammonium has other positively charged ions in the vicinity. Both situations do exist in the imprinting and binding of **10** by our cationic micelle. By taking the neutral amino form, template **10** can migrate deeper into the micelle of **1** and avoid electrostatic repulsion at the same time. Tryptophan **9**, however, had to stay near the surface of the micelle because of its two ionic groups.[53] Its advantage, of course, is the lack of electrostatic repulsion with the cationic micelle. In these ways, each template could optimize its interactions with the cationic micelle within its own capability and constraints; the end result was that the two showed similar binding toward the cationic MINP.

In Table 1, we also included two columns of cross-reactivity ratio (CRR), defined as the binding constant of a guest relative to that of the template for a particular MINP. The term is frequently used in immunology, and measures the selectivity of our "synthetic antibodies" for closely related structural analogues. Based on the definition, CRR is 1 for the template and, the smaller the ratio for a particular guest, the weaker is the binding and the higher the selectivity of that MINP is for its template molecule.

Our data shows that the zwitterionic $MINP_4$ was able to distinguish its template from closely related structural analogues, regardless of the ionic characteristics of the template. For example, when the anionic template **8** was used as the template, zwitterionic **9** and cationic **10** gave a CRR of 0.59 and 0.62, respectively, for $MINP_4$(**8**) (Table 1, entries 2 and 3). Although the exact values differed somewhat for $MINP_4$(**9**) and $MINP_4$(**10**), the same trend persisted, i.e., MINP made with the zwitterionic surfactant always bound its template more strongly than structural analogues (entries 4–9).

In contrast, when cationic surfactant **1** was used to prepare MINP, a very different behavior was observed. Instead of favoring the template itself, $MINP_1$(**9**) showed a strong preference for guest **8** (Table 1, entries 1–3, under $MINP_1$). The same happened with $MINP_1$(**10**). All these are considered imprinting failure, when the imprinted material shows weaker binding for its template than structural analogues. In fact, when the cationic surfactant was used to prepare MINPs, regardless of the template, the binding of the final MINP always followed the order of **8** > **9** > **10**. Clearly, when hydrophobic group was kept constant, the binding affinity was mainly controlled by electrostatic interactions for the cationic MINPs.

The cationic MINP was not completely without merit in selectivity, however. When the anionic guest (**8**) was the template, the selectivity for the template was much higher than what was obtained by the zwitterionic MINP. The CRR for **9** and **10**, for example, was 0.07 and 0.03 toward MINP$_1$(**8**). These numbers were much lower than the corresponding values toward MINP$_4$(**8**), i.e., 0.59 and 0.62, respectively (Table 1, entries 2 and 3).

As for the binding between the guests and the nonimprinted nanoparticles, the K_a values were very similar for NINP$_4$ (0.05–0.06 × 10^5 M^{-1}) (Table 1, entries 10–12). Thus >100:1 IF was consistently obtained for all three guests. The results also support the minor importance of electrostatic interactions for the zwitterionic micelles. For the cationic NINP$_1$, although the bindings were also weak (0.01–0.09 × 10^5 M^{-1}), the binding affinity did follow the expected order **8** > **9** > **10**, indicating that the electrostatic interactions also dominated nonspecific binding of the cationic cross-linked micelles.

Binding of Alkaloids by Zwitterionic MINPs. The zwitterionic cross-linkable surfactant, thus, gave stronger binding affinities and higher selectivities when the template was zwitterionic or cationic. These results encouraged us to use **4** to imprint alkaloids, an extremely important class of biomolecules containing basic nitrogens and frequently administered in the cationic salt form.[28,29] As a proof of concept, we first studied three structurally similar alkaloids **11**–**13**. Among the three alkaloids, 1-phenylcyclohexanecarboxylic acid derive **11** is a potential antispasmodic.[54] Proadifen hydrochloride **12** has quite a similar structure but has completely different biological properties, showing inhibiting effects on cytochrome P450 enzymes[55] and suppressing proliferation of certain cancers.[56] Compound **12** is marketed under many different names (Ansmin, Cefadol, Celmidol, Difenidol, Maniol, Vontrol, etc.). With a slight variation of structure, this alkaloid is an antiemetic and antivertigo agent.

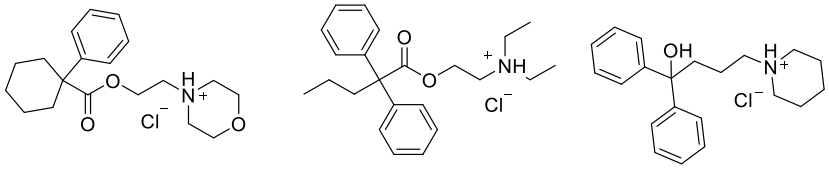

11 **12** **13**

Among the three alkaloids, **11** and **13** are quite similar and **12** is more different. For example, although there is a difference of ester versus hydroxyl in the center of the structure for **11** and **13**, the two are quite similar in size, shape, and amphiphilicity. Compound **12**, on the other hand, has an extra butyl near the two phenyls and also has a diethylamino instead of piperidinyl group on the other end of the structure. To see whether our imprinted micelles could differentiate the two groups of compounds, we prepared MINPs with **4** as the cross-linkable surfactant for **11** and **12** and studied their binding for all three compounds. Because the compounds were not fluorescent, we measured the binding by ITC.

Table 2 shows that both MINP$_4$(**11**) and MINP$_4$(**12**) bound their template more strongly than other alkaloids. The binding constant for **11** and **12** was 3.15 and 4.60 × 10^5 M^{-1}, respectively, by their own MINP receptor (entries 1 and 5). When **11** was used as the template, CRR was 0.16 for **12** and 0.63 for **13**. Thus, **13** was more similar to **11** than **12**, as far as the binding was concerned. When **12** was used as the template, CRR was 0.08 for **11** and 0.05 for **13**. Thus, once again, **11** and **13** were quite similar and differed quite a bit from **12**, on the basis of their interactions with the MINP.

Table 2. Binding data for MINPs obtained by ITC.[a]

entry	template	guest	*N*	K_a (10^5 M^{-1})	CRR	-Δ*G* (kcal/mol)	-Δ*H* (kcal/mol)	TΔ*S* (kcal/mol)
1	**11**	**11**	0.8 ± 0.2	3.15 ± 0.33	1	7.5	26.6 ± 2.4	-19.1
2	**11**	**12**	0.8 ± 0.1	0.516 ± 0.048	0.16	6.4	9.8 ± 1.3	-3.4
3	**11**	**13**	0.7 ± 0.1	1.97 ± 0.14	0.63	7.2	31.5 ± 3.1	-24.3
4	**12**	**11**	1.3 ± 0.2	0.360 ± 0.028	0.08	6.2	2.5 ± 0.3	3.7
5	**12**	**12**	0.7 ± 0.1	4.60 ± 0.67	1	7.7	11.1 ± 3.1	-3.4
6	**12**	**13**	1.1 ± 0.1	0.222 ± 0.034	0.05	5.9	4.3 ± 0.5	1.6
7	**14**	**14**	0.8 ± 0.1	7.81 ± 0.31	-	8.0	3.3 ± 0.6	4.7

[a] Binding was measured in 50 mM Tris buffer (pH = 7.4). The titrations were performed in duplicates and the errors between the runs were <20%.

Unlike molecular synthesis of receptors that gets more difficult with increasing complexity of ligands, molecular imprinting of complex guests can be as straightforward as that of simple ones. Vinblastine **14** is a dimeric indole-based alkaloid with a very complex structure. It is able to inhibit the formation of microtubules[57,58] and normally administered together with other anticancer drugs against a wide range of cancers. In our hands, it could be imprinted as easily as the other much simpler templates. We also measured the binding of the alkaloid by the MINP. The binding constant was 7.81 × 10^5 M^{-1} (Table 2, entry 7), in line with those for other alkaloids (by their own MINP receptors).

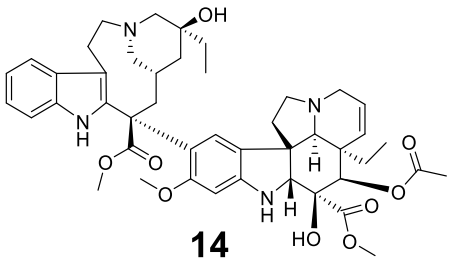

14

Conclusions

Synthetic receptors have potential applications in the isolation, extraction, and monitoring of biologically interesting molecules including drugs and natural products. They could also be used to probe or intervene biological interactions. Despite all these applications, design and synthesis of molecular receptors become too difficult as the guest gets more complicated in structure and larger in size. This work shows that micellar imprinting affords a convenient method to create protein-sized, water-soluble organic nanoparticles for natural products/drugs. It also revealed that zwitterionic cross-linkable surfactant **4** outperformed the cationic one (**1**) in most cases when the guests carried identical hydrophobes but different ionic groups. Imprinted receptors prepared with this surfactant was able to categorize and recognize closely related alkaloids. The one-pot, 2-day synthesis of MINP at room temperature was straightforward to perform for complex as well as simple alkaloids. Given that many important alkaloids are isolated from natural sources—e.g., vinblastine from the leaves of *Catharanthus roseus*[57,58]—a facile preparation of their receptors is significant for their isolation and purification.

Acknowledgments

We thank NIGMS (R01GM113883) for financial support of this research

Experimental Section

General Method. Routine ^{1}H and ^{13}C NMR spectra were recorded on a 400 and 600 MHz NMR spectrometer. ESI-MS mass was recorded on Shimadzu LCMS-2010 mass spectrometer. Dynamic light scattering (DLS) data were recorded at 25 °C using PDDLS/CoolBatch 90T with PD2000DLS instrument. Isothermal titration calorimetry (ITC) was performed using a MicroCal VP-ITC Microcalorimeter with Origin 7 software and VPViewer2000 (GE Healthcare, Northampton, MA). Syntheses of compounds **1**–**3** and **6** were reported previously.[21]

Compound 4. N,N-Diisopropylethylamine (DIPEA) (84 mg, 0.65 mmol) was added slowly to stirred solution of **6** (135 mg, 0.5 mmol) and **7** (71 mg, 0.5 mmol) in anhydrous THF (2 mL) at 0 °C. The reaction mixture was warmed up to room temperature. After 2 h, the mixture was filtered through a pad of celite and the filtrate was concentrated under reduced pressure. The colorless oil was dissolved in anhydrous methylene chloride (3 mL) at 0 °C, followed by addition of trimethylsilyl triflate (111 mg, 0.5 mmol) and tripropargylamine (200 mg, 1.5 mmol). The reaction mixture was warmed to room temperature and stirred for 12 h. The reaction mixture was diluted with chloroform (10 mL) and neutralized with saturated sodium bicarbonate solution. The organic layer was separated, dried over anhydrous Na_2SO_4, and concentrated under reduced pressure. The residue was purified by column chromatography over silica gel using 4:1 methylene chloride/methanol and then 55:45:3 methylene chloride/methanol/water as eluents to afford a colorless oil (139 mg, 55%). ^{1}H NMR (600 MHz, $CDCl_3$, δ): 6.09 (s, 1H), 5.54 (s, 1H), 4.78 (s, 6H), 4.40 (s, 2H), 4.13 (t, J = 6.7 Hz, 2H), 3.99

(s, 2H), 3.84 (m, 2H), 3.42 (s, 3H), 1.94 (s, 3H), 1.65 (m, 4H), 1.19 (m, 16H). $^{13}C\{H\}$ NMR (100 MHz, $CDCl_3$, δ): 167.6, 136.5, 125.2, 83.4, 70.8, 66.0, 60.20, 58.8, 51.2, 30.9, 30.9, 29.72, 29.70, 29.63, 29.57, 29.3, 28.6, 26.0, 25.91 18.3. HRMS (ESI/QTOF) m/z: $[M + H]^+$ calcd for $C_{27}H_{43}NO_6P$, 508.2823; found 508.2835.

Preparation of MINPs and NINPs. Preparation of MINP**1** followed previously reported procedures and typical yields were 70–80%.[21] In the preparation of MINP**4**, copper chloride used in the click reaction (for surface-cross-linking and functionalization) precipitated in the presence of **4**. The click reaction was performed with copper chloride as the precatalyst with additional 4 equivalents of a tridentate ligand N,N,N′,N″,N″-pentamethyldiethylenetriamine (PMDTA).[59] For the purification of MINP**4**, the final reaction mixture was poured into acetone (8 mL). The precipitate was collected by centrifugation and washed with a mixture of methanol (5 mL) three times. The off-white powder was dried in air to afford the final MINPs with typically 70% yield. The preparation of nonimprinted nanoparticles (NINP**1** and NINP**4**) followed the same procedures, except that the template was not used.

Determination of Binding Constants by Fluorescence Titration. A typical procedure is as follows. A stock solution containing MINP**4**(**8**) (200 μM) was prepared in 50 mM Tris buffer (pH = 7.4). Aliquots (2 μL) of the MINP stock solution were added to 2.00 mL of the solutions of **8**–**10** in the same buffer (2.0 μM). After each addition, the sample was allowed to sit for 1 min at room temperature before the fluorescence spectrum was collected. The excitation wavelength (λ_{ex}) was 300 nm. The excitation slit width was 10 nm, and the emission slit width was 10 nm. The binding constant was obtained by nonlinear least squares fitting of the emission intensity at 363 nm to 1:1 binding isotherm.

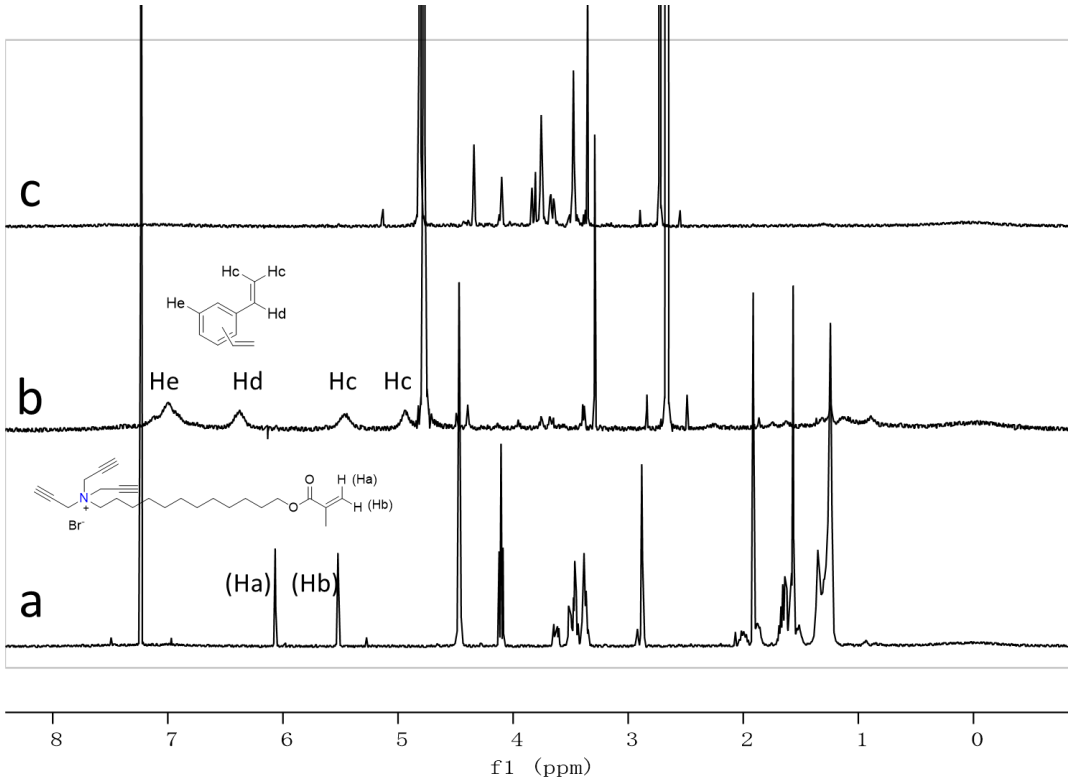

Figure S1. ^{1}H NMR spectra of (a) **1** in $CDCl_3$, (b) alkynyl-SCM in D_2O, and (c) MINP$_1$(**8**) in D_2O.

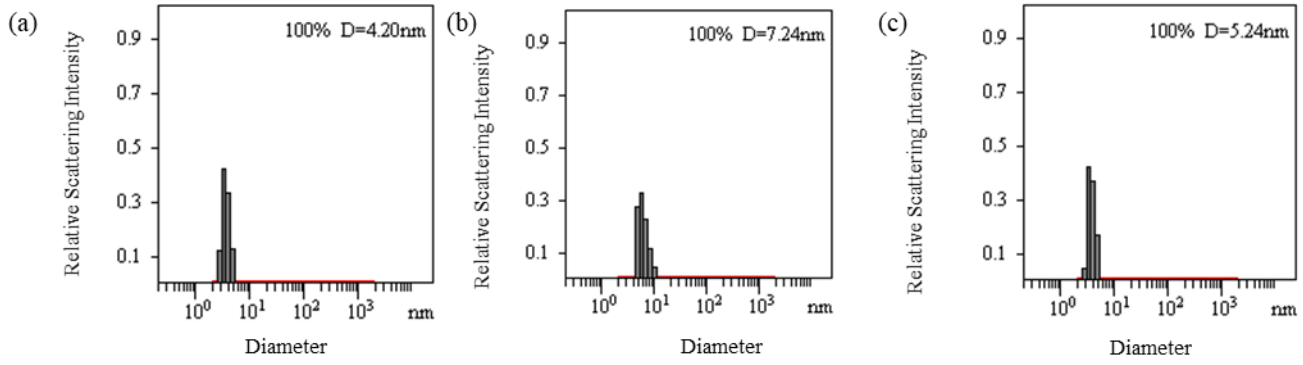

Figure S2. Distribution of the hydrodynamic diameters of the nanoparticles in water as determined by DLS for (a) alkynyl-SCM, (b) surface-functionalized SCM, and (c) MINP$_1$(**8**) after purification.

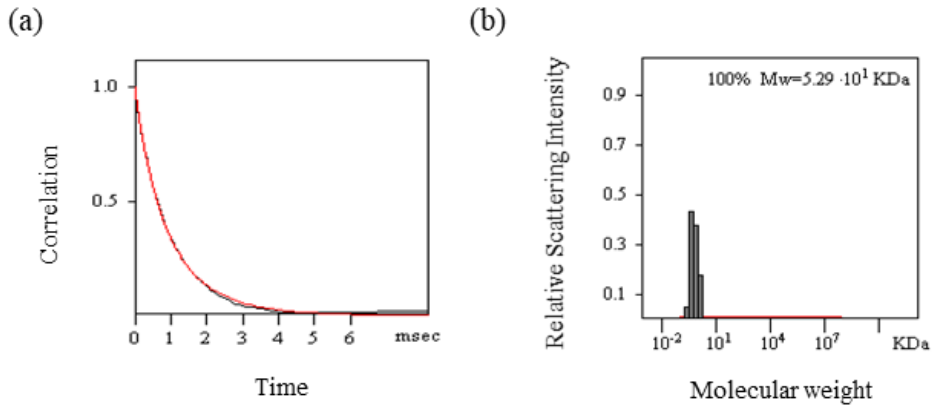

Figure S3. The correlation curve and the distribution of the molecular weight for MINP$_1$(**8**) from the DLS. The PRECISION DECONVOLVE program assumes the intensity of scattering is proportional to the mass of the particle squared. If each unit of building block for the MINP$_1$(**8**) is assumed to contain one molecule of compound **1** (MW = 465 g/mol), 1.2 molecules of compound **2** (MW = 172 g/mol), one molecule of DVB (MW = 130 g/mol), and 0.8 molecules of compound **3** (MW = 264 g/mol), the molecular weight of MINP$_1$(**8**) translates to 51 [= 52900 / (465 + 1.2×172 + 130 + 0.8×264)] of such units.

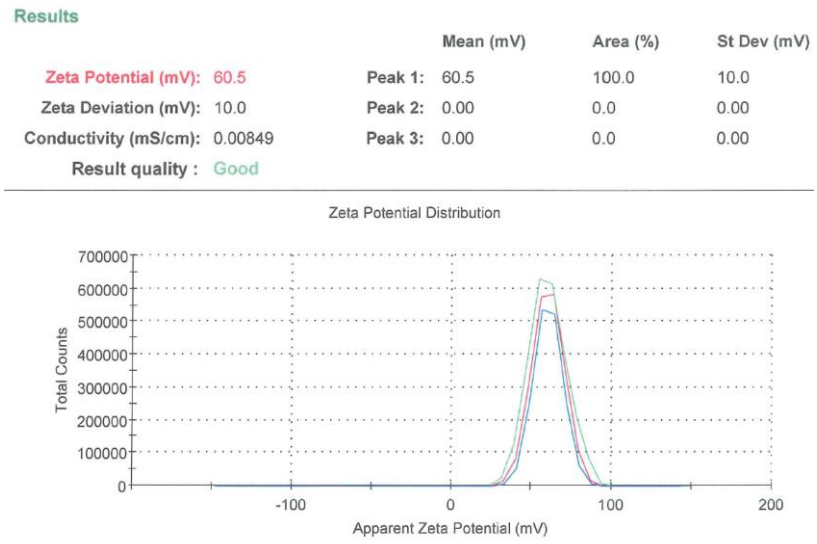

Figure S4. The zeta potential of typical MINP$_1$(**8**) after purification.

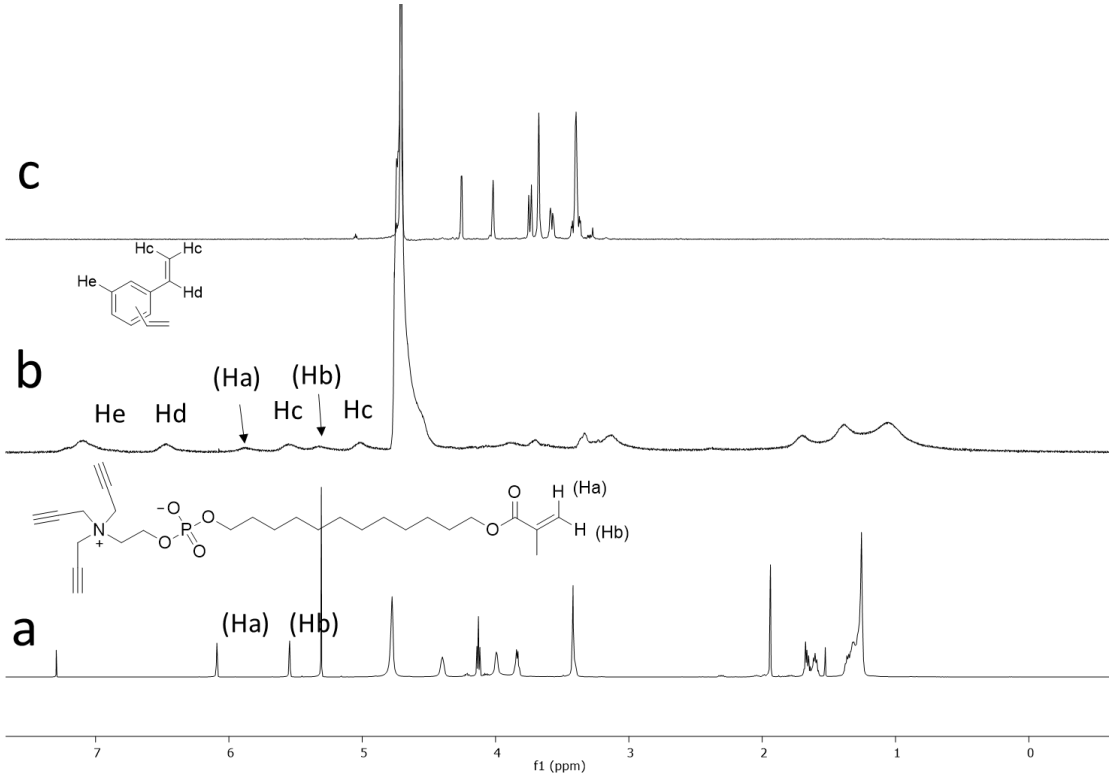

Figure S5. ^{1}H NMR spectra of (a) **4** in $CDCl_3$, (b) alkynyl-SCM in D_2O, and (c) MINP$_4$(**8**) in D_2O.

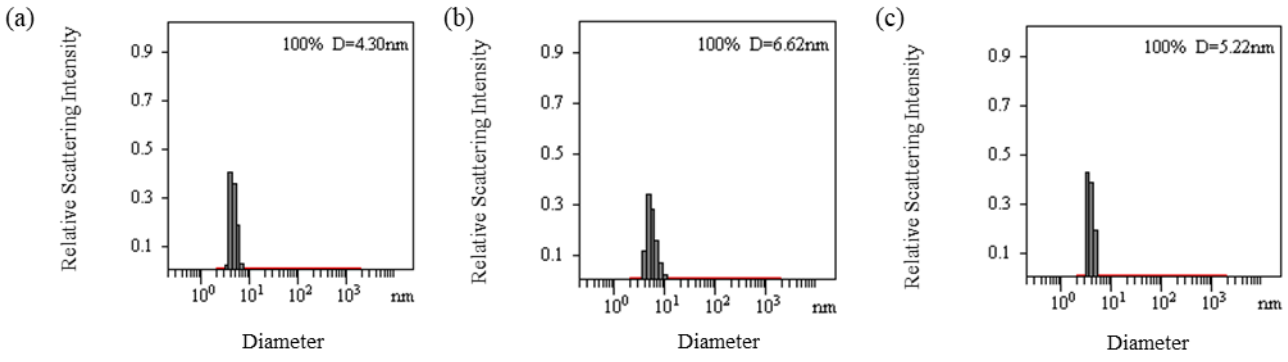

Figure S6. Distribution of the hydrodynamic diameters of the nanoparticles in water as determined by DLS for (a) alkynyl-SCM, (b) surface-functionalized SCM, and (c) MINP$_4$(**8**) after purification.

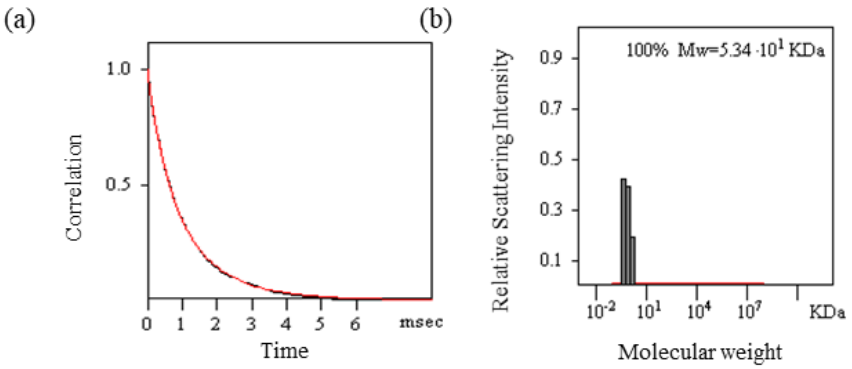

Figure S7. The correlation curve and the distribution of the molecular weight for MINP$_4$(**8**) from the DLS. The PRECISION DECONVOLVE program assumes the intensity of scattering is proportional to the mass of the particle squared. If each unit of building block for the MINP$_4$(**8**) is assumed to contain one molecule of compound **4** (MW = 508 g/mol), 1.2 molecules of compound **2** (MW = 172 g/mol), one molecule of DVB (MW = 130 g/mol), and 0.8 molecules of compound **3** (MW = 264 g/mol), the molecular weight of MINP$_4$(**8**) translates to 51 [= 53400 / (508 + 1.2×172 + 130 + 0.8×264)] of such units.

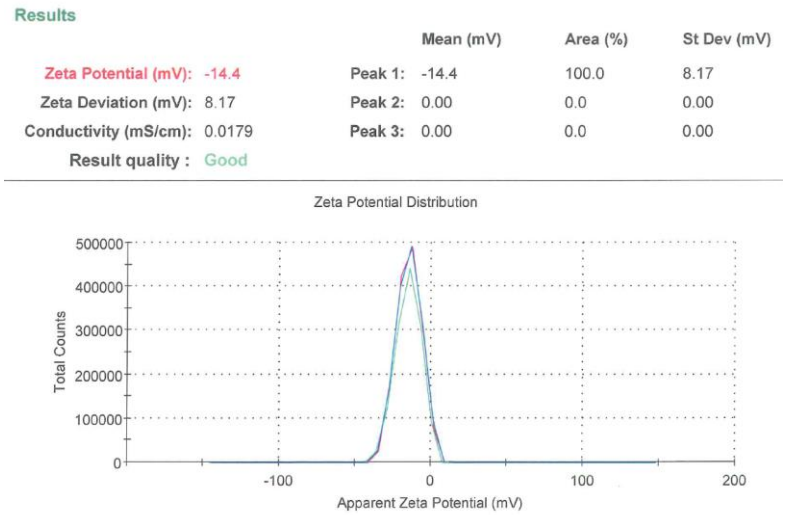

Figure S8. The zeta potential of typical MINP$_4$(**8**) after purification.

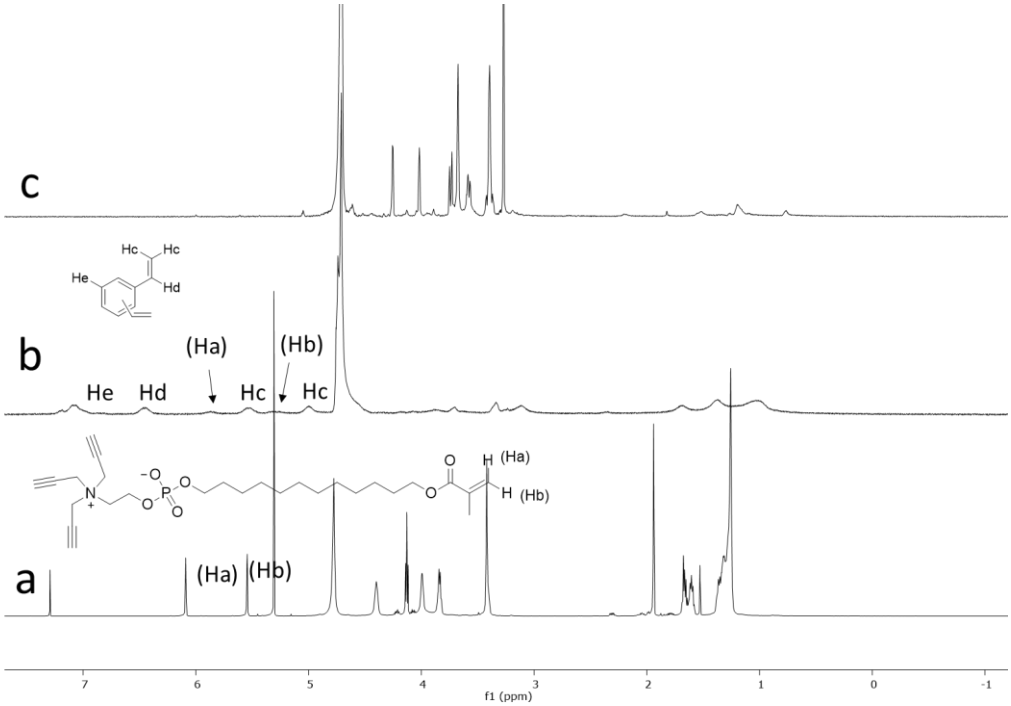

Figure S9. ^{1}H NMR spectra of (a) **4** in $CDCl_3$, (b) alkynyl-SCM in D_2O, and (c) MINP$_4$(**11**) in D_2O.

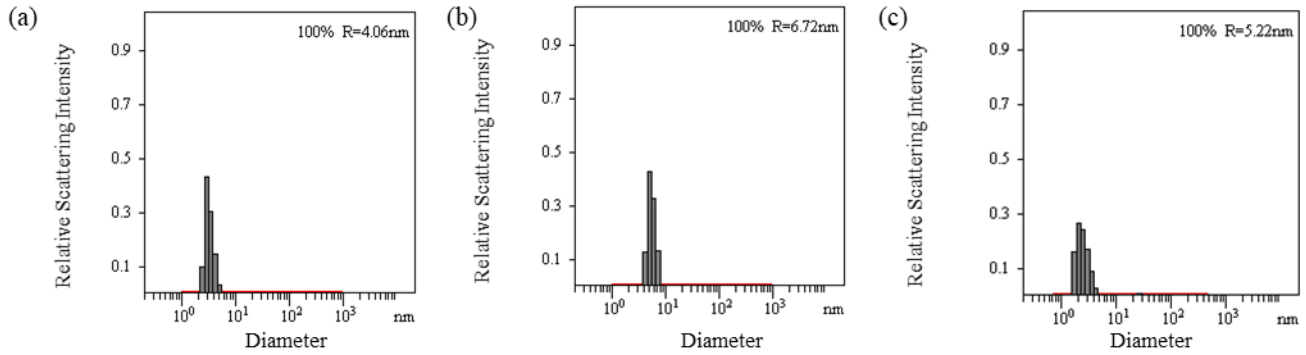

Figure S10. Distribution of the hydrodynamic diameters of the nanoparticles in water as determined by DLS for (a) alkynyl-SCM, (b) surface-functionalized SCM, and (c) MINP$_4$(**11**) after purification.

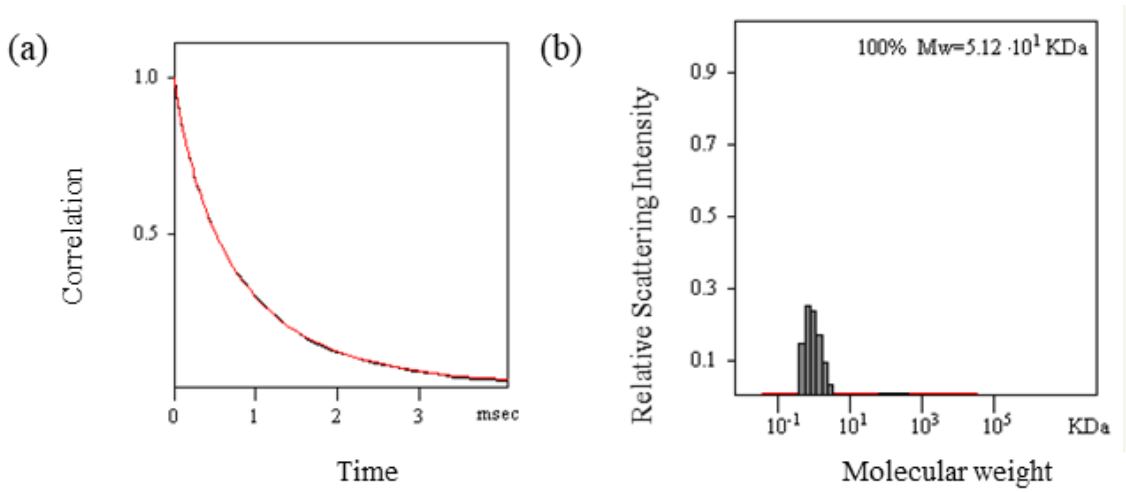

Figure S11. The correlation curve and the distribution of the molecular weight for MINP$_4$(**11**) from the DLS. The PRECISION DECONVOLVE program assumes the intensity of scattering is proportional to the mass of the particle squared. If each unit of building block for the MINP$_4$(**11**) is assumed to contain one molecule of compound **4** (MW = 508 g/mol), 1.2 molecules of compound **2** (MW = 172 g/mol), one molecule of DVB (MW = 130 g/mol), and 0.8 molecules of compound **3** (MW = 264 g/mol), the molecular weight of MINP$_4$(**11**) translates to 49 [= 51200 / (508 + 1.2×172 + 130 + 0.8×264)] of such units.

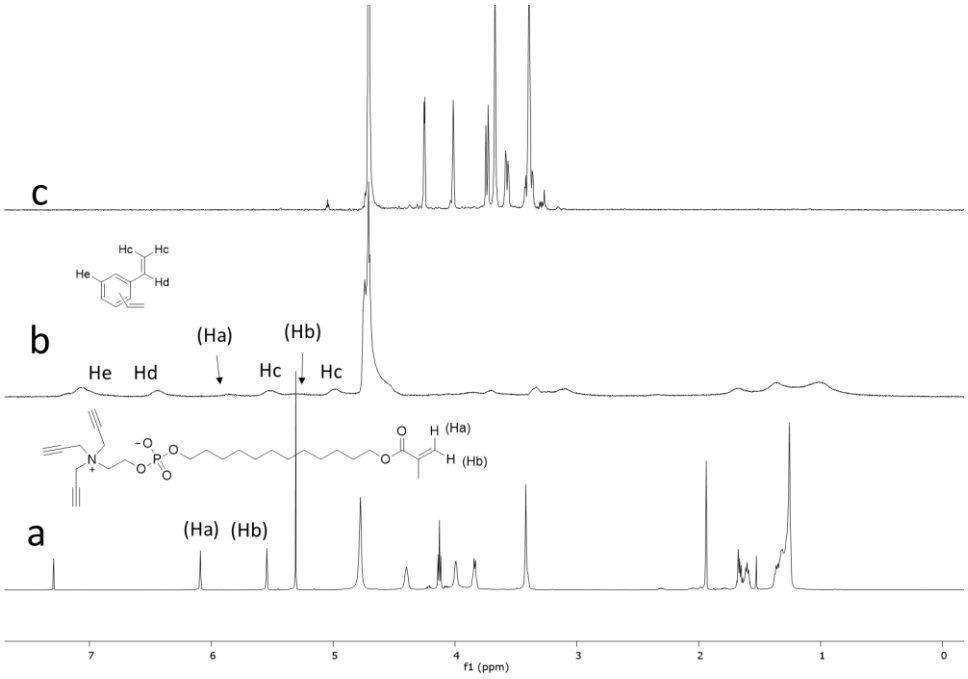

Figure S12. ^{1}H NMR spectra of (a) **4** in $CDCl_3$, (b) alkynyl-SCM in D_2O, and (c) MINP$_4$(**12**) in D_2O.

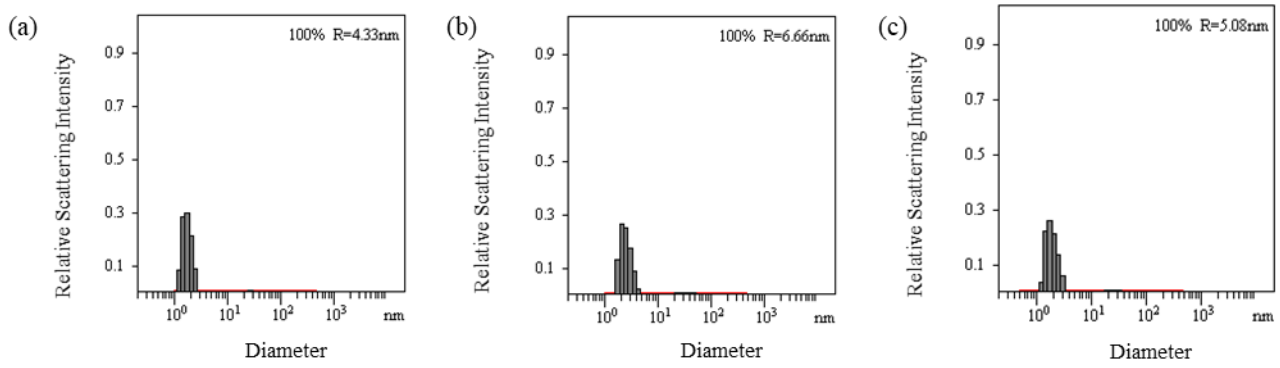

Figure S13. Distribution of the hydrodynamic diameters of the nanoparticles in water as determined by DLS for (a) alkynyl-SCM, (b) surface-functionalized SCM, and (c) MINP$_4$(**12**) after purification.

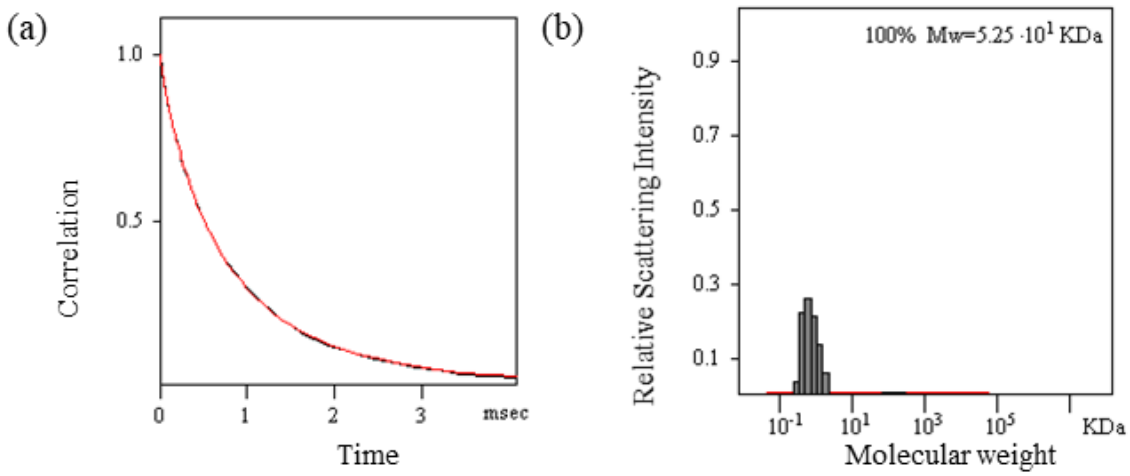

Figure S14. The correlation curve and the distribution of the molecular weight for MINP$_4$(**12**) from the DLS. The PRECISION DECONVOLVE program assumes the intensity of scattering is proportional to the mass of the particle squared. If each unit of building block for the MINP$_4$(**12**) is assumed to contain one molecule of compound 5 (MW = 508 g/mol), 1.2 molecules of compound **2** (MW = 172 g/mol), one molecule of DVB (MW = 130 g/mol), and 0.8 molecules of compound **3** (MW = 264 g/mol), the molecular weight of MINP$_4$(**12**) translates to 50 [= 52500 / (508 + 1.2×172 + 130 + 0.8×264)] of such units.

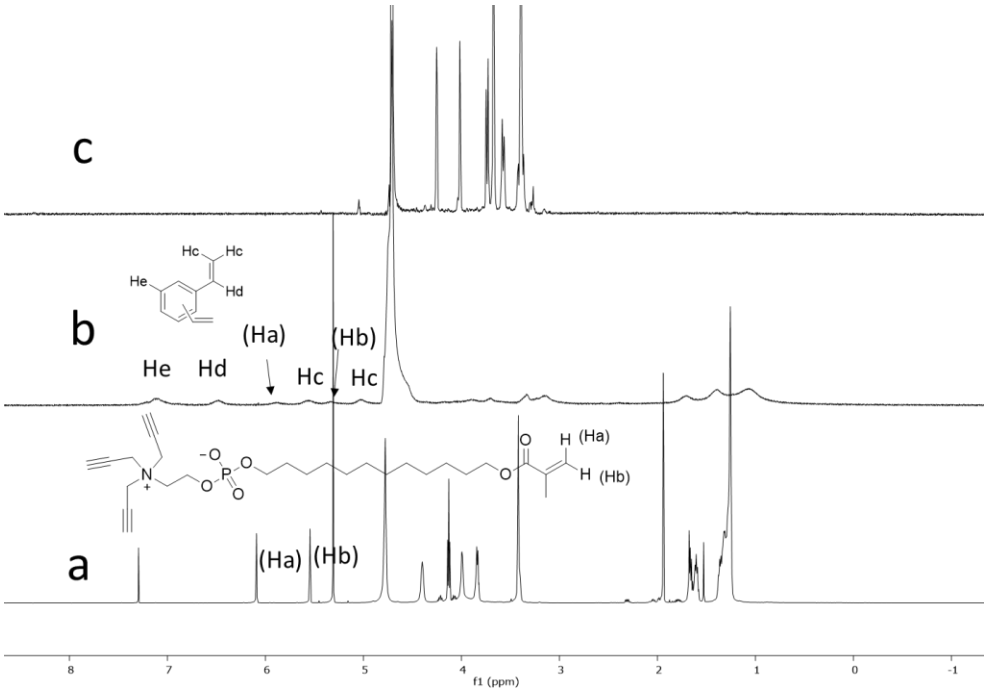

Figure S15. ^{1}H NMR spectra of (a) **4** in $CDCl_3$, (b) alkynyl-SCM in D_2O, and (c) MINP$_4$(**14**) in D_2O.

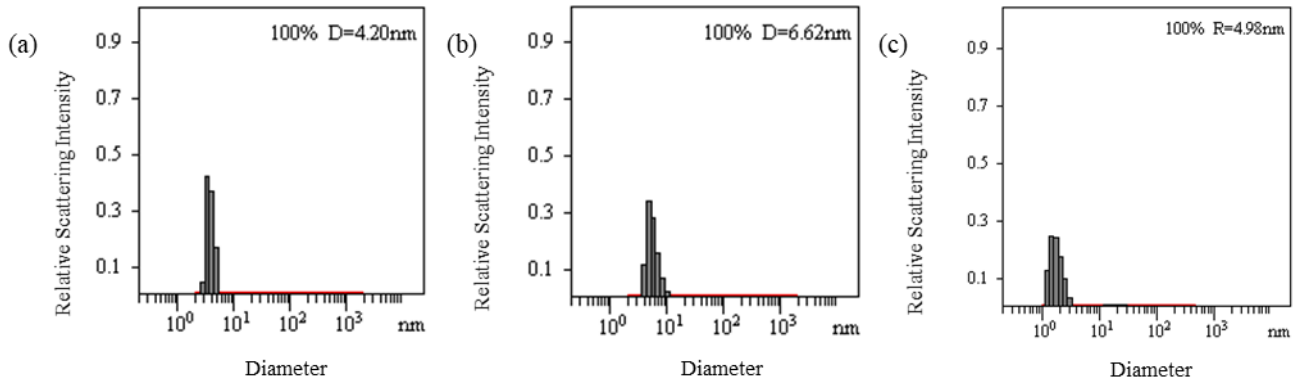

Figure S16. Distribution of the hydrodynamic diameters of the nanoparticles in water as determined by DLS for (a) alkynyl-SCM, (b) surface-functionalized SCM, and (c) MINP$_4$(**14**) after purification.

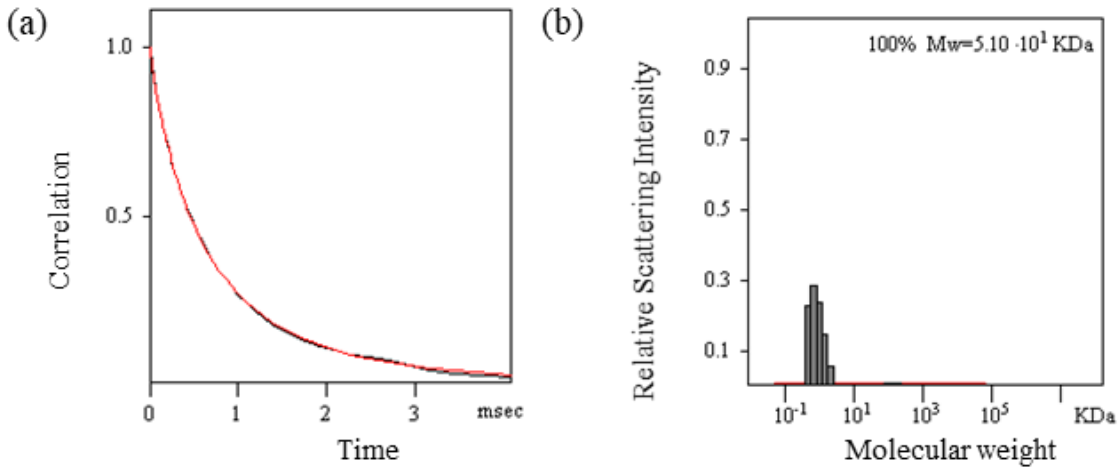

Figure S17. The correlation curve and the distribution of the molecular weight for MINP$_4$(**14**) from the DLS. The PRECISION DECONVOLVE program assumes the intensity of scattering is proportional to the mass of the particle squared. If each unit of building block for the MINP$_4$(**14**) is assumed to contain one molecule of compound 5 (MW = 508 g/mol), 1.2 molecules of compound **2** (MW = 172 g/mol), one molecule of DVB (MW = 130 g/mol), and 0.8 molecules of compound **3** (MW = 264 g/mol), the molecular weight of MINP$_4$(**14**) translates to 49 [= 51000 / (508 + 1.2×172 + 130 + 0.8×264)] of such units.

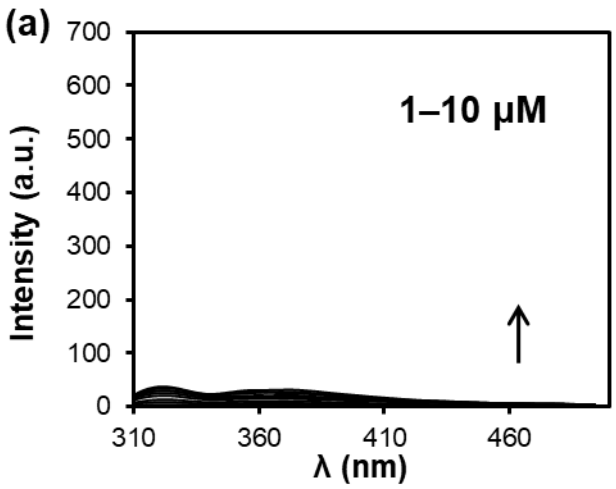

Figure S18. (a) Fluorescence emission spectrum of MINP$_4$(**8**) at different concentrations in 50 mM Tris buffer (pH 7.4).

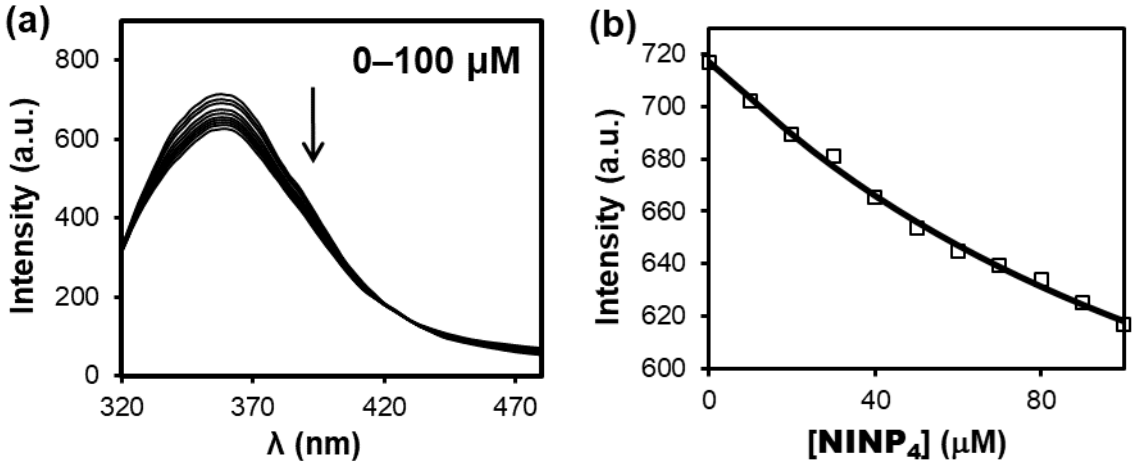

Figure S19. (a) Fluorescence emission spectra of guest **8** (λ_{ex} = 300 nm) upon addition of different concentrations of NINP$_4$ in 50 mM Tris buffer (pH 7.4). [**8**] = 2.0 μM. (b) Nonlinear least squares fitting of the emission intensity of **8** at 363 nm to a 1:1 binding isotherm; corresponding to entry 10 in Table 1.

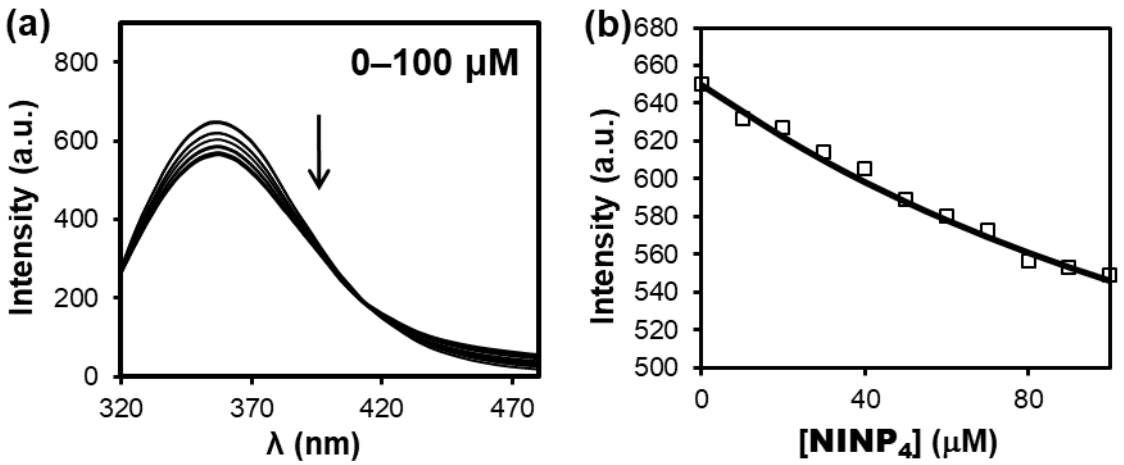

Figure S20. (a) Fluorescence emission spectra of guest **9** (λ_{ex} = 300 nm) upon addition of different concentrations of $NINP_4$ in 50 mM Tris buffer (pH 7.4). [**9**] = 2.0 μM. (b) Nonlinear least squares fitting of the emission intensity of **9** at 363 nm to a 1:1 binding isotherm; corresponding to entry 10 in Table 1.

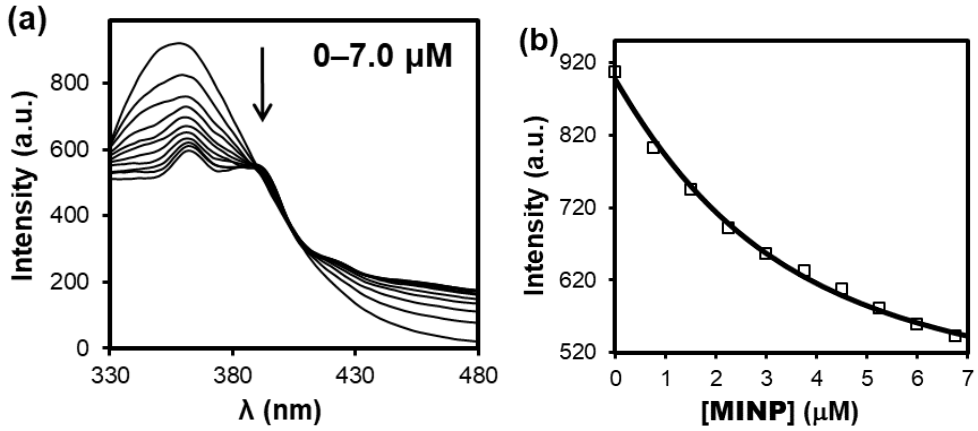

Figure S21. (a) Fluorescence emission spectra of guest **9** (λ_{ex} = 300 nm) upon addition of different concentrations of $MINP_4$(**8**) in 50 mM Tris buffer (pH 7.4). [**9**] = 2.0 μM. (b) Nonlinear least squares fitting of the emission intensity of **9** at 363 nm to a 1:1 binding isotherm; corresponding to entry 2 in Table 1.

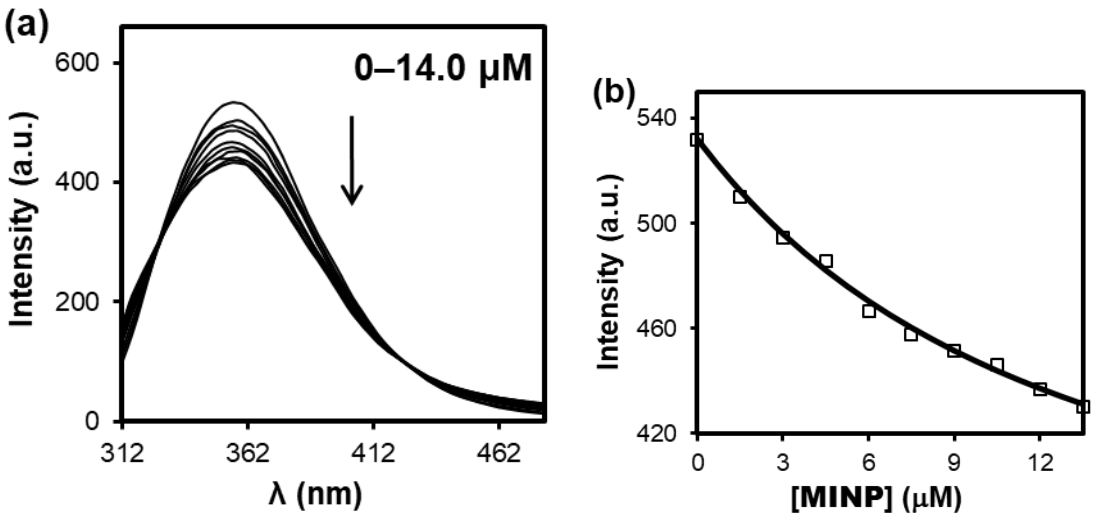

Figure S22. (a) Fluorescence emission spectra of guest **9** (λ_{ex} = 300 nm) upon addition of different concentrations of MINP$_1$(**8**) in 50 mM Tris buffer (pH 7.4). [**9**] = 2.0 μM. (b) Nonlinear least squares fitting of the emission intensity of **9** at 363 nm to a 1:1 binding isotherm; corresponding to entry 2 in Table 1.

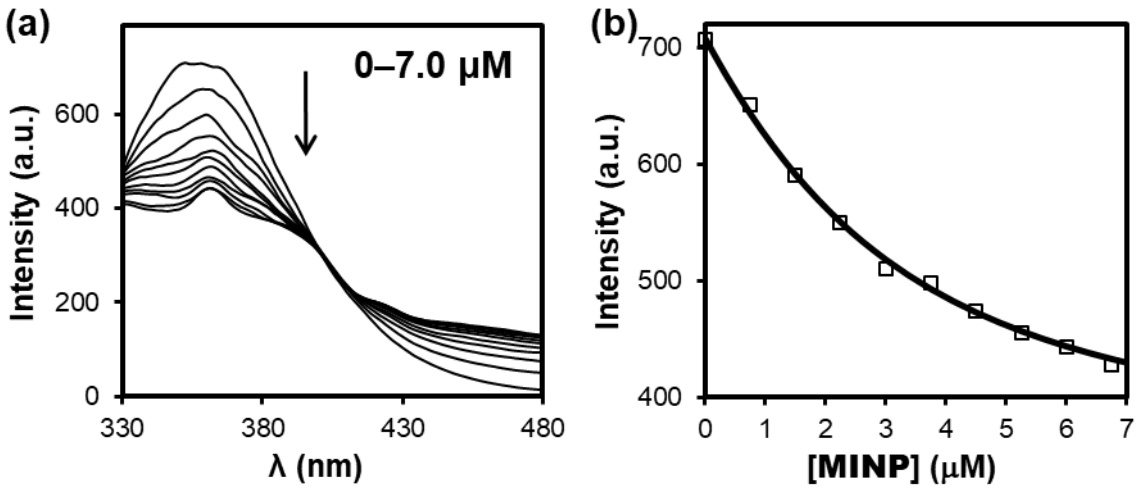

Figure S23. (a) Fluorescence emission spectra of guest **10** (λ_{ex} = 300 nm) upon addition of different concentrations of MINP$_4$(**8**) in 50 mM Tris buffer (pH 7.4). [**10**] = 2.0 μM. (b) Nonlinear least squares fitting of the emission intensity of **10** at 363 nm to a 1:1 binding isotherm; corresponding to entry 3 in Table 1.

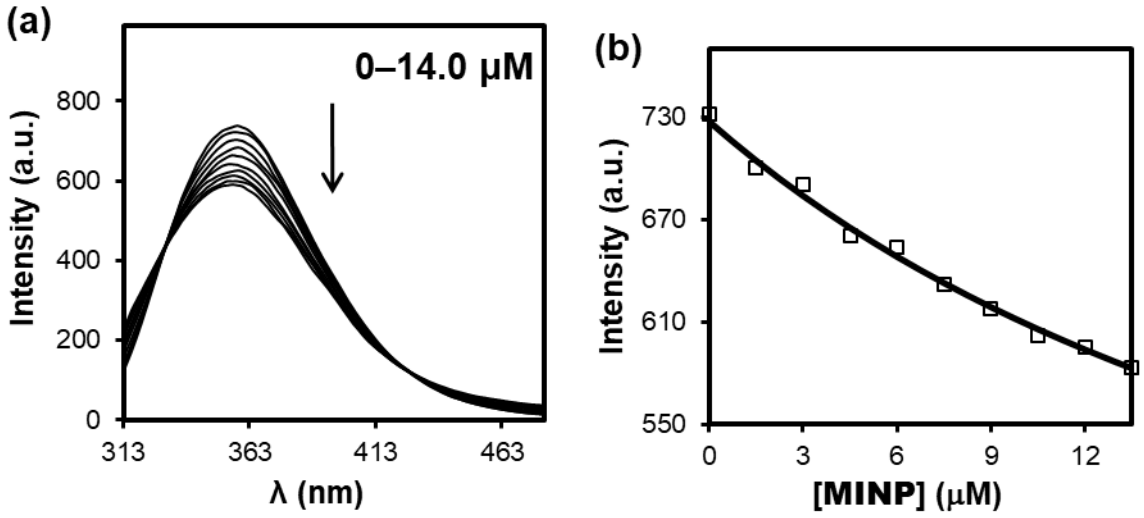

Figure S24. (a) Fluorescence emission spectra of guest **10** (λ_{ex} = 300 nm) upon addition of different concentrations of MINP$_1$(**8**) in 50 mM Tris buffer (pH 7.4). [**10**] = 2.0 μM. (b) Nonlinear least squares fitting of the emission intensity of **10** at 363 nm to a 1:1 binding isotherm; corresponding to entry 3 in Table 1.

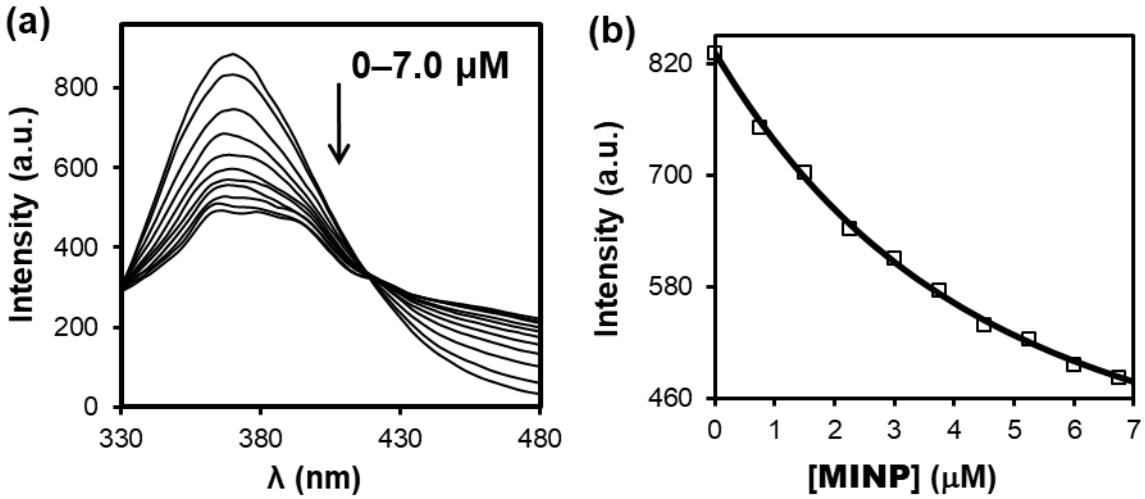

Figure S25. (a) Fluorescence emission spectra of guest **8** (λ_{ex} = 300 nm) upon addition of different concentrations of MINP$_4$(**9**) in 50 mM Tris buffer (pH 7.4). [**8**] = 2.0 μM. (b) Nonlinear least squares fitting of the emission intensity of **8** at 363 nm to a 1:1 binding isotherm; corresponding to entry 4 in Table 1.

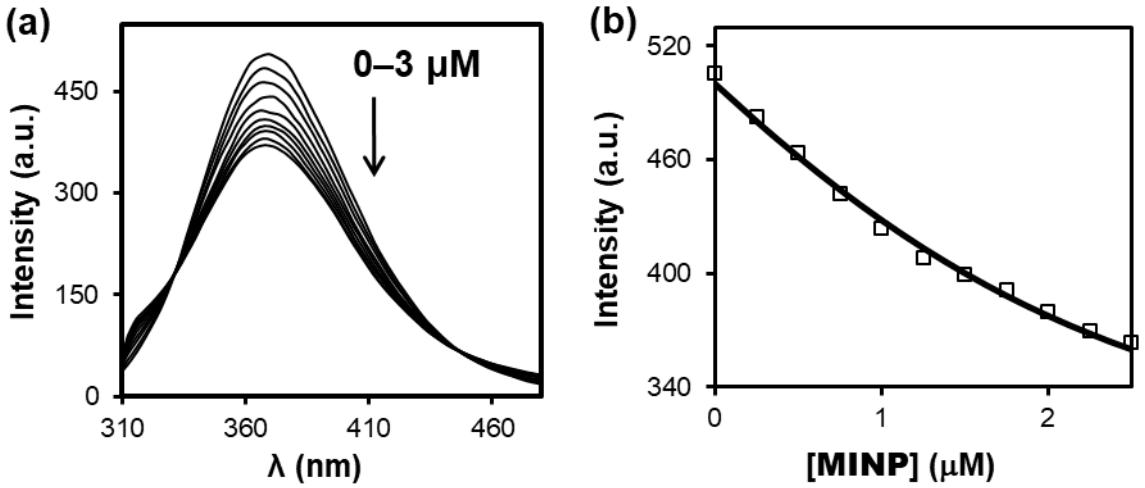

Figure S26. (a) Fluorescence emission spectra of guest **8** (λ_{ex} = 300 nm) upon addition of different concentrations of MINP$_1$(**9**) in 50 mM Tris buffer (pH 7.4). [**8**] = 2.0 μM. (b)

Nonlinear least squares fitting of the emission intensity of **8** at 363 nm to a 1:1 binding isotherm; corresponding to entry 4 in Table 1.

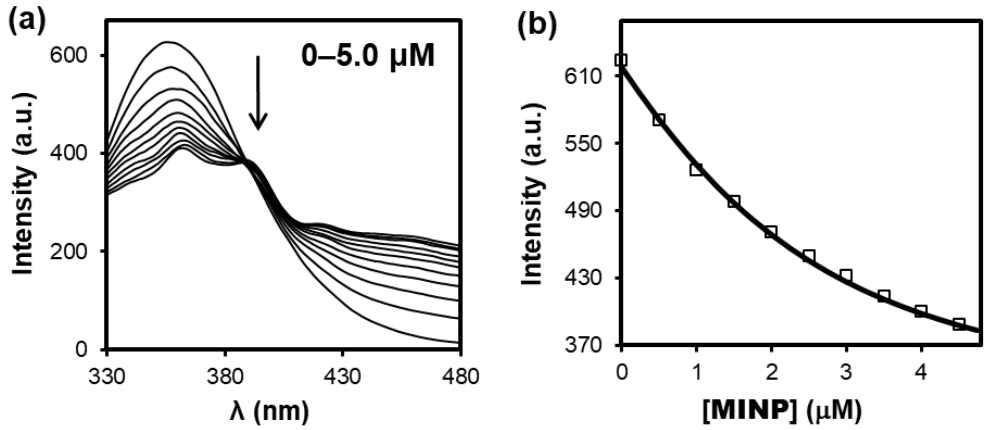

Figure S27. Fluorescence Titration of 9 by MINP$_4$(9) (a) Fluorescence emission spectra of guest **9** (λ_{ex} = 300 nm) upon addition of different concentrations of MINP$_4$(**9**) in 50 mM Tris buffer (pH 7.4). [**9**] = 2.0 μM. (b) Nonlinear least squares fitting of the emission intensity of **9** at 363 nm to a 1:1 binding isotherm; corresponding to entry 5 in Table 1.

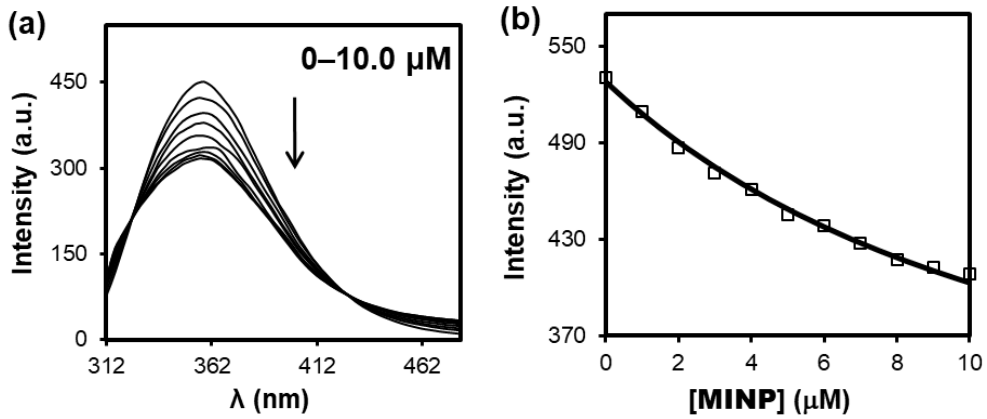

Figure S28. Fluorescence Titration of 9 by MINP$_1$(9) (a) Fluorescence emission spectra of guest **9** (λ_{ex} = 300 nm) upon addition of different concentrations of MINP$_1$(**9**) in 50 mM Tris buffer (pH 7.4). [**9**] = 2.0 μM. (b) Nonlinear least squares fitting of the emission intensity of **9** at 363 nm to a 1:1 binding isotherm; corresponding to entry 5 in Table 1.

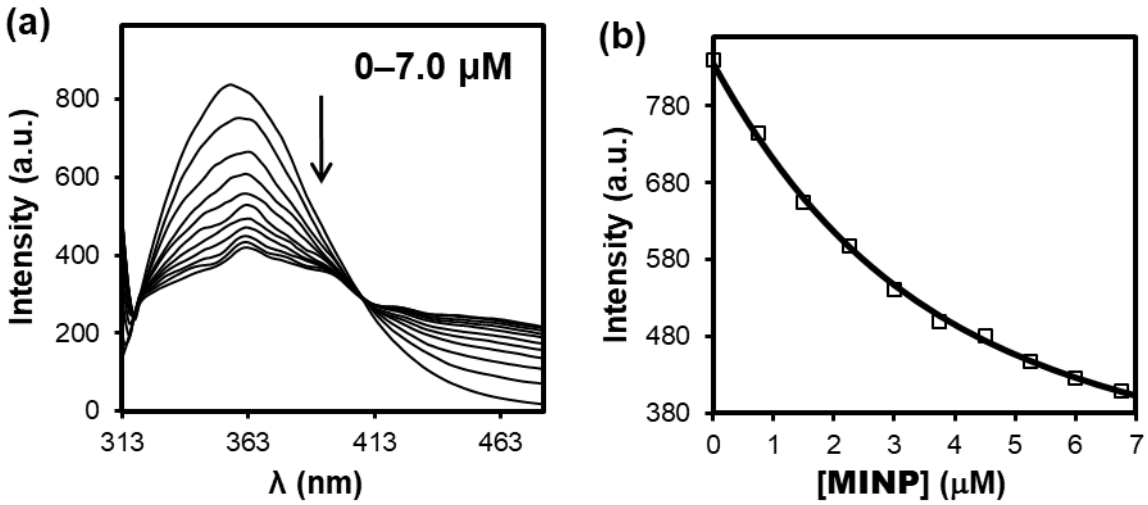

Figure S29. (a) Fluorescence emission spectra of guest **10** (λ_{ex} = 300 nm) upon addition of different concentrations of MINP$_4$(**9**) in 50 mM Tris buffer (pH 7.4). [**10**] = 2.0 μM. (b) Nonlinear least squares fitting of the emission intensity of **10** at 363 nm to a 1:1 binding isotherm; corresponding to entry 6 in Table 1.

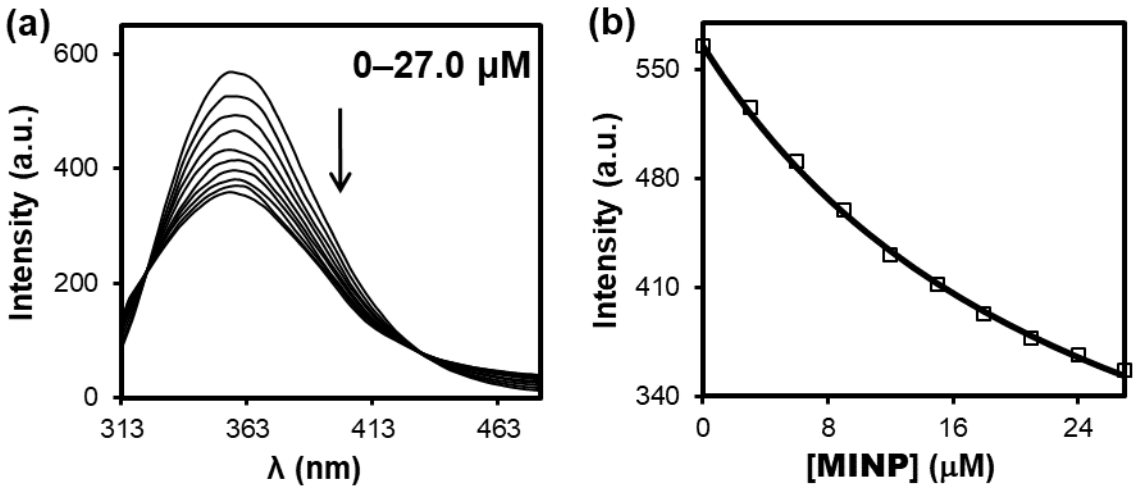

Figure S30. (a) Fluorescence emission spectra of guest **10** (λ_{ex} = 300 nm) upon addition of different concentrations of MINP$_1$(**9**) in 50 mM Tris buffer (pH 7.4). [**10**] = 2.0 μM. (b) Nonlinear least squares fitting of the emission intensity of **10** at 363 nm to a 1:1 binding isotherm; corresponding to entry 6 in Table 1.

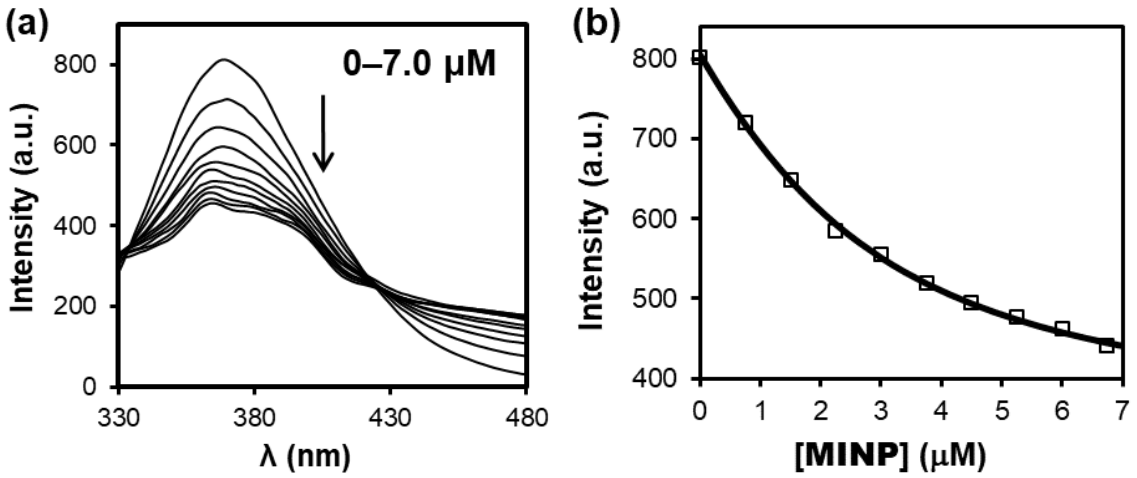

Figure S31. (a) Fluorescence emission spectra of guest **8** (λ_{ex} = 300 nm) upon addition of different concentrations of MINP$_4$(**10**) in 50 mM Tris buffer (pH 7.4). [**8**] = 2.0 μM. (b) Nonlinear least squares fitting of the emission intensity of **8** at 363 nm to a 1:1 binding isotherm; corresponding to entry 7 in Table 1.

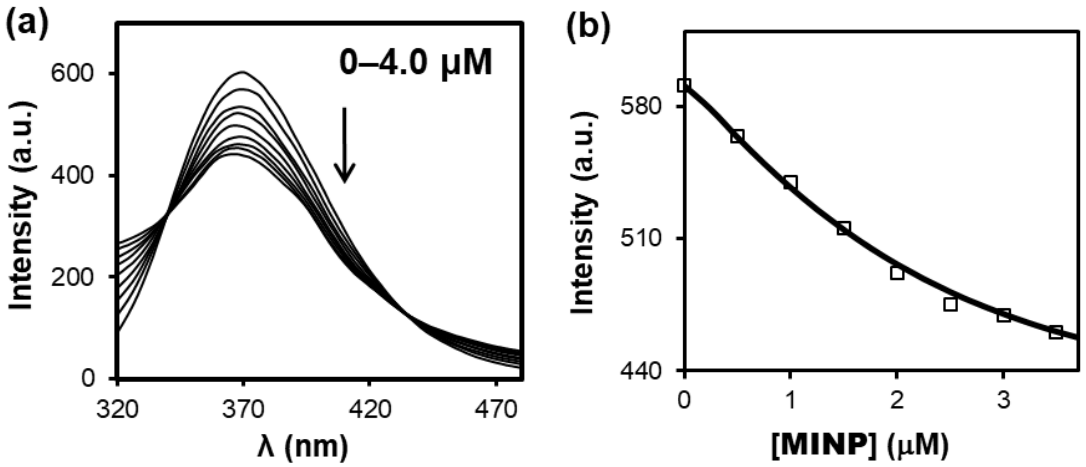

Figure S32. (a) Fluorescence emission spectra of guest **8** (λ_{ex} = 300 nm) upon addition of different concentrations of MINP$_1$(**10**) in 50 mM Tris buffer (pH 7.4). [**8**] = 2.0 μM. (b) Nonlinear least squares fitting of the emission intensity of **8** at 363 nm to a 1:1 binding isotherm; corresponding to entry 7 in Table 1.

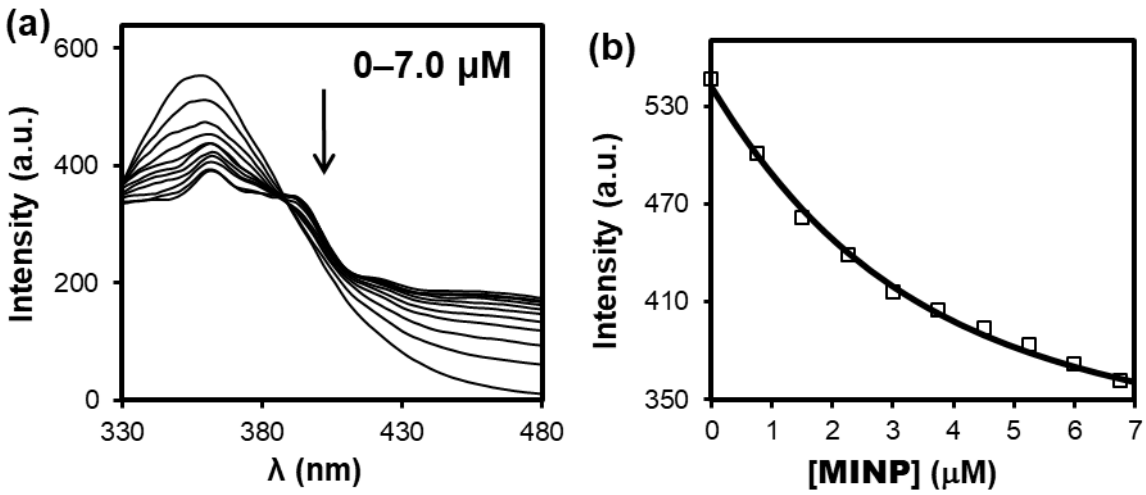

Figure S33. (a) Fluorescence emission spectra of guest **9** (λ_{ex} = 300 nm) upon addition of different concentrations of MINP$_4$(**10**) in 50 mM Tris buffer (pH 7.4). [**9**] = 2.0 μM. (b) Nonlinear least squares fitting of the emission intensity of **9** at 363 nm to a 1:1 binding isotherm; corresponding to entry 8 in Table 1.

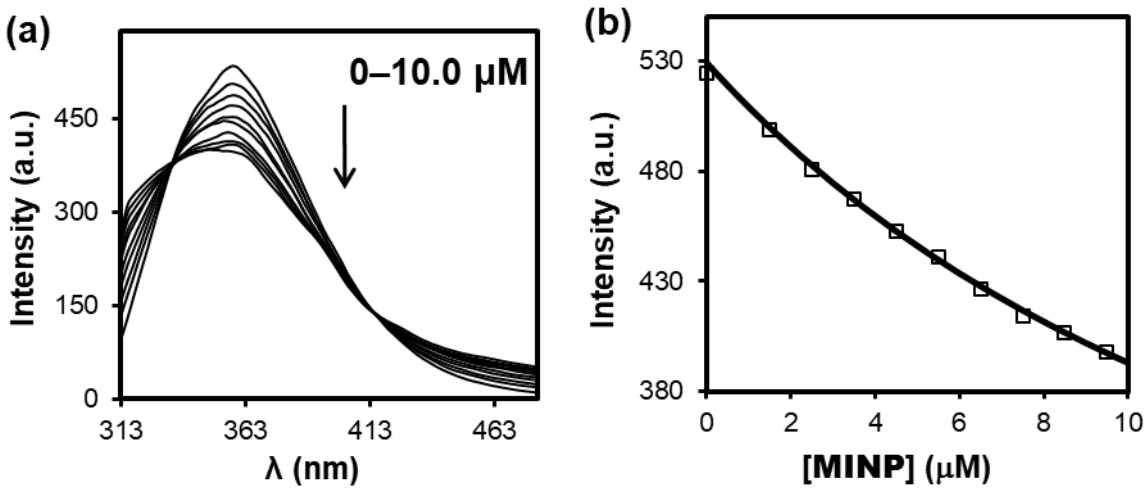

Figure S34. (a) Fluorescence emission spectra of guest **9** (λ_{ex} = 300 nm) upon addition of different concentrations of MINP$_1$(**10**) in 50 mM Tris buffer (pH 7.4). [**9**] = 2.0 μM. (b) Nonlinear least squares fitting of the emission intensity of **9** at 363 nm to a 1:1 binding isotherm; corresponding to entry 8 in Table 1.

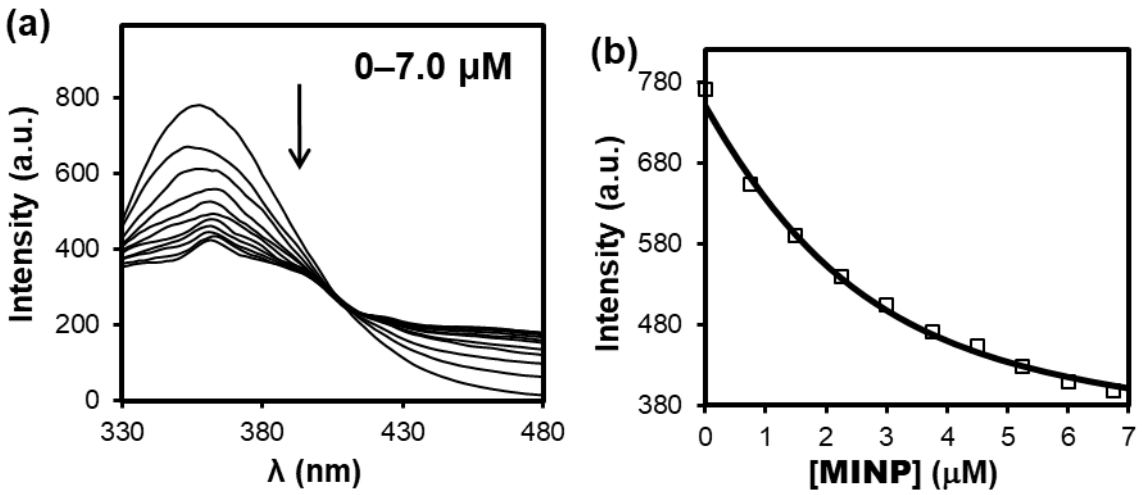

Figure S35. (a) Fluorescence emission spectra of guest **10** (λ_{ex} = 300 nm) upon addition of different concentrations of MINP$_4$(**10**) in 50 mM Tris buffer (pH 7.4). [**10**] = 2.0 μM. (b) Nonlinear least squares fitting of the emission intensity of **10** at 363 nm to a 1:1 binding isotherm; corresponding to entry 9 in Table 1.

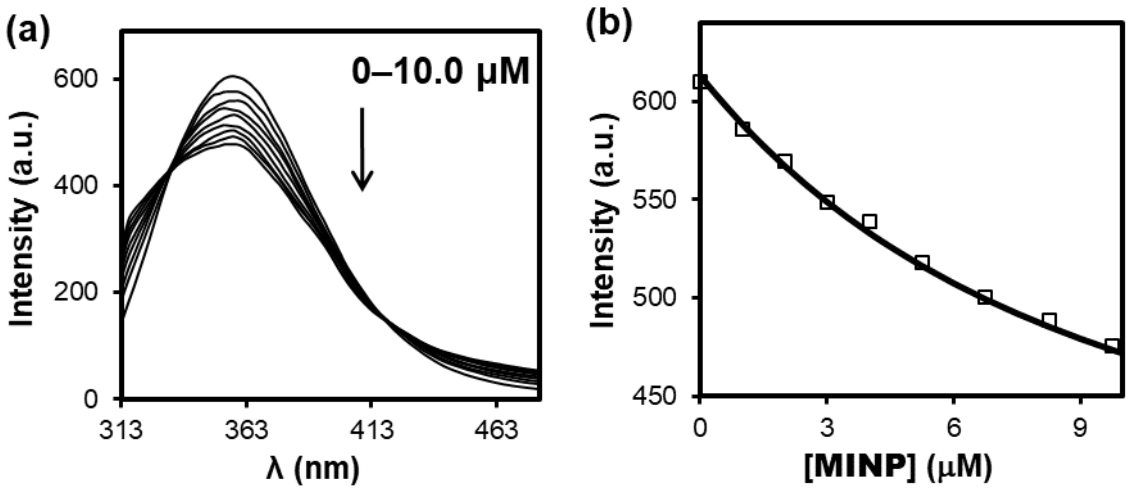

Figure S36. (a) Fluorescence emission spectra of guest **10** (λ_{ex} = 300 nm) upon addition of different concentrations of MINP$_1$(**10**) in 50 mM Tris buffer (pH 7.4). [**10**] = 2.0 μM. (b) Nonlinear least squares fitting of the emission intensity of **10** at 363 nm to a 1:1 binding isotherm; corresponding to entry 9 in Table 1.

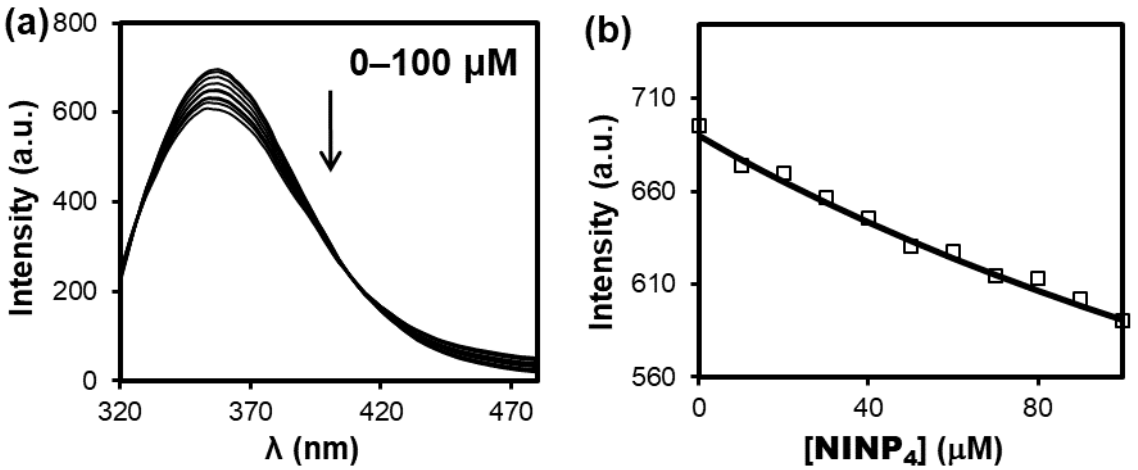

Figure S37. (a) Fluorescence emission spectra of guest **10** (λ_{ex} = 300 nm) upon addition of different concentrations of $NINP_4$ in 50 mM Tris buffer (pH 7.4). [**10**] = 2.0 μM. (b) Nonlinear least squares fitting of the emission intensity of **10** at 363 nm to a 1:1 binding isotherm; corresponding to entry 11 in Table 1.

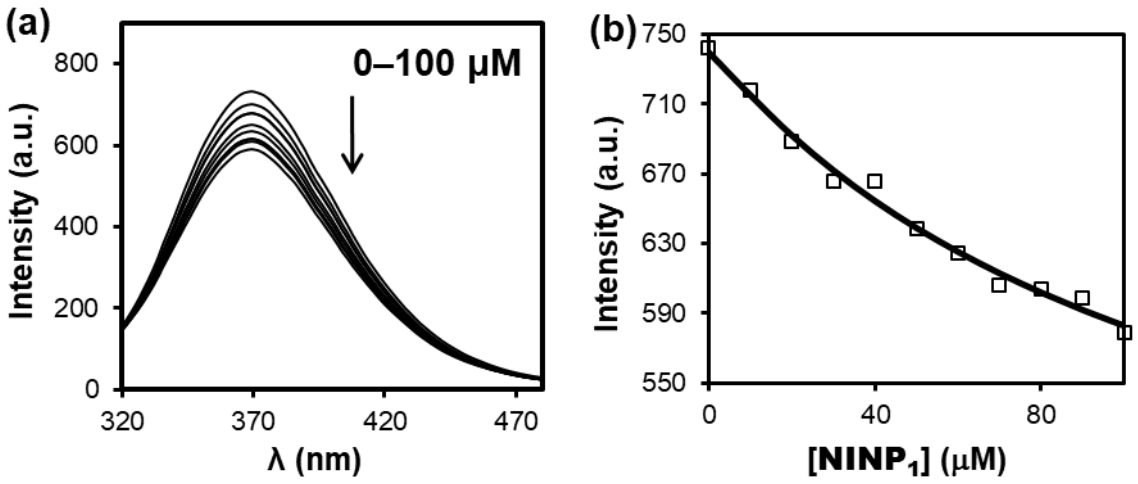

Figure S38. (a) Fluorescence emission spectra of guest **8** (λ_{ex} = 300 nm) upon addition of different concentrations of $NINP_1$ in 50 mM Tris buffer (pH 7.4). [**8**] = 2.0 μM. (b) Nonlinear least squares fitting of the emission intensity of **8** at 363 nm to a 1:1 binding isotherm; corresponding to entry 11 in Table 1.

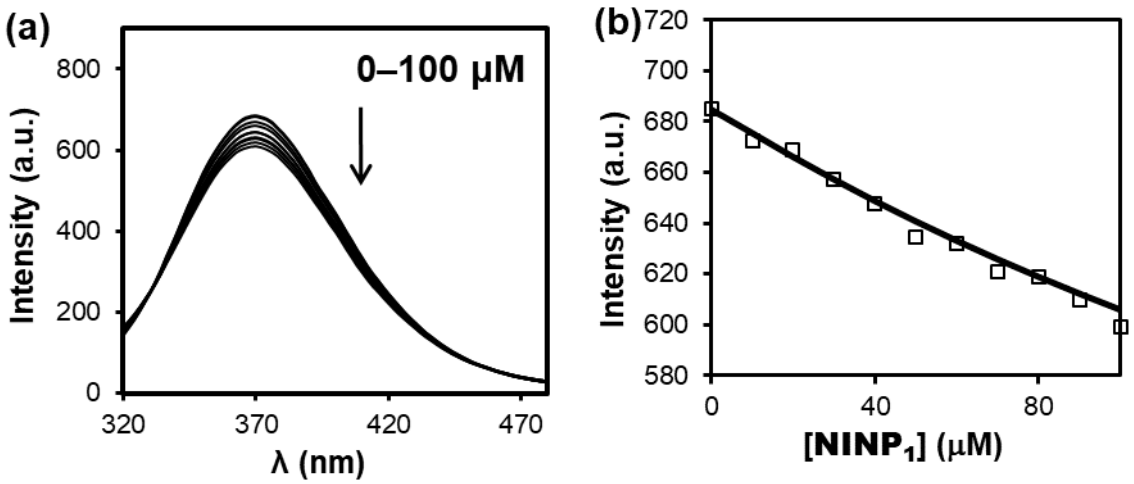

Figure S39. (a) Fluorescence emission spectra of guest **9** (λ_{ex} = 300 nm) upon addition of different concentrations of NINP$_1$ in 50 mM Tris buffer (pH 7.4). [**9**] = 2.0 μM. (b) Nonlinear least squares fitting of the emission intensity of **9** at 363 nm to a 1:1 binding isotherm; corresponding to entry 12 in Table 1.

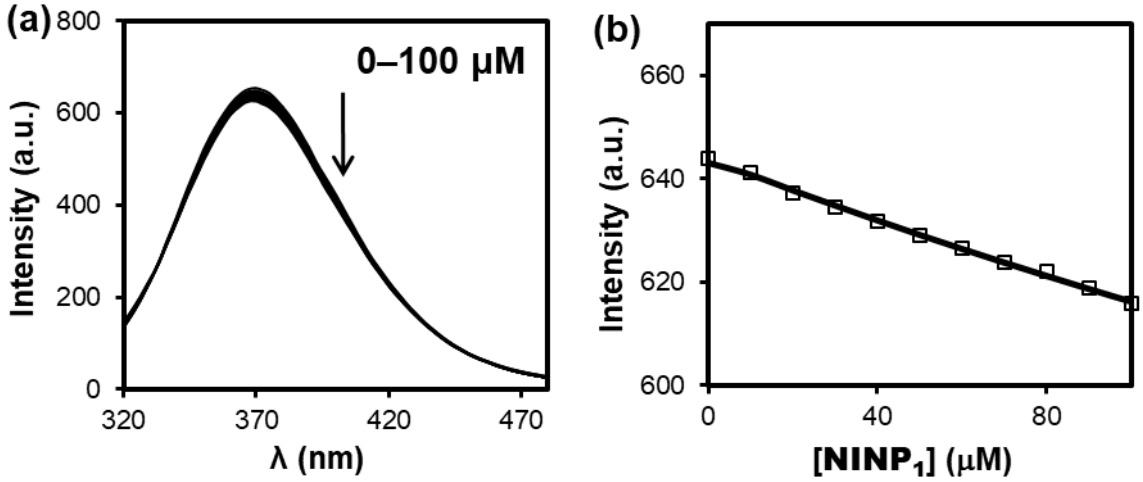

Figure S40. (a) Fluorescence emission spectra of guest **10** (λ_{ex} = 300 nm) upon addition of different concentrations of NINP$_1$ in 50 mM Tris buffer (pH 7.4). [**10**] = 2.0 μM. (b) Nonlinear least squares fitting of the emission intensity of **10** at 363 nm to a 1:1 binding isotherm; corresponding to entry 12 in Table 1.

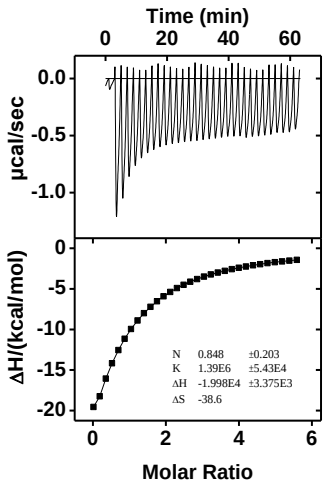

Figure S41. ITC titration curves obtained at 298 K for the titration of MINP$_1$(**8**) with guest **8** in 50 mM Tris buffer (pH 7.4). The data correspond to entry 9 in Table 1. The top panel shows the raw calorimetric data. The area under each peak represents the amount of heat generated at each ejection and is plotted against the molar ratio of MINP to the substrate. The solid line is the best fit of the experimental data to the sequential binding of N equal and independent binding sites on the MINP. The heat of dilution for the substrate, obtained by adding the substrate to the buffer, was subtracted from the heat released during the binding. Binding parameters were auto-generated after curve fitting using Microcal Origin 7.

(a) (b) (c)

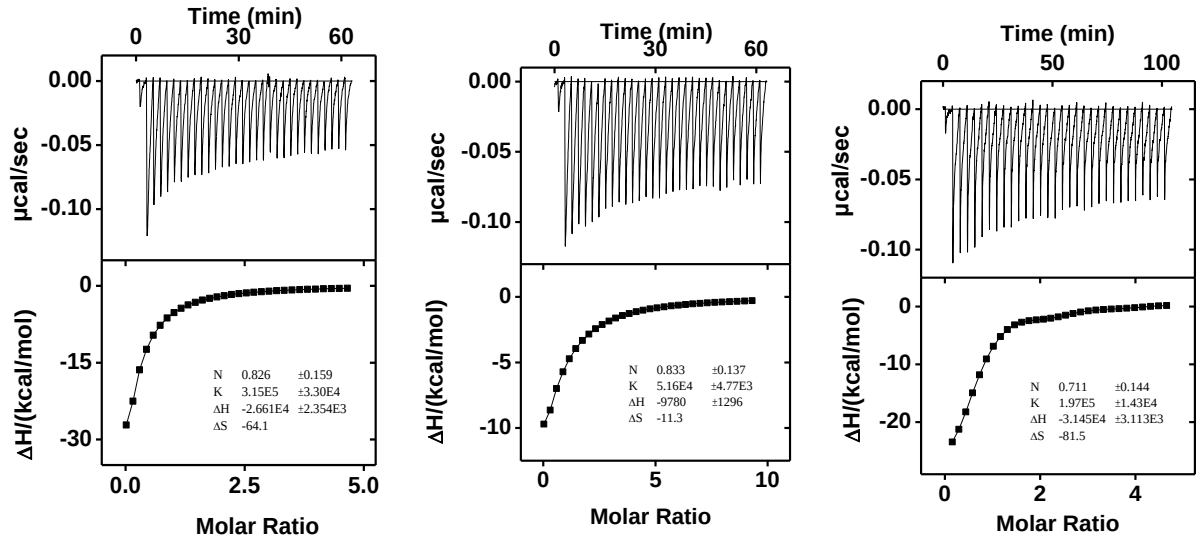

Figure S42. ITC titration curves obtained at 298 K for the titration of MINP$_4$(**11**) with alkaloid guest **11** (a), MINP$_4$(**11**) with guest **12** (b), and MINP$_4$(**11**) with guest **13** (c) in 50 mM Tris buffer (pH 7.4). The data correspond to entries 1-3, respectively, in Table 2. The top panel shows the raw calorimetric data. The area under each peak represents the amount of heat generated at each ejection and is plotted against the molar ratio of MINP to the substrate. The solid line is the best fit of the experimental data to the sequential binding of N equal and independent binding sites on the MINP. The heat of dilution for the substrate, obtained by adding the substrate to the buffer, was subtracted from the heat released during the binding. Binding parameters were auto-generated after curve fitting using Microcal Origin 7.

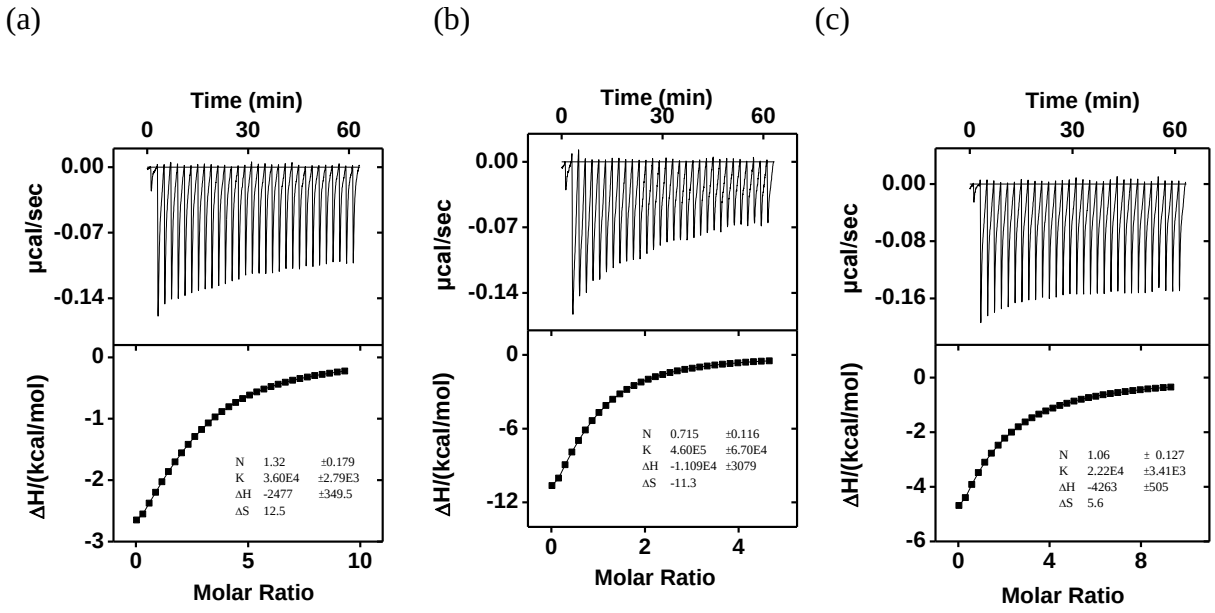

Figure S43. ITC titration curves obtained at 298 K for the titration of MINP$_4$(**12**) with alkaloid guest **11** (a), MINP$_4$(**12**) with guest **12** (b), and MINP$_4$(**12**) with guest **13** (c) in 50 mM Tris buffer (pH 7.4). The data correspond to entries 4-6, respectively, in Table 2. The top panel shows the raw calorimetric data. The area under each peak represents the amount of heat generated at each ejection and is plotted against the molar ratio of MINP to the substrate. The solid line is the best fit of the experimental data to the sequential binding of N equal and independent binding sites on the MINP. The heat of dilution for the substrate, obtained by adding the substrate to the buffer, was subtracted from the heat released during the binding. Binding parameters were auto-generated after curve fitting using Microcal Origin 7.

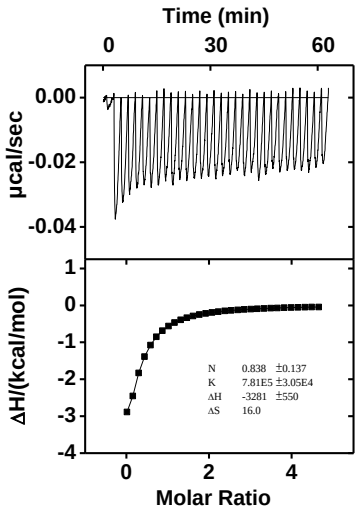

Figure S44. ITC titration curves obtained at 298 K for the titration of MINP$_4$(**14**) with alkaloid guest **14** in 50 mM Tris buffer (pH 7.4). The data correspond to entries 7 in Table 2. The top panel shows the raw calorimetric data. The area under each peak represents the amount of heat generated at each ejection and is plotted against the molar ratio of MINP to the substrate. The solid line is the best fit of the experimental data to the sequential binding of N equal and independent binding sites on the MINP. The heat of dilution for the substrate, obtained by adding the substrate to the buffer, was subtracted from the heat released during the binding. Binding parameters were auto-generated after curve fitting using Microcal Origin 7.

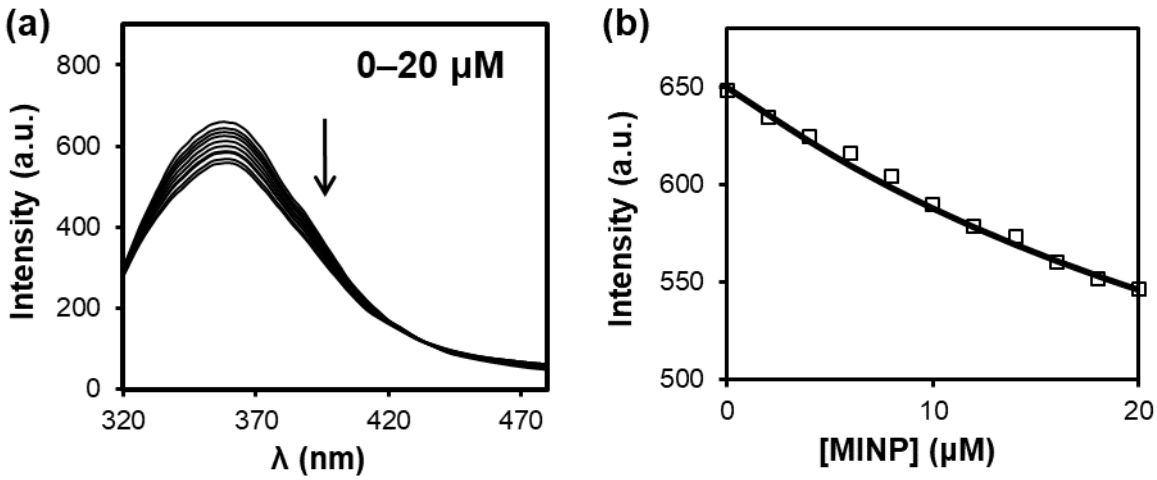

Figure S45. (a) Fluorescence emission spectra of guest **8** (λ_{ex} = 300 nm) upon addition of different concentrations of MINP$_4$(**11**) in 50 mM Tris buffer (pH 7.4). [**8**] = 2.0 μM. (b) Nonlinear least squares fitting of the emission intensity of **8** at 363 nm to a 1:1 binding isotherm; corresponding to entry 1 in Table 2S.

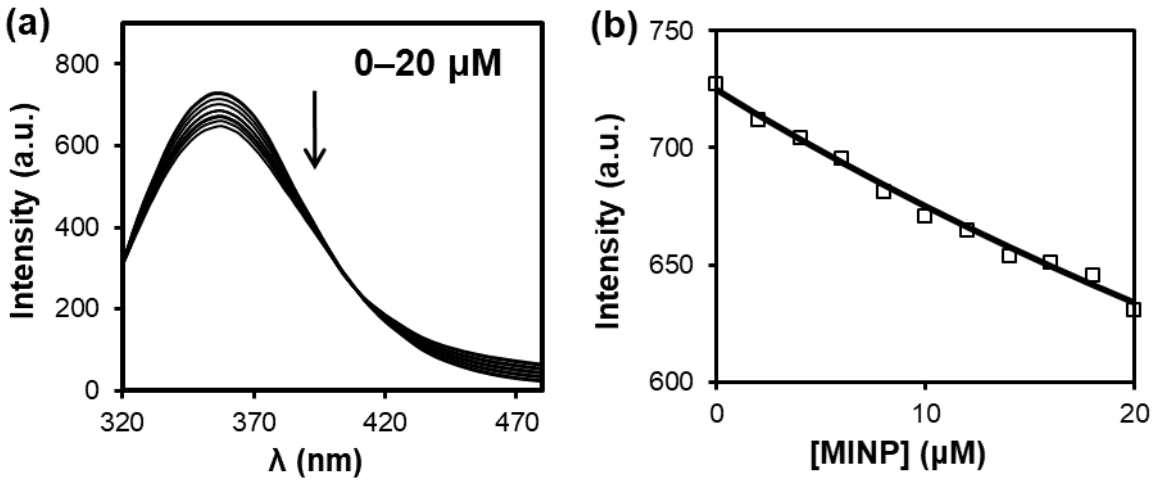

Figure S46. (a) Fluorescence emission spectra of guest **9** (λ_{ex} = 300 nm) upon addition of different concentrations of MINP$_4$(**11**) in 50 mM Tris buffer (pH 7.4). [**9**] = 2.0 μM. (b) Nonlinear least squares fitting of the emission intensity of **9** at 363 nm to a 1:1 binding isotherm; corresponding to entry 2 in Table 2S.

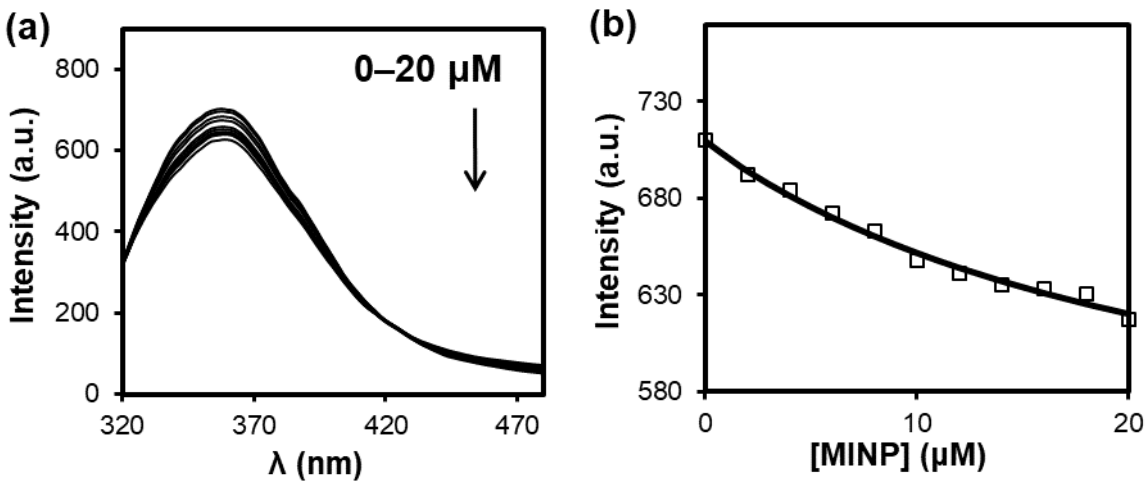

Figure S47. (a) Fluorescence emission spectra of guest **10** (λ_{ex} = 300 nm) upon addition of different concentrations of MINP$_4$(**11**) in 50 mM Tris buffer (pH 7.4). [**10**] = 2.0 μM. (b) Nonlinear least squares fitting of the emission intensity of **10** at 363 nm to a 1:1 binding isotherm; corresponding to entry 3 in Table 2S.

^{1}H NMR spectrum

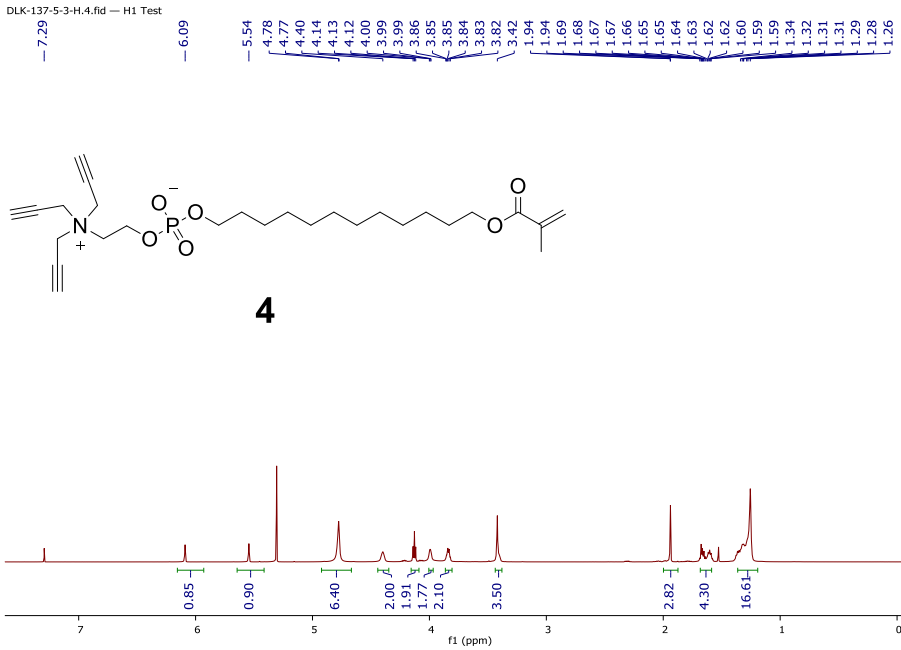

^{13}C NMR spectrum

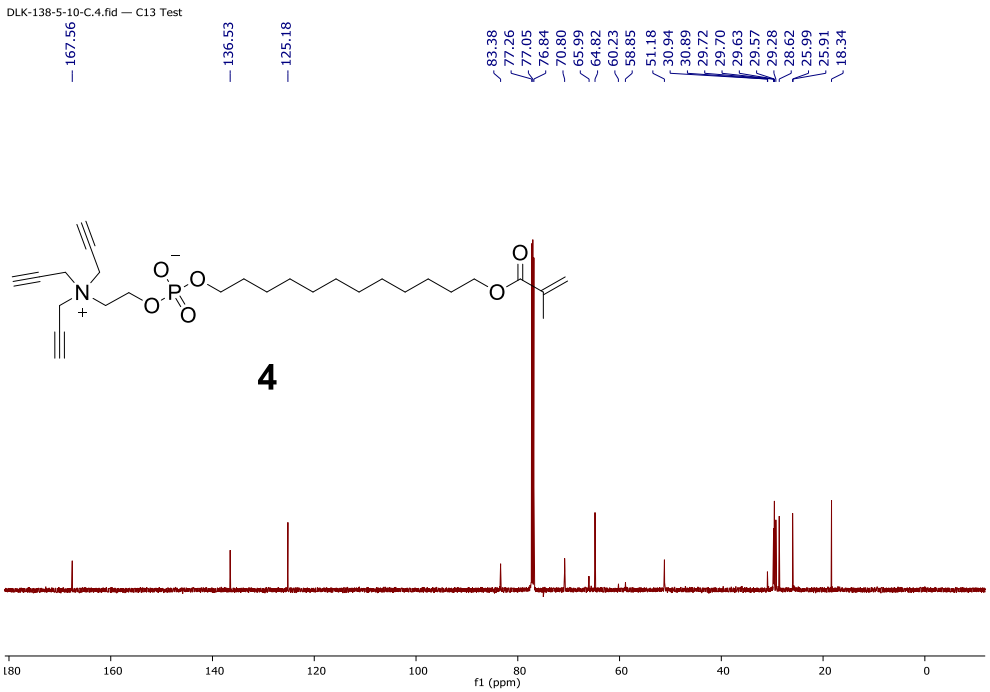

References

(1) Wulff, G. Enzyme-Like Catalysis by Molecularly Imprinted Polymers. *Chem. Rev.* **2001**, *102*, 1-28.

(2) Haupt, K.; Mosbach, K. Molecularly Imprinted Polymers and Their Use in Biomimetic Sensors. *Chem. Rev.* **2000**, *100*, 2495-2504.

(3) Aherne, A.; Alexander, C.; Payne, M. J.; Perez, N.; Vulfson, E. N. Bacteria-Mediated Lithography of Polymer Surfaces. *J. Am. Chem. Soc.* **1996**, *118*, 8771-8772.

(4) Ren, K.; Zare, R. N. Chemical Recognition in Cell-Imprinted Polymers. *ACS Nano* **2012**, *6*, 4314-4318.

(5) Borovička, J.; Stoyanov, S. D.; Paunov, V. N. Shape Recognition of Microbial Cells by Colloidal Cell Imprints. *Nanoscale* **2013**, *5*, 8560-8568.

(6) Shen, X.; Bonde, J. S.; Kamra, T.; Bülow, L.; Leo, J. C.; Linke, D.; Ye, L. Bacterial Imprinting at Pickering Emulsion Interfaces. *Angew. Chem. Int. Ed.* **2014**, *53*, 10687-10690.

(7) Bao, H.; Yang, B.; Zhang, X.; Lei, L.; Li, Z. Bacteria-Templated Fabrication of a Charge Heterogeneous Polymeric Interface for Highly Specific Bacterial Recognition. *Chem. Commun.* **2017**, *53*, 2319-2322.

(8) Pan, J.; Chen, W.; Ma, Y.; Pan, G. Molecularly Imprinted Polymers as Receptor Mimics for Selective Cell Recognition. *Chem. Soc. Rev.* **2018**, *47*, 5574-5587.

(9) Lakshmi, D.; Bossi, A.; Whitcombe, M. J.; Chianella, I.; Fowler, S. A.; Subrahmanyam, S.; Piletska, E. V.; Piletsky, S. A. Electrochemical Sensor for Catechol and Dopamine Based on a Catalytic Molecularly Imprinted Polymer-Conducting Polymer Hybrid Recognition Element. *Anal. Chem.* **2009**, *81*, 3576-3584.

(10) Hoshino, Y.; Koide, H.; Urakami, T.; Kanazawa, H.; Kodama, T.; Oku, N.; Shea, K. J. Recognition, Neutralization, and Clearance of Target Peptides in the Bloodstream of Living Mice by Molecularly Imprinted Polymer Nanoparticles: A Plastic Antibody. *J. Am. Chem. Soc.* **2010**, *132*, 6644-6645.

(11) Hoshino, Y.; Kodama, T.; Okahata, Y.; Shea, K. J. Peptide Imprinted Polymer Nanoparticles: A Plastic Antibody. *J. Am. Chem. Soc.* **2008**, *130*, 15242-15243.

(12) Urraca, J. L.; Aureliano, C. S. A.; Schillinger, E.; Esselmann, H.; Wiltfang, J.; Sellergren, B. Polymeric Complements to the Alzheimer's Disease Biomarker B-Amyloid Isoforms Aβ1–40 and Aβ1–42 for Blood Serum Analysis under Denaturing Conditions. *J. Am. Chem. Soc.* **2011**, *133*, 9220-9223.

(13) Ma, Y.; Pan, G. Q.; Zhang, Y.; Guo, X. Z.; Zhang, H. Q. Narrowly Dispersed Hydrophilic Molecularly Imprinted Polymer Nanoparticles for Efficient Molecular Recognition in Real Aqueous Samples Including River Water, Milk, and Bovine Serum. *Angew. Chem. Int. Ed.* **2013**, *52*, 1511-1514.

(14) Kuwata, T.; Uchida, A.; Takano, E.; Kitayama, Y.; Takeuchi, T. Molecularly Imprinted Polymer Arrays as Synthetic Protein Chips Prepared by Transcription-Type Molecular Imprinting by Use of Protein-Immobilized Dots as Stamps. *Anal. Chem.* **2015**, *87*, 11784-11791.

(15) Liu, Y. B.; Fang, S. M.; Zhai, J. Q.; Zhao, M. P. Construction of Antibody-Like Nanoparticles for Selective Protein Sequestration in Living Cells. *Nanoscale* **2015**, *7*, 7162-7167.

(16) Liu, J.; Yin, D.; Wang, S.; Chen, H. Y.; Liu, Z. Probing Low‐Copy‐Number Proteins in a Single Living Cell. *Angew. Chem. Int. Ed.* **2016**, *55*, 13215-13218.

(17) Horikawa, R.; Sunayama, H.; Kitayama, Y.; Takano, E.; Takeuchi, T. A Programmable Signaling Molecular Recognition Nanocavity Prepared by Molecular Imprinting and Post-Imprinting Modifications. *Angew. Chem. Int. Ed.* **2016**, *55*, 13023-13027.

(18) Panagiotopoulou, M.; Salinas, Y.; Beyazit, S.; Kunath, S.; Duma, L.; Prost, E.; Mayes, A. G.; Resmini, M.; Bui, B. T. S.; Haupt, K. Molecularly Imprinted Polymer Coated Quantum Dots for Multiplexed Cell Targeting and Imaging. *Angew. Chem. Int. Ed.* **2016**, *55*, 8244-8248.

(19) Bertolla, M.; Cenci, L.; Anesi, A.; Ambrosi, E.; Tagliaro, F.; Vanzetti, L.; Guella, G.; Bossi, A. M. Solvent-Responsive Molecularly Imprinted Nanogels for Targeted Protein Analysis in Maldi-Tof Mass Spectrometry. *ACS Appl. Mater. Interfaces* **2017**, *9*, 6908-6915.

(20) Pan, G.; Shinde, S.; Yeung, S. Y.; Jakštaitė, M.; Li, Q.; Wingren, A. G.; Sellergren, B. An Epitope‐Imprinted Biointerface with Dynamic Bioactivity for Modulating Cell–Biomaterial Interactions. *Angew. Chem. Int. Ed.* **2017**, *56*, 15959-15963.

(21) Awino, J. K.; Zhao, Y. Protein-Mimetic, Molecularly Imprinted Nanoparticles for Selective Binding of Bile Salt Derivatives in Water. *J. Am. Chem. Soc.* **2013**, *135*, 12552-12555.

(22) Nowick, J. S.; Chen, J. S.; Noronha, G. Molecular Recognition in Micelles - the Roles of Hydrogen-Bonding and Hydrophobicity in Adenine Thymine Base-Pairing in Sds Micelles. *J. Am. Chem. Soc.* **1993**, *115*, 7636-7644.

(23) Nowick, J. S.; Chen, J. S. Molecular Recognition in Aqueous Micellar Solution - Adenine Thymine Base-Pairing in Sds Micelles. *J. Am. Chem. Soc.* **1992**, *114*, 1107-1108.

(24) Awino, J. K.; Gunasekara, R. W.; Zhao, Y. Sequence-Selective Binding of Oligopeptides in Water through Hydrophobic Coding. *J. Am. Chem. Soc.* **2017**, *139*, 2188-2191.

(25) Gunasekara, R. W.; Zhao, Y. A General Method for Selective Recognition of Monosaccharides and Oligosaccharides in Water. *J. Am. Chem. Soc.* **2017**, *139*, 829-835.

(26) Hu, L.; Arifuzzaman, M. D.; Zhao, Y. Controlling Product Inhibition through Substrate-Specific Active Sites in Nanoparticle-Based Phosphodiesterase and Esterase. *Acs Catal* **2019**, *9*, 5019-5024.

(27) Arifuzzaman, M. D.; Zhao, Y. Water-Soluble Molecularly Imprinted Nanoparticle Receptors with Hydrogen-Bond-Assisted Hydrophobic Binding. *J. Org. Chem.* **2016**, *81*, 7518-7526.

(28) Brossi, A.: The Alkaloids. Chemistry and Pharmacology. Academic Press: New York, San Diego, 1983.

(29) Aniszewski, T.: *Alkaloids - Secrets of Life: Alkaloid Chemistry, Biological Significance, Applications and Ecological Role*; Elsevier: Amsterdam, 2007.

(30) Lee, A. G.: *Biomembranes: A Multi-Volume Treatise*; JAI Press: Greenwich, 1995.

(31) Yeagle, P.: *The Structure of Biological Membranes, 2nd Ed.*; CRC Press: Boca Raton, 2005.

(32) Ishihara, K.; Ueda, T.; Nakabayashi, N. Preparation of Phospholipid Polylners and Their Properties as Polymer Hydrogel Membranes. *Polym. J.* **1990**, *22*, 355-360.

(33) Ishihara, K.; Nomura, H.; Mihara, T.; Kurita, K.; Iwasaki, Y.; Nakabayashi, N. Why Do Phospholipid Polymers Reduce Protein Adsorption? *J. Biomed. Mater. Res.* **1998**, *39*, 323-330.

(34) Patel, J. D.; Iwasaki, Y.; Ishihara, K.; Anderson, J. M. Phospholipid Polymer Surfaces Reduce Bacteria and Leukocyte Adhesion under Dynamic Flow Conditions. *J. Biomed. Mater. Res.: Part A* **2005**, *73A*, 359-366.

(35) Chen, M.; Briscoe, W. H.; Armes, S. P.; Klein, J. Lubrication at Physiological Pressures by Polyzwitterionic Brushes. *Science* **2009**, *323*, 1698-1701.

(36) Seuring, J.; Reiss, P.; Koert, U.; Agarwal, S. Synthesis, Characterization and Properties of a New Polymerisable Surfactant: 12-Methacryloyl Dodecylphosphocholine. *Chem. Phys. Lipids* **2010**, *163*, 367-372.

(37) Rosen, M. J.: *Surfactants and Interfacial Phenomena*; 2nd ed.; Wiley: New York, 1989. pp. 108-168.

(38) Kalyanasundaram, K.; Thomas, J. K. Environmental Effects of Vibronic Band Intensities in Pyrene Monomer Fluorescence and Their Application in Studies of Micellar Systems. *J. Am. Chem. Soc.* **1977**, *99*, 2039-2044.

(39) Zhang, S.; Zhao, Y. Facile Synthesis of Multivalent Water-Soluble Organic Nanoparticles Via "Surface Clicking" of Alkynylated Surfactant Micelles. *Macromolecules* **2010**, *43*, 4020-4022.

(40) Bendheim, P. E.; Poeggeler, B.; Neria, E.; Ziv, V.; Pappolla, M. A.; Chain, D. G. Development of Indole-3-Propionic Acid (Oxigon) for Alzheimer's Disease. *J. Mol. Neurosci.* **2002**, *19*, 213-217.

(41) Khan, M. Z.; Nawaz, W. The Emerging Roles of Human Trace Amines and Human Trace Amine-Associated Receptors (Htaars) in Central Nervous System. *Biomed. Pharmacother.* **2016**, *83*, 439-449.

(42) Li, X.; Zhao, Y. Protection/Deprotection of Surface Activity and Its Applications in the Controlled Release of Liposomal Contents. *Langmuir* **2012**, *28*, 4152-4159.

(43) Fa, S.; Zhao, Y. Peptide-Binding Nanoparticle Materials with Tailored Recognition Sites for Basic Peptides. *Chem. Mater.* **2017**, *29*, 9284-9291.

(44) Fa, S.; Zhao, Y. Water-Soluble Nanoparticle Receptors Supramolecularly Coded for Acidic Peptides. *Chem. -Eur. J.* **2018**, *24*, 150-158.

(45) Slater, L. S.; Callis, P. R. Molecular Orbital Theory of the ^1l_a and ^1l_b States of Indole. 2. An Ab Initio Study. *J. Phys. Chem.* **1995**, *99*, 8572-8581.

(46) Pierce, D. W.; Boxer, S. G. Stark Effect Spectroscopy of Tryptophan. *Biophys. J.* **1995**, *68*, 1583-1591.

(47) Lami, H.; Glasser, N. Indole's Solvatochromism Revisited. *J. Chem. Phys.* **1986**, *84*, 597-604.

(48) Callis, P. R.: [7] ^1l_a and ^1l_b Transitions of Tryptophan: Applications of Theory and Experimental Observations to Fluorescence of Proteins. In *Methods in Enzymology*; Academic Press, 1997; Vol. 278; pp 113-150.

(49) Valeur, B.; Weber, G. Resolution of the Fluorescence Excitation Spectrum of Indole into the 1la and 1lb Excitation Bands*. *Photochem. Photobiol.* **1977**, *25*, 441-444.

(50) Gasymov, O. K.; Abduragimov, A. R.; Glasgow, B. J. Probing Tertiary Structure of Proteins Using Single Trp Mutations with Circular Dichroism at Low Temperature. *J. Phys. Chem. B* **2014**, *118*, 986-995.

(51) Seredyuk, V.; Alami, E.; Nydén, M.; Holmberg, K.; Peresypkin, A. V.; Menger, F. M. Micellization and Adsorption Properties of Novel Zwitterionic Surfactants. *Langmuir* **2001**, *17*, 5160-5165.

(52) Isom, D. G.; Castañeda, C. A.; Cannon, B. R.; García-Moreno E., B. Large Shifts in Pk_a Values of Lysine Residues Buried inside a Protein. *Proc. Natl. Acad. Sci. U. S. A.* **2011**, *108*, 5260-5265.

(53) The pKa shift is less significant when the ammonium group is on the surface of the micelle, strongly solvated by water.

(54) Rubin, M.; Wishinsky, H. 1-Arylcyclohexanecarboxylic Acids. *J. Am. Chem. Soc.* **1946**, *68*, 828-832.

(55) Marshall, F. N.; Williamson, H. E. Natruretic Response During Infusion of Beta-Diethylaminoethyl-Diphenylpropyl Acetate Hydrocloride (Skf 525-a). *The Journal of pharmacology and experimental therapeutics* **1964**, *143*, 395-400.

(56) Jendzelovsky, R.; Koval, J.; Mikes, J.; Papcova, Z.; Plsikova, J.; Fedorocko, P. Inhibition of Gsk-3beta Reverses the Pro-Apoptotic Effect of Proadifen (Skf-525a) in Ht-29 Colon Adenocarcinoma Cells. *Toxicol. In Vitro.* **2012**, *26*, 775-782.

(57) Na, G. C.; Timasheff, S. N. Stoichiometry of the Vinblastine-Induced Self-Association of Calf Brain Tubulin. *Biochemistry* **1980**, *19*, 1347-1354.

(58) Jordan, M. A.; Wilson, L. Microtubules as a Target for Anticancer Drugs. *Nat. Rev. Cancer* **2004**, *4*, 253-265.

(59) Zhang, S.; Zhao, Y. Controlled Release from Cleavable Polymerized Liposomes Upon Redox and Ph Stimulation. *Bioconjugate Chem.* **2011**, *22*, 523-528.

CHAPTER 3. SELECTIVE BINDING OF FOLIC ACID AND DERIVATIVES BY IMPRINTED NANOPARTICLE RECEPTORS IN WATER

Modified from a paper published in *Bioconjugate Chemistry*, **2018**, 29, 1438.

Likun Duan[1], Yan Zhao[1]*

[1]Department of chemistry, Iowa State University, Ames, Iowa, 50011 United States

* Corresponding Authors

Abstract

Folate receptors are overexpressed on cancer cells and frequently used for targeted delivery. Creation of synthetic receptors to bind folic acid and analogues in water, however, is challenging because of its complex hydrogen-bonding patterns and competition for hydrogen bonds from the solvent. Micellar imprinting within cross-linkable surfactants circumvented these problems because the nonpolar micellar environment strengthened the hydrogen bonds between the amide group in the surfactant and the template molecule. Polymerizable thiouronium functional monomers further enhanced the binding through hydrogen-bond-reinforced ion pairs with the glutamate moiety of folate. The resulting imprinted micelles were able to bind folate and their analogues with submicromolar affinity and distinguish small changes in the hydrogen bonding patterns, as well as the number/position of carboxylic acids. The binding constant obtained was 2–3 orders of magnitude higher than those reported for small molecule synthetic receptors. Our binding study also revealed interesting details in the binding.

For example, the relative contributions of different segments of the molecule to the binding followed the order of carboxylates > pyrimidine ring > pyrazine ring.

Introduction

Biological systems rely on molecular recognition for important processes such as binding, catalysis, and transport. Because individual noncovalent interactions are quite weak, they are used together to achieve sufficient strength. Chemists over the last several decades have used the same strategy to construct receptors for ions and small organic molecules, mainly in organic solvents.[1,2]

To bind a guest molecule with high affinity and selectivity, its receptor needs to have a highly complementary binding interface for the guest. Macrocycles are a perfect platform for receptors, as long as their concave structure has the appropriate size and functionality for the guest molecule. A more recent platform is linear foldamers,[3-7] with a particular benefit of using guest-triggered conformational changes to amplify the guest binding.[8,9]

Both macrocycles and foldamers represent the molecular approach to the construction of receptors. Herein, the receptor, typically larger than the guest molecule, is built step-by-step to encompass the guest. As the guest molecule becomes more complex, the receptors necessarily grow in size and complexity and their synthesis could become very difficult.

Molecular recognition in water takes the challenge to the next level,[10,11] as hydrogen bonds, one of the best tools for directional molecular interaction, are compromised by competition from the solvent. Furthermore, when the receptor is built from a molecular scaffold, water-solubilizing groups need to be installed on the structure, in addition to the binding groups. As we move from simple organic guests to more complex biological molecules, design and synthesis of the corresponding molecular receptors could become an unsurmountable task.

Molecular imprinting is a very different approach to constructing receptors.[12-22] The method aims to trap the noncovalent or covalent complex between the template/guest molecule and functional monomers (FMs) in a polymeric matrix by heavy cross-linking. Removal of the templates leaves behind guest-complementary binding sites in the matrix, potentially with a high level of fidelity. In this method, the binding site is formed by facile covalent capture instead of total synthesis, making the synthesis much easier to perform. Not surprisingly, since their discovery, molecularly imprinted polymer (MIPs) have been used by researchers of diverse backgrounds for applications including separation, enzyme-mimetic catalysis, and chemical sensing. Over the years, many different techniques have been developed to improve the properties of traditional MIPs, including imprinting unimolecularly within dendrimers,[23,24] on polymeric nanoparticles,[25-32] and within micro/nanogels[33-38]

Folic acid is an important biological molecule. Because folate receptors are overexpressed on many cancerous cells,[39] folic acids are frequently used for targeted delivery of anticancer drugs.[40,41] Creation of synthetic receptors for folic acid illustrates the typical challenges in the molecular recognition of biomolecules in water.[42-46] The molecule is highly functional, with a glutamate coupled to a pteroate moiety. It is fully water-soluble with numerous hydrogen-bond donors and acceptors and two ionizable carboxylic acids. A particular challenge with biomolecules is their selective recognition among close relatives: molecules **2**–**4** differ subtly from folic acid, sometimes by only one or two hydrogen-bond donor/acceptor. Yet, they play very different roles in biology.

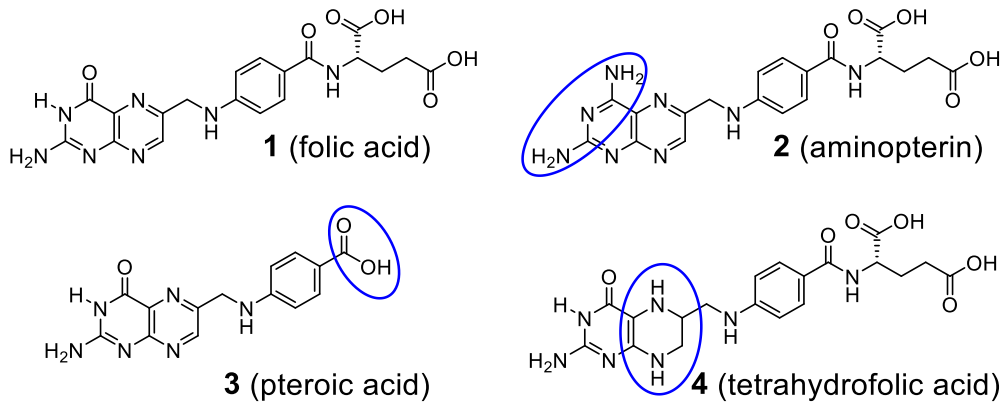

Chart 1. Structures of folic acid and analogues, with the differences from folic acid highlighted by blue circles.

These challenges, together with our interest of designing biomimetic receptors,[47-49] prompted us to develop synthetic receptors for folic acid and analogues. In this paper, we report that highly selective folate receptors could be prepared by molecular imprinting within doubly cross-likable micelles. The resulting molecularly imprinted nanoparticles (MINPs) use hydrogen bonds, salt bridges, and hydrophobic interactions to achieve strong and selective binding. The binding constant obtained by our receptor was 2–3 orders of magnitude higher than those reported in the literature by small-molecule receptors. The materials bridge the gap between molecular receptors and macroscopic MIPs. Similar to traditional MIPs, they can be prepared conveniently in one-pot reaction without special techniques. Unlike macroscopic polymers, however, they behave like soluble molecular receptors due to their nanodimension and a controllable number of binding sites.

Results and Discussion

Design and Synthesis of Functionalized MINPs. Preparation of MINP receptors is shown in Scheme 1. Cross-linkable surfactant **5** contains two sets of orthogonal cross-linkable groups and is dissolved in water above its CMC (0.41 mM).[50] We first cross-linked its micelle on the

surface by the Cu(I)-catalyzed click reaction with diazide **6**.[56,57] The surface-cross-linked micelle was further functionalized by the click reaction with monoazide **7**. The functionalization decorates the micelle with a layer of hydrophilic ligands to improve its water-solubility. The micelle contained divinylbenzene (DVB) and DMPA (a photolytic radical initiator). Free radical polymerization was initiated normally after the surface-cross-linking and functionalization to cross-link the core between the methacrylate of **5** and DVB. The template molecule typically had significant hydrophobicity and was incorporated into the micelle very easily. It served as a place holder inside the micelle as the surface–core double cross-linking "solidified" the micelle. Once the template was removed by repeated solvent washing, the resulting nanoparticle possessed a binding site complementary to the template molecule. The surfactant/template ratio was typically maintained at 50:1 in the preparation because dynamic light scattering (DLS) showed that each MINP consisted of approximately 50 (cross-linked) surfactants. The 50:1 surfactant/template ratio translated to an average of one binding site per nanoparticle. We have shown that this number is fully tunable, simply by using different surfactant/template ratio in the preparation.[51]

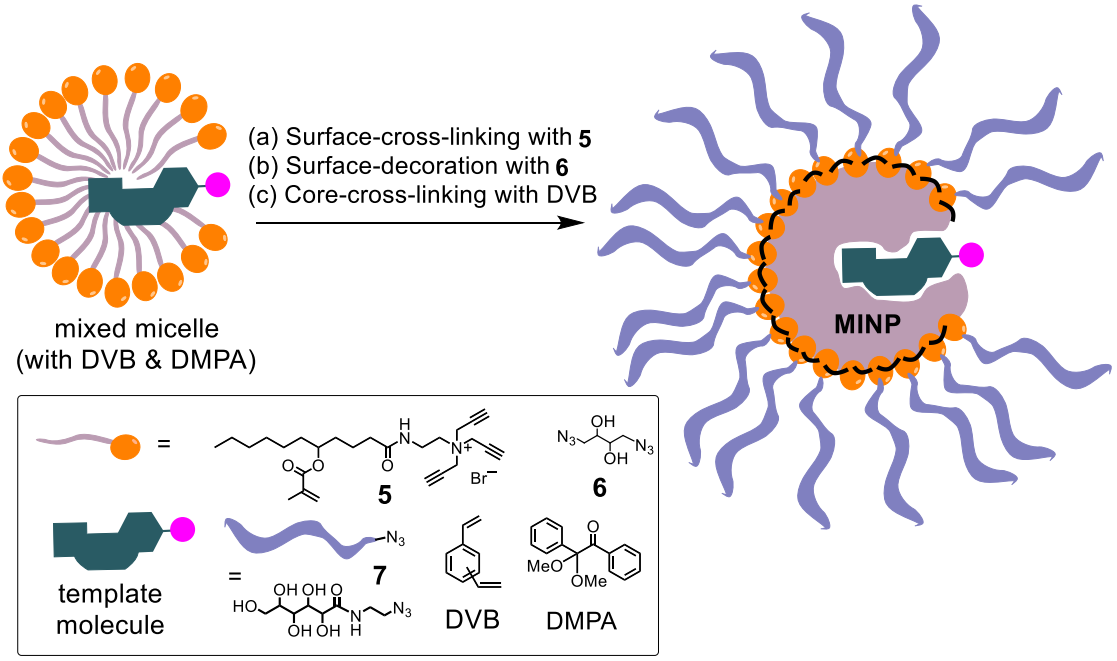

Scheme 1. Preparation of MINP from templated polymerization of cross-linkable micelle.

The detailed procedures for the MINP preparation are reported in the Experimental Section. In general, the surface-cross-linking and core-polymerization/cross-linking was monitored by ^{1}H NMR spectroscopy and DLS (Supporting Information).[51] As the surfactant and DVB (core-cross-linker) underwent free radical polymerization, ^{1}H NMR spectroscopy showed disappearance of alkenic protons. DLS, on the other hand, revealed an increase in size for the nanoparticles as surface ligands were attached and a slight decrease in size when core-polymerization shrank the cross-linked micelles. DLS could also help us estimate the molecular weight of the MINP. The surface-cross-linking has been confirmed by mass spectrometry (after cleaving the surface-cross-linkages)[56] and the DLS size by transmission electron microscopy (TEM).[58]

Binding Properties of MINPs. Folic acid is rich in hydrogen-bonding functionalities and has two carboxylic acids. This was why we used amide-functionalized surfactant **5** in the majority of our MINP preparation. Folic acid is anionic under physiological conditions. The

usage of a cationic cross-linkable surfactant is envisioned to help its inclusion in the micelle. Once incorporated into the micelle, folic acid is expected to stay close to the micellar surface to be solvated by water, due to its strong hydrophilicity. The amide bond of **5** is only two carbons away from the ammonium headgroup and thus should be very close to the surface as well. We reasoned that the numerous surfactant molecules surrounding the template would hydrogen-bond with it using the amide. Although competition from solvent often makes hydrogen bonds ineffective for molecular recognition in water, the hydrophobic microenvironment of a micelle is known to strengthen hydrogen bonds.[59,60] As a comparison, we prepared a MINP from compound **8**, another cross-linkable surfactant we frequently used.[61,62] It has little hydrogen-bonding ability in the headgroup but the same cross-linkable functionalities (tripropargylammonium headgroup and methacrylate on the hydrophobic tail). As will be shown by the binding data (vide infra), surfactant **5** afforded a MINP with significantly stronger binding than **8**.

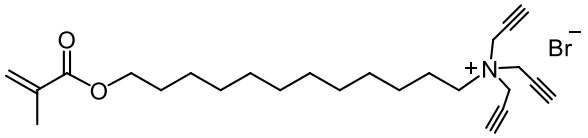

8

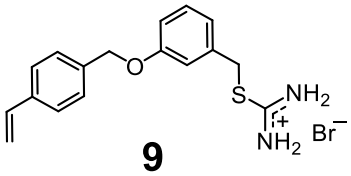

9

To recognize the glutamate moiety, we included FM **9** in the formulation. It is amphiphilic, just like the cross-linkable surfactant. The two hydrophobic aromatic rings help the molecule stay within the micelle. The thiouronium group, similar to guanidinium or amidinium,[63-66] is known to form strong hydrogen-bond-reinforced salt bridge with carboxylate.[52] Its vinyl group will copolymerize with the methacrylate and DVB to covalently fix the binding group on the MINP.

Folic acid is weakly fluorescent. As different concentrations of MINP$_5$(**1**)—i.e., MINP prepared with cross-linkable surfactant **5** and template **1**—were added to folic acid in 50 mM Tris buffer (pH 7.4), its fluorescence was slightly quenched (Figure 1a). Two isoemissive points were observed at 417 and 511 nm, indicating that the titration caused a continuous transition from the free to the bound guest. The emission intensity at 448 nm fit nicely to a 1:1 binding isotherm, yielding a binding constant (K_a) of (17.2 ± 2.7) × 10^5 M^{-1} in Tris buffer (Figure 1b). The submicromolar binding affinity was very impressive for a completely water-soluble guest. In comparison, molecularly constructed receptors in the literature were reported to bind folate with K_a = 10^2–10^4 M^{-1}.[45] The 1:1 binding stoichiometry was confirmed in our case by the Job plot, which showed a clear maximum at a molar fraction of 0.5 (Figure 1c).

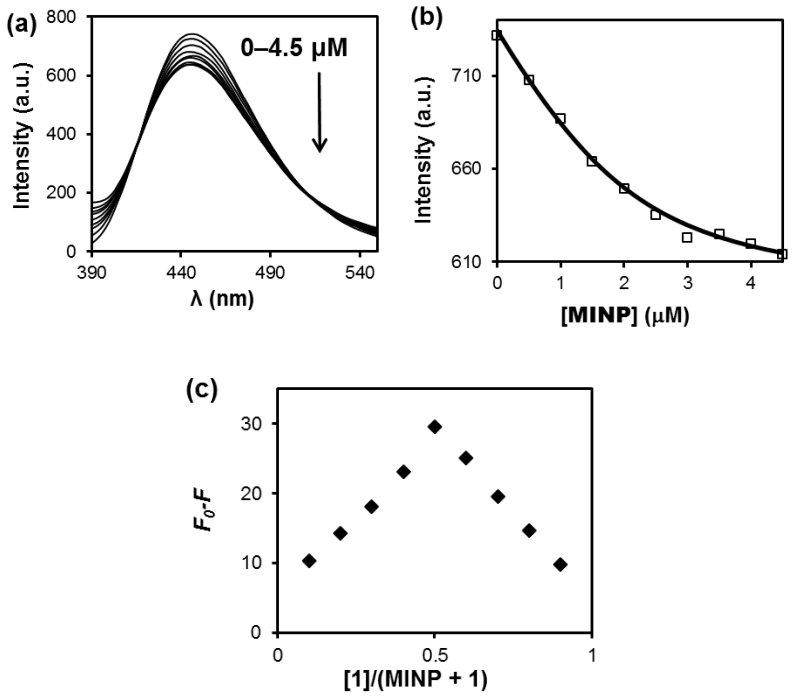

Figure 1. (a) Emission spectra of folic acid **1** in the presence of 0–4.5 μM of MINP$_5$(**1**) in 50 mM Tris bugger (pH 7.4). The MINP was prepared with 2 equiv FM **9** to bind the glutamate. [**1**] = 2.0 μM. λ_{ex} = 350 nm. (b) Nonlinear least squares curve fitting of the fluorescence

intensity at 448 nm to a 1:1 binding isotherm. (c) Job plot for the binding of **1** by MINP$_5$(**1**), in which the emission intensity at 448 nm was plotted against the molar fraction of **1**, at a constant total concentration of 10.0 μM in 50 mM Tris buffer (pH = 7.4).

We also confirmed the binding constant obtained from the fluorescence titration by isothermal titration calorimetry (ITC). It is considered one of the most reliable methods for studying intermolecular interactions.[67] It has the benefit of giving a number of important parameters including binding enthalpy (ΔH) and the number of binding sites per particle (N), in addition to the binding constant. The binding free energy (ΔG) can be calculated from K_a using equation $-\Delta G = RT\ln(K_a)$, and ΔS from ΔG and ΔH. The ITC titration of **1** showed a negative/favorable enthalpy. The data afforded a K_a value of $(17.0 \pm 1.0) \times 10^5$ M^{-1} (Table 1, entry 1), in excellent agreement with the value obtained by fluorescence titration. The ITC titration gave the number of binding site of $N = 1.2 \pm 0.4$, consistent with our surfactant/template ratio in the preparation and also the Job plot.

Table 1 summarizes the binding data obtained in the study. The binding data were generally obtained from ITC and selected examples were verified by fluorescence titration, with the K_a values obtained by the latter shown in parentheses.

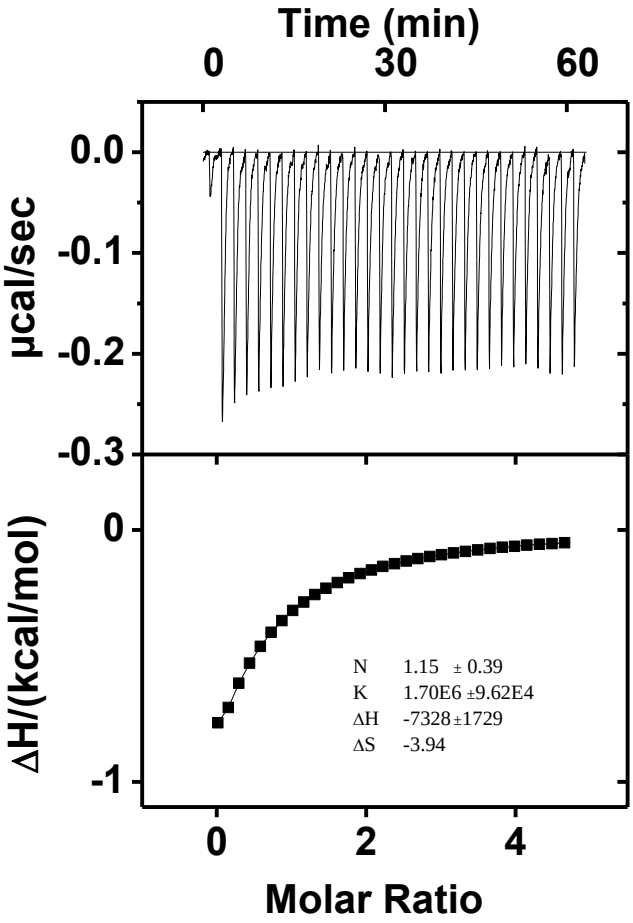

Figure 2. ITC curve obtained at 298.15 K from titration of MINP$_5$(**1**) with **1** in 50 mM Tris buffer (pH = 7.4). The MINP was prepared with 2 equiv FM **9** to bind the glutamate. MINP$_5$(**1**) = 10 µM in the cell. The concentration of **1** in the syringe was 0.2 mM.

Entries 1–4 of Table 1 show the effects of FM **9** on the MINP binding. As the amount of the FM increased in the formulation, the binding constant of the corresponding MINP for folic acid (**1**) peaked at 2 equiv **9**. Since folic acid has two carboxylates, the results indicate that a 1:1 stoichiometry is optimal for the imprinting and binding. MINP$_5$(**1**) prepared without FM **9** also gave a significant binding constant ($K_a = 4.55 \times 10^5$ M^{-1}). Thus, even without the thiouronium FM, the template was readily included into the micelle. The discrete number of binding sites

Table 1. Binding data for MINPs (obtained by ITC unless indicated otherwise)[a]

Entry	MINP[b]	FM	Guest	$-\Delta G$ (kcal/mol)	N[c]	K_a ($\times 10^5$ M^{-1})	$-\Delta H$ (kcal/mol)	$T\Delta S$ (kcal/mol)
1	MINP$_5$(**1**)	0 equiv **9**	**1**	7.7	0.9 ± 0.3	4.55 ± 1.3 (4.60 ± 1.40)	3.4 ± 1.1	4.3
2	MINP$_5$(**1**)	1 equiv **9**	**1**	8.2	0.9 ± 0.1	10.1 ± 2.5 (10.0 ± 2.2)	1.0 ± 0.1	7.2
3	MINP$_5$(**1**)	2 equiv **9**	**1**	8.5	1.2 ± 0.4	17.0 ± 1.0 (17.2 ± 2.7)	7.3 ± 1.7	1.2
4	MINP$_5$(**1**)	3 equiv **9**	**1**	8.4	0.8 ± 0.1	16.0 ± 1.0 (16.1 ± 2.3)	5.8 ± 0.8	2.6
5	MINP$_8$(**1**)	2 equiv **9**	**1**	7.4	0.7 ± 0.2	2.47 ± 0.14	3.8 ± 0.5	3.6
6	MINP$_5$(**1**)	2 equiv **9**	**2**	7.5	0.8 ± 0.2	3.50 ± 1.0 (3.70 ± 0.94)	9.7 ± 1.3	-2.2
7	MINP$_5$(**1**)	2 equiv **9**	**3**	5.9	0.9 ± 0.1	0.217 ± 0.052	19.5 ± 1.7	-13.6
8	MINP$_5$(**1**)	2 equiv **9**	**4**	8.1	1.3 ± 0.1	9.01 ± 0.22	15.2 ± 1.3	-7.1
9	MINP$_5$(**2**)	2 equiv **9**	**1**	7.4	0.8 ± 0.1	2.81 ± 0.31	3.2 ± 0.6	4.2
10	MINP$_5$(**2**)	2 equiv **9**	**2**	8.4	1.2 ± 0.3	13.6 ± 1.6	10.9 ± 3.0	-2.5
11	MINP$_5$(**2**)	2 equiv **9**	**3**	5.6	1.0 ± 0.2	0.127 ± 0.011	1.3 ± 0.2	4.3
12	MINP$_5$(**2**)	2 equiv **9**	**4**	7	1.0 ± 0.1	1.44 ± 0.16	29.0 ± 1.8	-22

[a] The titrations were generally performed in duplicates in 50 mM Tris buffer (pH = 7.4) and the errors between the runs were <20%. The binding constants in parentheses were from fluorescence titration and thus the number of binding sites and binding enthalpy/entropy were not available. [b] The subscript denotes the cross-linkable surfactant used in the MINP synthesis and the number in parentheses the template molecule. [c] Binding was too weak to be detected by ITC. [c] *N* is the number of binding site per nanoparticle measured by ITC.

and clear trends in the binding constants ruled out any significant nonspecific binding during the titrations.

Entry 5 shows the binding of MINP$_8$(**1**) prepared with 2 equiv FM **9**. The binding constant (K_a = 2.47 10^5 M^{-1}) was 1/7 of that from MINP$_5$(**1**) prepared under the same conditions. The results support the importance of the amide groups in the imprinting, most likely from the proposed hydrogen-bonding interactions mentioned above.

Compounds **2**–**4** are close structural analogues of folic acid (**1**). Aminopterin **2** has an identical glutamate moiety and a 4-aminobenzoyl spacer as folic acid. The only difference is at the left end of the molecule, in the hydrogen-bonding pattern. Instead of D-D-A in the pyrimidine ring of **1**, compound **2** has a D-A-D motif, with everything else being the same (Chart 1). Yet, MINP$_5$(**1**) showed significant selectivity, with **2** only bound by MINP$_5$(**1**) with $K_a = 3.50 \times 10^5$ M^{-1} (Table 1, entry 6). This number is about 1/5 of that for **1**, corresponding to about 1 kcal/mol difference in the binding free energy. Clearly, hydrogen bonds played an important role in the imprinting and binding of the folate derivatives, as supported by our earlier data. This is an important feature of our imprinting method. Molecular imprinting in water traditionally is considered a highly challenging topic.[68] In our case, the micellar environment circumvented the problem of solvent competition. Given the polarity of folic acid, it must stay near the surface of the micelle. It is very good news that hydrogen bonds between the amide of the surfactant and the template played noticeable roles in the imprinting and binding.

Pteroic acid **3** is missing the glutamate of folic acid. Its binding by MINP$_5$(**1**), thus, tests the importance of the carboxylic acids in the molecular imprinting. The binding constant was even weaker, with $K_a = 0.217 \times 10^5$ M^{-1} (Table 1, entry 7) or nearly 1/80 of the value for **1**. Thus, the carboxylates contributed very strongly to the binding. The result is in agreement with entries 1–4, illustrating the importance of thiouronium FM **9** in our study.

Tetrahydrofolic acid **4** is similar to **2** in that the hydrogen-bonding motifs of the molecule is changed by the reduction of the pyrazine ring. Instead of two hydrogen-bond acceptors in **1**, the same place now has two hydrogen-bond donors instead. MINP$_5$(**1**) again was able to detect the change, with $K_a = 9.01 \times 10^5$ M^{-1} (Table 1, entry 8). This binding constant is stronger than that for **2** (entry 6) by nearly 3 times, suggesting that the pyrazine part of the molecule played a less important role than pyrimidine in the molecular imprinting and binding of the receptor.

The benefit of creating receptors by molecular imprinting is that different receptors can be prepared with the same ease, without the need of any individual design, as formation of the binding pocket is taken care of by similar template–FM complexation and covalent capture. We thus prepared MINP$_5$(**2**) following similar procedures, with aminopterin as the template molecule. As shown by the binding data (Table 1, entries 9–12), this receptor showed as good binding properties as MINP$_5$(**1**): the receptor shows the strongest binding for its own template (**2**) among the structural analogues. This is another indication for the success of the imprinting. The guest that was bound most weakly was pteroic acid **3**, once again highlighting the key roles of the thiouronium–carboxylate salt bridge in the imprinting and binding. If the change around the pyrazine ring between **1** and **4** were detected with a little difficulty by MINP$_5$(**1**) (relatively speaking), MINP$_5$(**2**) had no problem distinguishing **4**—its binding was nearly one order of magnitude lower than that for the template (**2**) itself. The results make sense. The only

difference between **1** and **4** are in the pyrazine, which according to the earlier discussion contributed not as importantly as other parts of the molecule to the binding. The difference between **2** and **4** are in both the pyrazine and the pyrimidine ring in the hydrogen-bonding motifs. Since the latter seemed to be key contributors to the binding, differentiation between these two molecules is expected to be easier than between **1** and **2**.

Conclusions

Although molecular recognition in water is a very challenging topic in supramolecular chemistry,[10,11] this work shows that molecular imprinting in cross-linked micelles is an effective and convenient solution to the problem. Despite the complexity of folate derivatives and their subtle structural differences, our MINP receptors easily distinguished them in the binding. The initial applications of MINPs focused on relatively hydrophobic molecules.[51,69] This work demonstrates that very hydrophilic molecules can be imprinted just as easily, as long as appropriate FMs are present. It also shows that MINP could be used to reveal the relative contributions of different functional groups to the binding, by comparing structural analogues in the binding. In the case of MINP receptors for folate, the relative contributions followed the order of carboxylates > pyrimidine > pyrazine. This is an extremely useful feature of our imprinted receptors, as it can help reveal the effectiveness of different functional groups in molecular recognition and allow researchers to focus on the most effective groups. Although it is difficult to measure the importance of hydrophobic interactions in folate recognition directly, the interactions are expected to be the "background", always present in molecular recognition in water. Even for the binding of carbohydrates (which typically lack any significantly hydrophobic groups) by lectins (their protein receptors in nature), release of water-molecules from the binding pockets is considered an important part of the binding free energy.[70] Prior to

binding, the imprinted binding site of MINP is occupied by water molecules. Even though folic acid itself is not very hydrophobic, its binding releases these “high-energy” water molecules, similar to the binding of carbohydrates by lectins.

Acknowledgments

We thank NIGMS (R01GM113883) for financial support of this research

Experimental Section

Syntheses of compounds **5**,[50] **6**–**8**,[51] and **9**[52] were previously reported.

Preparation of Molecularly Imprinted Nanoparticles (MINPs). A typical procedure is as follows.[51] To a micellar solution of compound **5** (10.2 mg, 0.02 mmol) in H_2O (2.0 mL), divinylbenzene (DVB, 2.8 μL, 0.02 mmol), compound **1** in H_2O (10 μL of a solution of 18.5 mg/mL, 0.0004 mmol), and 2,2-dimethoxy-2-phenylacetophenone (DMPA,10 μL of a 12.8 mg/mL solution in DMSO, 0.0005 mmol) were added. The mixture was subjected to ultrasonication for 10 min before compound **6** (4.13 mg, 0.024 mmol), $CuCl_2$ (10 μL of a 6.7 mg/mL solution in H_2O, 0.0005 mmol), and sodium ascorbate (10 μL of a 99 mg/mL solution in H_2O, 0.005 mmol) were added. After the reaction mixture was stirred slowly at room temperature for 12 h, compound **7** (10.6 mg, 0.04 mmol), $CuCl_2$ (10 μL of a 6.7 mg/mL solution in H_2O, 0.0005 mmol l), and sodium ascorbate (10 μL of a 99 mg/mL solution in H_2O, 0.005 mmol) were added. After being stirred for another 6 h at room temperature, the reaction mixture was transferred to a glass vial, purged with nitrogen for 15 min, sealed with a rubber stopper, and irradiated in a Rayonet reactor for 12 h. ^{1}H NMR spectroscopy was used to monitor the progress of reaction. The reaction mixture was poured into acetone (8 mL). The precipitate was

collected by centrifugation and washed with a mixture of acetone/water (5 mL/1 mL) three times. The crude produce was washed by methanol/acetic acid (5 mL/0.1 mL) three times until the emission peak at 448 nm (for the dansyl) disappeared and then with excess methanol. The off white powder was dried in air to afford the final MINP (16 mg, 80%).

Determination of Binding Constants by Fluorescence Titration. A typical procedure is as follows. A stock solution containing MINP$_5$(**1**) (100 μM) was prepared in 50 mM Tris buffer (pH 7.4). Aliquots (1.0 μL) of the MINP stock solution were added to 2.00 mL of the solution of **1** in 50 mM Tris buffer (pH 7.4) (2 μM). After each addition, the sample was allowed to sit for 1 min at room temperature before the fluorescence spectrum was collected. The excitation wavelength (λ_{ex}) was 350 nm. The excitation slit width was 10 nm, and the emission slit width was 10 nm. The binding constant was obtained by nonlinear least squares curve fitting of the fluorescence intensity at 448 nm to a 1:1 binding isotherm.

Determination of Binding Constants by ITC. The determination of binding constants by ITC followed standard procedures.[53-55] In general, a solution of an appropriate guest in in 50 mM Tris buffer (pH 7.4) was injected in equal steps into 1.43 mL of the corresponding MINP in the same solution. The top panel shows the raw calorimetric data. The area under each peak represents the amount of heat generated at each ejection and is plotted against the molar ratio of the MINP to the guest. The smooth solid line is the best fit of the experimental data to the sequential binding of *N* binding site on the MINP. The heat of dilution for the guest, obtained by titration carried out beyond the saturation point, was subtracted from the heat released during the binding. Binding parameters were auto-generated after curve fitting using Microcal Origin 7.

General Method

Routine ^{1}H and ^{13}C NMR spectra were recorded on a Bruker DRX-400, on a Bruker AV II 600 or on a Varian VXR-400 spectrometer. ESI-MS mass was recorded on Shimadzu LCMS-2010 mass spectrometer. Dynamic light scattering (DLS) data were recorded at 25 °C using PDDLS/ CoolBatch 90T with PD2000DLS instrument. Isothermal titration calorimetry (ITC) was performed using a MicroCal VP-ITC Microcalorimeter with Origin 7 software and VPViewer2000 (GE Healthcare, Northampton, MA).

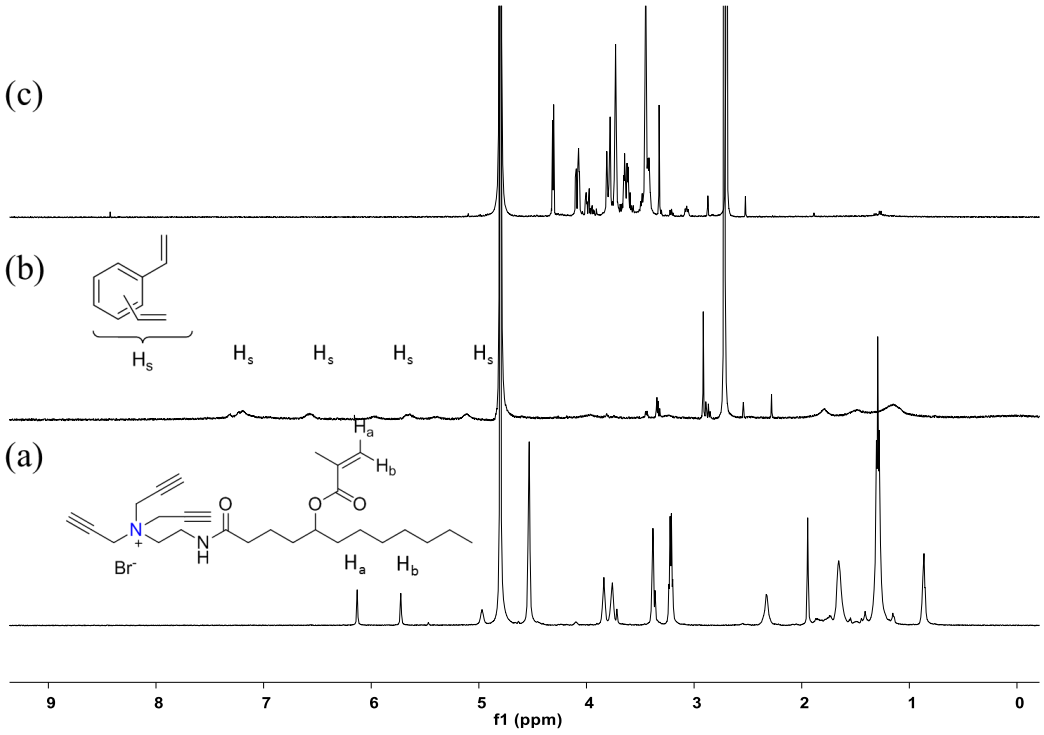

Figure 1S. ^{1}H NMR spectra of (a) **5** in D_2O, (b) alkynyl-SCM in D_2O, and (c) $MINP_5$(**1**) in D_2O.

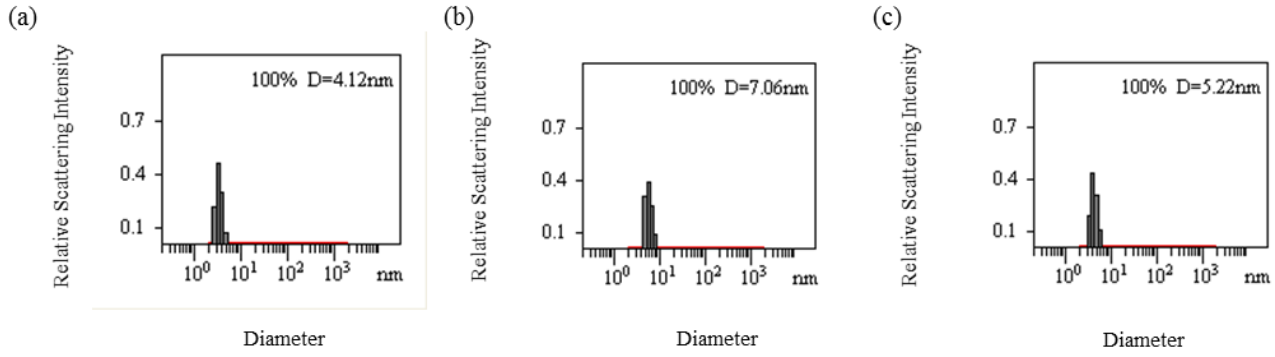

Figure 2S. Distribution of the hydrodynamic diameters of the nanoparticles in water as determined by DLS for (a) alkynyl-SCM, (b) surface-functionalized SCM, and (c) $MINP_5$(**1**) after purification.

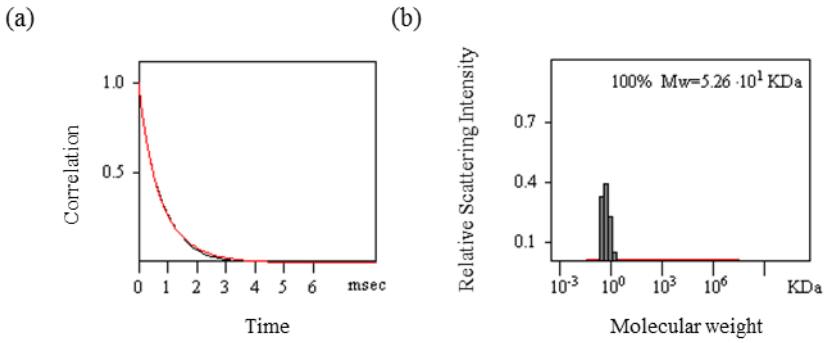

Figure 3S. The correlation curve and the distribution of the molecular weight for MINP(glucose) from the DLS. The PRECISION DECONVOLVE program assumes the intensity of scattering is proportional to the mass of the particle squared. If each unit of building block for the MINP(glucose) is assumed to contain one molecule of compound **5** (MW = 520 g/mol), 1.2 molecules of compound **6** (MW = 172 g/mol), one molecule of DVB (MW = 130 g/mol), and 0.8 molecules of compound **7** (MW = 264 g/mol), the molecular weight of MINP(glucose) translates to 50 [= 52600 / (520 + 1.2×172 + 130 + 0.8×264)] of such units.

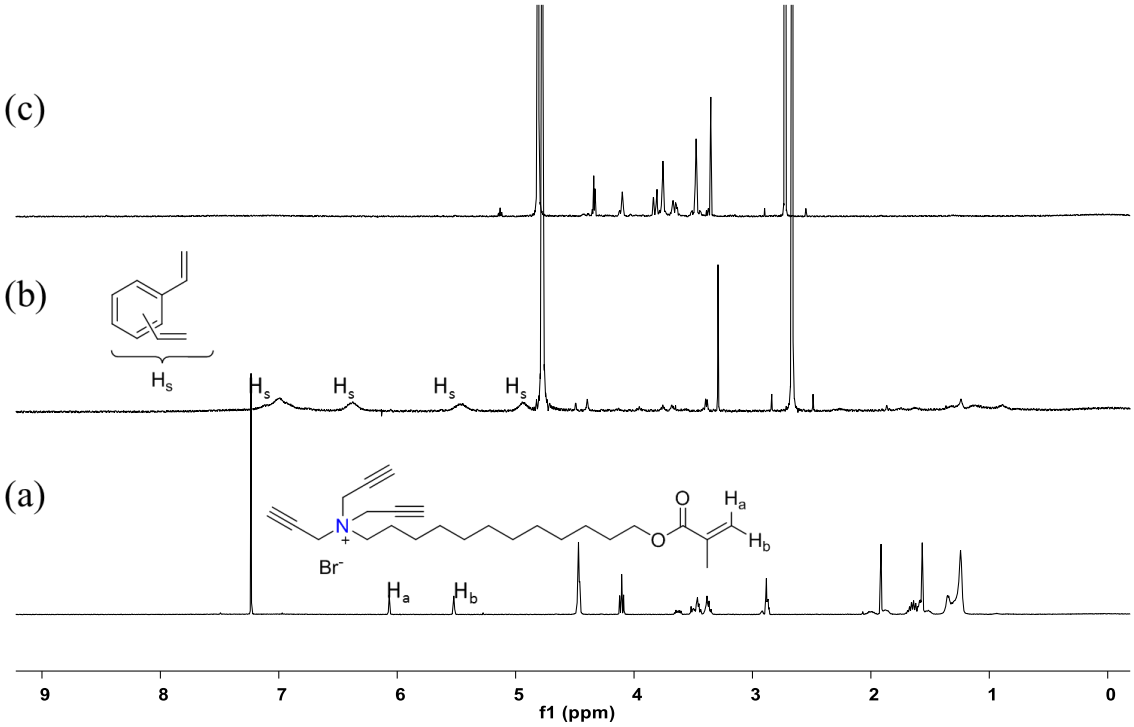

Figure 4S. ^{1}H NMR spectra of (a) **8** in $CDCl_3$, (b) alkynyl-SCM in D_2O, and (c) $MINP_8$(**1**) in D_2O.

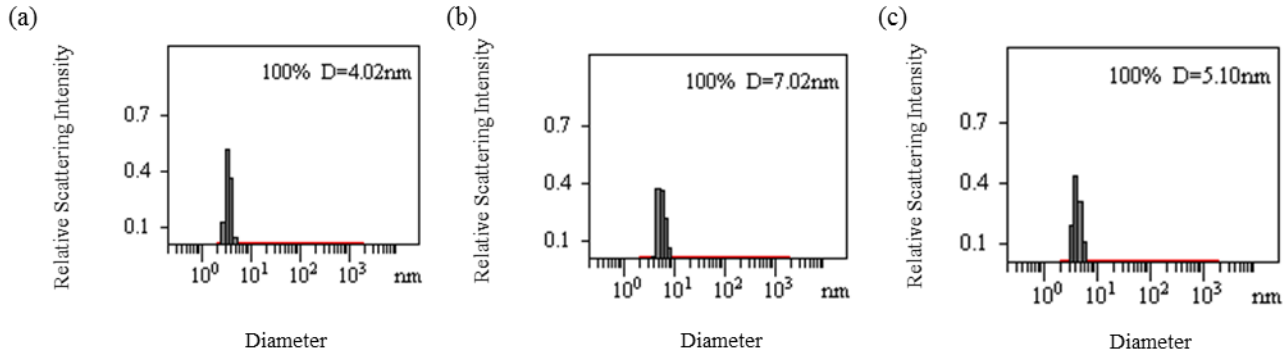

Figure 5S. Distribution of the hydrodynamic diameters of the nanoparticles in water as determined by DLS for (a) alkynyl-SCM, (b) surface-functionalized SCM, and (c) $MINP_8$(**1**) after purification.

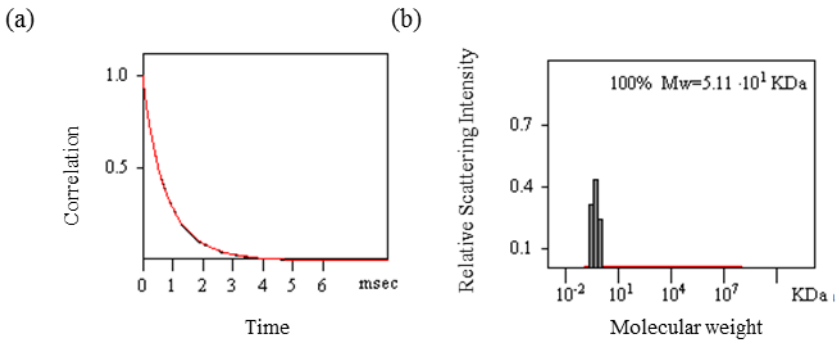

Figure 6S. The correlation curve and the distribution of the molecular weight for MINP(glucose) from the DLS. The PRECISION DECONVOLVE program assumes the intensity of scattering is proportional to the mass of the particle squared. If each unit of building block for the MINP(glucose) is assumed to contain one molecule of compound **8** (MW = 465 g/mol), 1.2 molecules of compound **6** (MW = 172 g/mol), one molecule of DVB (MW = 130 g/mol), and 0.8 molecules of compound **7** (MW = 264 g/mol), the molecular weight of MINP(glucose) translates to 51 [= 51100 / (465 + 1.2×172 + 130 + 0.8×264)] of such units.

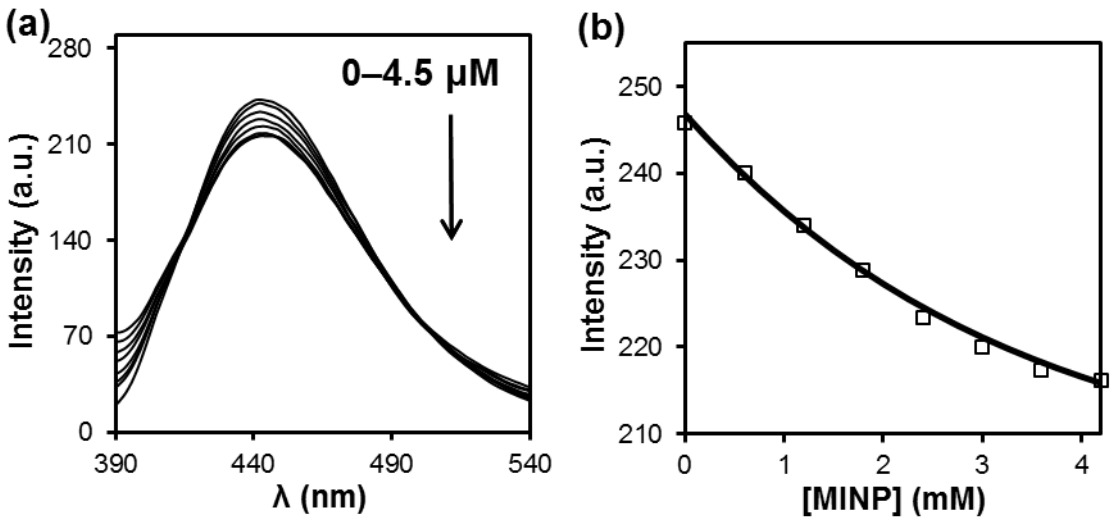

Figure 7S. (a) Emission spectra of compound **1** (2.0 μM) upon the addition of different concentrations of $MINP_5$(**1**) (0 equiv FM **9**) in 50 mM Tris buffer (pH = 7.4). (b) Nonlinear least squares fitting of the emission intensity of compound **1** at 448 nm to a 1:1 binding isotherm. The data correspond to entry 1 in Table 1.

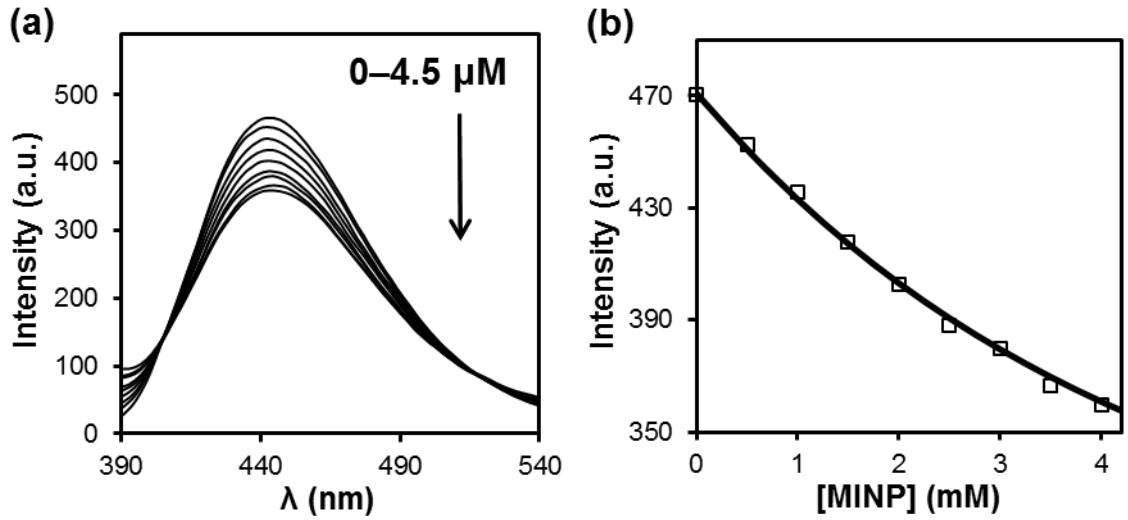

Figure 8S. (a) Emission spectra of compound **1** (2.0 μM) upon the addition of different concentrations of $MINP_5$(**1**) (1 equiv FM **9**) in 50 mM Tris buffer (pH = 7.4). (b) Nonlinear least squares fitting of the emission intensity of compound **1** at 448 nm to a 1:1 binding isotherm. The data correspond to entry 2 in Table 1.

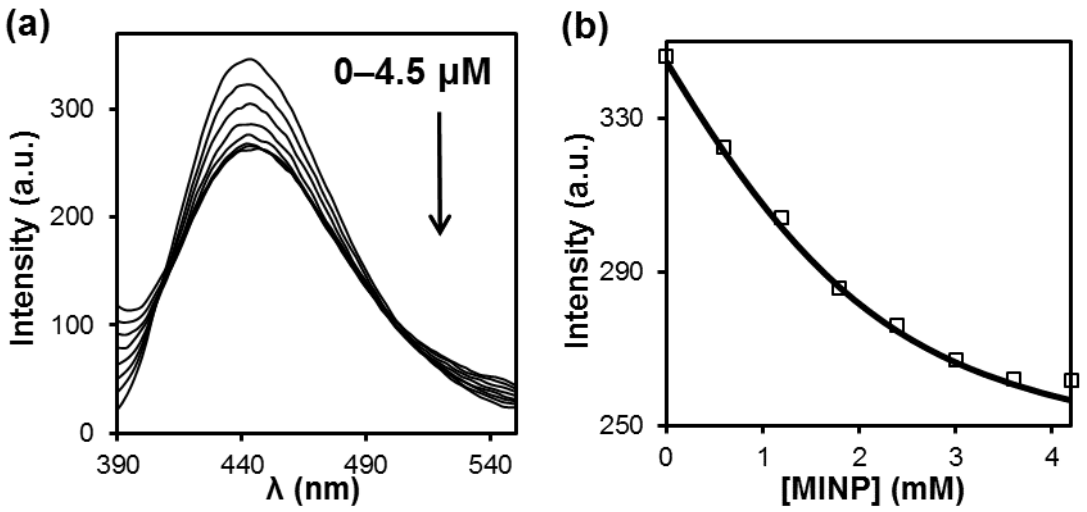

Figure 9S. (a) Emission spectra of compound **1** (2.0 μM) upon the addition of different concentrations of $MINP_5$(**1**) (3 equiv FM **9**) in 50 mM Tris buffer (pH = 7.4). (b) Nonlinear least squares fitting of the emission intensity of compound **1** at 448 nm to a 1:1 binding isotherm. The data correspond to entry 4 in Table 1.

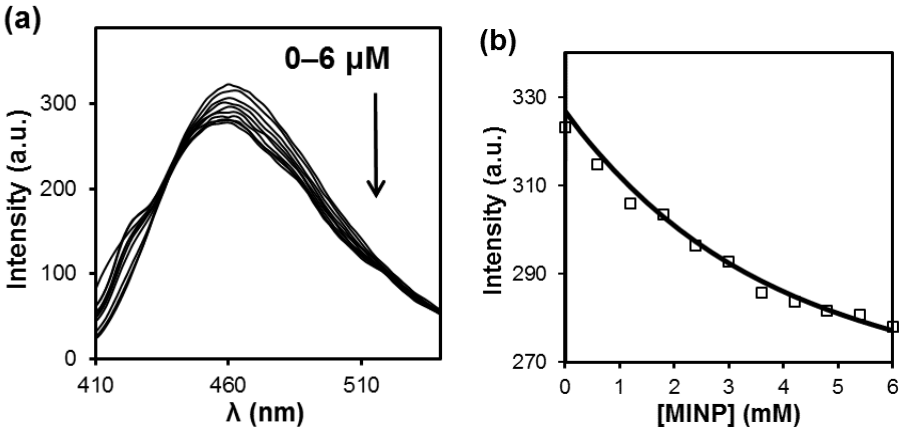

Figure 10S. (a) Emission spectra of compound **2** (2.0 μM) upon the addition of different concentrations of $MINP_5$(**1**) (2 equiv FM **9**) in 50 mM Tris buffer (pH = 7.4). (b) Nonlinear least squares fitting of the emission intensity of compound **2** at 460 nm to a 1:1 binding isotherm. The data correspond to entry 6 in Table 1.

(a) (b) (c)

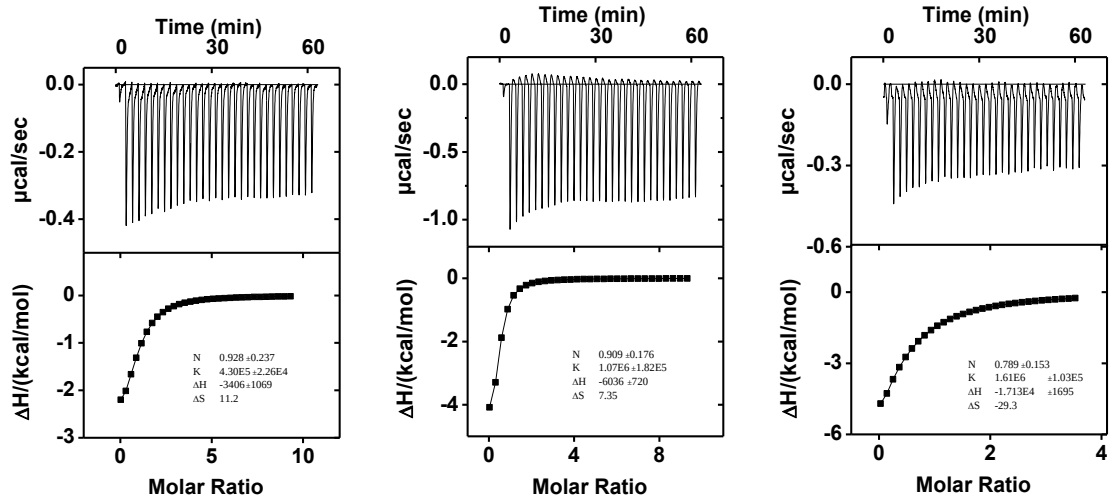

Figure 11S. ITC titration curves obtained at 298 K for the titration of 10 µM of (a) $MINP_5$(**1**) with 0 equiv FM **9**, (b) $MINP_5$(**1**) with 1 equiv FM **9** (1:1), and (c) $MINP_5$(**1**) with 3 equiv FM **9** (1:3) by compound **1** (0.2 mM) in 50 mM Tris buffer (pH = 7.4). The data correspond to entries 1, 2, 4 in Table 1, respectively.

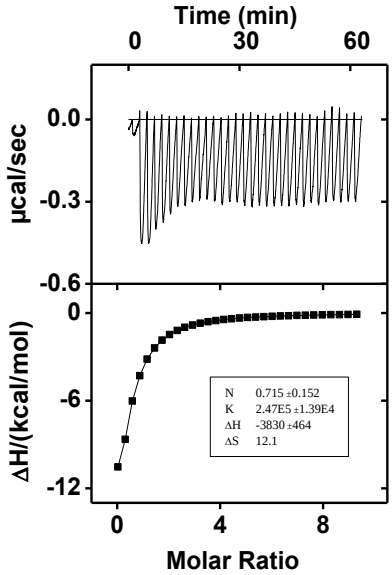

Figure 12S. ITC titration curves obtained at 298 K for the titration of 10 µM of $MINP_8$(**1**) with 2 equiv FM **9** (1:2) by compound **1** (0.2 mM) in 50 mM Tris buffer (pH = 7.4). The data correspond to entries 5 in Table 1.

(a) (b) (c)

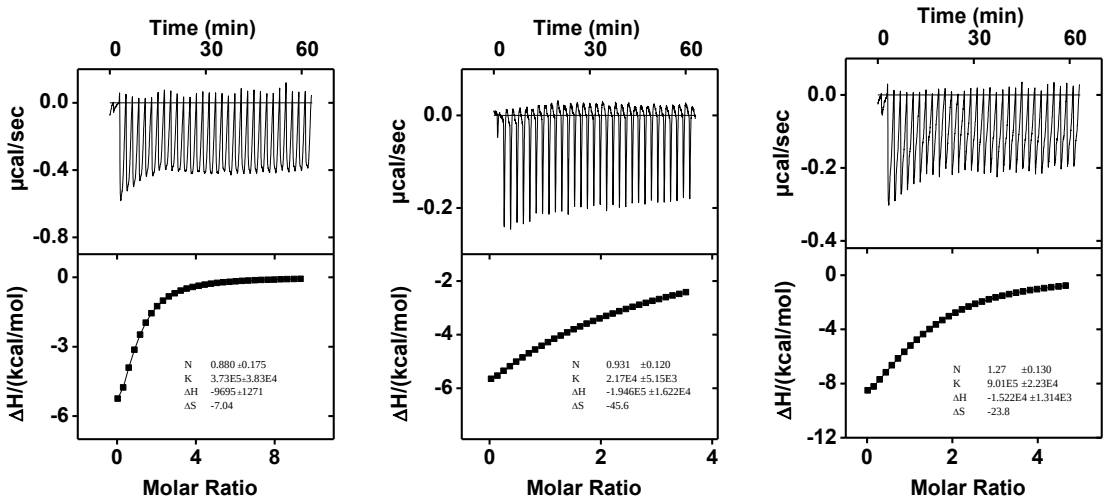

Figure 13S. ITC titration curves obtained at 298 K for the titration of 10 µM of $MINP_1$(**2**) with 2 equiv FM **9** (1:2) by compound **2** (0.2 mM), compound **3** (0.2 mM), and compound **4** (0.2 mM) in 50 mM Tris buffer (pH = 7.4). The data correspond to entries 6, 7, 8 in Table 1.

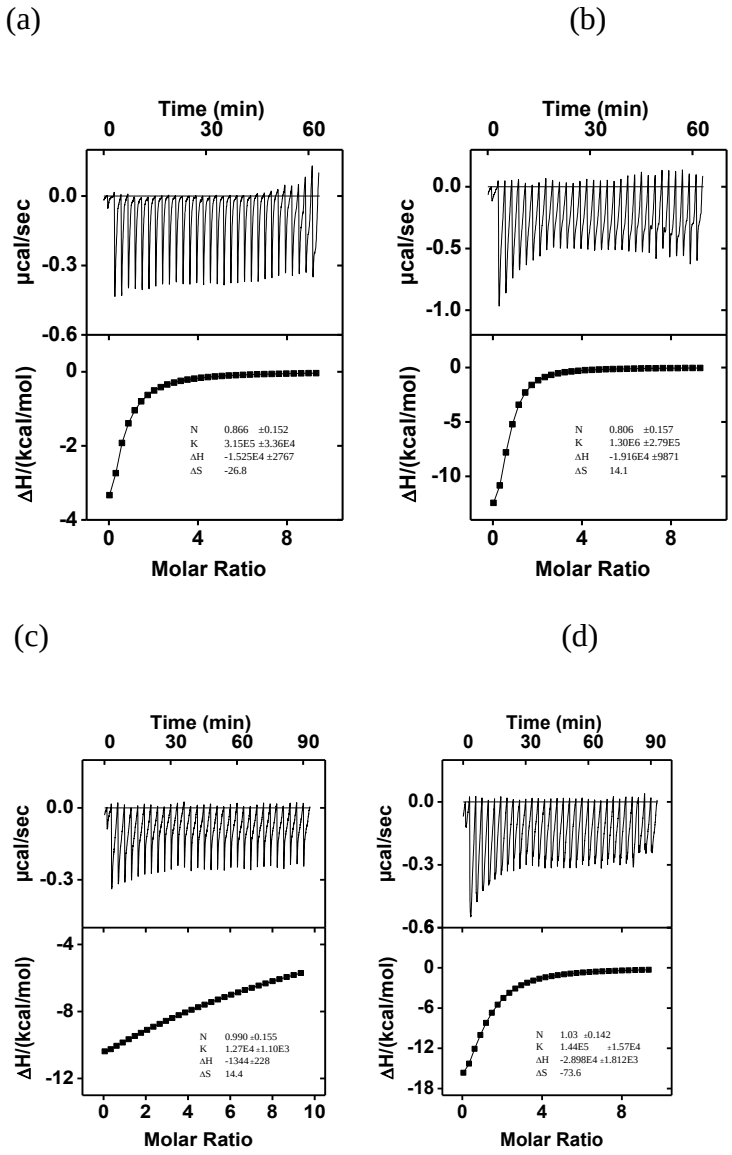

Figure 14S. ITC titration curves obtained at 298 K for the titration of 10 µM of $MINP_5$(**2**) with 2 equiv FM **9** (1:2) by compound **1** (0.2 mM), compound **2** (0.2 mM), compound **3** (0.2 mM), and compound **4** (0.2 mM) in 50 mM Tris buffer (pH = 7.4). The data correspond to entries 9, 10, 11, 12 in Table 1.

Notes and References

(1) Atwood, J. L.; Lehn, J. M.: *Comprehensive Supramolecular Chemistry*; Pergamon: New York, 1996.

(2) Steed, J. W.; Gale, P. A.: *Supramolecular Chemistry: From Molecules to Nanomaterials*; Wiley: Weinheim, 2012.

(3) Juwarker, H.; Suk, J. M.; Jeong, K. S. Foldamers with Helical Cavities for Binding Complementary Guests. *Chem. Soc. Rev.* **2009**, *38*, 3316-3325.

(4) Hua, Y.; Liu, Y.; Chen, C.-H.; Flood, A. H. Hydrophobic Collapse of Foldamer Capsules Drives Picomolar-Level Chloride Binding in Aqueous Acetonitrile Solutions. *J. Am. Chem. Soc.* **2013**, *135*, 14401-14412.

(5) Gan, Q. A.; Ferrand, Y.; Bao, C. Y.; Kauffmann, B.; Grelard, A.; Jiang, H.; Huc, I. Helix-Rod Host-Guest Complexes with Shuttling Rates Much Faster Than Disassembly. *Science* **2011**, *331*, 1172-1175.

(6) Zhao, Y.; Zhong, Z. Tuning the Sensitivity of a Foldamer-Based Mercury Sensor by Its Folding Energy. *J. Am. Chem. Soc.* **2006**, *128*, 9988-9989.

(7) Hou, J. L.; Shao, X. B.; Chen, G. J.; Zhou, Y. X.; Jiang, X. K.; Li, Z. T. Hydrogen Bonded Oligohydrazide Foldamers and Their Recognition for Saccharides. *J. Am. Chem. Soc.* **2004**, *126*, 12386-12394.

(8) Zhong, Z.; Li, X.; Zhao, Y. Enhancing Binding Affinity by the Cooperativity between Host Conformation and Host–Guest Interactions. *J. Am. Chem. Soc.* **2011**, *133*, 8862-8865.

(9) Zhao, Y. Cooperatively Enhanced Receptors for Biomimetic Molecular Recognition. *ChemPhysChem* **2013**, *14*, 3878-3885.

(10) Oshovsky, G. V.; Reinhoudt, D. N.; Verboom, W. Supramolecular Chemistry in Water. *Angew. Chem. Int. Ed.* **2007**, *46*, 2366-2393.

(11) Kataev, E. A.; Müller, C. Recent Advances in Molecular Recognition in Water: Artificial Receptors and Supramolecular Catalysis. *Tetrahedron* **2014**, *70*, 137-167.

(12) Wulff, G. Molecular Imprinting in Cross-Linked Materials with the Aid of Molecular Templates— a Way Towards Artificial Antibodies. *Angew. Chem. Int. Ed. Engl.* **1995**, *34*, 1812-1832.

(13) Wulff, G. Enzyme-Like Catalysis by Molecularly Imprinted Polymers. *Chem. Rev.* **2001**, *102*, 1-28.

(14) Haupt, K.; Mosbach, K. Molecularly Imprinted Polymers and Their Use in Biomimetic Sensors. *Chem. Rev.* **2000**, *100*, 2495-2504.

(15) Ye, L.; Mosbach, K. Molecular Imprinting: Synthetic Materials as Substitutes for Biological Antibodies and Receptors. *Chem. Mater.* **2008**, *20*, 859-868.

(16) Shea, K. J. Molecular Imprinting of Synthetic Network Polymers: The De Novo Synthesis of Macromolecular Binding and Catalytic Sites. *Trends Polym. Sci.* **1994**, *2*, 166-173.

(17) Sellergren, B.: *Molecularly Imprinted Polymers: Man-Made Mimics of Antibodies and Their Applications in Analytical Chemistry*; Elsevier: Amsterdam, 2001.

(18) Komiyama, M.: *Molecular Imprinting: From Fundamentals to Applications*; Wiley-VCH: Weinheim, 2003.

(19) Yan, M.; Ramström, O.: *Molecularly Imprinted Materials: Science and Technology*; Marcel Dekker: New York, 2005.

(20) Alexander, C.; Andersson, H. S.; Andersson, L. I.; Ansell, R. J.; Kirsch, N.; Nicholls, I. A.; O'Mahony, J.; Whitcombe, M. J. Molecular Imprinting Science and Technology: A Survey of the Literature for the Years up to and Including 2003. *J. Mol. Recognit.* **2006**, *19*, 106-180.

(21) Sellergren, B.; Hall, A. J.: Molecularly Imprinted Polymers. In *Supramolecular Chemistry: From Molecules to Nanomaterials*; Steed, J. W., Gale, P. A., Eds.; Wiley: Online, 2012.

(22) Haupt, K.: *Molecular Imprinting*; Springer: Heidelberg ; New York, 2012.

(23) Zimmerman, S. C.; Wendland, M. S.; Rakow, N. A.; Zharov, I.; Suslick, K. S. Synthetic Hosts by Monomolecular Imprinting inside Dendrimers. *Nature* **2002**, *418*, 399-403.

(24) Zimmerman, S. C.; Zharov, I.; Wendland, M. S.; Rakow, N. A.; Suslick, K. S. Molecular Imprinting inside Dendrimers. *J. Am. Chem. Soc.* **2003**, *125*, 13504-13518.

(25) Li, Z.; Ding, J.; Day, M.; Tao, Y. Molecularly Imprinted Polymeric Nanospheres by Diblock Copolymer Self-Assembly. *Macromolecules* **2006**, *39*, 2629-2636.

(26) Hoshino, Y.; Kodama, T.; Okahata, Y.; Shea, K. J. Peptide Imprinted Polymer Nanoparticles: A Plastic Antibody. *J. Am. Chem. Soc.* **2008**, *130*, 15242-15243.

(27) Priego-Capote, F.; Ye, L.; Shakil, S.; Shamsi, S. A.; Nilsson, S. Monoclonal Behavior of Molecularly Imprinted Polymer Nanoparticles in Capillary Electrochromatography. *Anal. Chem.* **2008**, *80*, 2881-2887.

(28) Cutivet, A.; Schembri, C.; Kovensky, J.; Haupt, K. Molecularly Imprinted Microgels as Enzyme Inhibitors. *J. Am. Chem. Soc.* **2009**, *131*, 14699-14702.

(29) Yang, K. G.; Berg, M. M.; Zhao, C. S.; Ye, L. One-Pot Synthesis of Hydrophilic Molecularly Imprinted Nanoparticles. *Macromolecules* **2009**, *42*, 8739-8746.

(30) Zeng, Z. Y.; Patel, J.; Lee, S. H.; McCallum, M.; Tyagi, A.; Yan, M. D.; Shea, K. J. Synthetic Polymer Nanoparticle-Polysaccharide Interactions: A Systematic Study. *J. Am. Chem. Soc.* **2012**, *134*, 2681-2690.

(31) Ma, Y.; Pan, G. Q.; Zhang, Y.; Guo, X. Z.; Zhang, H. Q. Narrowly Dispersed Hydrophilic Molecularly Imprinted Polymer Nanoparticles for Efficient Molecular Recognition in Real Aqueous Samples Including River Water, Milk, and Bovine Serum. *Angew. Chem. Int. Ed.* **2013**, *52*, 1511-1514.

(32) Zhang, Y.; Deng, C.; Liu, S.; Wu, J.; Chen, Z.; Li, C.; Lu, W. Active Targeting of Tumors through Conformational Epitope Imprinting. *Angew. Chem. Int. Ed.* **2015**, *54*, 5157-5160.

(33) Biffis, A.; Graham, N. B.; Siedlaczek, G.; Stalberg, S.; Wulff, G. The Synthesis, Characterization and Molecular Recognition Properties of Imprinted Microgels. *Macromol. Chem. Phys.* **2001**, *202*, 163-171.

(34) Maddock, S. C.; Pasetto, P.; Resmini, M. Novel Imprinted Soluble Microgels with Hydrolytic Catalytic Activity. *Chem. Commun.* **2004**, 536-537.

(35) Wulff, G.; Chong, B. O.; Kolb, U. Soluble Single-Molecule Nanogels of Controlled Structure as a Matrix for Efficient Artificial Enzymes. *Angew. Chem. Int. Ed.* **2006**, *45*, 2955-2958.

(36) Carboni, D.; Flavin, K.; Servant, A.; Gouverneur, V.; Resmini, M. The First Example of Molecularly Imprinted Nanogels with Aldolase Type I Activity. *Chem. -Eur. J.* **2008**, *14*, 7059-7065.

(37) Servant, A.; Haupt, K.; Resmini, M. Tuning Molecular Recognition in Water-Soluble Nanogels with Enzyme-Like Activity for the Kemp Elimination. *Chem.-Eur. J.* **2011**, *17*, 11052-11059.

(38) Çakir, P.; Cutivet, A.; Resmini, M.; Bui, B. T.; Haupt, K. Protein-Size Molecularly Imprinted Polymer Nanogels as Synthetic Antibodies, by Localized Polymerization with Multi-Initiators. *Adv. Mater.* **2013**, *25*, 1048-1051.

(39) Chen, C.; Ke, J. Y.; Zhou, X. E.; Yi, W.; Brunzelle, J. S.; Li, J.; Yong, E. L.; Xu, H. E.; Melcher, K. Structural Basis for Molecular Recognition of Folic Acid by Folate Receptors. *Nature* **2013**, *500*, 486-+.

(40) Sudimack, J.; Lee, R. J. Targeted Drug Delivery Via the Folate Receptor. *Adv. Drug Deliv. Rev.* **2000**, *41*, 147-162.

(41) Low, P. S.; Henne, W. A.; Doorneweerd, D. D. Discovery and Development of Folic-Acid-Based Receptor Targeting for Imaging and Therapy of Cancer and Inflammatory Diseases. *Acc. Chem. Res.* **2008**, *41*, 120-129.

(42) Quaglia, M.; Chenon, K.; Hall, A. J.; De Lorenzi, E.; Sellergren, B. Target Analogue Imprinted Polymers with Affinity for Folic Acid and Related Compounds. *J. Am. Chem. Soc.* **2001**, *123*, 2146-2154.

(43) Hall, A. J.; Quaglia, M.; Manesiotis, P.; De Lorenzi, E.; Sellergren, B. Polymeric Receptors for the Recognition of Folic Acid and Related Compounds Via Substructure Imprinting. *Anal. Chem.* **2006**, *78*, 8362-8367.

(44) Prasad, B. B.; Tiwari, M. P.; Madhuri, R.; Sharma, P. S. Development of a Highly Sensitive and Selective Hyphenated Technique (Molecularly Imprinted Micro-Solid Phase Extraction Fiber–Molecularly Imprinted Polymer Fiber Sensor) for Ultratrace Analysis of Folic Acid. *Anal. Chim. Acta* **2010**, *662*, 14-22.

(45) Quiñonero, D.; López, K. A.; Deyà, P. M.; Piña, M. N.; Morey, J. Synthetic Tripodal Squaramido-Based Receptors for the Complexation of Antineoplastic Folates in Water (Eur. J. Org. Chem. 31/2011). *Eur J Org Chem* **2011**, *2011*, n/a-n/a.

(46) de Oliveira, F. M.; Segatelli, M. G.; Tarley, C. R. T. Evaluation of a New Water-Compatible Hybrid Molecularly Imprinted Polymer Combined with Restricted Access

for the Selective Recognition of Folic Acid in Binding Assays. *J. Appl. Polym. Sci* **2016**, *133*, n/a-n/a.

(47) Cho, H.; Zhao, Y. Environmental Effects Dominate the Folding of Oligocholates in Solution, Surfactant Micelles, and Lipid Membranes. *J. Am. Chem. Soc.* **2010**, *132*, 9890-9899.

(48) Gunasekara, R. W.; Zhao, Y. Rationally Designed Cooperatively Enhanced Receptors to Magnify Host–Guest Binding in Water. *J. Am. Chem. Soc.* **2015**, *137*, 843-849.

(49) Gunasekara, R. W.; Zhao, Y. Enhancing Binding Affinity and Selectivity through Preorganization and Cooperative Enhancement of the Receptor. *Chem. Commun.* **2016**, *52*, 4345-4348.

(50) Arifuzzaman, M. D.; Zhao, Y. Water-Soluble Molecularly Imprinted Nanoparticle Receptors with Hydrogen-Bond-Assisted Hydrophobic Binding. *J. Org. Chem.* **2016**, *81*, 7518-7526.

(51) Awino, J. K.; Zhao, Y. Protein-Mimetic, Molecularly Imprinted Nanoparticles for Selective Binding of Bile Salt Derivatives in Water. *J. Am. Chem. Soc.* **2013**, *135*, 12552-12555.

(52) Fa, S.; Zhao, Y. Water-Soluble Nanoparticle Receptors Supramolecularly Coded for Acidic Peptides. *Chem. -Eur. J.* **2018**, *24*, 150-158.

(53) Wiseman, T.; Williston, S.; Brandts, J. F.; Lin, L. N. Rapid Measurement of Binding Constants and Heats of Binding Using a New Titration Calorimeter. *Anal. Biochem.* **1989**, *179*, 131-137.

(54) Jelesarov, I.; Bosshard, H. R. Isothermal Titration Calorimetry and Differential Scanning Calorimetry as Complementary Tools to Investigate the Energetics of Biomolecular Recognition. *J. Mol. Recognit.* **1999**, *12*, 3-18.

(55) Velazquez-Campoy, A.; Leavitt, S. A.; Freire, E. Characterization of Protein-Protein Interactions by Isothermal Titration Calorimetry. *Methods Mol. Biol.* **2004**, *261*, 35-54.

(56) Zhang, S.; Zhao, Y. Facile Synthesis of Multivalent Water-Soluble Organic Nanoparticles Via "Surface Clicking" of Alkynylated Surfactant Micelles. *Macromolecules* **2010**, *43*, 4020-4022.

(57) Peng, H.-Q.; Chen, Y.-Z.; Zhao, Y.; Yang, Q.-Z.; Wu, L.-Z.; Tung, C.-H.; Zhang, L.-P.; Tong, Q.-X. Artificial Light-Harvesting System Based on Multifunctional Surface-Cross-Linked Micelles. *Angew. Chem. Int. Ed.* **2012**, *51*, 2088-2092.

(58) Fa, S.; Zhao, Y. Peptide-Binding Nanoparticle Materials with Tailored Recognition Sites for Basic Peptides. *Chem. Mater.* **2017**, *29*, 9284-9291.

(59) Nowick, J. S.; Chen, J. S. Molecular Recognition in Aqueous Micellar Solution - Adenine Thymine Base-Pairing in Sds Micelles. *J. Am. Chem. Soc.* **1992**, *114*, 1107-1108.

(60) Nowick, J. S.; Chen, J. S.; Noronha, G. Molecular Recognition in Micelles - the Roles of Hydrogen-Bonding and Hydrophobicity in Adenine Thymine Base-Pairing in Sds Micelles. *J. Am. Chem. Soc.* **1993**, *115*, 7636-7644.

(61) Awino, J. K.; Zhao, Y. Water-Soluble Molecularly Imprinted Nanoparticles (Minps) with Tailored, Functionalized, Modifiable Binding Pockets. *Chem.-Eur. J.* **2015**, *21*, 655-661.

(62) Awino, J. K.; Hu, L.; Zhao, Y. Molecularly Responsive Binding through Co-Occupation of Binding Space: A Lock–Key Story. *Org. Lett.* **2016**, *18*, 1650-1653.

(63) Hannon, C. L.; Anslyn, E. V.: The Guanidinium Group: Its Biological Role; Synthetic Analogs. In *Bioorganic Chemistry Frontiers*; Dugas, H., Schmidtchen, F. P., Eds.; Springer: Heidelberg, 1993; pp 193-255.

(64) Schmidtchen, F. P.; Berger, M. Artificial Organic Host Molecules for Anions. *Chem. Rev.* **1997**, *97*, 1609-1646.

(65) Ariga, K.; Kunitake, T. Molecular Recognition at Air-Water and Related Interfaces: Complementary Hydrogen Bonding and Multisite Interaction. *Acc. Chem. Res.* **1998**, *31*, 371-378.

(66) Orner, B. P.; Hamilton, A. D. The Guanidinium Group in Molecular Recognition: Design and Synthetic Approaches. *J Incl Phenom Macro* **2001**, *41*, 141-147.

(67) Schmidtchen, F. P.: Isothermal Titration Calorimetry in Supramolecular Chemistry. In *Supramolecular Chemistry: From Molecules to Nanomaterials*; Steed, J. W., Gale, P. A., Eds.; Wiley: Online, 2012.

(68) Chen, L. X.; Xu, S. F.; Li, J. H. Recent Advances in Molecular Imprinting Technology: Current Status, Challenges and Highlighted Applications. *Chem. Soc. Rev.* **2011**, *40*, 2922-2942.

(69) Awino, J. K.; Zhao, Y. Polymeric Nanoparticle Receptors as Synthetic Antibodies for Nonsteroidal Anti-Inflammatory Drugs (Nsaids). *ACS Biomater. Sci. Eng.* **2015**, *1*, 425-430.

(70) Ball, P. Water as an Active Constituent in Cell Biology. *Chem. Rev.* **2008**, *108*, 74-108.

CHAPTER 4. SENSING OF NONSTEROIDAL ANTI-INFLAMMATORY DRUGS (NSAIDS) BY MOLECULARLY IMPRINTED NANOPARTICLES

Likun Duan[1], Yan Zhao[1]*

[1]Department of chemistry, Iowa State University, Ames, Iowa, 50011 United States

* Corresponding Authors

ABSTRACT. Nonsteroidal anti-inflammatory drugs (NSAIDs) are widely used over-the-counter drugs and their uncontrolled disposal is a significant environmental concern. Although their fluorescent sensing is a desirable method of detection for its sensitivity and simplicity, the structural similarity of the drugs makes the design of selective sensors highly challenging. A thiourea-based fluorescent functional monomer was identified in this work to enable highly efficient synthesis of molecularly imprinted nanoparticle (MINP) sensors for NSAIDs such as Indomethacin or Tolmetin. Micromolar binding affinities were obtained in aqueous solution, with binding selectivities comparable to those reported for polyclonal antibodies. The detection limit was ~50 ng/mL in aqueous solution, and common carboxylic acids such as acetic acid, benzoic acid, and citric acid showed negligible interference.

Introduction

Nonsteroidal anti-inflammatory drugs (NSAIDs) are the most commonly administered over-the-counter drugs to reduce pain, decrease fever, and control inflammation.[1] Due to their potential effects on different organisms, their wide usage and uncontrolled disposal are a significant environmental concern.[2,3] Although many NSAIDs are degraded by microorganisms

in soil, rate of degradation varies greatly depending on the types of soil and other environmental conditions.[4]

The important biological activity of NSAIDs and their environmental risks have motivated many researchers to develop sensitive methods for their detection and monitoring. Traditional analyses include electrophoresis[5] and liquid chromatography–mass spectrometry[6] but the sophisticated instruments utilized are inconvenient for rapid in-field monitoring. Recognition-based fluorescent sensing is a method of choice for its simplicity, high sensitivity, and ease of operation.[7-11] However, NSAIDs have very similar structures, with a carboxylic acid on a similarly sized hydrophobic aromatic moiety (Chart 1). The structural similarity represents a difficult challenge in the selective detection of these drugs by fluorescence,[12-14] and traditional macrocyclic supramolecular hosts such as cyclodextrins tend to bind NSAIDs nondisciminately.[15] The difficulty prompted researchers to explore alternative formats of sensing, such as arrays of sensors, which showed good promise.[16] Other choices include enzyme-linked immunosorbent assays (ELISA),[17,18] but the structural similarity even challenges antibodies which are known for their highly specific binding.[17]

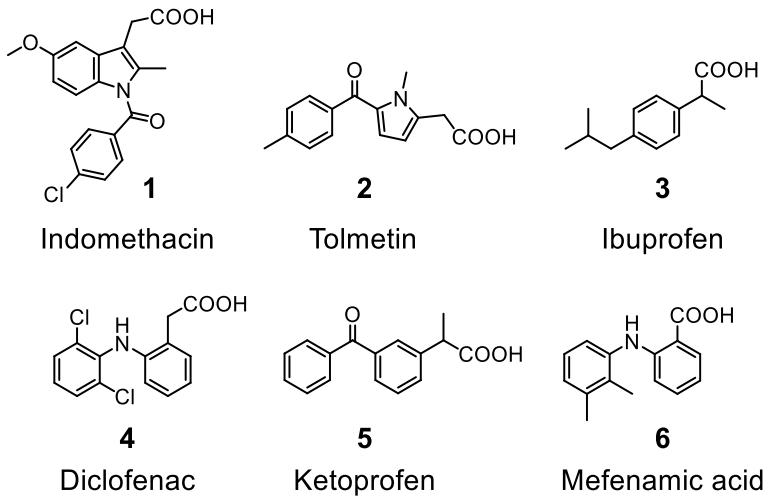

Chart 1. Structures of common NSAIDs.

One way to prepare a receptor for a target analyte is through molecular imprinting.[19,20] The technique uses the analyte (or a surrogate) as the template and, through templated polymerization, creates analyte-complementary binding sites in a highly cross-linked polymer network. Molecularly imprinted polymers (MIPs) have been referred to as "plastic antibodies" and found numerous applications.[21-30] Indeed, MIPs generated for NSAIDs displayed selective adoption of these drugs,[31-34] but their conversion into selective fluorescent sensors is hampered by the insolubility, heterogeneous distribution of binding sites, and other challenges associated with traditional MIPs.

Our group developed a method of molecular imprinting in doubly cross-linked micelles (Scheme 1).[35] The method involves first surface-crosslinking of micelle of **6** with diazide **7** using the click reaction and then core-cross-linking with divinylbenzene (DVB) using free-radical polymerization. The cross-linked micelles are also functionalized with a layer of hydrophilic ligand (i.e., **8**) for increased hydrophilicity and facile purification. The method can be applied to a wide range of small-molecule drugs,[35,36] peptides,[37] and carbohydrates.[38,39] The resulting molecularly imprinted nanoparticles (MINPs) showed strong abilities to distinguish closely related structures including leucine and isoleucine in peptides[37] and inversion of a single hydroxyl in oligosaccharides.[38,39] MINPs are ~5 nm in diameter, and mimic proteins in their nanosize, hydrophilic exterior, and hydrophobic core. The number of binding sites per MINP can be conveniently controlled by the surfactant/template ratio.

In this work, we report the design and synthesis of several fluorescent functional monomers (FMs) for selective NSAID detection. Structure of fluorophore was found to impact the sensing strongly, with minor variation in substitution pattern totally changing the behavior of the resulting sensor. One FM, containing a thiourea group bonded to a sulfonated 1,5-naphthalene

derivative, allowed highly selective binding of the drugs. Strong binding between the thiourea group of the FM and the carboxylic acid of NSAID helped the fluorescent probe reside near the imprinted binding site so that the guest binding was readily detected by fluorescent change.

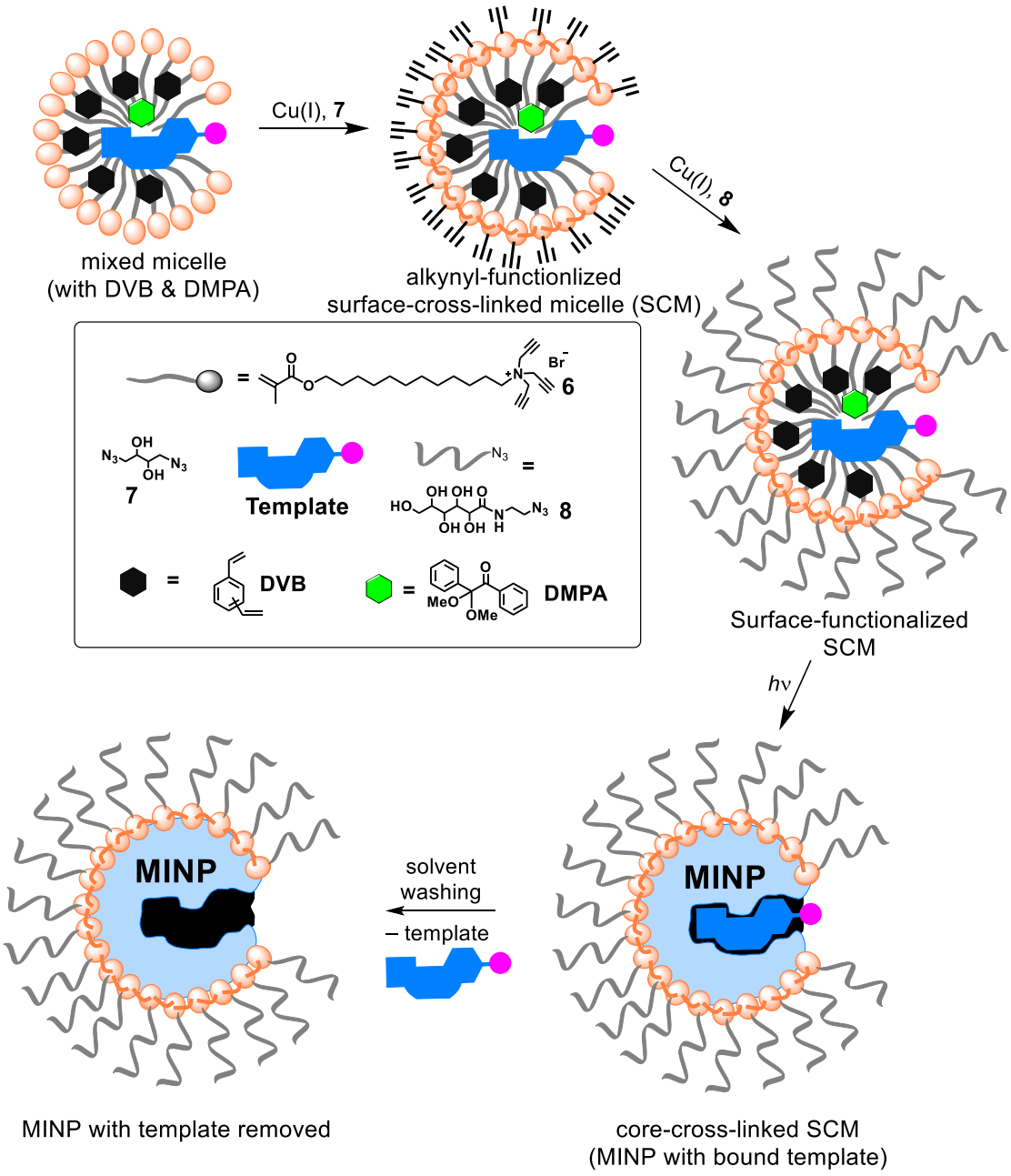

Scheme 1. Preparation of MINP by surface–core double cross-linking of template-containing micelle of **1**.

Results and Discussion

Design and Synthesis of Fluorescent Functional Monomers to Bind Carboxylates. Molecular imprinting can be very effective at creating template-specific binding sites in a polymer network. To create a fluorescent sensor for NSAIDs, however, we need to not only have a strong and selective binding for the drug but also convert the binding into an easy-to-detect fluorescent signal.[31-34,36] Our strategy is to employ a functional monomer containing an environmentally sensitive fluorophore and a strong carboxylate-binding moiety in close proximity.[40] In addition, highly specific, strong binding must exist between the FM and the NSAID drug so that the fluorophore will stay near the imprinted site.

Compounds **9**–**12** fit the above criteria. The FMs generally have a push–pull fluorophore known to be highly sensitive to its microenvironment, based on either the amino-nitrobenzoxadiazole (amino-NBD) or aminonaphalenesulfonate (ANS) framework. All compounds have at least one polymerizable vinyl group from a methacrylate, methacrylamide, or styrene. All have a reasonable level of hydrophobicity for their facile incorporation into of micelle for the MINP preparation. FM **9** has a guanidinium cation to bind a carboxylate through a hydrogen-bond-reinforced salt bridge. FMs **10**–**12** employ either a urea or thiourea group to form double hydrogen bonds with a carboxylate. In all cases, the carboxylate-binding moiety is adjacent to the fluorophore, in the hope that the binding would trigger a noticeable change in the latter's emission. Although hydrogen-bonds are weakened by strong solvent competition in aqueous solution, they are known to become much stronger in the hydrophobic core of micelles[41,42] and at the surfactant/water interface.[43]

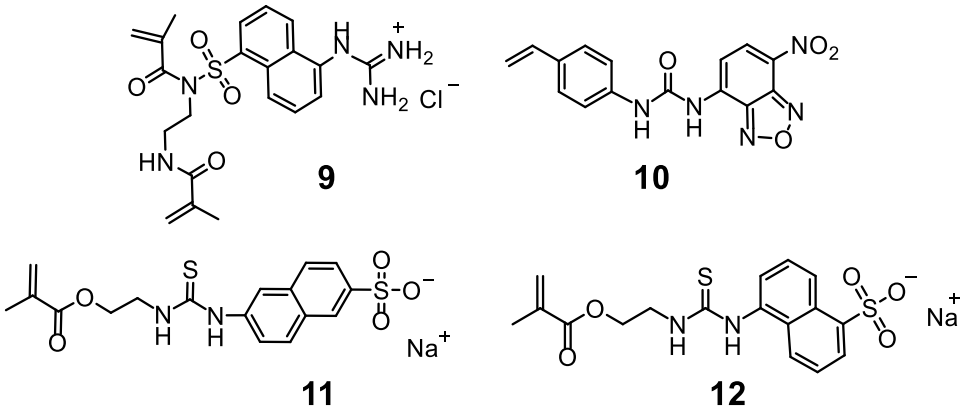

Table 1. Binding constants between carboxylate guests and FM **9**–**12** in CTAB solution.[a]

entry	FM	guest	K_a (10^3 M^{-1})
1	**9**	sodium acetate	-[b]
2	**9**	sodium butyrate	-[b]
3	**9**	sodium octanoate	-[b]
4	**10**	sodium acetate	0.016 ± 0.3
5	**10**	sodium butyrate	0.34 ± 0.05
6	**10**	sodium octanoate	3.01 ± 0.26
7	**11**	sodium acetate	0.17 ± 0.06
8	**11**	sodium butyrate	0.49 ± 0.04
9	**11**	sodium octanoate	1.51 ± 0.14
10	**12**	sodium acetate	0.18 ± 0.06
11	**12**	sodium butyrate	0.78 ± 0.23
12	**12**	sodium octanoate	5.18 ± 0.12

[a] The binding constants were obtained from fluorescence titrations performed in duplicates in 2 mM CTAB solution. [FM] = 2.0 μM. [b] Binding constant could not be obtained because of weak emission of the fluorophore.

To test the suitability of these compounds as fluorescent FMs for NSAID sensing, we first studied their binding of simple carboxylates in a micellar solution of CTAB (cetyl trimethylammonium bromide) (Table 1). The cationic surfactant is commercially available and mimics **6** without any concerns of polymerization. We evaluated the binding with sodium acetate, butyrate, and octanoate, respectively, with the expectation that a more hydrophobic carboxylate would have a stronger driving force to enter the micelle and display an enhanced binding. As mentioned above, a successful fluorescent sensor could only be obtained if the fluorescent FM stayed near the template during polymerization/cross-linking. A strong binding between the FM and the template in the aqueous micellar solution thus is a prerequisite.

In our hands, the emission of **9** in CTAB solution was very weak and showed little response to the addition of the carboxylate salts. Meanwhile, even though the emission of **10** was quenched strongly by the carboxylates and good binding properties were obtained (Table 1, entries 4–6), the solubility of the molecule in micellar solutions, whether of CTAB or **6**, was very low. The poor solubility made **10** unsuitable as a FM because our previous studies showed that MINP prepared with **6** as the cross-linkable surfactant contained ~50 cross-linked surfactants. For typical MINPs, we want to reach at least 1:50 for the FM/surfactant ratio, so that the final MINP will have an average of one binding site per nanoparticle.[35]

We suspected that the poor solubility of **10** was caused by strong intermolecular interactions among the molecules as a result of the neutral, relatively rigid structure. In addition, a urea group has an excellent hydrogen-bond acceptor (carbonyl) and two good hydrogen-bond donors (NH), making self-association of the FM very strong. In view of these challenges, we designed and synthesized **11** and **12**, which had a more flexible structure, an anionic sulfonate group, and

a thiourea instead. Without a strong hydrogen-bond acceptor, thioureas tend to self-associate much weakly than ureas.

Both **11** and **12**, to our delight, were easily incorporated into micelles and were actually soluble in water themselves. In addition, they both bound the carboxylates, exhibiting larger bonding constants (K_a) with an increase in the hydrocarbon chain length of the guest (Table 1, entries 7–12). The submillimolar binding affinities suggest, under typical MINP preparation conditions (i.e., 10 mM of **6** and 0.2 mM of FM), a substantial amount of the carboxylate guest will be complexed with the FM.[44] Upon further screening, compound **11** was rejected because its resulting MINP displayed very little fluorescence response to the template. Fortunately, compound **12**, with a simple change of substitution pattern from 2,6- to 1,5 on the naphthalene ring, showed strong binding for hydrophobic carboxylates in the CTAB micelle (Table 1, entries 10–12) and the resulting MINP also worked well (vide infra).

Fluorescent MINPs for Indomethacin (1). Our initial NSAID target was Indomethacin (**1**). Not only is this drug commonly used to treat osteoarthritis and rheumatoid arthritis, the COX-2 inhibitor has been used to construct fluorescent probes to target the Golgi apparatus of cancer cells.[45] Preparation of MINP(**1**), i.e., MINP prepared with Indomethacin (**1**) as the template, follows previously reported procedures and is described in the Experimental Section. The surface- and core-cross-linking of the micelle was monitored by ^{1}H NMR spectroscopy. The surface-cross-linking chemistry had been confirmed by mass spectrometry previously.[46] The micelles underwent characteristic changes in size during the surface-cross-linking, surface-functionalization, and core-cross-linking, and could be monitored by dynamic light scattering (DLS). The DLS size had been confirmed by transmission electron microscopy (TEM).[47,48]

Figure 1a shows the emission spectra of 2.0 μM MINP(**1**) in 50 mM Tris buffer (pH = 7.4) upon the addition of 0–10 μM Indomethacin. The MINP was prepared with a 2:1 ratio of FM/template. The emission maximum (λ_{em}) for the MINP occurred at 414 nm. The number was significantly shifted to the blue than the value in CTAB solution, 430 nm (Figure S15). This is in agreement with the common behavior of ANS-based fluorophores that tend to emit at a shorter wavelength in a less polar environment.[49] A CTAB micelle is highly dynamic. FM **12** in the uncross-linked micelle thus had a much higher chance to be exposed to water than in the doubly cross-linked MINP.[50]

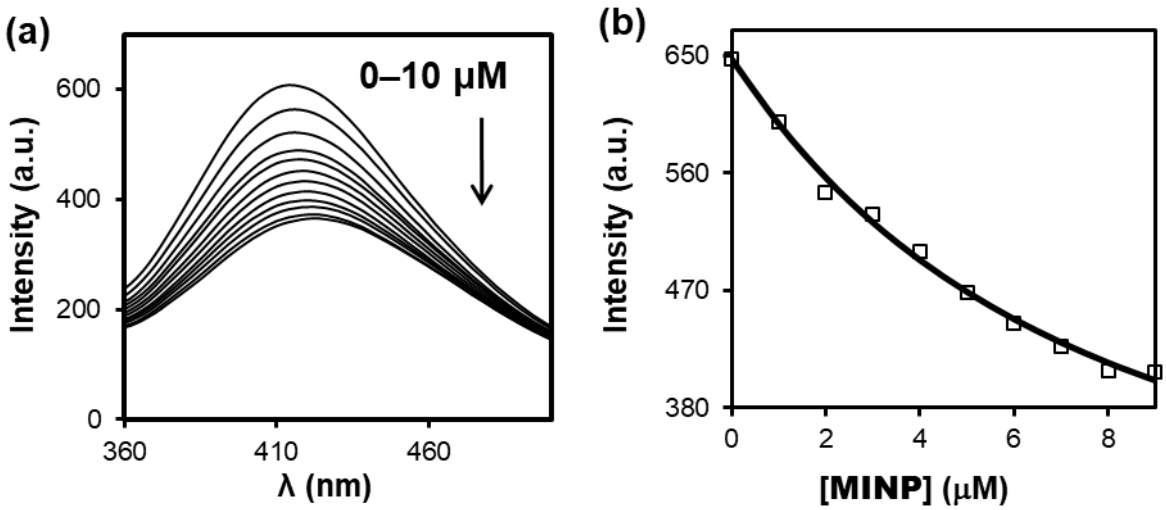

Figure 1. (a) Emission spectra of MINP(**1**) in 50 mM Tris buffer (pH = 7.4) upon the addition of different concentrations of **1**. The MINP was prepared with a 2:1 FM/template ratio. λ_{ex} = 310nm. [MINP(**1**)] = 2.0 μM. The concentration of MINP was calculated based on a M.W. of 49300 g/mol determined by DLS. (b) Nonlinear least squares fitting of the emission intensity of MINP(**1**) at 414 nm to a 1:1 binding isotherm.

The addition of 0–10 μM Indomethacin caused significant quenching of the MINP's emission. Meanwhile, a small red shift was observed during the titration. As shown in Figure

1b, the emission intensity at 414 nm fit nearly perfectly to a 1:1 binding isotherm, affording a binding constant of $K_a = (1.68 \pm 0.20) \times 10^5\ M^{-1}$. This value was substantially higher than those observed between FM **12** and octanoate in CTAB micelles ($5.18 \times 10^3\ M^{-1}$). Although the two guests have a different hydrophobe, the nearly 30-times stronger binding in MINP suggests that an imprinted micelle did provide a better binding environment to the guest than the generic nonpolar core of a CTAB micelle.

An important parameter to optimize is the ratio of FM/template in the MINP preparation. Too small an amount of the FM would leave many templates uncomplexed during cross-linking and polymerization. Although imprinted sites would form under such a situation, the binding pocket would not have a nearby fluorescent group to report the binding. Too large an amount of the FM during the MINP preparation, on the other hand, would incorporate many polymerized fluorophores in the MINPs without a nearby binding site for the guest. Neither situation is desirable.

To identify the optimal FM/T ratio, we prepared MINPs with **1** as the template and 1, 2, and 3 equivalents of FM **12**. We then measured the K_a values for not only the template itself, but also two other NSAIDs, Tolmetin (**2**) and Ibuprofen (**3**). We wanted to the know the best FM/T ratio for both the binding affinity and selectivity.

As shown by entries 1 and 4 of Table 2, the binding constant of MINP(**1**) for the template more than doubled from 79×10^3 to $168 \times 10^3\ M^{-1}$ when the FM/T ratio increased from 1:1 to 2:1. However, a further increase of the FM in the preparation reversed the trend and afforded a binding constant of $120 \times 10^3\ M^{-1}$ (entry 14). Meanwhile, the binding selectivity displayed a

Table 2. Binding constants of MINP(**1**) prepared with different FM/T ratios for NSAIDs and selected small-molecule acids.[a]

entry	FM/T ratio	guest	K_a (10^3 M^{-1})	CRR[b]
1	1:1	Indomethacin (**1**)	79 ± 0.3	1
2	1:1	Tolmetin (**2**)	14 ± 2	0.18
3	1:1	Ibuprofen (**3**)	0.7 ± 0.3	0.01
4	2:1	Indomethacin (**1**)	168 ± 20	1
5	2:1	Tolmetin (**2**)	22 ± 3	0.13
6	2:1	Ibuprofen (**3**)	1.1 ± 0.3	0.01
7	2:1	Diclofenac (**4**)	5.1 ± 0.5	0.03
8	2:1	Ketoprofen (**5**)	15 ± 0.1	0.12
9	2:1	Mefenamic acid (**6**)	4.7 ± 0.6	0.03
10	2:1	acetic acid	0.3 ± 0.1	0.002
11	2:1	butyric acid	0.1 ± 0.1	0.0006
12	2:1	benzoic acid	0.3 ± 0.2	0.002
13	2:1	citric acid	0.2 ± 0.1	0.001
14	3:1	Indomethacin (**1**)	120 ± 27	1
15	3:1	Tolmetin (**2**)	25 ± 4	0.21
16	3:1	Ibuprofen (**3**)	1.2 ± 0.1	0.01

[a] The binding constants were obtained from fluorescence titrations performed in duplicates in 50 mM Tris buffer (pH = 7.4). λ_{ex} = 310 nm. [MINP(**1**)] = 2.0 μM. [b] CRR is the cross-reactivity ratio, defined as the binding constant of a guest relative to that of the template for a particular MINP.

similar trend, as measured by the cross-reactivity ratio (CRR), defined as the binding constant of a guest relative to that of the template for a particular MINP. Among the two analogues studied, Tolmetin (**2**) is more similar to Indomethacin (**1**) than Ibuprofen (**3**), in terms of both functionality and size. Indeed, the CRR for Tolmetin was 0.18, 0.13, and 0.21, respectively as the FM/T increased from 1 to 3. The absolute binding constant for Tolmetin was 14, 22, and 25 $\times 10^3$ M^{-1} for these MINPs (entries 2, 5, and 15). The data, thus, suggests that the 2:1 FM/T ratio gave the best selectivity for the template as a result of increasing the binding for the template more than it did for its structural analogue.

For the best MINP(**1**), we also measured its binding constant for all the other NSAIDs shown in Chart 1, as well as several carboxylic acids (acetic acid, butyric acid, and citric acid). Among the structural analogues, Tolmetin (**2**) and Ketoprofen (**5**) showed the highest cross reactivity (CRR = 0.13 and 0.12, respectively). The other three NSAIDs (Ibuprofen, Diclofenac, and Mefenamic acid) showed very little binding (CRR = 0.01–0.03).

Polyclonal antibodies have been generated and used in competitive ELISA assays for Indomethacin.[51] Tolmetin gave about 0.09 corss reactivity in the assay, slightly better than our 0.13. However, Dichlofenac displayed 0.09 cross-reactivity with the natural antibody but only 0.03 in our case. Thus, the selectivity of our synthetic antibody compares very favorably overall with that of natural polyclonal antibodies which require live animal and a much longter time to produce. As cross-linked polymeric nanoparticles, MINPs also have the benefit of tolerating high temperature,[35,52] organic solvent,[52] extreme pH,[53].

For MINP binding in water, hydrophobic interactions are known to contribute strongly.[35] Although these interactions are nonspecific in nature, complementarity can come from matching size and shape between the guest molecule and the imprinted site. Since we have a

strong carboxyl-binding thiourea in our MINP, complementarity in hydrogen bonds is also expected to be important.

Figure 2a gives a schematic representation of the binding of the template (Indomethacin) by MINP(**1**). Despite the simplistic comparison, the model does help to explain the binding data given in Table 2. Guests **2** and **5**, for example, gave the highest cross-reactivity (0.12–0.13) in binding among the five NSAID analogues. For comparison purposes, we colored the original template (**1**) red, as well as the substructures in the analogous drugs that resemble the original template. Tolmetin (**2**), as shown in Figure 2b, contains a pyrrole ring bonded to the α-carbon of the carboxyl. Although the methyl group is next to the pyrrole nitrogen in **1** and on the pyrrole nitrogen in **2**, the overall shape of the five-membered ring (including the methyl) and the *para*-substituted benzoyl group in the two compounds are very similar. The great structural resemblance suggests that, no matter how perfectly the binding site will be created for **1**, it will always bind **2**, albeit with a lower affinity due to the incomplete filling of the binding site.

The other guest that showed a high CRR value was Ketoprofen (**5**), shown in Figure 2e. The most obvious mismatch between the molecule and the template is the extra methyl group on the α-carbon of the carboxyl, shown in black. Although a phenyl instead of a pyrrole is bonded to the α-carbon in **5**, the *meta*-substituted benzoyl group was oriented similarly as that in **1**. Thus, the overall similarity of Ketoprofen was quite high to the template, consistent with the 0.12 CRR (Table 2, entry 8).

The guests that fit most poorly in the imprinted site were **4** and **6** (Figure 2d,f). Their carboxylic acid is directly bonded to the phenyl ring, without a methylene in between as in the template. In addition, the *ortho* substitution in the carboxyl-containing phenyl ring makes the

overall shape of these molecules very different from that of the template. Their weak binding, thus, was fully expected.

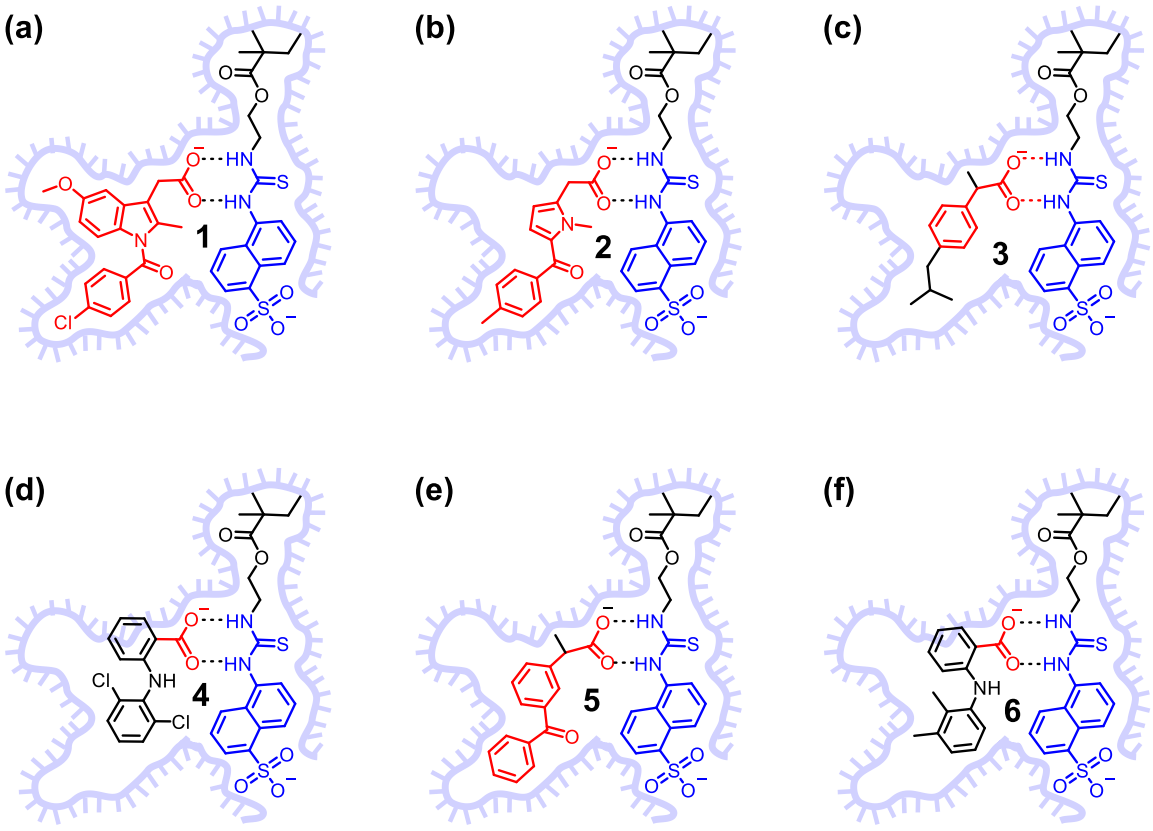

Figure 2. Schematic representation of the binding of **1**–**6** inside the binding site of MINP(**1**).

Ibuprofen (**3**) also displayed a very weak binding relative to the template, with a CRR of 0.01 (Table 2, entries 5–9). Given the reasonable level of similarity between **3** and **5**, we had not expected **3** to be so much worse a guest for MINP(**1**), since **5** was the best among the nonmatching NSAIDs. Nonetheless, there were several reasons that disfavored the binding of Ibuprofen: it contains an extra methyl on the α-carbon of the carboxyl; it is overall the smallest among the NSAIDs, with a single aromatic ring; its isobutyl group on the phenyl ring is located

on the *para* carbon, with respect to the carboxylic acid. It is possible that there were just too many mismatches and together they tipped the balance.

Finally, none of the other potentially interfering carboxylic acids showed any significant binding, including acetic acid, butyric acid, benzoic acid and citric acid (Table 2, entries 10–13).

Table 3. Binding constants of MINP(**2**) prepared with different FM/T ratios for NSAIDs and selected small-molecule acids.[a]

Entry	guest	K_a (10^3 M^{-1})	CRR[b]
1	Indomethacin (**1**)	8.9 ± 1.8	0.11
2	Tolmetin (**2**)	84 ± 17	1
3	Ibuprofen (**3**)	1.3 ± 0.3	0.02
4	Diclofenac (**4**)	5.4 ± 1.1	0.06
5	Ketoprofen (**5**)	19 ± 3	0.23
6	Mefenamic acid (**6**)	4.3 ± 0.5	0.05
7	acetic acid	0.3 ± 0.1	0.004
8	butyric acid	0.7 ± 0.2	0.008
9	benzoic acid	1.3 ± 0.4	0.02
10	citric acid	0.6 ± 0.1	0.007

[a] The binding constants were obtained from fluorescence titrations performed in duplicates in in 50 mM Tris buffer (pH = 7.4). λ_{ex} = 310 nm. [MINP(**2**)] = 2.0 μM. [b] CRR is the cross-reactivity ratio, defined as the binding constant of a guest relative to that of the template for a particular MINP.

To demonstrate the generality of our method, we also prepared MINP with Tolmetin (**2**) as the template. Table 2 summarizes its binding constants obtained for various guests. Consistent with successful imprinting, the MINP bound its template most strongly among the analogues. The binding constant (84×10^3 M^{-1}) was about half of that observed for **1** by MINP(**1**). This trend was reasonable, given the larger size of Indomethacin. It is well known that the strength of hydrophobic interactions is directly proportional to the area of hydrophobic surface being buried upon binding.[54] As long as the imprinted sites match their templates well, a larger template will have a stronger driving force to enter its imprinted site than a small template (to its own).

Table 1 shows that NSAID **2** and **5** showed the strongest cross-reactivities in the binding of MINP(**1**), suggesting these two drugs were more similar to each other than other NSAIDs examined in our work. Table 3 shows that, when **2** was used as the template, the drug that showed the strongest cross-reactivity was **5**, with a CRR of 0.23. Thus, both binding studies were able to classify NSAIDs according to their structural similarity.

The low CRR values for **4** and **6** are expected, given the *ortho* substitution and the direct connection of the carboxylic acid to the first phenyl ring (Table 3, entries 4 and 6). The weak binding of **3** was not surprising either (entry 3), considering the *para* substitution and the mismatched size. None of the other, non-NSAID carboxylic acids showed significant binding (entries 7–10)—also an expected result.

The most surprising result in Table 3 was the relative large cross-reactivity of Indomethacin (**1**) toward MINP(2), with CRR = 0.11 (Table 3, entry 1). We have found in multiple examples that larger guests could not enter imprinted sites created from smaller templates but smaller

guests can be bound by a larger imprinted site, with reduced affinity.[35,37,55] From this stand point, a weaker binding of **2** by MINP(**1**) was reasonable (Table 2, entry 2) but a weaker and yet significant binding of **1** by the MINP made with the much smaller template (**2**) did not make sense.

A plausible reason for the above abnormity comes from the depth of the imprinted binding site, which is formed through double cross-linking of the micelle (Scheme 1). However, the surface cross-linker used in the MINP preparation was diazide **2**, which has four methylene groups between the two azides. There are, therefore, many rotatable bonds in between two cross-linked ammonium headgroups, making the surface-cross-linking density quite low. The core-cross-linking, on the other hand, happens through radical polymerization of the methacrylate with nearly 50 DVB molecules in each micelle, and thus should have a considerably higher density. The template–FM complex formed by **12** with either **1** or **2** are quite polar, with an anionic sulfonate and another anionic carboxylate. Because polar and, especially, ionic groups have a strong need to be solvated by water on the surface of the micelle, the template–FM complex should be located near the surfactant/water interface and the imprinted site from the complex will also be quite close to the surface of the micelle. If this assumption is true, a higher plasticity of the binding site would be anticipated, due to the low surface-cross-linking density mentioned above. Nevertheless, both MINP(**1**) and MINP(**2**) displayed strong selectivities among most NSAIDs, especially toward **4** and **6**. Thus, it seems, even for a relatively flexible network, the imprinted site still has a good memory of the original template, so that guests more similar to the template are bound better than those that are more different.

Fluorescent Sensing of NSAIDs. Figure 3 shows the change of fluorescence intensity of MINP(**1**) by 10 μM of different acids in 50 mM Tris buffer (blue columns). The red columns are the responses of the nonimprinted nanoparticle (NINP), prepared with FM **12** but without any template. The imprinting effect was very strong in our MINP, as shown by the large difference in the responses of the imprinted versus nonimprinted sensor. The other acids all had a smaller effect on the emission intensity of MINP(**1**) and the responses seemed to largely follow the binding affinities. Table 2, for example, shows that Tolmetin (**2**) and Ketoprofen (**5**) gave the highest CRR for MINP(**1**) among the non-templating NSAIDs. In Figure 3, these two drugs also showed the largest responses, after the template itself. Fluorescent sensing was also performed with MINP(**2**). As shown by Figure 4, excellent selectivity was observed again for the templating drug, Tolmetin.

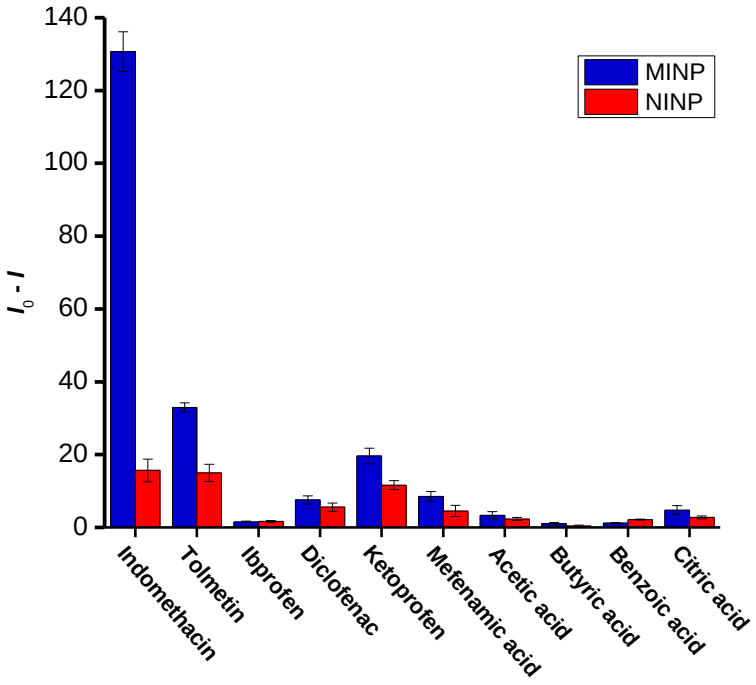

Figure 3. Change of fluorescence emission intensity of MINP(**1**) caused by different carboxylic acids in 50 mM Tris buffer (pH = 7.4). [MINP(**1**)] = 2.0 μM. [Acid] = 10 μM. λ_{ex} = 310 nm.

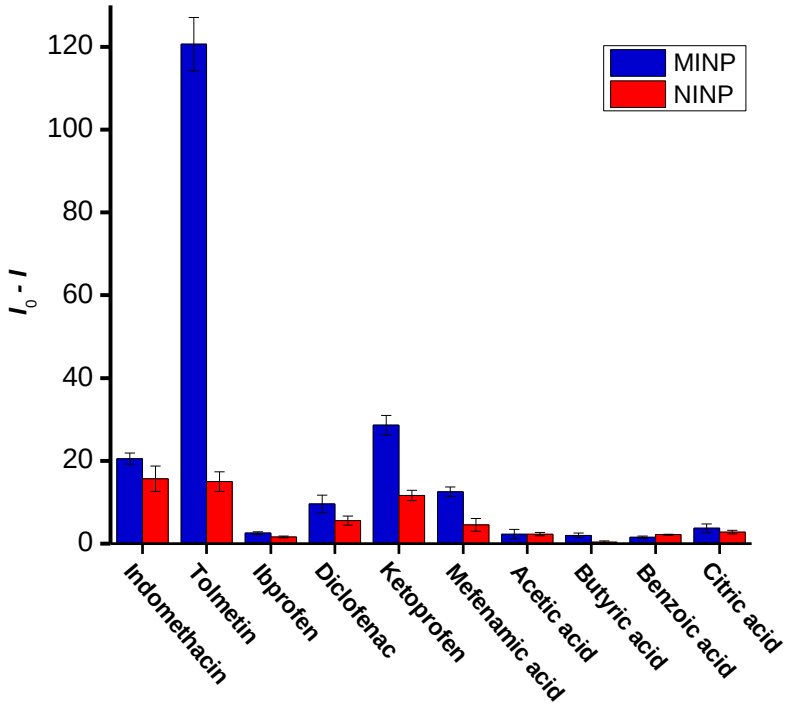

Figure 3. Change of fluorescence emission intensity of MINP(**2**) caused by different carboxylic acids in 50 mM Tris buffer (pH = 7.4). [MINP(**1**)] = 2.0 μM. [Acid] = 10 μM. λ_{ex} = 310 nm.

The strong binding of MINP(**1**) and MINP(**2**) for their targeted drugs suggestion the detection for Indomethacin and Tolmetin should be quite sensitive. To calculate the detection limit, we measured the emission intensity of 2.0 μM MINP(**1**) in the presence of 1–5 μM Indomethacin in 50 mM Tris buffer. The detection limit, calculated from 3δ/slope, was about 140 nM (Figure S41). The concentration translates to 50 ng/mL, a little over three times of what was reported for the antibody-based ELISA assay (15 ng/mL).[51] For Tolmetin, our detection limit was 200 nM or 51 ng/mL by MINP(**2**) (Figure S42).

Conclusions

The high structural similarity among NSAIDs makes it difficult even for natural antibodies to distinguish the drugs. The molecularly imprinted cross-linked micelles, nonetheless, displayed excellent abilities to bind and distinguish these drugs. The choice of fluorescent

functional monomer is highly important, with compound **12** being the only one useful among the four synthesized. Once the correct FM and all the other ingredients of MINPs are available, MINP-based fluorescent sensors can be prepared and purified in less than 2 days for different drugs. The binding studies showed that these sensors could bind the desired drug selectively among analogues and also classified the analogues based on their structural similarity to the original template. Fluorescent sensing could easily detect 100–200 nM or ~50 ng/mL of the drugs in water.

Acknowledgments

We thank NIGMS (R01GM113883) for financial support of this research

Experimental Section

General Method. Routine ^{1}H and ^{13}C NMR spectra were recorded on a 400 and 600 MHz NMR spectrometer. ESI-MS mass was recorded on Shimadzu LCMS-2010 mass spectrometer. Dynamic light scattering (DLS) data were recorded at 25 °C using PDDLS/CoolBatch 90T with PD2000DLS instrument. Isothermal titration calorimetry (ITC) was performed using a MicroCal VP-ITC Microcalorimeter with Origin 7 software and VPViewer2000 (GE Healthcare, Northampton, MA). Syntheses of compounds **6**–**8** were reported previously.[35] Syntheses of the fluorescent functional monomers (9–12) are reported in the Supporting Information (SI).

Preparation of MINPs and NINPs. A typical procedure is as follows.[35] To a micellar solution of compound **6** (10.2 mg, 0.02 mmol) in H_2O (2.0 mL), divinylbenzene (DVB, 2.8 μL, 0.02 mmol), compound **1** in H_2O (10 μL of a solution of 18.5 mg/mL, 0.0004 mmol), and 2,2-dimethoxy-2-phenylacetophenone (DMPA,10 μL of a 12.8 mg/mL solution in DMSO, 0.0005

mmol) were added. The mixture was subjected to ultrasonication for 10 min before compound **7** (4.13 mg, 0.024 mmol), $CuCl_2$ (10 μL of a 6.7 mg/mL solution in H_2O, 0.0005 mmol), and sodium ascorbate (10 μL of a 99 mg/mL solution in H_2O, 0.005 mmol) were added. After the reaction mixture was stirred slowly at room temperature for 12 h, compound **8** (10.6 mg, 0.04 mmol), $CuCl_2$ (10 μL of a 6.7 mg/mL solution in H_2O, 0.0005 mmol l), and sodium ascorbate (10 μL of a 99 mg/mL solution in H_2O, 0.005 mmol) were added. After being stirred for another 6 h at room temperature, the reaction mixture was transferred to a glass vial, purged with nitrogen for 15 min, sealed with a rubber stopper, and irradiated in a Rayonet reactor for 12 h. ^1H NMR spectroscopy was used to monitor the progress of reaction. The reaction mixture was poured into acetone (8 mL). The precipitate was collected by centrifugation and washed with a mixture of acetone/water (5 mL/1 mL) three times. The crude produce was washed by methanol/acetic acid (5 mL/0.1 mL) three times until the emission peak at 448 nm (for the dansyl) disappeared and then with excess methanol. The off white powder was dried in air to afford the final MINPs (16 mg, 80%). NINPs were prepared following similar procedures except no template was used.

Determination of Binding Constants by Fluorescence Titration. A typical procedure is as follows. A stock solution of the acid (200 μM) was prepared in 50 mM Tris buffer (pH = 7.4). Aliquots (2 μL) of the acid stock solution were added to 2.00 mL of MINP(**1**) solution (2.0 μM) in the same buffer. After each addition, the sample was allowed to sit for 1 min at room temperature before the fluorescence spectrum was collected. The excitation wavelength (λ_{ex}) was 370 nm. The excitation slit width was 10 nm, and the emission slit width was 10 nm. The binding constant was obtained by nonlinear least squares fitting of the emission intensity at 420 nm to 1:1 binding isotherm.

General Method

Routine ^{1}H and ^{13}C NMR spectra were recorded on a Bruker DRX-400, on a Bruker AV II 600 or on a Varian VXR-400 spectrometer. ESI-MS mass was recorded on Shimadzu LCMS-2010 mass spectrometer. Dynamic light scattering (DLS) data were recorded at 25 °C using PDDLS/ CoolBatch 90T with PD2000DLS instrument. Isothermal titration calorimetry (ITC) was performed using a MicroCal VP-ITC Microcalorimeter with Origin 7 software and VPViewer2000 (GE Healthcare, Northampton, MA).

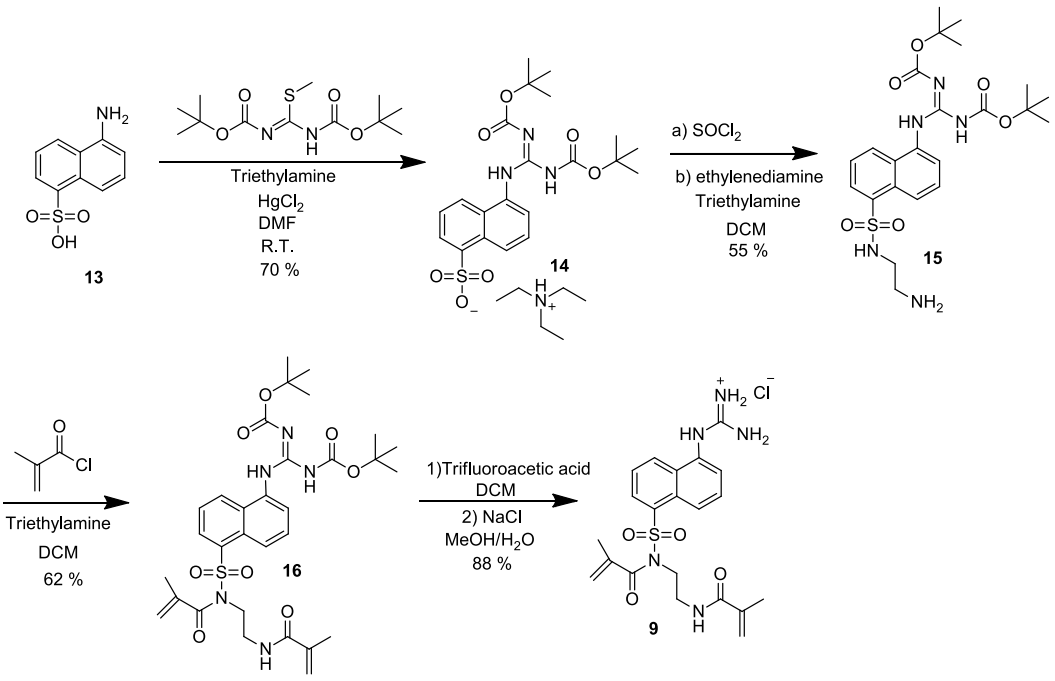

Scheme S1. *Syntheses of fluorescent functional monomer* ***9***

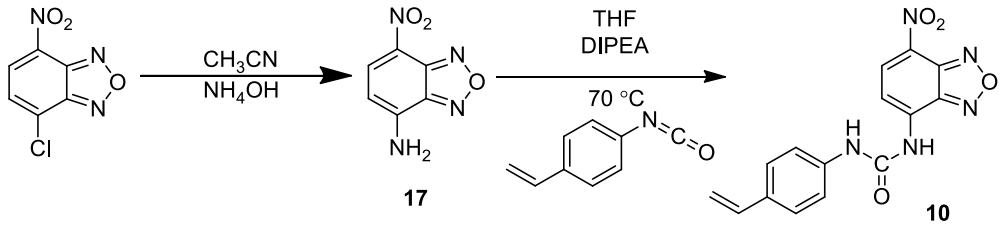

Scheme S2. *Syntheses of fluorescent functional monomer 10.*

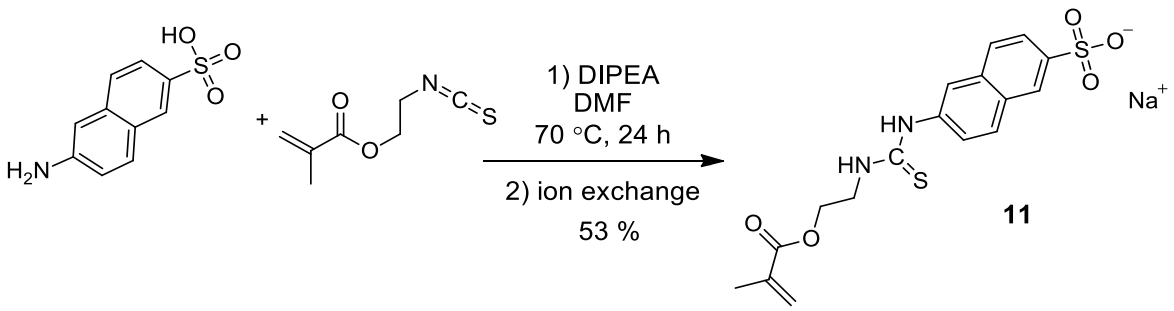

Scheme S3. *Syntheses of fluorescent functional monomer **11**.*

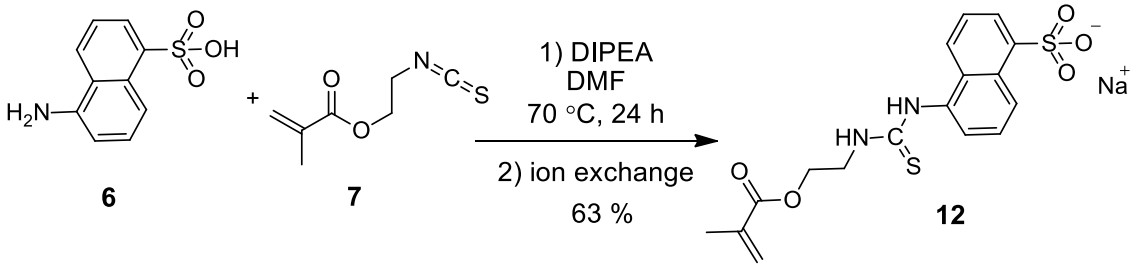

Scheme S4. *Syntheses of fluorescent functional monomer **12**.*

Syntheses

Compound 14. To a solution of 5-aminonaphthalene-1-sulfonic acid (0.223 g, 1 mmol) in anhydrous DMF(10 mL) was added 1,3-bis(tert-butoxycarbonyl)-2-methylthiopseudourea (0.75 g, 2.5 mmol), triethylamine (0.61 g, 6 mmol) and mercury chloride (0.68 g, 2.5 mmol). The suspension was stirred at room temperature overnight. The reaction mixture was diluted with CH_2Cl_2. The organic phase was washed with Na_2CO_3 solution, filtered through a pad of Celite, washed with water 3 times, dried over anhydrous Na_2SO_4, and concentrated by rotary evaporation. The residue was purified by column chromatography over silica gel using 10:1 CH_2Cl_2/MeOH as the eluent to give a light brown powder (0.39 g, 70%). ^{1}H NMR (400 MHz, CD_3OD, δ): 8.75 (d, J = 8.7 Hz, 1H), 8.13 (d, J = 7.2 Hz, 1H), 8.03 (m, 1H), 7.71 (s, 1H), 7.52

(m, 2H), 3.06 (q, *J* = 7.3 Hz, 6H), 1.64–1.22 (m, 18H), 1.22–1.12 (m, 9H). ^{13}C NMR (151 MHz, CD_3OD, δ) 163.4, 157.8, 141.7, 129.8, 129.6, 126.0, 125.7, 125.4, 125.0, 124.8, 124.8, 123.7, 53.8, 46.5, 27.3, 8.0. HRMS (ESI/QTOF) m/z: calcd for $C_{21}H_{28}N_3O_7S^+$ $[M + H - Et_3N]^+$ 466.1642, found 466.1652.

Compound 15. A catalytic amount of DMF was added to a solution of compound **14** (57 mg, 0.1 mmol) in 2 mL of thionyl chloride. After the mixture was stirred at room temperature for 3 h, thionyl chloride was removed by rotary evaporation. The residue was dissolved in 2 mL of anhydrous dichloromethane, followed by the addition of triethylamine (50 mg, 0.5 mmol). The above mixture was slowly added to a solution of ethylenediamine (60 mg, 1 mmol) dichloromethane at 0 °C. The ice bath was removed after 20 min and stirring was continued at room temperature for 3 h. After the solvent was removed by rotary evaporation, the residue was purified by column chromatography over silica gel using 10:1 CH_2Cl_2/MeOH as the eluent to give a light brown powder (28 mg, 55%). ^{1}H NMR (400 MHz, CD_3OD, δ) 8.64 (d, J = 8.5 Hz, 1H), 8.29 (m, 2H), 7.73 (m, 3H), 3.02 (t, J = 5.9 Hz, 2H), 2.94 (t, J = 5.9 Hz, 2H), 1.50 (1s, 18H). ^{13}C NMR (151 MHz, CD_3OD, δ) 162.5, 157.2, 135.0, 130.3, 129.5, 129.3, 128.8, 128.2, 127.7, 127.6, 124.7, 123.3, 54.0, 40.7, 39.7, 27.1. HRMS (ESI/QTOF) m/z: calcd for $C_{23}H_{34}N_5O_6S^+$ $[M + H]^+$ 508.2224, found 508.2222.

Compound 16. Methacryloyl chloride (22 mg, 2.2 mmol) in anhydrous dichloromethane (5 mL) was added slowly to a mixture of compound **15** (51 mg, 1 mmol) and triethylamine (30 mg 3 mmol) in anhydrous dichloromethane (5 mL) at 0 °C. After the mixture was stirred for 3 h, the solvent was removed by rotary evaporation. The residue was purified by column

chromatography over silica gel using 4:1 hexane/ethyl acetate as the eluent to give a light brown powder (40 mg, 62%). ^{1}H NMR (600 MHz, CD_3OD, δ) 8.46–8.35 (m, 2H), 8.29 (s, 1H), 7.90 (s, 1H), 7.76 (m, 2H), 5.83 (s, 1H), 5.46 (s, 1H), 5.34 (s, 1H), 5.26 (s, 1H), 4.20 (s, 2H), 3.60 (s, 2H), 2.02 (s, 3H), 1.74 (s, 3H), 1.52 (s, 18H). ^{13}C NMR (151 MHz, CD_3OD, δ) 175.2, 172.0, 171.5, 170.0, 139.9, 139.7, 133.9, 133.89, 133.88, 133.6, 132.6, 128.6, 128.3, 124.5, 124.4, 120.3, 119.6, 60.2, 45.4, 38.8, 27.0, 18.2, 17.4. HRMS (ESI/QTOF) m/z: calcd for $C_{31}H_{42}N_5O_8S^+$ $[M + H]^+$ 644.2749, found 644.2762.

Compound 9. Compound **16** (64 mg, 1 mmol) was dissolved in 4 mL of dichloromethane, followed with the addition of 4 mL of trifluoroacetic acid. The mixture was stirred for 3 h. After the solvent was removed by rotary evaporation, the residue was purified by column chromatography over silica gel using 5:1 CH_2Cl_2/MeOH as the eluent. The material obtained was dissolved in methanol (5 mL), followed by the addition of sodium chloride (290 mg, 5 mmol) in water (5 mL). After being stirred for 6 h, the mixture was diluted with CH_2Cl_2 (10 mL). The organic layer was washed with water (2 × 30 mL), dried over sodium sulfate, and concentrated by rotary evaporation to give a light brown powder (39 mg, 81%). ^{1}H NMR (400 MHz, CD_3OD, δ) 8.47 (d, J = 8.6 Hz, 2H), 8.39 (d, J = 8.5 Hz, 1H), 7.87–7.75 (m, 2H), 7.68 (d, J = 7.5, 1H), 5.74 (t, J = 1.1 Hz, 1H), 5.39 (m, 1H), 5.30 (d, J = 1.8 Hz, 1H), 5.19 (d, J = 1.3 Hz, 1H), 4.15 (t, J = 5.9 Hz, 2H), 3.51 (m, 2H), 1.94 (t, J = 1.2 Hz, 3H), 1.71 (d, J = 1.2 Hz, 3H). ^{13}C NMR (100 MHz, CD_3OD, δ) 171.9, 170.1, 157.6, 139.6, 134.4, 133.0, 131.8, 131.3, 129.2, 129.1, 128.4, 127.02, 126.99, 125.4, 125.4, 124.3, 120.2, 45.5, 38.7, 18.2, 17.4. HRMS (ESI/QTOF) m/z: calcd for $C_{21}H_{26}N_5O_4S^+$ $[M - Cl]^+$ 444.1700, found 444.1704.

Compound 10. Compound **17** (90 mg, 0.5 mmol) and *N*,*N*-diisopropylethylamine (DIPEA, 97 mg) were added to a solution of 4-vinylphenyl isocyanate (73 mg, 0.5 mmol) in dry THF (10 mL). After the reaction mixture was stirred overnight under nitrogen, the solvent was removed by rotary evaporation. The residue was purified by column chromatography over silica gel using 4:1 dichloromethane/methanol as the eluent to give a red powder (88 mg, 54%). ^{1}H NMR (600 MHz, acetone-d_6) δ 8.76 (d, J = 8.4 Hz, 1H), 8.42 (d, J = 8.5 Hz, 1H), 7.62 (d, J = 8.1 Hz, 2H), 7.50 (d, J = 8.2 Hz, 2H), 6.84–6.67 (m, 1H), 5.77 (d, J = 17.6 Hz, 1H), 5.20 (d, J = 10.9 Hz, 1H). ^{13}C NMR (101 MHz, acetone-d_6) δ 150.8, 145.5, 143.5, 136.3, 136.0, 135.6, 133.0, 126.8, 126.6, 118.9, 118.3, 112.1, HRMS (ESI/QTOF) m/z: calcd for $C_{15}H_{10}N_5O_4$ $[M - H]^-$ 324.0738, found 324.0741.

Compound 11. Compound **18** (18 mg, 0.11 mmol) was added slowly to a stirred solution of 6-aminonaphthalene-2-sulfonic acid (23 mg, 0.1 mmol) and DIPEA (20 mg, 0.15 mmol) in DMF (5 mL). The reaction mixture was heated to 70 °C for 24 h. After the mixture was cooled to room temperature, water (15 mL) was added. The mixture was extracted with ether (3 × 10 mL). The combined organic solution was concentrated by rotary evaporation and the residue was mixed with sodium dodecyl sulfate (56 mg) in water (5 mL). After the micellar solution was stirred at room temperature for 2 h, it was extracted with dichloromethane (3 × 10 mL). The combined organic solution was dried over sodium sulfate and concentrated by rotary evaporation. The residue was purified by column chromatography over silica gel using 4:1 dichloromethane/methanol as the eluent to give a white powder (22 mg, 52%). ^{1}H NMR (600 MHz, D_2O, δ) 8.23 (s, 1H), 7.91 (d, J = 8.7 Hz, 1H), 7.82 (d, J = 8.6 Hz, 1H), 7.80 – 7.71 (m, 1H), 7.63 (s, 1H), 7.31 (s, 1H), 5.99 (s, 1H), 5.58 (s, 1H), 4.28 (t, J = 5.0 Hz, 2H), 3.82 (s, 2H),

1.77 (s, 3H). ^{13}C NMR (126 MHz, D_2O, δ) 179.7, 169.5, 139.7, 135.9, 135.6, 134.3, 130.7, 130.5, 128.8, 127.1, 125.3, 125.1, 123.0, 122. 7, 63.2, 43.4, 17.3. HRMS (ESI/QTOF) calcd for $C_{17}H_{19}N_2O_5S_2$ $[M+H]^+$ 395.0730, found 395.0738.

Compound 12. Compound **18** (18 mg, 0.11 mmol) was added slowly to a stirred solution of 6-aminonaphthalene-2-sulfonic acid (23 mg, 0.1 mmol) and DIPEA (20 mg, 0.15 mmol) in DMF (5 mL). The reaction mixture was heated to 70 °C for 24 h. After the mixture was cooled to room temperature, water (15 mL) was added. The mixture was extracted with ether (3 × 10 mL). The combined organic solution was concentrated by rotary evaporation and the residue was mixed with sodium dodecyl sulfate (56 mg) in water (5 mL). After the micellar solution was stirred at room temperature for 2 h, it was extracted with dichloromethane (3 × 10 mL). The combined organic solution was dried over sodium sulfate and concentrated by rotary evaporation. The residue was purified by column chromatography over silica gel using 4:1 dichloromethane/methanol as the eluent to give a white powder (26 mg, 61%). ^{1}H NMR (400 MHz, CD3OD, δ) 8.84 (d, *J* = 8.8 Hz, 1H), 8.14 (d, *J* = 7.2 Hz, 1H), 8.00 (d, *J* = 8.5 Hz, 1H), 7.56 (dd, *J* = 8.7, 7.3 Hz, 1H), 7.51–7.37 (m, 2H), 5.88 (s, 1H), 5.49 (s, 1H), 4.18 (t, *J* = 5.4 Hz, 2H), 3.79 (t, *J* = 5.4 Hz, 2H), 1.77 (s, 3H). ^{13}C NMR (100 MHz, CD3OD, δ) 186.2, 171.2, 145.1, 139.9, 135.1, 134.1, 131.0, 130.0, 129.9, 129.7, 129.6, 129.2, 128.8, 111.0, 66.7, 47.3, 20.9. HRMS (ESI/QTOF) m/z: calcd for $C_{17}H_{17}N_2O_5S_2$ $[M - Na]^-$ 393.0584, found 393.0583.

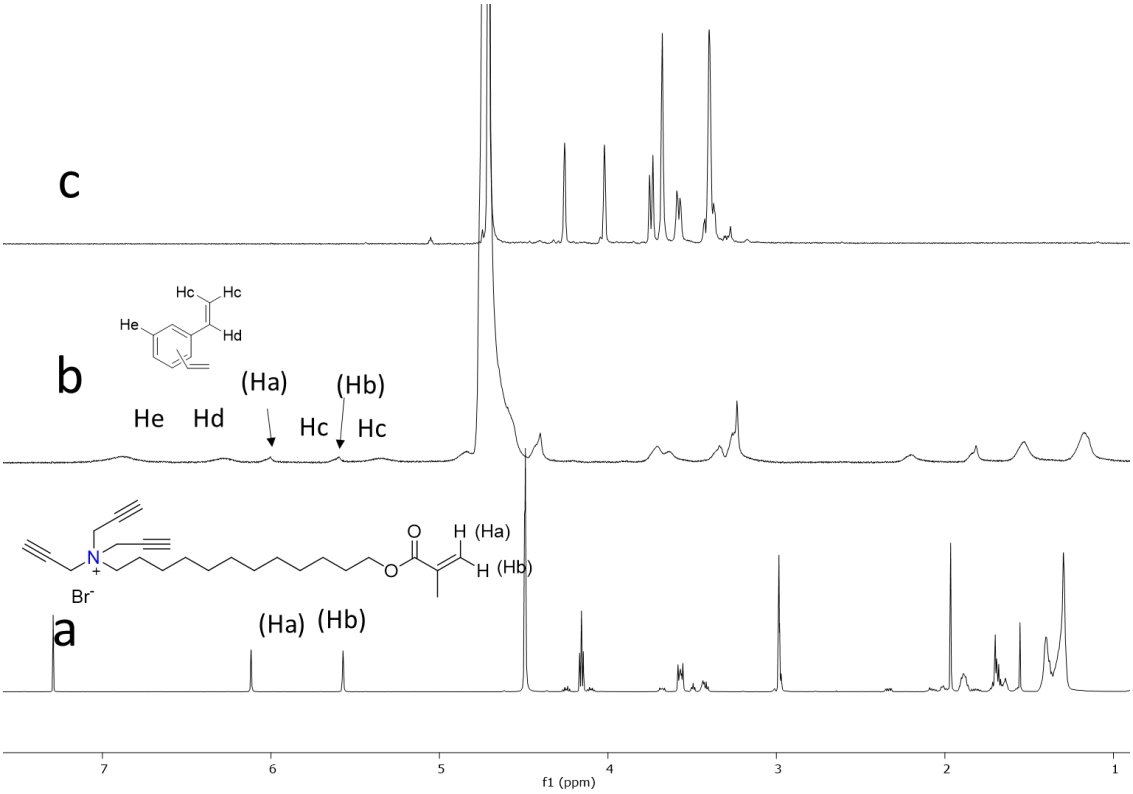

Figure S1. ^{1}H NMR for MINP(1). ^{1}H NMR spectra of (a) **6** in $CDCl_3$, (b) alkynyl-SCM in D_2O, and (c) **MINP(1)** in D_2O.

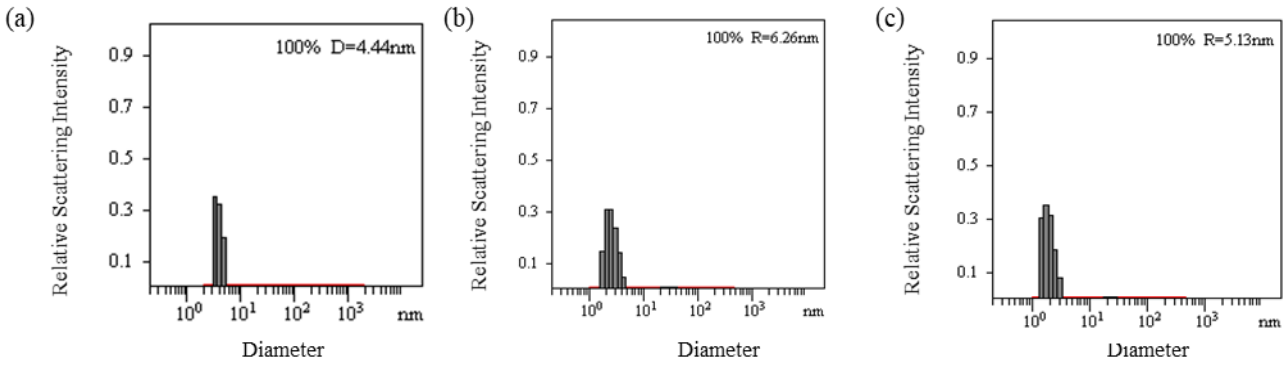

Figure S2 DLS for MINP(1). Distribution of the hydrodynamic diameters of the nanoparticles in water as determined by DLS for (a) alkynyl-SCM, (b) surface-functionalized SCM, and (c) **MINP(1)** after purification.

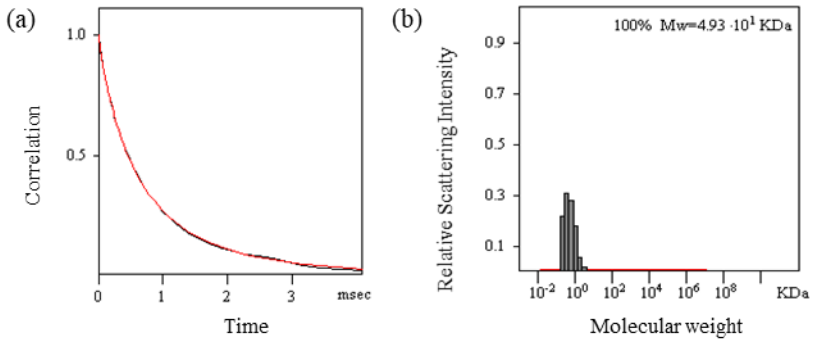

Figure S3. DLS for MINP(1). The correlation curve and the distribution of the molecular weight for MINP(**1**) from the DLS. The PRECISION DECONVOLVE program assumes the intensity of scattering is proportional to the mass of the particle squared. If each unit of building block for the MINP(**1**) is assumed to contain one molecule of compound **6** (MW = 465 g/mol), 1.2 molecules of compound **7** (MW = 172 g/mol), one molecule of DVB (MW = 130 g/mol), and 0.8 molecules of compound **8** (MW = 264 g/mol), the molecular weight of MINP(**1**) translates to 49 [= 49300 / (465 + 1.2×172 + 130 + 0.8×264)] of such units.

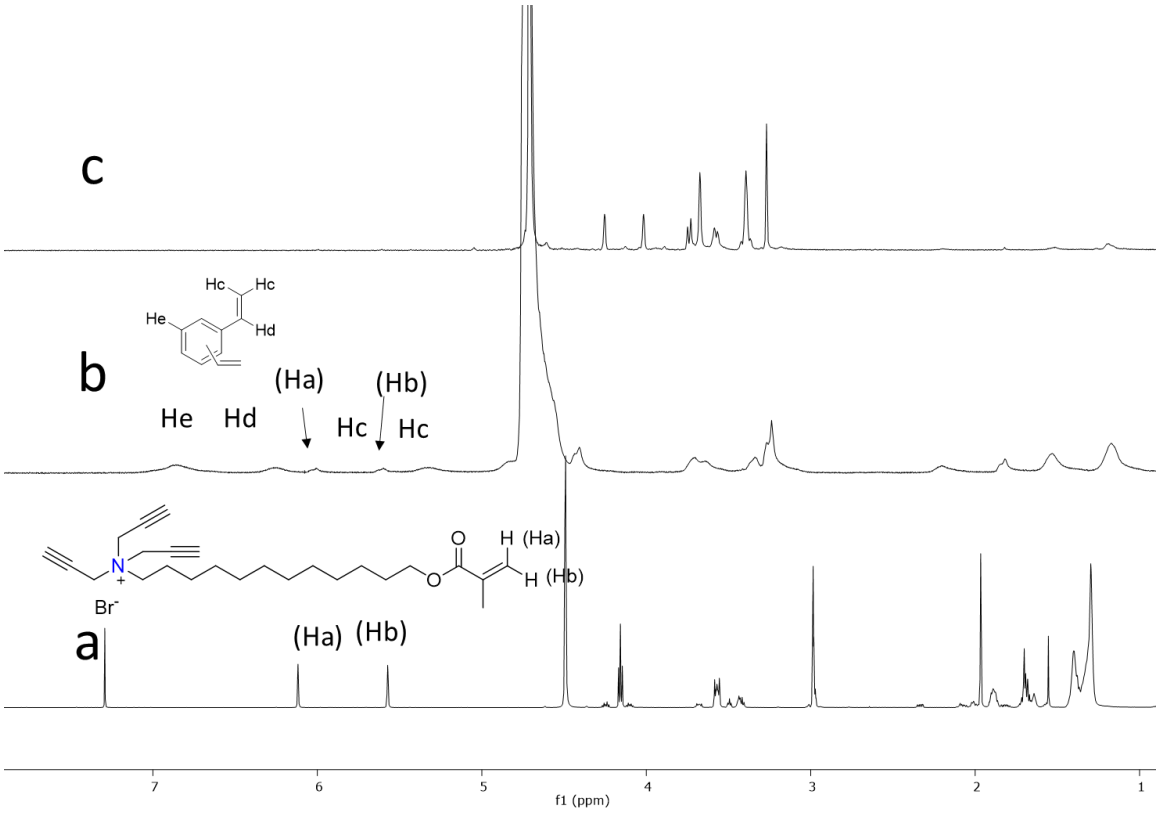

Figure S4. ^{1}H NMR for MINP(2). ^{1}H NMR spectra of (a) **6** in $CDCl_3$, (b) alkynyl-SCM in D_2O, and (c) MINP (**2**) in D_2O.

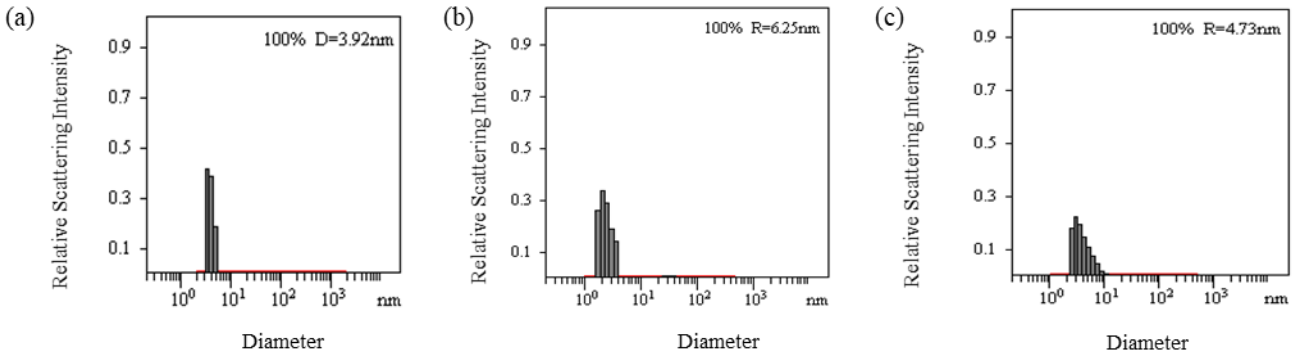

Figure S5. DLS for MINP(2). Distribution of the hydrodynamic diameters of the nanoparticles in water as determined by DLS for (a) alkynyl-SCM, (b) surface-functionalized SCM, and (c) MINP(**2**) after purification.

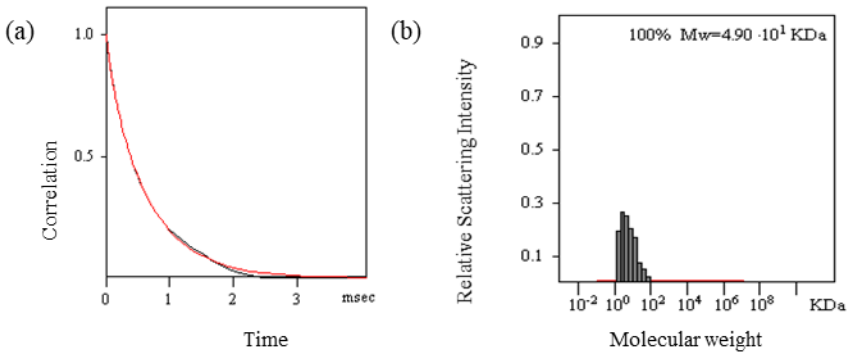

Figure S6. DLS for MINP(2). The correlation curve and the distribution of the molecular weight for MINP(**2**) from the DLS. The PRECISION DECONVOLVE program assumes the intensity of scattering is proportional to the mass of the particle squared. If each unit of building block for the MINP(**2**) is assumed to contain one molecule of compound **6** (MW = 465 g/mol), 1.2 molecules of compound **7** (MW = 172 g/mol), one molecule of DVB (MW = 130 g/mol), and 0.8 molecules of compound **8** (MW = 264 g/mol), the molecular weight of MINP(**2**) translates to 48 [= 49000 / (465 + 1.2×172 + 130 + 0.8×264)] of such units.

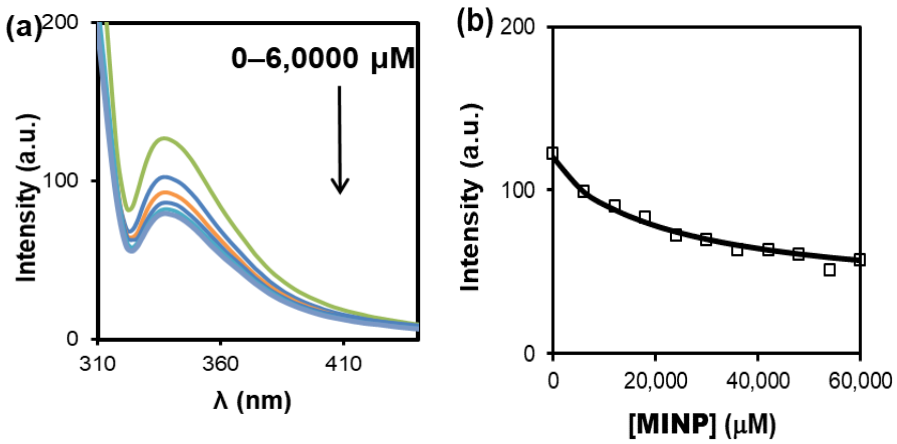

Figure S7. Fluorescence Titration of FM 10 by sodium acetate. (a) Fluorescence emission spectra of **FM 10** (λ_{ex} = 280 nm) upon addition of different concentrations of sodium acetate in CTAB solution. [CTAB] = 2 mM. [**FM 10**] = 2.0 μM. (b) Nonlinear least squares fitting of the emission intensity of **FM 10** at 340 nm to a 1:1 binding isotherm. The data corresponds to entry 12 in Table 1.

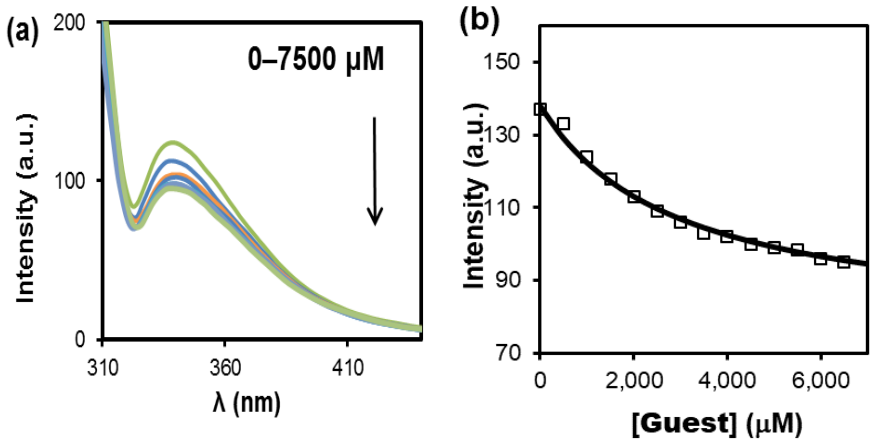

Figure S8. Fluorescence Titration of FM 10 by sodium butyrate. (a) Fluorescence emission spectra of **FM 10** (λ_{ex} = 280 nm) upon addition of different concentrations of sodium butyrate in CTAB solution. [CTAB] = 2 mM. [**FM 10**] = 2.0 μM. (b) Nonlinear least squares fitting of the emission intensity of **FM 10** at 340 nm to a 1:1 binding isotherm. The data corresponds to entry 12 in Table 1.

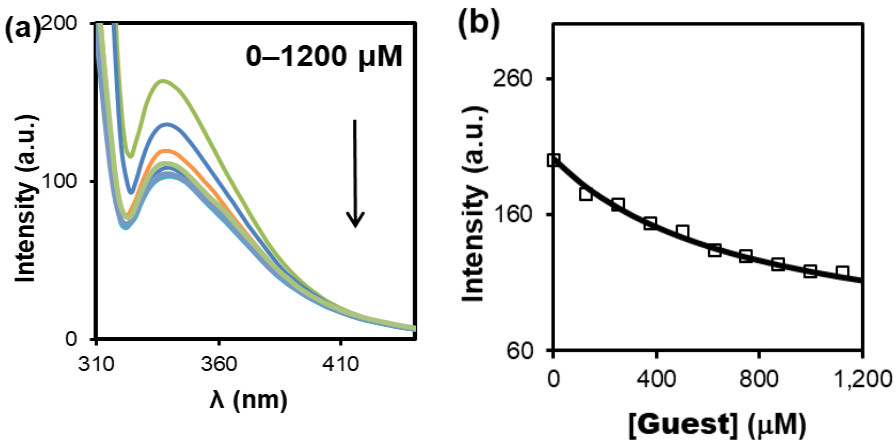

Figure S9. Fluorescence Titration of FM 10 by sodium octanoate. (a) Fluorescence emission spectra of **FM 10** (λ_{ex} = 280 nm) upon addition of different concentrations of sodium octanoate in CTAB solution. [CTAB] = 2 mM. [**FM 10**] = 2.0 μM. (b) Nonlinear least squares fitting of the emission intensity **of FM 10** at 340 nm to a 1:1 binding isotherm. The data corresponds to entry 12 in Table 1.

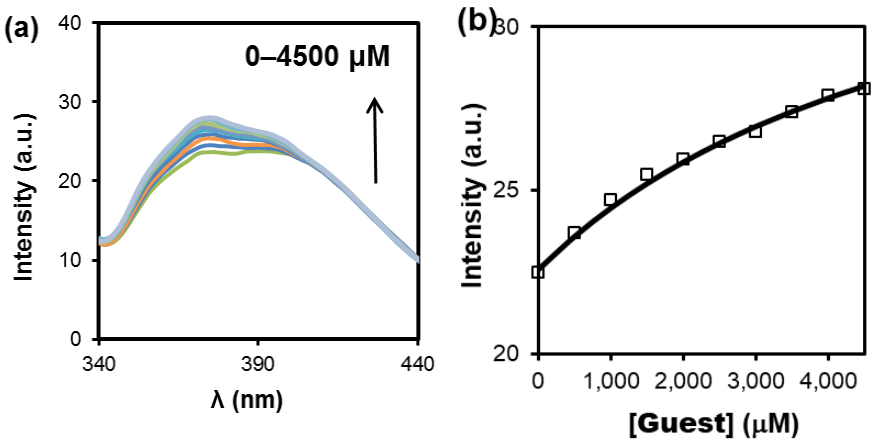

Figure S10. Flluorescence Titration of FM 11 by sodium acetate. (a) Fluorescence emission spectra **of FM 11** (λ_{ex} = 300 nm) upon addition of different concentrations of sodium acetate in CTAB solution. [CTAB] = 2 mM. [**FM 11**] = 2.0 μM. (b) Nonlinear least squares fitting of the emission intensity of **FM 11** at 370 nm to a 1:1 binding isotherm. The data corresponds to entry 12 in Table 1.

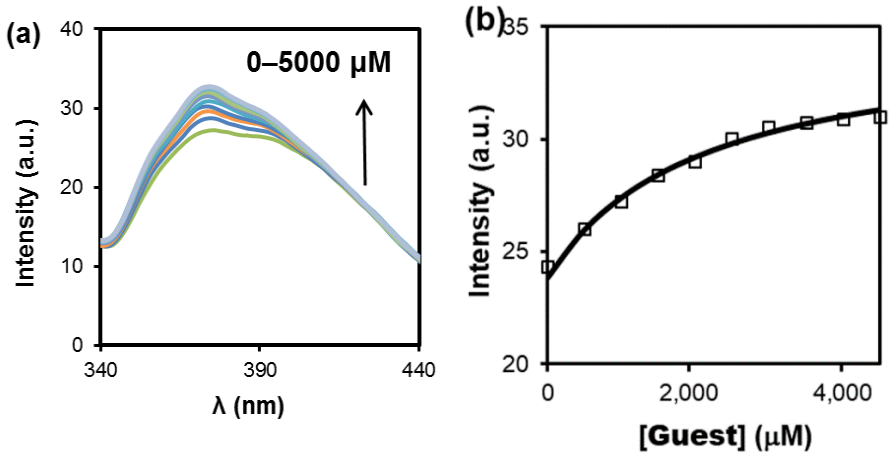

Figure S11. Fluorescence Titration of FM 11 by sodium butyrate. (a) Fluorescence emission spectra of **FM 11** (λ_{ex} = 300 nm) upon addition of different concentrations of sodium butyrate in CTAB solution. [CTAB] = 2 mM. [**FM 11**] = 2.0 μM. (b) Nonlinear least squares fitting of the emission intensity of **FM 11** at 370 nm to a 1:1 binding isotherm. The data corresponds to entry 12 in Table 1.

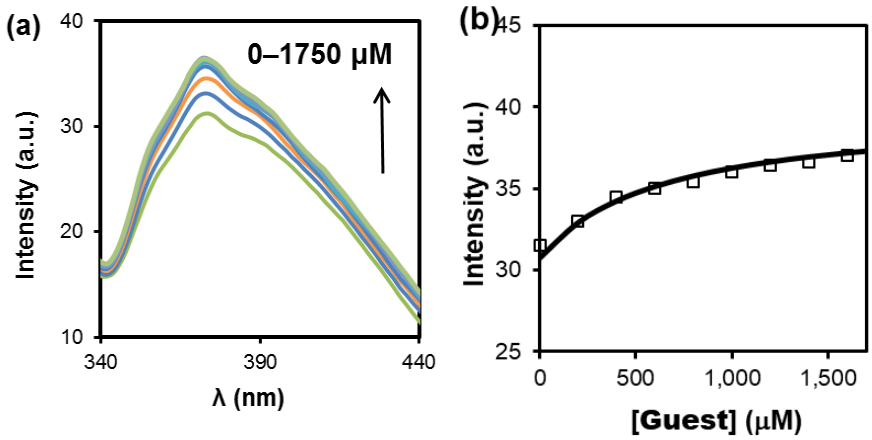

Figure S12. Fluorescence Titration of FM 11 by sodium octanoate. (a) Fluorescence emission spectra **of FM 11** (λ_{ex} = 300 nm) upon addition of different concentrations of sodium octanoate in CTAB solution. [CTAB] = 2 mM. [**FM 11**] = 2.0 μM. (b) Nonlinear least squares fitting of the emission intensity of **FM 11** at 370 nm to a 1:1 binding isotherm. The data corresponds to entry 12 in Table 1.

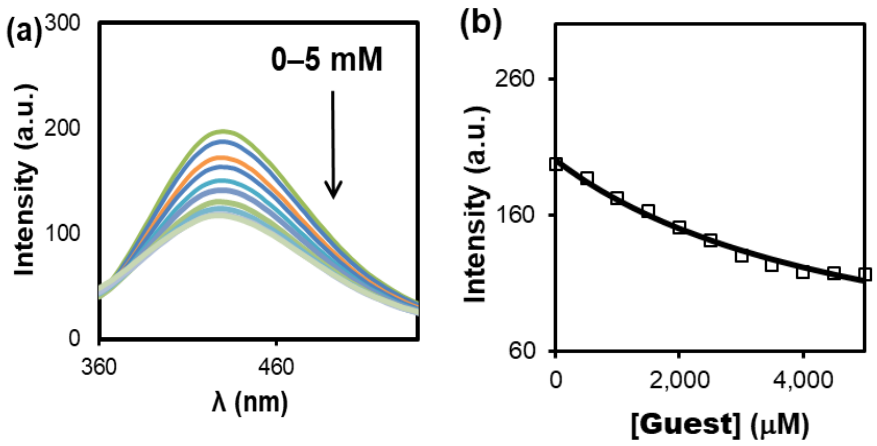

Figure S13. Fluorescence Titration of FM 12 by sodium acetate. (a) Fluorescence emission spectra of **FM 12** (λ_{ex} = 340 nm) upon addition of different concentrations of sodium acetate in CTAB solution. [CTAB] = 2 mM. [**FM 12**] = 2.0 μM. (b) Nonlinear least squares fitting of the emission intensity of **FM 12** at 430 nm to a 1:1 binding isotherm. The data corresponds to entry 12 in Table 1.

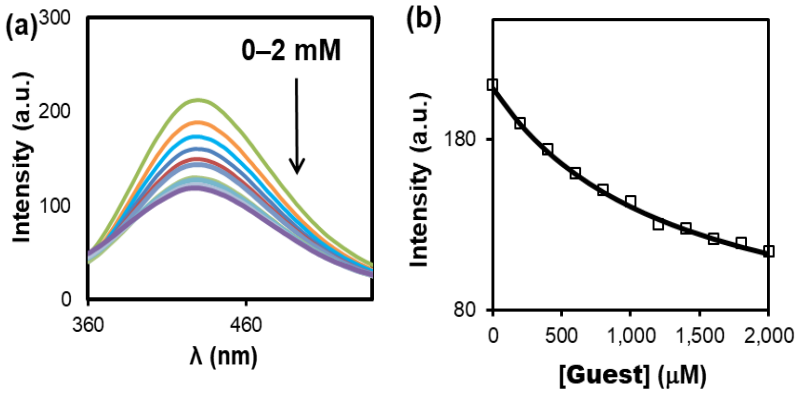

Figure S14. Fluorescence Titration of FM 12 by sodium butyrate. (a) Fluorescence emission spectra of **FM 12** (λ_{ex} = 340 nm) upon addition of different concentrations of sodium butyrate in CTAB solution. [CTAB] = 2 mM. [**FM 12**] = 2.0 μM. (b) Nonlinear least squares fitting of the emission intensity of **FM 12** at 430 nm to a 1:1 binding isotherm. The data corresponds to entry 12 in Table 1.

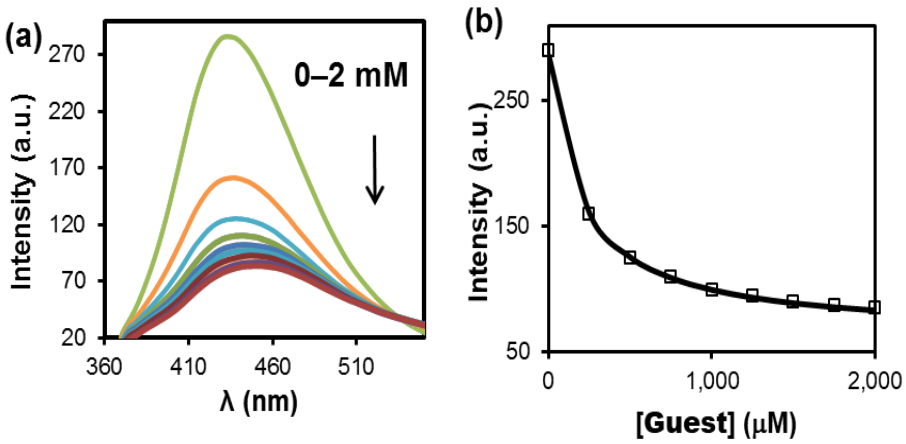

Figure S15. Fluorescence Titration of FM 12 by sodium octanoate. (a) Fluorescence emission spectra of **FM 12** (λ_{ex} = 340 nm) upon addition of different concentrations of sodium octanoate in CTAB solution. [CTAB] = 2 mM. [**FM 12**] = 2.0 μM. (b) Nonlinear least squares fitting of the emission intensity of **FM 12** at 430 nm to a 1:1 binding isotherm. The data corresponds to entry 12 in Table 1.

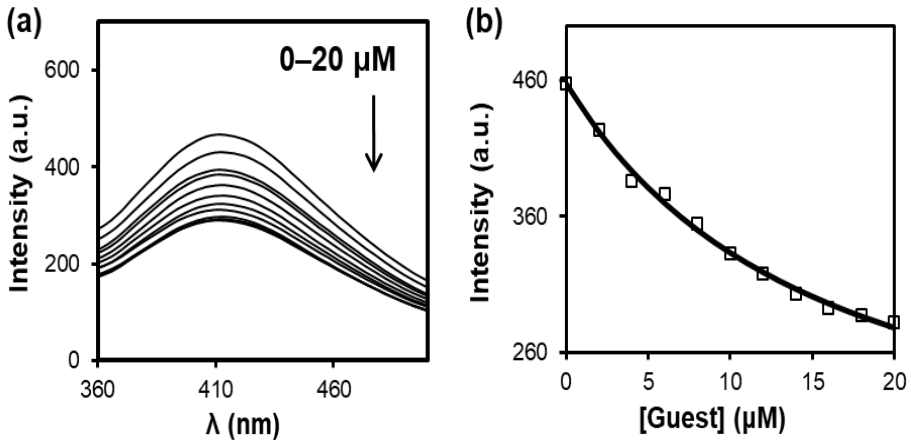

Figure S16. Fluorescence Titration of MINP(1) (1 equiv. FM) by 1. (a) Fluorescence emission spectra of **MINP(1)** (1 equiv. FM) (λ_{ex} = 340 nm) upon addition of different concentrations of guest **1** in 50 mM Tris buffer (pH 7.4). [**MINP(1)**] = 2.0 μM. (b) Nonlinear least squares fitting of the emission intensity of **MINP(1)** at 420 nm to a 1:1 binding isotherm. The data corresponds to entry 1 in Table 2.

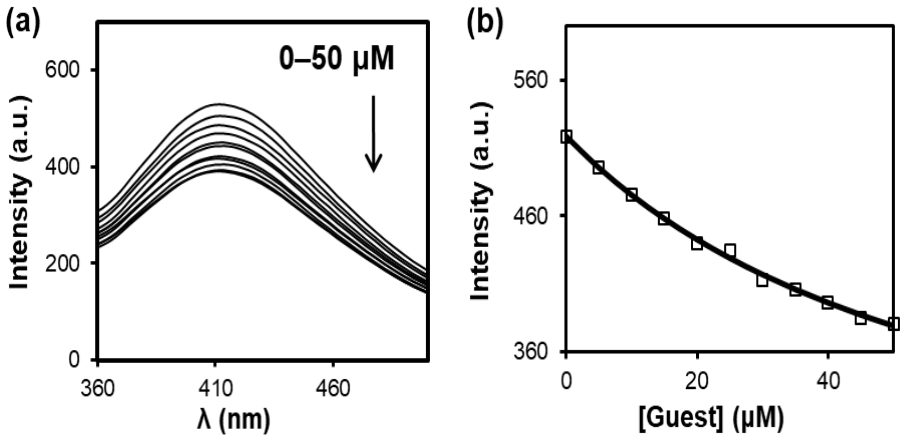

Figure S17. Fluorescence Titration of MINP(1) (1 equiv. FM) by 2. (a) Fluorescence emission spectra of MINP**(1)** (1 equiv. FM) (λ_{ex} = 340 nm) upon addition of different concentrations of guest **2** in 50 mM Tris buffer (pH 7.4). [MINP**(1)**] = 2.0 μM. (b) Nonlinear least squares fitting of the emission intensity of MINP**(1)** at 420 nm to a 1:1 binding isotherm. The data corresponds to entry 2 in Table 2.

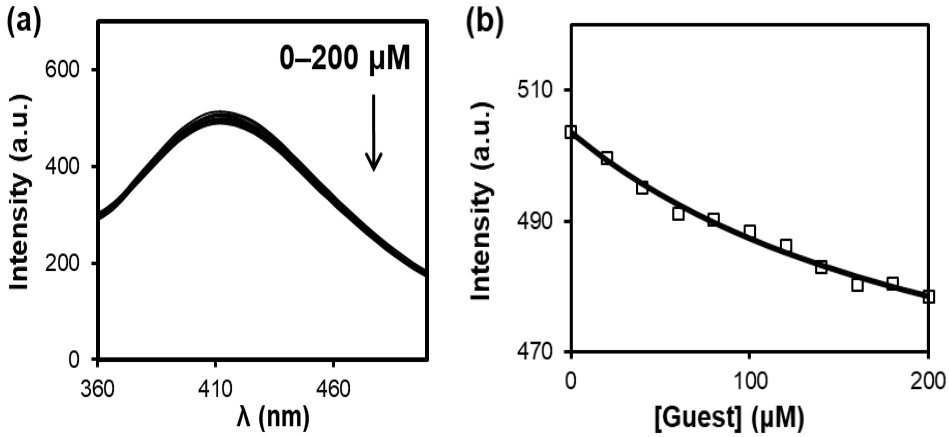

Figure S18. Fluorescence Titration of MINP(1) (1 equiv. FM) by 3. (a) Fluorescence emission spectra of MINP(**1**) (1 equiv. FM) (λ_{ex} = 340 nm) upon addition of different concentrations of guest **3** in 50 mM Tris buffer (pH 7.4). [MINP**(1)**] = 2.0 μM. (b) Nonlinear least squares fitting of the emission intensity of MINP**(1)** at 420 nm to a 1:1 binding isotherm. The data corresponds to entry 3 in Table 2.

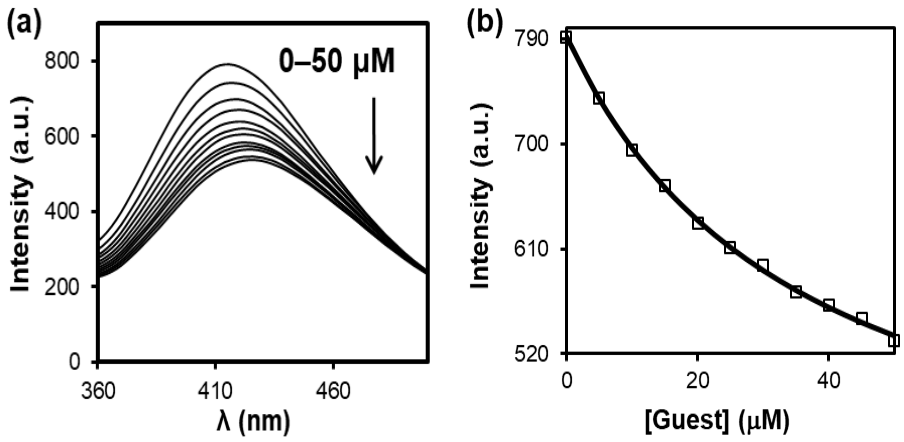

Figure S19. Fluorescence Titration of MINP(1) (2 equiv. FM) by 2. (a) Fluorescence emission spectra of MINP**(1)** (2 equiv. FM) (λ_{ex} = 340 nm) upon addition of different concentrations of guest **2** in 50 mM Tris buffer (pH 7.4). [MINP**(1)**] = 2.0 μM. (b) Nonlinear least squares fitting of the emission intensity of MINP**(1)** at 420 nm to a 1:1 binding isotherm. The data corresponds to entry 5 in Table 2.

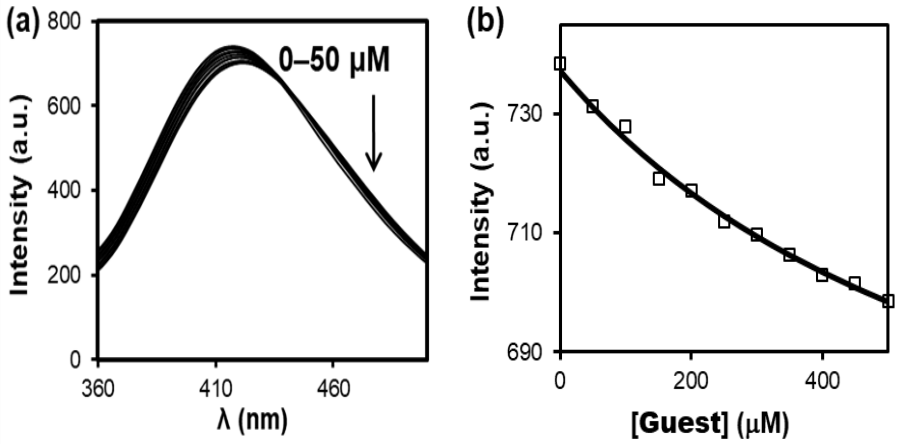

Figure S20. Fluorescence Titration of MINP(1) (2 equiv. FM) by 3. (a) Fluorescence emission spectra of MINP**(1)** (2 equiv. FM) (λ_{ex} = 340 nm) upon addition of different concentrations of guest **3** in 50 mM Tris buffer (pH 7.4). [MINP**(1)**] = 2.0 μM. (b) Nonlinear least squares fitting of the emission intensity of MINP**(1)** at 420 nm to a 1:1 binding isotherm. The data corresponds to entry 6 in Table 2.

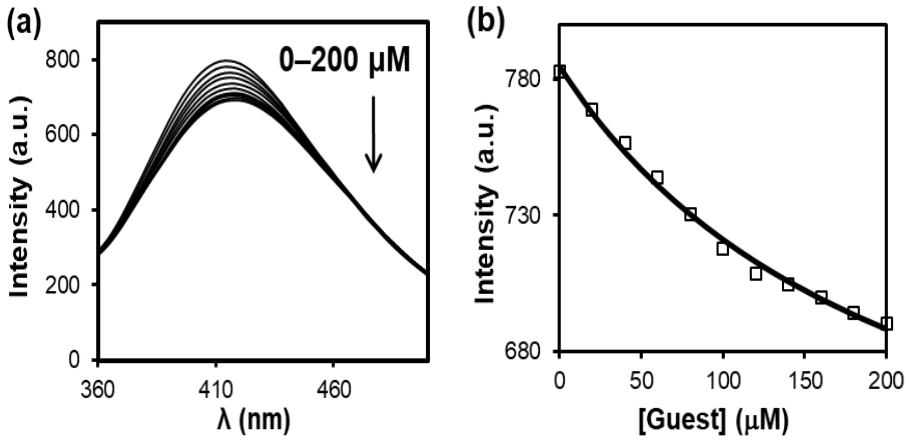

Figure S21. Fluorescence Titration of MINP(1) (2 equiv. FM) by 4. (a) Fluorescence emission spectra of MINP**(1)** (2 equiv. FM) (λ_{ex} = 340 nm) upon addition of different concentrations of guest **4** in 50 mM Tris buffer (pH 7.4). [MINP**(1)**] = 2.0 μM. (b) Nonlinear least squares fitting of the emission intensity of MINP**(1)** at 420 nm to a 1:1 binding isotherm. The data corresponds to entry 7 in Table 2.

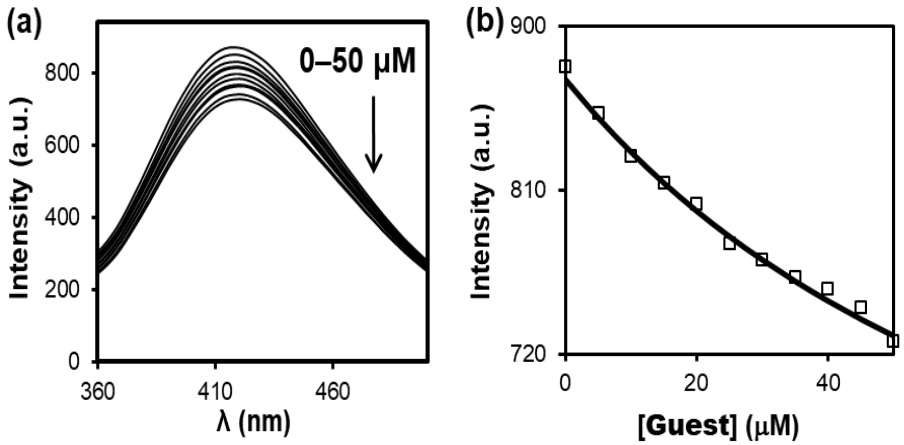

Figure S22. Fluorescence Titration of MINP(1) (2 equiv. FM) by 5. (a) Fluorescence emission spectra of MINP**(1)** (2 equiv. FM) (λ_{ex} = 340 nm) upon addition of different concentrations of guest **5** in 50 mM Tris buffer (pH 7.4). [MINP**(1)**] = 2.0 μM. (b) Nonlinear least squares fitting of the emission intensity of MINP**(1)** at 420 nm to a 1:1 binding isotherm. The data corresponds to entry 8 in Table 2.

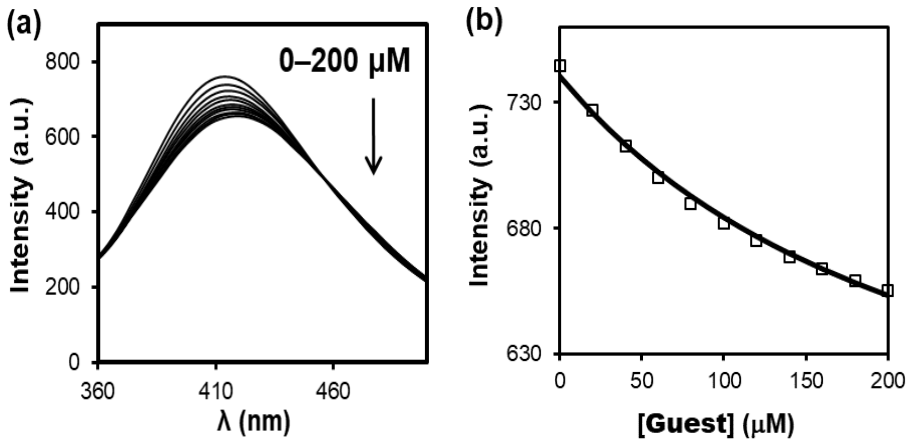

Figure S23. Fluorescence Titration of MINP(1) (2 equiv. FM) by 6. (a) Fluorescence emission spectra of MINP**(1)** (2 equiv. FM) (λ_{ex} = 340 nm) upon addition of different concentrations of guest **6** in 50 mM Tris buffer (pH 7.4). [MINP**(1)**] = 2.0 μM. (b) Nonlinear least squares fitting of the emission intensity of MINP**(1)** at 420 nm to a 1:1 binding isotherm. The data corresponds to entry 9 in Table 2.

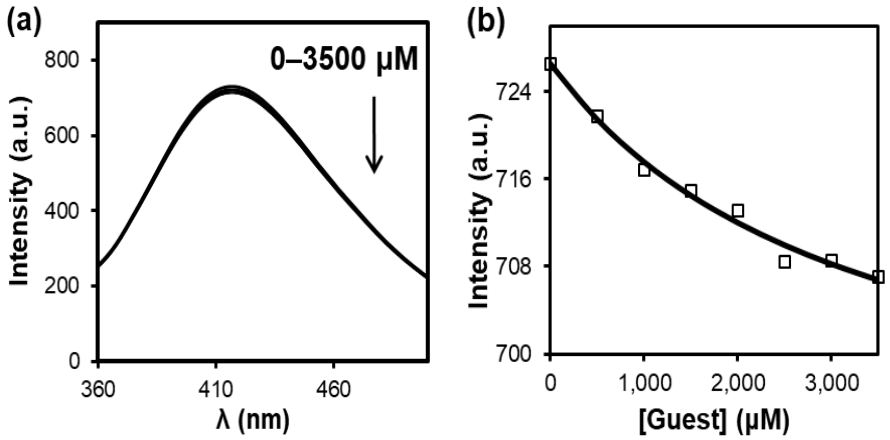

Figure S24. Fluorescence Titration of MINP(1) (2 equiv. FM) by acetic acid. (a) Fluorescence emission spectra of MINP**(1)** (2 equiv. FM) (λ_{ex} = 340 nm) upon addition of different concentrations of acetic acid in 50 mM Tris buffer (pH 7.4). [MINP**(1)**] = 2.0 μM. (b) Nonlinear least squares fitting of the emission intensity of MINP**(1)** at 420 nm to a 1:1 binding isotherm. The data corresponds to entry 10 in Table 2.

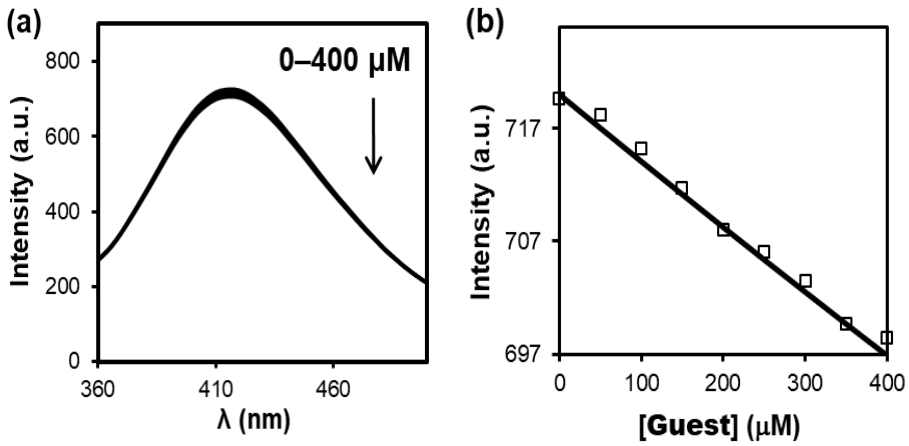

Figure S25. Fluorescence Titration of MINP(1) (2 equiv. FM) by butyric acid. (a) Fluorescence emission spectra of MINP**(1)** (2 equiv. FM) (λ_{ex} = 340 nm) upon addition of different concentrations of butyric acid in 50 mM Tris buffer (pH 7.4). [MINP**(1)**] = 2.0 μM. (b) Nonlinear least squares fitting of the emission intensity of MINP**(1)** at 420 nm to a 1:1 binding isotherm. The data corresponds to entry 11 in Table 2.

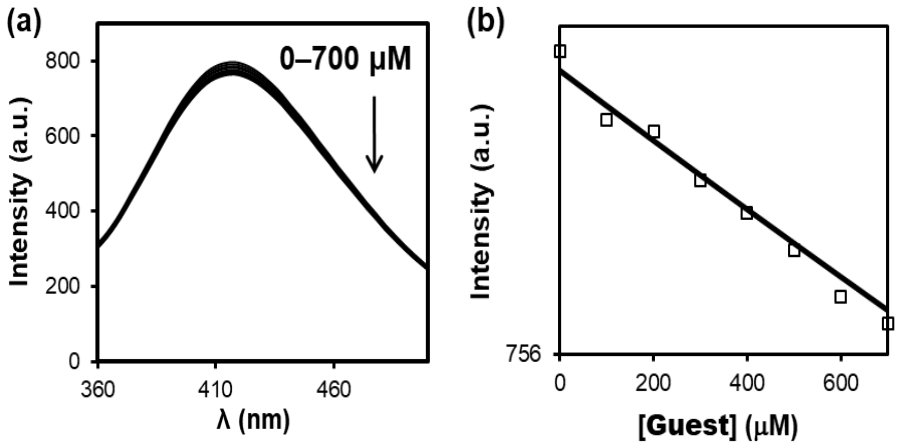

Figure S26. Fluorescence Titration of MINP(1) (2 equiv. FM) by benzoic acid. (a) Fluorescence emission spectra of MINP**(1)** (2 equiv. FM) (λ_{ex} = 340 nm) upon addition of different concentrations of benzoic acid in 50 mM Tris buffer (pH 7.4). [MINP**(1)**] = 2.0 μM. (b) Nonlinear least squares fitting of the emission intensity of MINP**(1)** at 420 nm to a 1:1 binding isotherm. The data corresponds to entry 12 in Table 2.

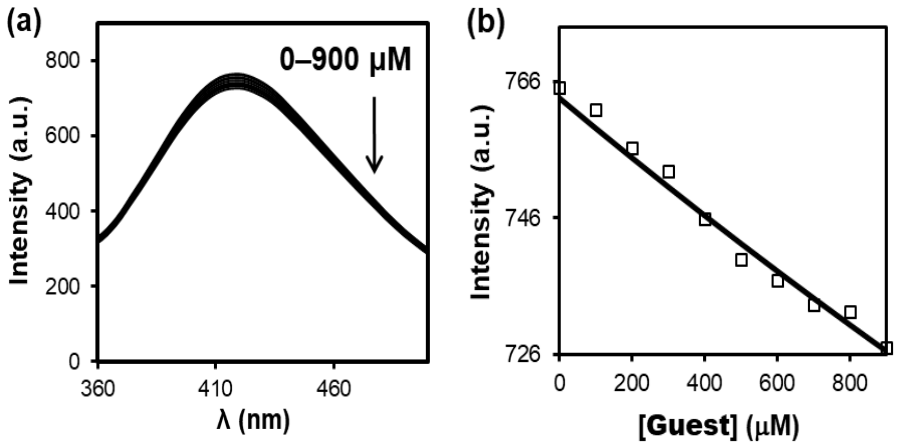

Figure S27. Fluorescence Titration of MINP(1) (2 equiv. FM) by citric acid. (a) Fluorescence emission spectra of MINP**(1)** (2 equiv. FM) (λ_{ex} = 340 nm) upon addition of different concentrations of citric acid in 50 mM Tris buffer (pH 7.4). [MINP**(1)**] = 2.0 μM. (b) Nonlinear least squares fitting of the emission intensity of MINP**(1)** at 420 nm to a 1:1 binding isotherm. The data corresponds to entry 13 in Table 2.

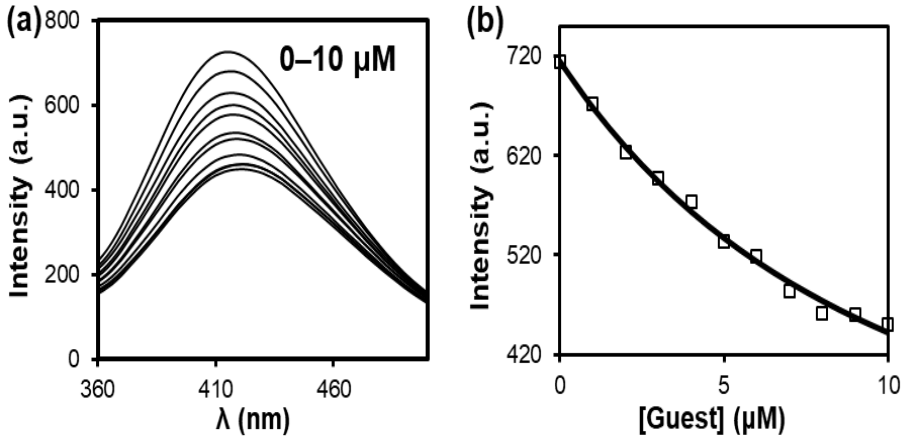

Figure S28. Fluorescence Titration of MINP(1) (3 equiv. FM) by 1. (a) Fluorescence emission spectra of MINP**(1)** (3 equiv. FM) (λ_{ex} = 340 nm) upon addition of different concentrations of guest **1** in 50 mM Tris buffer (pH 7.4). [MINP**(1)**] = 2.0 μM. (b) Nonlinear least squares fitting of the emission intensity of MINP**(1)** at 420 nm to a 1:1 binding isotherm. The data corresponds to entry 14 in Table 2.

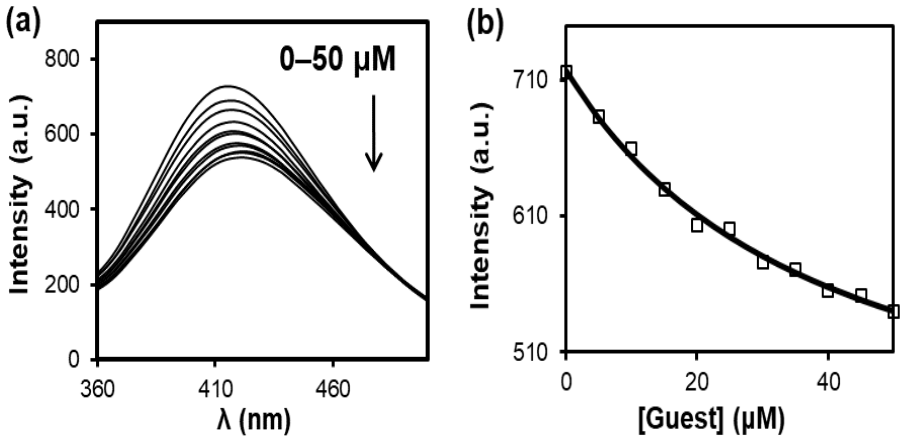

Figure S29. Fluorescence Titration of MINP(1) (3 equiv. FM) by 2. (a) Fluorescence emission spectra of MINP**(1)** (3 equiv. FM) (λ_{ex} = 340 nm) upon addition of different concentrations of guest **2** in 50 mM Tris buffer (pH 7.4). [MINP**(1)**] = 2.0 μM. (b) Nonlinear least squares fitting of the emission intensity of MINP**(1)** at 420 nm to a 1:1 binding isotherm. The data corresponds to entry 15 in Table 2.

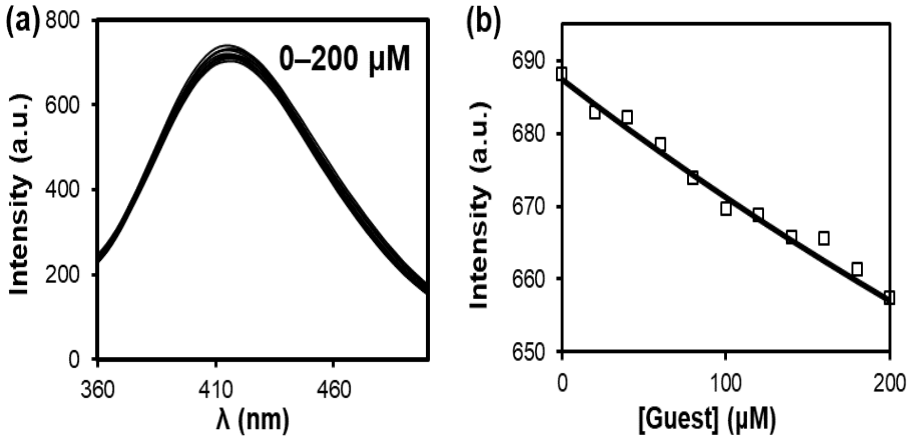

Figure S30. Fluorescence Titration of MINP(1) (3 equiv. FM) by 3. (a) Fluorescence emission spectra of MINP**(1)** (3 equiv. FM) (λ_{ex} = 340 nm) upon addition of different concentrations of guest **3** in 50 mM Tris buffer (pH 7.4). [MINP**(1)**] = 2.0 μM. (b) Nonlinear least squares fitting of the emission intensity of MINP**(1)** at 420 nm to a 1:1 binding isotherm. The data corresponds to entry 16 in Table 2.

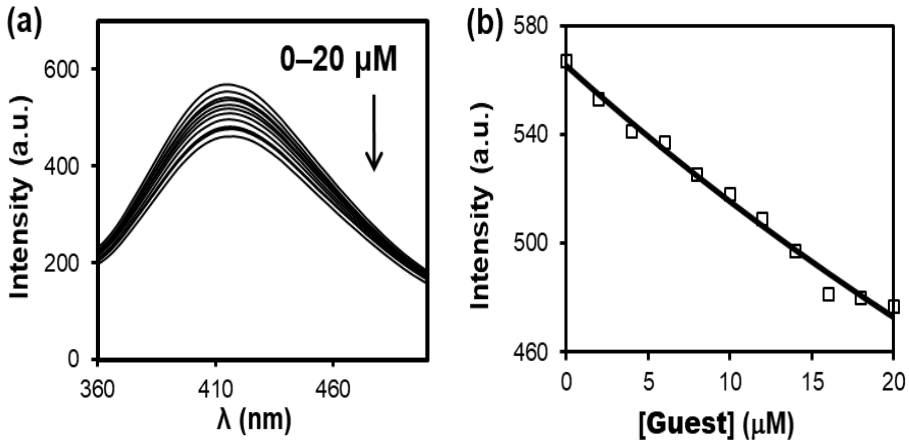

Figure S31. Fluorescence Titration of MINP(2) (2 equiv. FM) by 1. (a) Fluorescence emission spectra of MINP**(2)** (2 equiv. FM) (λ_{ex} = 340 nm) upon addition of different concentrations of guest **1** in 50 mM Tris buffer (pH 7.4). [MINP**(2)**] = 2.0 μM. (b) Nonlinear least squares fitting of the emission intensity of MINP**(2)** at 420 nm to a 1:1 binding isotherm. The data corresponds to entry 1 in Table 2.

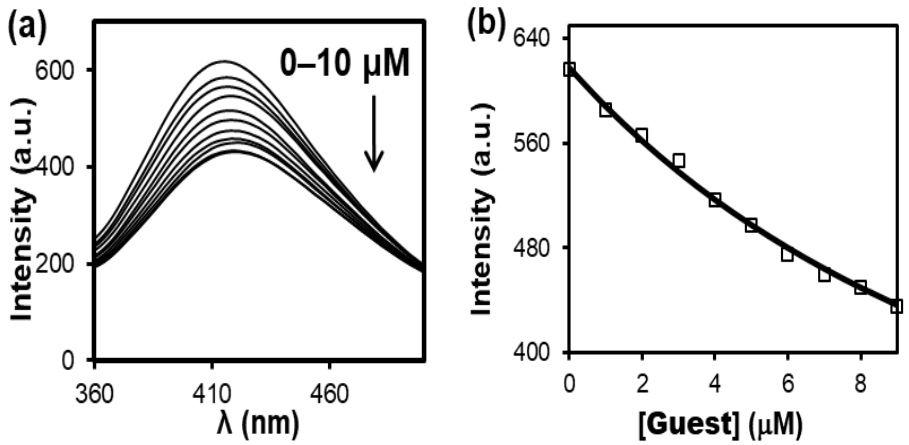

Figure S32. Fluorescence Titration of MINP(2) (2 equiv. FM) by 2. (a) Fluorescence emission spectra of MINP**(2)** (2 equiv. FM) (λ_{ex} = 340 nm) upon addition of different concentrations of guest **2** in 50 mM Tris buffer (pH 7.4). [MINP**(2)**] = 2.0 μM. (b) Nonlinear least squares fitting of the emission intensity of MINP**(2)** at 420 nm to a 1:1 binding isotherm. The data corresponds to entry 2 in Table 2.

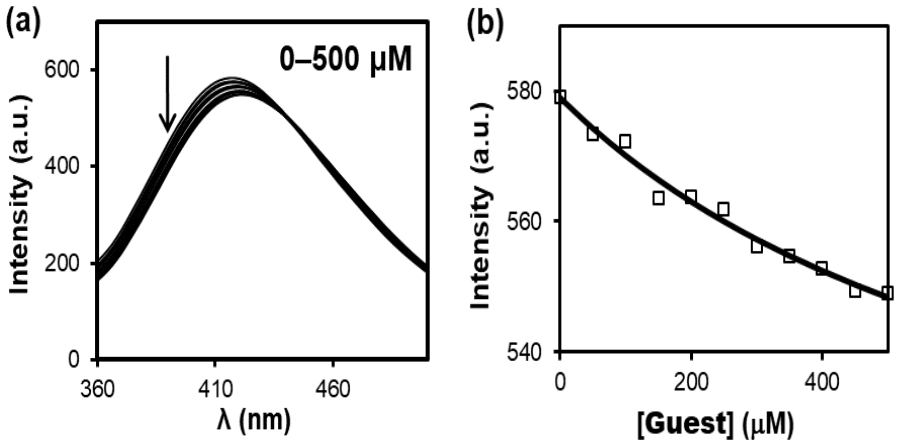

Figure S33. Fluorescence Titration of MINP(2) (2 equiv. FM) by 3. (a) Fluorescence emission spectra of MINP**(2)** (2 equiv. FM) (λ_{ex} = 340 nm) upon addition of different concentrations of guest **3** in 50 mM Tris buffer (pH 7.4). [MINP**(2)**] = 2.0 μM. (b) Nonlinear least squares fitting of the emission intensity of MINP**(2)** at 420 nm to a 1:1 binding isotherm. The data corresponds to entry 3 in Table 2.

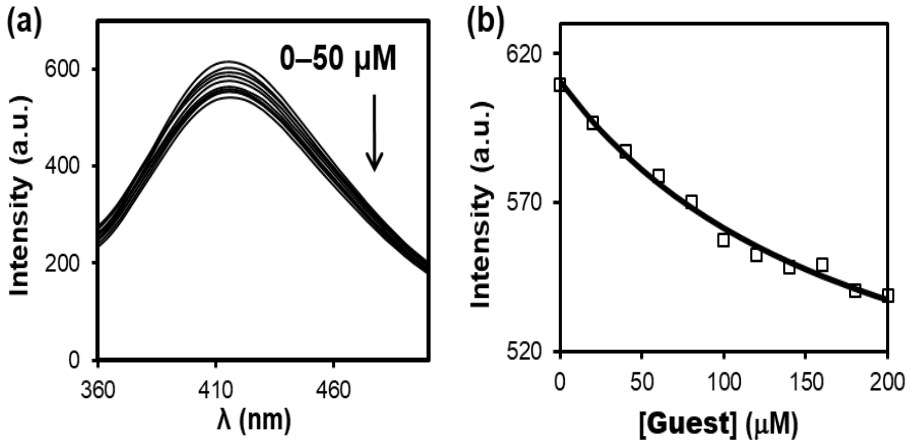

Figure S34. Fluorescence Titration of MINP(2) (2 equiv. FM) by 4. (a) Fluorescence emission spectra of MINP**(2)** (2 equiv. FM) (λ_{ex} = 340 nm) upon addition of different concentrations of guest **4** in 50 mM Tris buffer (pH 7.4). [MINP**(2)**] = 2.0 μM. (b) Nonlinear least squares fitting of the emission intensity of MINP**(2)** at 420 nm to a 1:1 binding isotherm. The data corresponds to entry 4 in Table 2.

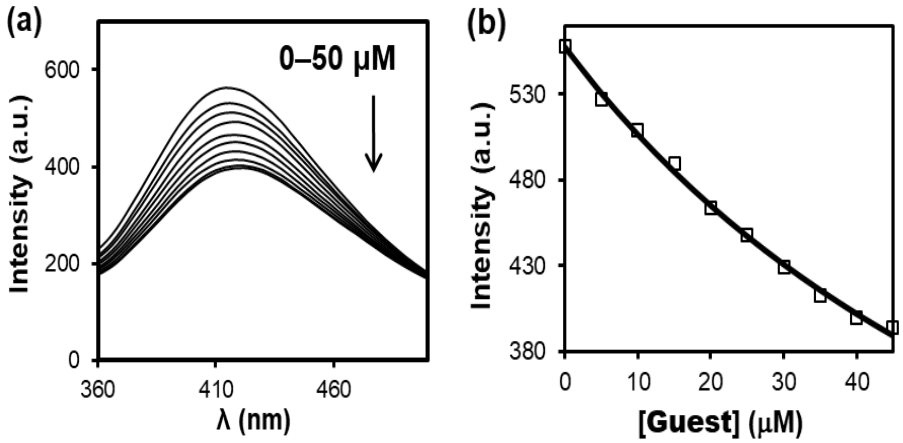

Figure S35. Fluorescence Titration of MINP(2) (2 equiv. FM) by 5. (a) Fluorescence emission spectra of MINP**(2)** (2 equiv. FM) (λ_{ex} = 340 nm) upon addition of different concentrations of guest **5** in 50 mM Tris buffer (pH 7.4). [MINP**(2)**] = 2.0 μM. (b) Nonlinear least squares fitting of the emission intensity of MINP**(2)** at 420 nm to a 1:1 binding isotherm. The data corresponds to entry 5 in Table 2.

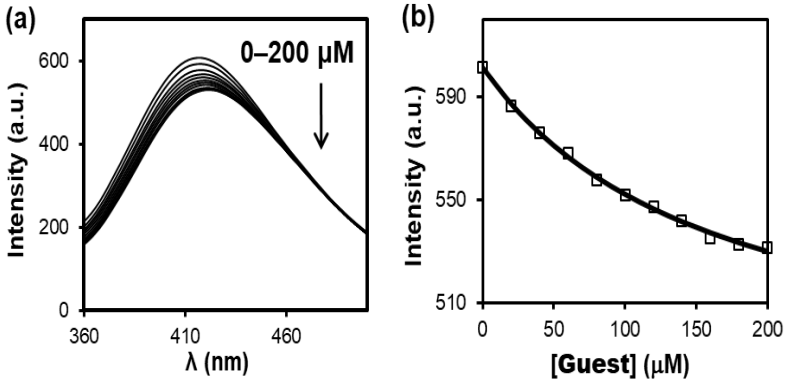

Figure S36. Fluorescence Titration of MINP(2) (2 equiv. FM) by 6. (a) Fluorescence emission spectra of MINP**(2)** (2 equiv. FM) (λ_{ex} = 340 nm) upon addition of different concentrations of guest **6** in 50 mM Tris buffer (pH 7.4). [MINP**(2)**] = 2.0 μM. (b) Nonlinear least squares fitting of the emission intensity of MINP**(2)** at 420 nm to a 1:1 binding isotherm. The data corresponds to entry 6 in Table 2.

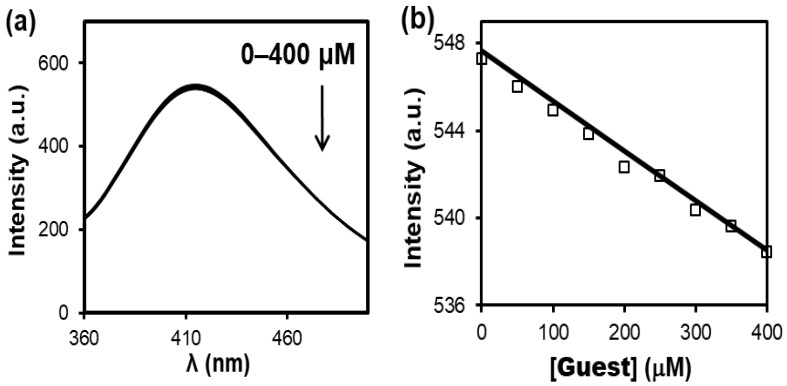

Figure S37. Fluorescence Titration of MINP(2) (2 equiv. FM) by acetic acid. (a) Fluorescence emission spectra of MINP**(2)** (2 equiv. FM) (λ_{ex} = 340 nm) upon addition of different concentrations of acetic acid in 50 mM Tris buffer (pH 7.4). [MINP**(2)**] = 2.0 μM. (b) Nonlinear least squares fitting of the emission intensity of MINP**(2)** at 420 nm to a 1:1 binding isotherm. The data corresponds to entry 7 in Table 2.

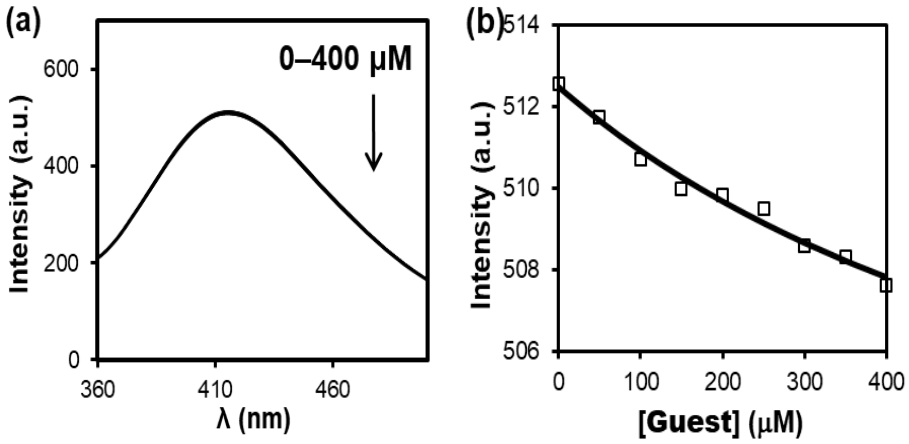

Figure S38. Fluorescence Titration of MINP(2) (2 equiv. FM) by butyric acid. (a) Fluorescence emission spectra of MINP**(2)** (2 equiv. FM) (λ_{ex} = 340 nm) upon addition of different concentrations of butyric acid in 50 mM Tris buffer (pH 7.4). [MINP**(2)**] = 2.0 μM. (b) Nonlinear least squares fitting of the emission intensity of MINP**(2)** at 420 nm to a 1:1 binding isotherm. The data corresponds to entry 8 in Table 2.

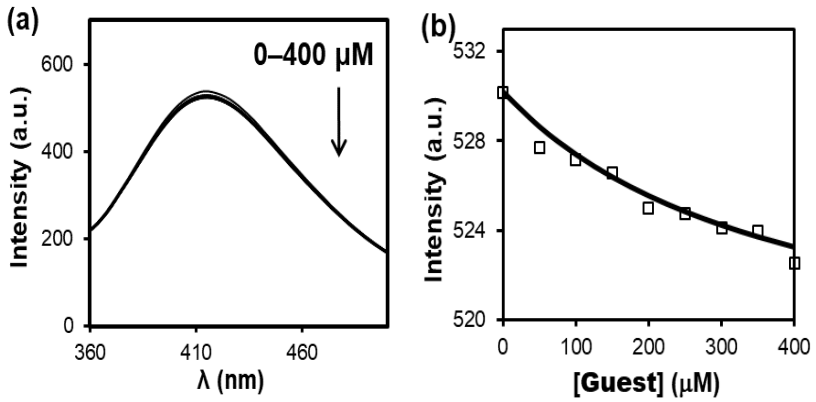

Figure S39. Fluorescence Titration of MINP(2) (2 equiv. FM) by benzoic acid. (a) Fluorescence emission spectra of MINP**(2)** (2 equiv. FM) (λ_{ex} = 340 nm) upon addition of different concentrations of benzoic acid in 50 mM Tris buffer (pH 7.4). [MINP**(2)**] = 2.0 μM. (b) Nonlinear least squares fitting of the emission intensity of MINP**(2)** at 420 nm to a 1:1 binding isotherm. The data corresponds to entry 9 in Table 2.

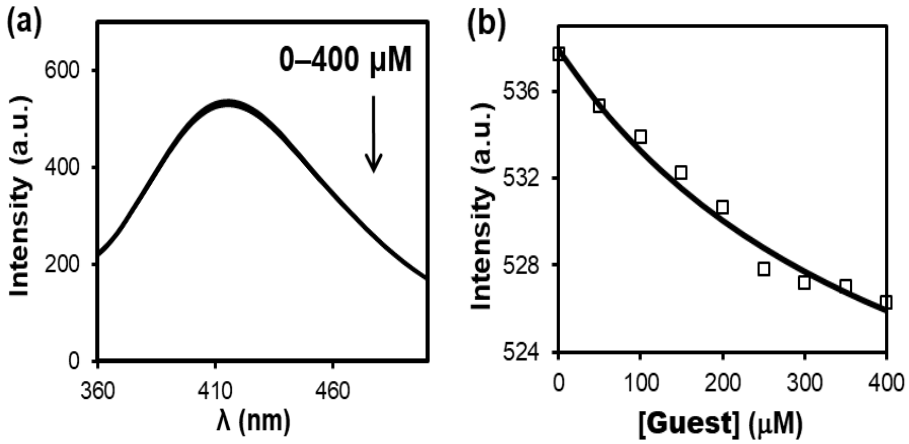

Figure S40. Fluorescence Titration of MINP(2) (2 equiv. FM) by citric acid. (a) Fluorescence emission spectra of MINP**(2)** (2 equiv. FM) (λ_{ex} = 340 nm) upon addition of different concentrations of citric acid in 50 mM Tris buffer (pH 7.4). [MINP**(2)**] = 2.0 μM. (b) Nonlinear least squares fitting of the emission intensity of MINP**(2)** at 420 nm to a 1:1 binding isotherm. The data corresponds to entry 10 in Table 2.

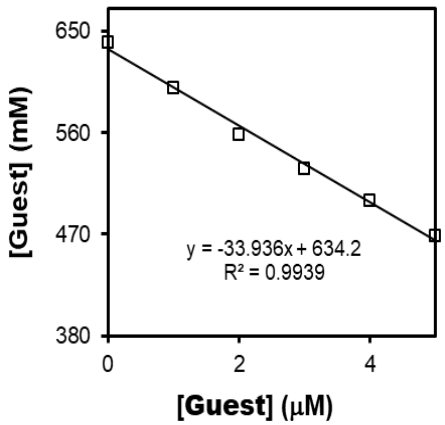

Figure S41. Limit of detection. Normalized response of fluorescence signal of MINP**(1)** in 50 mM Tris buffer (pH = 7.4, 2 μM) in the presence of increasing amount of **1** (1 μM to 5 μM) predissolved in buffer solution. (λ_{ex} = 370 nm; λ_{em} = 420 nm). The detection limit for **1** was calculated to be 144 nM (Detection limit = $3\sigma/K = 4.89/33.9 \times 10^{-6}$ M ≈ 144 nM).

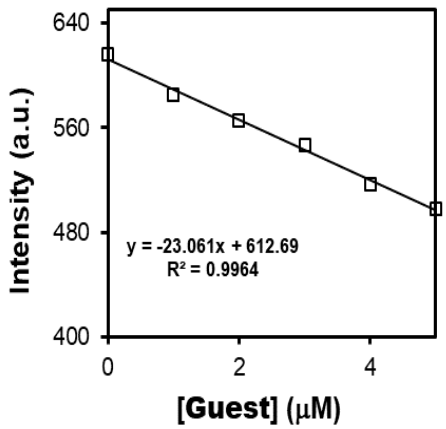

Figure S42. Limit of detection. Normalized response of fluorescence signal of MINP**(2)** in 50 mM Tris buffer (pH = 7.4, 2 μM) in the presence of increasing amount of **2** (1 μM to 5 μM) predissolved in buffer solution. (λ_{ex} = 370 nm; λ_{em} = 420 nm). The detection limit for **2** was calculated to be 204 nM (Detection limit = $3\sigma/K = 4.71/36.7 \times 10^{-6}$ M ≈ 204 nM).

^{1}H NMR, ^{13}C NMR

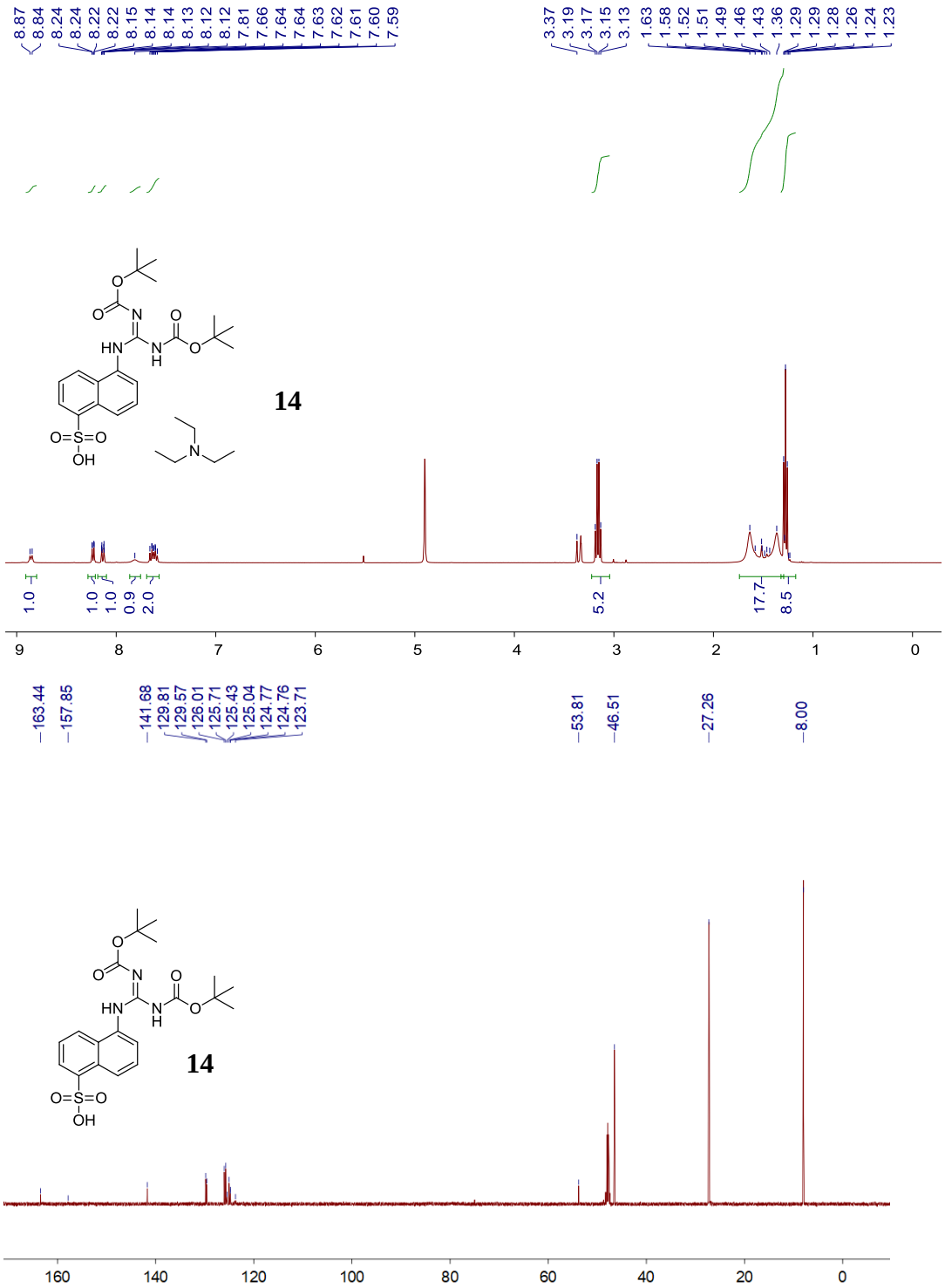

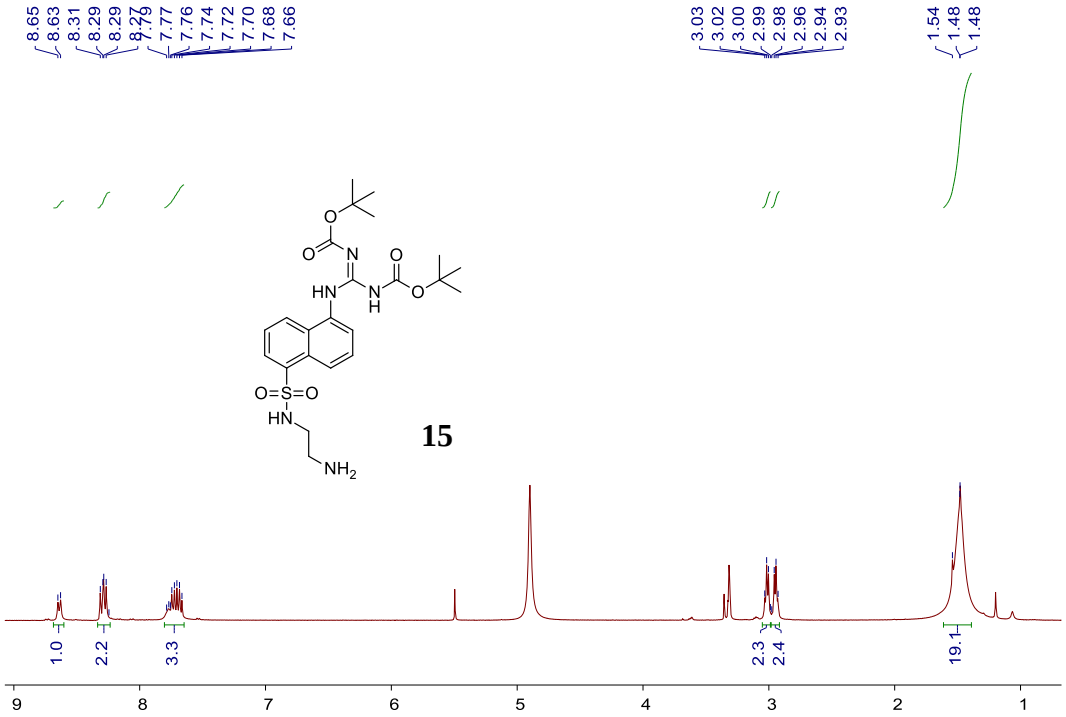

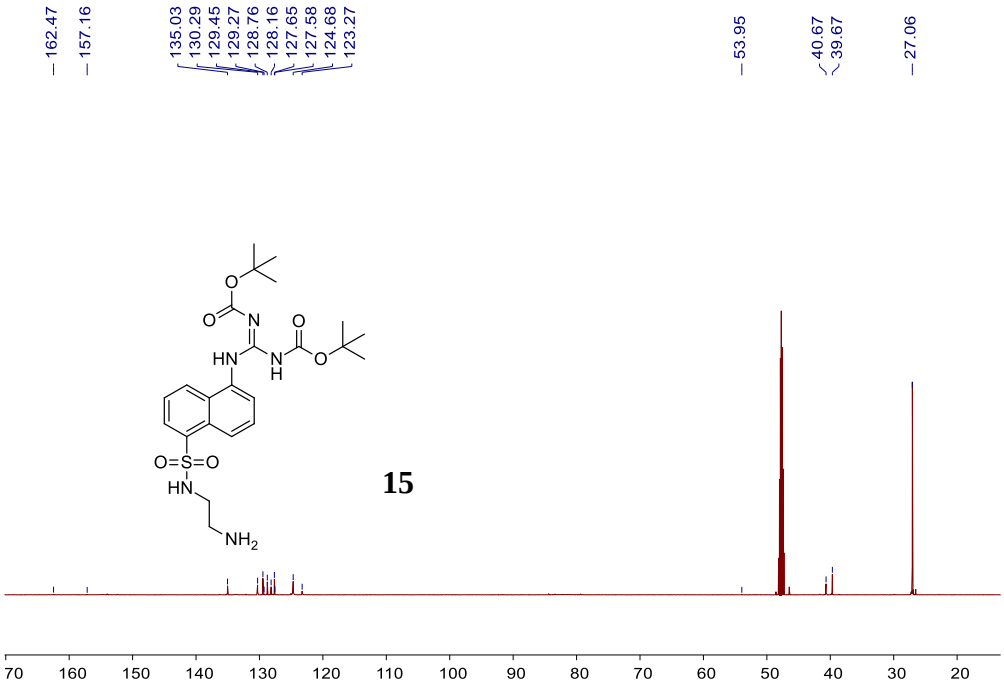

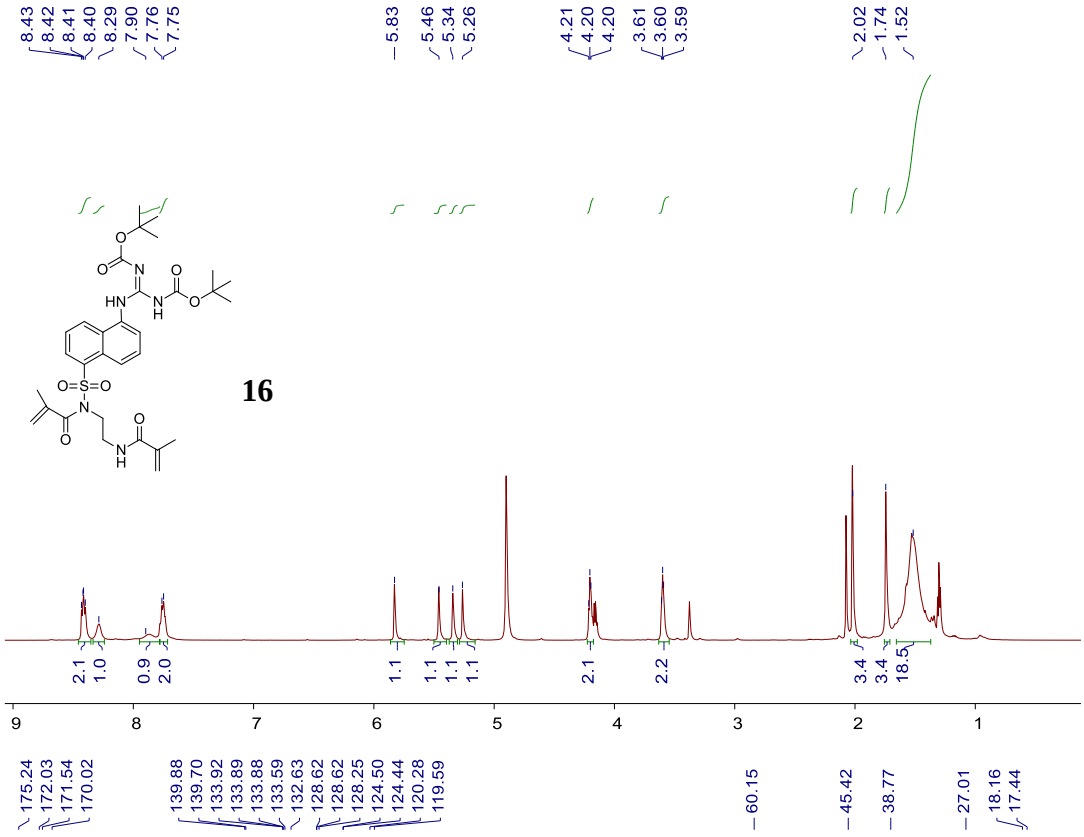

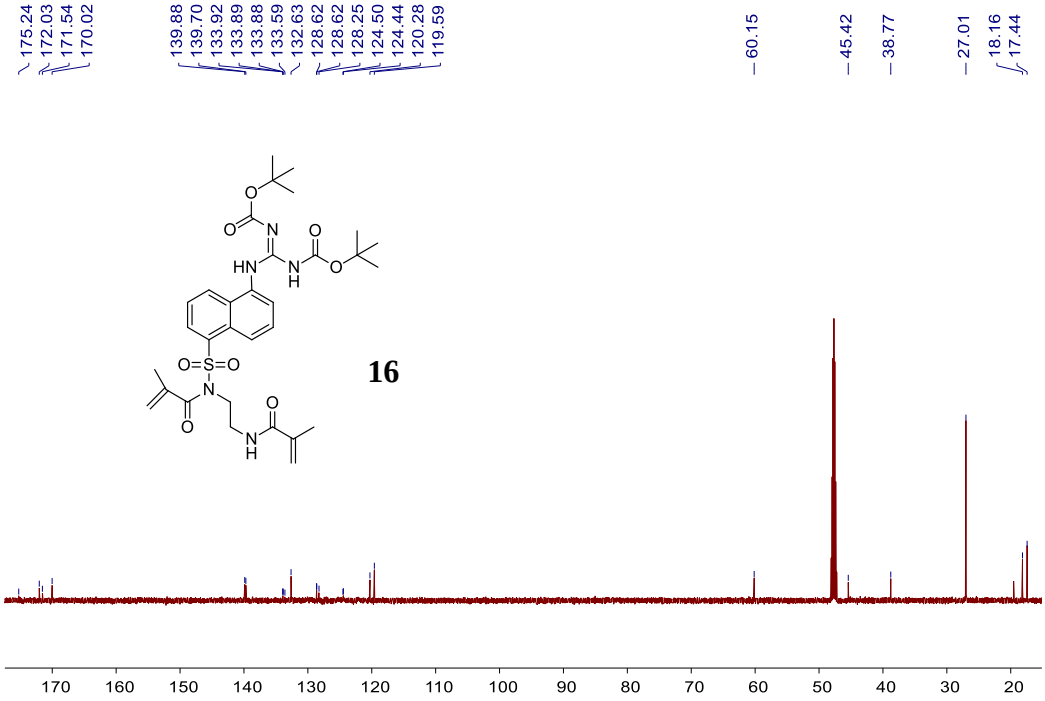

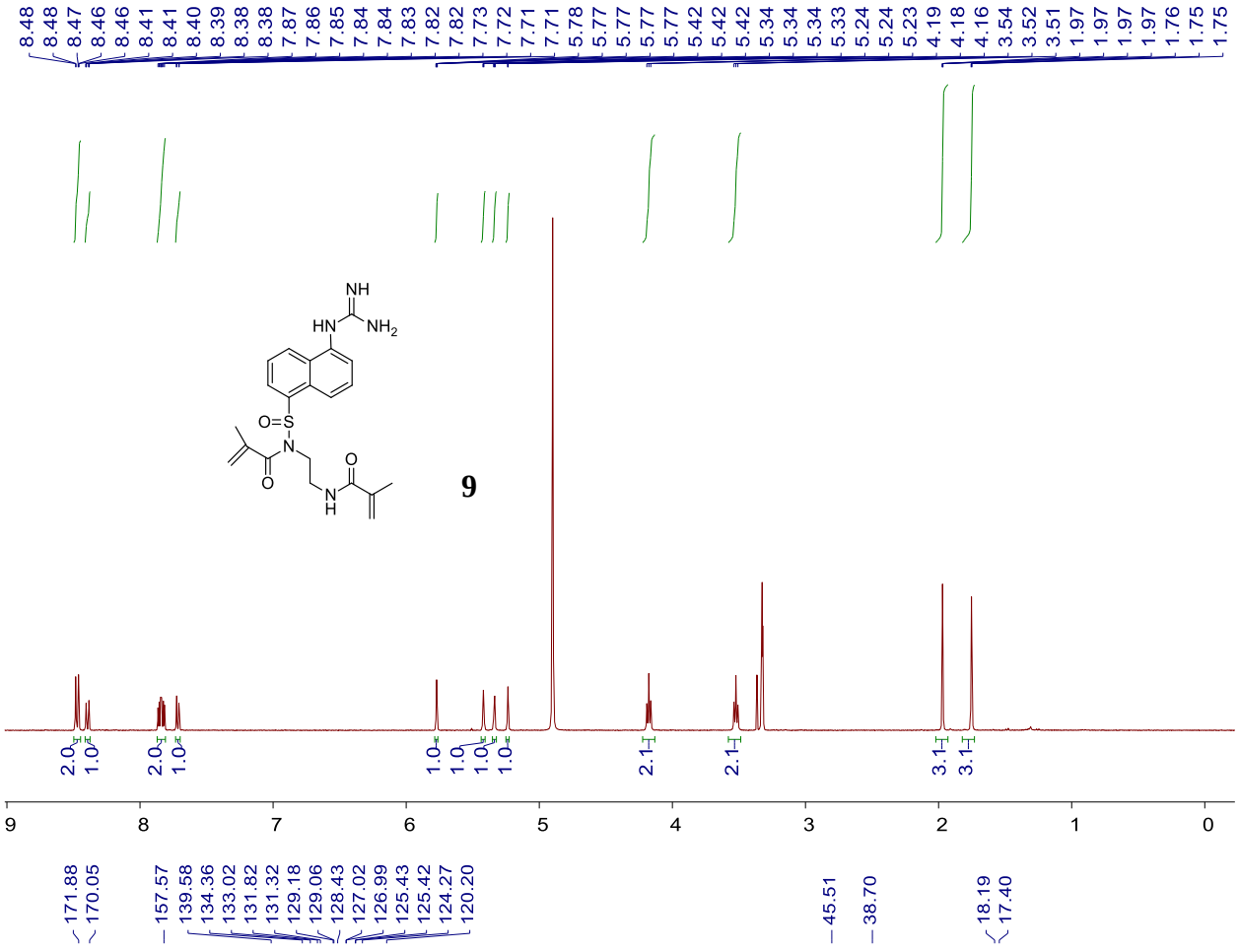

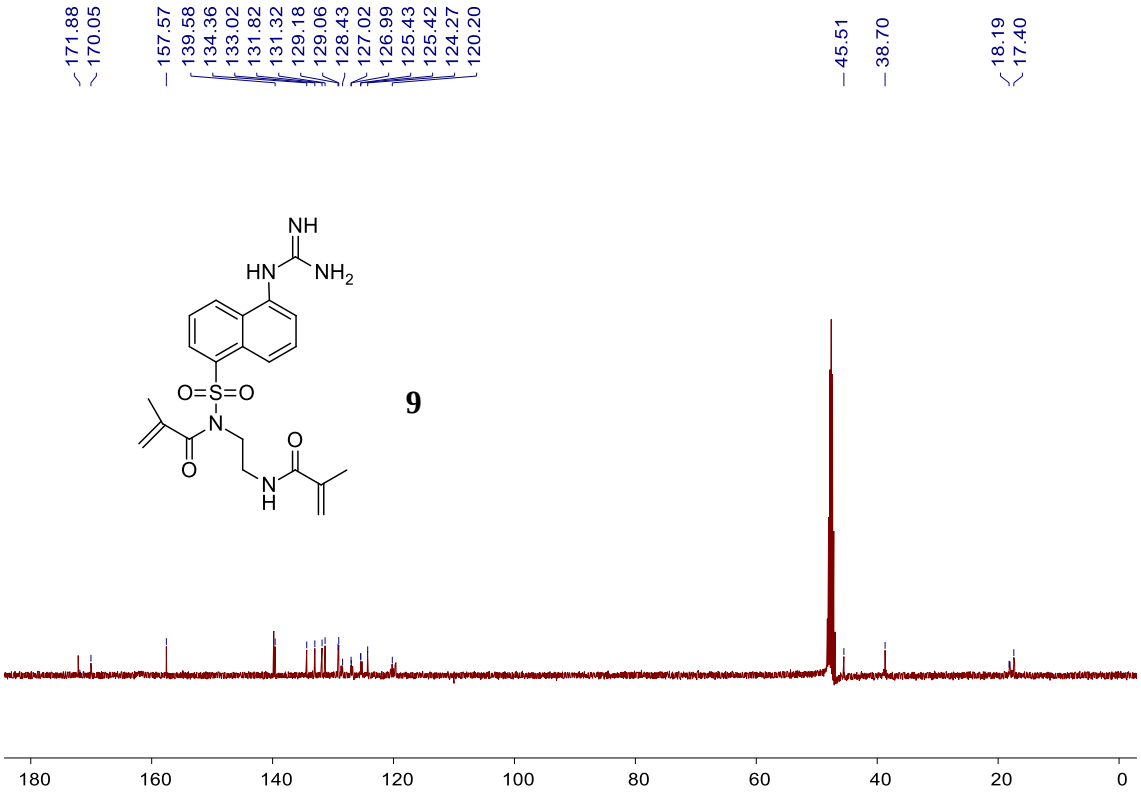

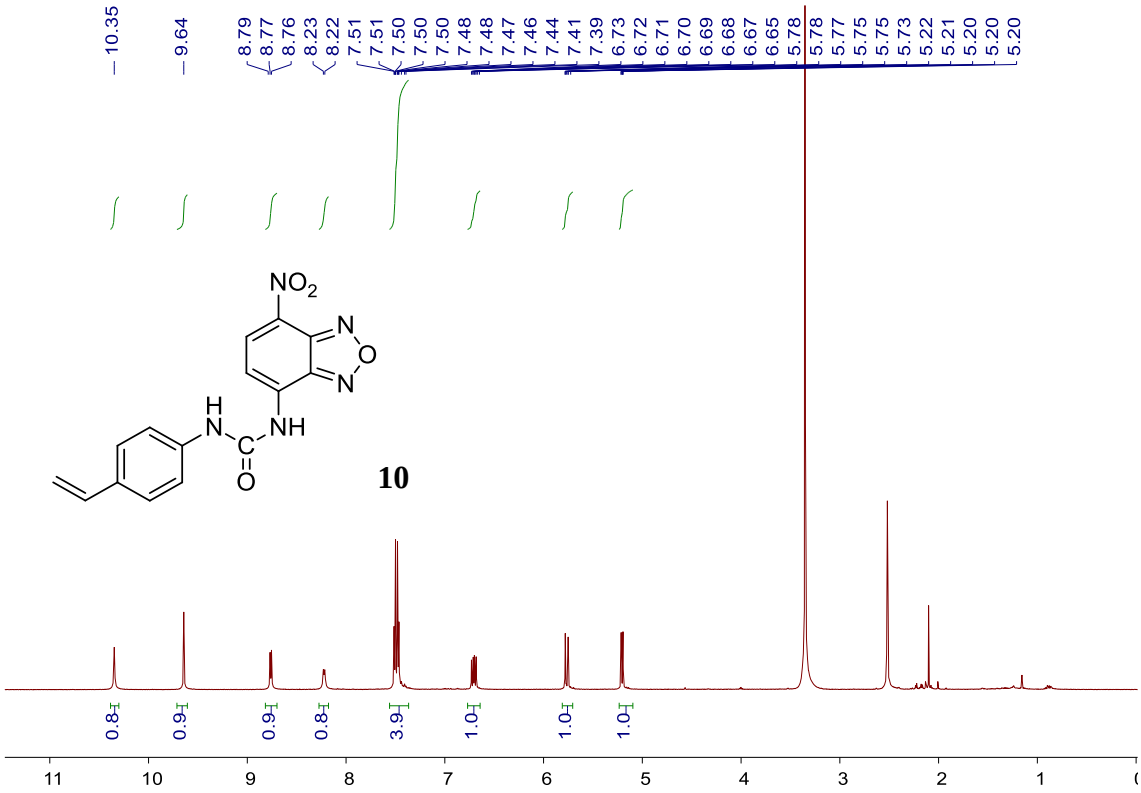

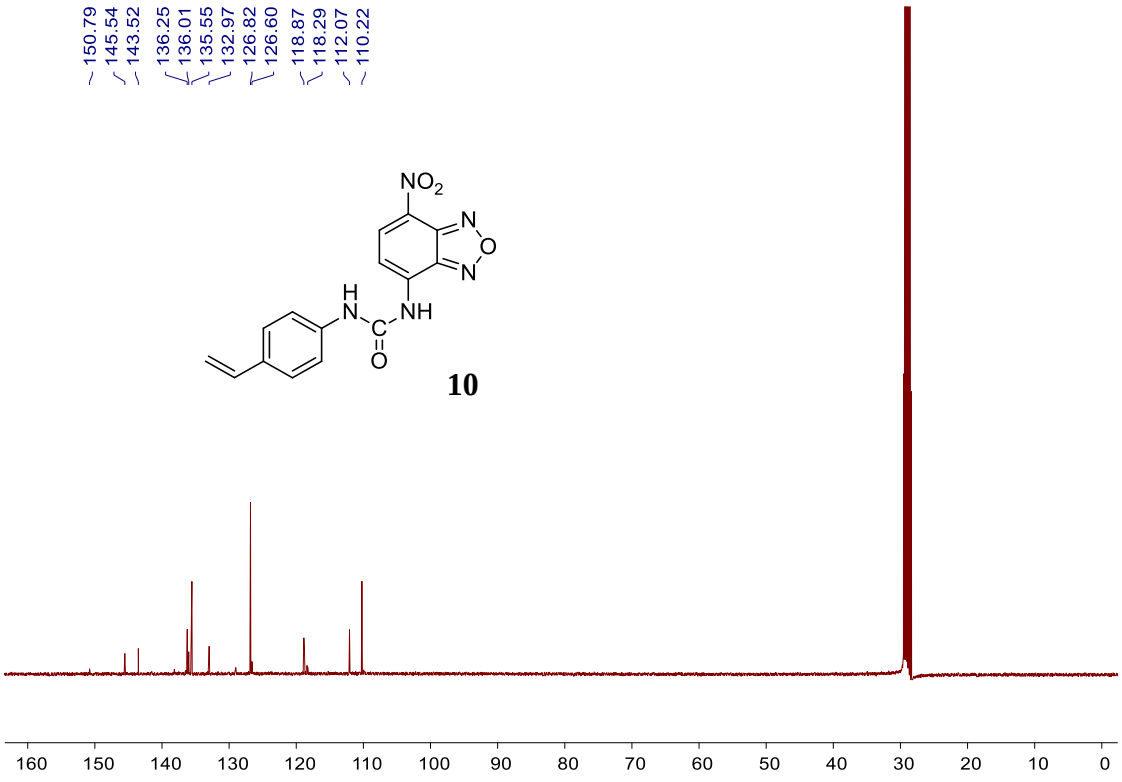

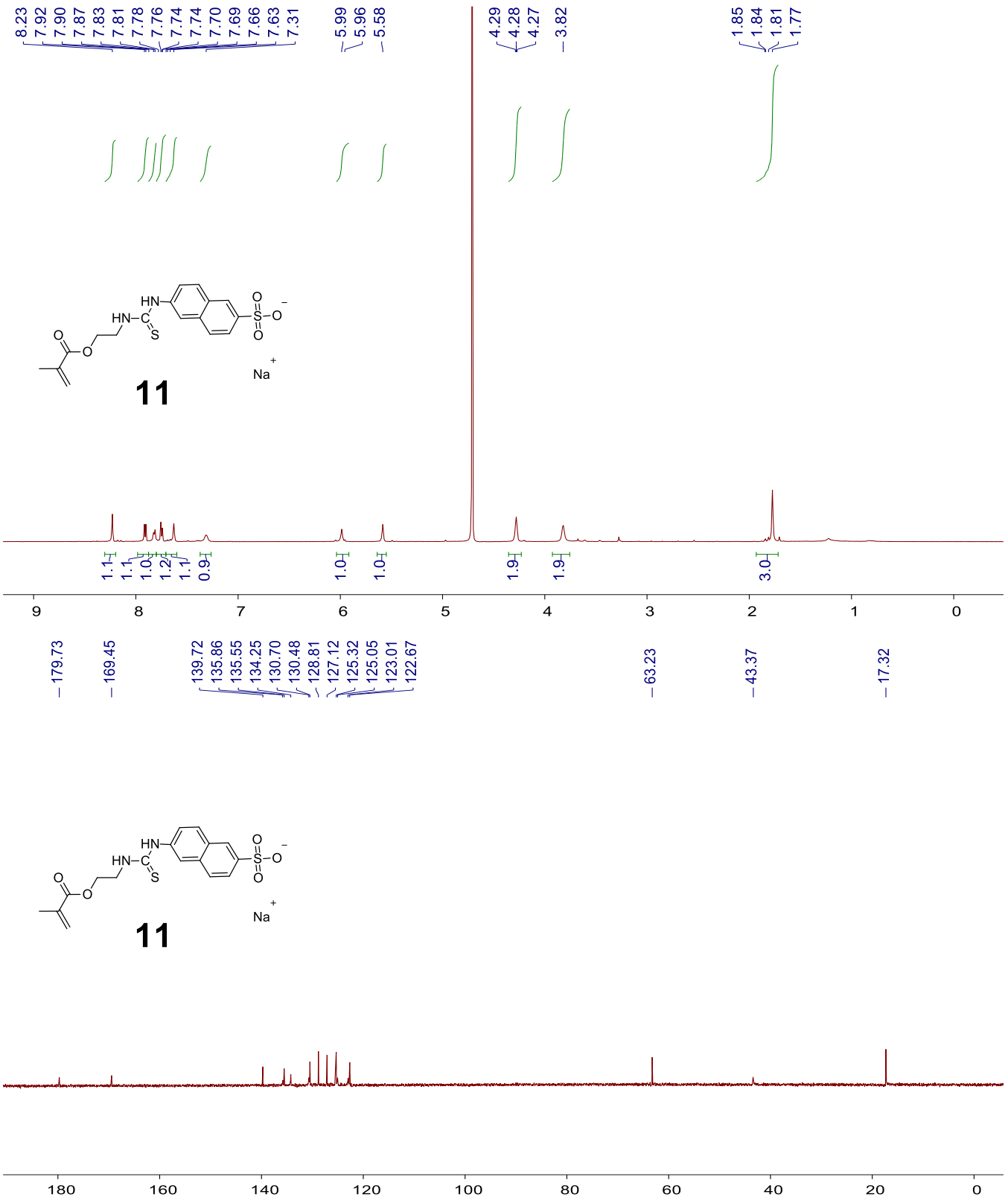

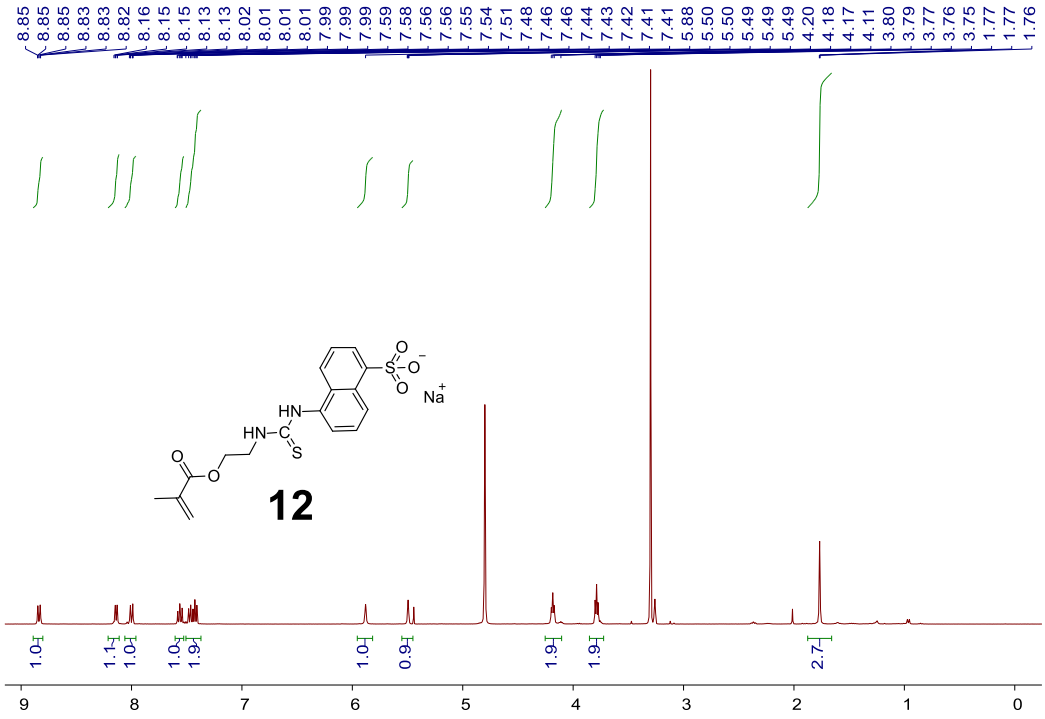

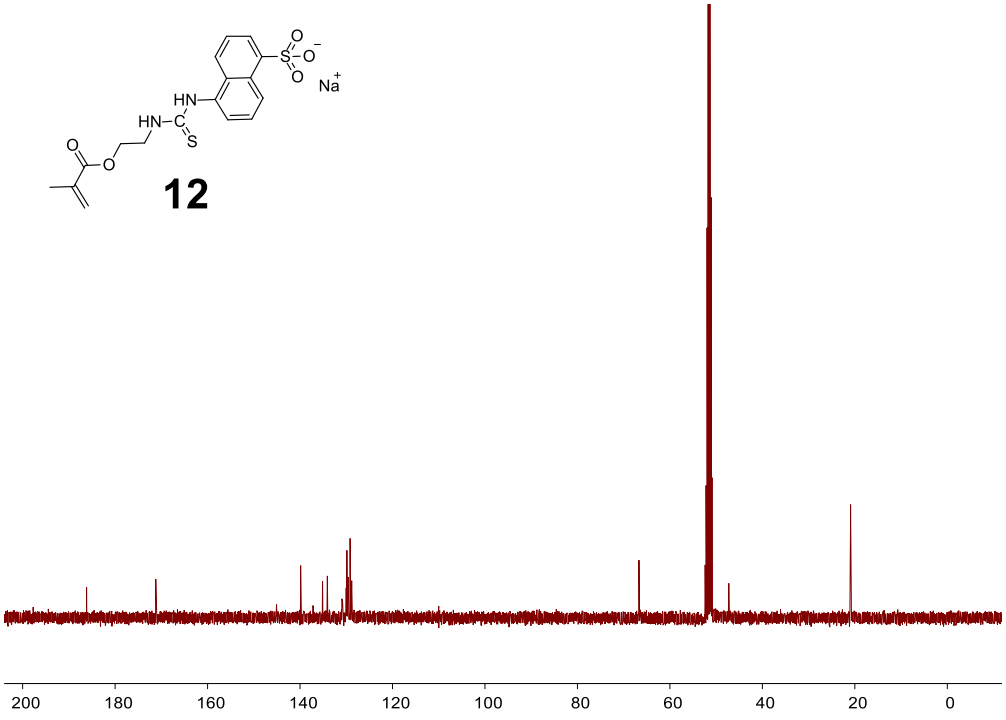

References

(1) Lewis, A.; Furst, D. E.: *Nonsteroidal Anti-Inflammatory Drugs: Mechanisms and Clinical Uses*; 2nd ed.; M. Dekker: New York, 1994.

(2) Zorita, S.; Mårtensson, L.; Mathiasson, L. Occurrence and Removal of Pharmaceuticals in a Municipal Sewage Treatment System in the South of Sweden. *Sci. Total Environ.* **2009**, *407*, 2760-2770.

(3) Camacho-Munoz, D.; Martin, J.; Santos, J. L.; Aparicio, I.; Alonso, E. Effectiveness of Conventional and Low-Cost Wastewater Treatments in the Removal of Pharmaceutically Active Compounds. *Water Air Soil Pollut.* **2012**, *223*, 2611-2621.

(4) Cycon, M.; Borymski, S.; Zolnierczyk, B.; Piotrowska-Seget, Z. Variable Effects of Non-Steroidal Anti-Inflammatory Drugs (Nsaids) on Selected Biochemical Processes Mediated by Soil Microorganisms. *Front. Microbiol.* **2016**, *7*, 1969.

(5) Chen, Y.-L.; Wu, S.-M. Capillary Zone Electrophoresis for Simultaneous Determination of Seven Nonsteroidal Anti-Inflammatory Drugs in Pharmaceuticals. *Anal. Bioanal. Chem.* **2005**, *381*, 907-912.

(6) Suenami, K.; Lim, L. W.; Takeuchi, T.; Sasajima, Y.; Sato, K.; Takekoshi, Y.; Kanno, S. Rapid and Simultaneous Determination of Nonsteroidal Anti-Inflammatory Drugs in Human Plasma by Lc–Ms with Solid-Phase Extraction. *Anal. Bioanal. Chem.* **2006**, *384*, 1501-1505.

(7) Wang, B.; Anslyn, E. V.: *Chemosensors : Principles, Strategies, and Applications*; Wiley: Hoboken, N.J., 2011.

(8) Mirsky, V. M.; Yatsimirsky, A. K.: *Artificial Receptors for Chemical Sensors*; Wiley-VCH Verlag: Weinheim, Germany, 2011.

(9) Carter, K. P.; Young, A. M.; Palmer, A. E. Fluorescent Sensors for Measuring Metal Ions in Living Systems. *Chem. Rev.* **2014**, *114*, 4564-4601.

(10) Niu, L. Y.; Chen, Y. Z.; Zheng, H. R.; Wu, L. Z.; Tung, C. H.; Yang, Q. Z. Design Strategies of Fluorescent Probes for Selective Detection among Biothiols. *Chem. Soc. Rev.* **2015**, *44*, 6143-6160.

(11) Mako, T. L.; Racicot, J. M.; Levine, M. Supramolecular Luminescent Sensors. *Chem. Rev.* **2019**, *119*, 322-477.

(12) Lapresta-Fernández, A.; Cywinski, P. J.; Moro, A. J.; Mohr, G. J. Fluorescent Polyacrylamide Nanoparticles for Naproxen Recognition. *Anal. Bioanal. Chem.* **2009**, *395*, 1821.

(13) Denat, F.; Diaz-Fernandez, Y. A.; Pasotti, L.; Sok, N.; Pallavicini, P. A Micellar Multitasking Device: Sensing Ph Windows and Gauging the Lipophilicity of Drugs with Fluorescent Signals. *Chem.-Eur. J.* **2010**, *16*, 1289-1295.

(14) Hallaj, T.; Amjadi, M.; Manzoori, J. L.; Azizi, N. A Novel Chemiluminescence Sensor for the Determination of Indomethacin Based on Sulfur and Nitrogen Co-Doped Carbon Quantum Dot-Kmno4 Reaction. *Luminescence* **2017**, *32*, 1174-1179.

(15) Loftsson, T.; Ólafsdóttir, B. J.; Friðriksdóttir, H.; Jónsdóttir, S. Cyclodextrin Complexation of Nsaidss: Physicochemical Characteristics. *Eur. J. Pharm. Sci.* **1993**, *1*, 95-101.

(16) Liu, Y.; Minami, T.; Nishiyabu, R.; Wang, Z.; Anzenbacher, P. Sensing of Carboxylate Drugs in Urine by a Supramolecular Sensor Array. *J. Am. Chem. Soc.* **2013**, *135*, 7705-7712.

(17) Meulenberg, E. P.; Peelen, G. O. H.; Lukkien, E.; Koopal, K. Immunochemical Detection Methods for Bioactive Pollutants. *Intern. J. Environ. Anal. Chem.* **2005**, *85*, 861-870.

(18) Deng, A.; Himmelsbach, M.; Zhu, Q.-Z.; Frey, S.; Sengl, M.; Buchberger, W.; Niessner, R.; Knopp, D. Residue Analysis of the Pharmaceutical Diclofenac in Different Water Types Using Elisa and Gc−Ms. *Environ. Sci. Technol.* **2003**, *37*, 3422-3429.

(19) Wulff, G. Enzyme-Like Catalysis by Molecularly Imprinted Polymers. *Chem. Rev.* **2001**, *102*, 1-28.

(20) Haupt, K.; Mosbach, K. Molecularly Imprinted Polymers and Their Use in Biomimetic Sensors. *Chem. Rev.* **2000**, *100*, 2495-2504.

(21) Lakshmi, D.; Bossi, A.; Whitcombe, M. J.; Chianella, I.; Fowler, S. A.; Subrahmanyam, S.; Piletska, E. V.; Piletsky, S. A. Electrochemical Sensor for Catechol and Dopamine Based on a Catalytic Molecularly Imprinted Polymer-Conducting Polymer Hybrid Recognition Element. *Anal. Chem.* **2009**, *81*, 3576-3584.

(22) Ma, Y.; Pan, G. Q.; Zhang, Y.; Guo, X. Z.; Zhang, H. Q. Narrowly Dispersed Hydrophilic Molecularly Imprinted Polymer Nanoparticles for Efficient Molecular Recognition in Real Aqueous Samples Including River Water, Milk, and Bovine Serum. *Angew. Chem. Int. Ed.* **2013**, *52*, 1511-1514.

(23) Kuwata, T.; Uchida, A.; Takano, E.; Kitayama, Y.; Takeuchi, T. Molecularly Imprinted Polymer Arrays as Synthetic Protein Chips Prepared by Transcription-Type Molecular Imprinting by Use of Protein-Immobilized Dots as Stamps. *Anal. Chem.* **2015**, *87*, 11784-11791.

(24) Liu, J.; Yin, D.; Wang, S.; Chen, H. Y.; Liu, Z. Probing Low‐Copy‐Number Proteins in a Single Living Cell. *Angew. Chem. Int. Ed.* **2016**, *55*, 13215-13218.

(25) Chen, L.; Wang, X.; Lu, W.; Wu, X.; Li, J. Molecular Imprinting: Perspectives and Applications. *Chem. Soc. Rev.* **2016**, *45*, 2137-2211.

(26) Horikawa, R.; Sunayama, H.; Kitayama, Y.; Takano, E.; Takeuchi, T. A Programmable Signaling Molecular Recognition Nanocavity Prepared by Molecular Imprinting and Post-Imprinting Modifications. *Angew. Chem. Int. Ed.* **2016**, *55*, 13023-13027.

(27) Panagiotopoulou, M.; Salinas, Y.; Beyazit, S.; Kunath, S.; Duma, L.; Prost, E.; Mayes, A. G.; Resmini, M.; Bui, B. T. S.; Haupt, K. Molecularly Imprinted Polymer Coated Quantum Dots for Multiplexed Cell Targeting and Imaging. *Angew. Chem. Int. Ed.* **2016**, *55*, 8244-8248.

(28) Bertolla, M.; Cenci, L.; Anesi, A.; Ambrosi, E.; Tagliaro, F.; Vanzetti, L.; Guella, G.; Bossi, A. M. Solvent-Responsive Molecularly Imprinted Nanogels for Targeted Protein

Analysis in Maldi-Tof Mass Spectrometry. *ACS Appl. Mater. Interfaces* **2017**, *9*, 6908-6915.

(29) Yang, Y. Q.; Niu, H.; Zhang, H. Q. Direct and Highly Selective Drug Optosensing in Real, Undiluted Biological Samples with Quantum-Dot-Labeled Hydrophilic Molecularly Imprinted Polymer Microparticles. *ACS Appl. Mater. Interfaces* **2016**, *8*, 15741-15749.

(30) Jiang, L.; Messing, M. E.; Ye, L. Temperature and Ph Dual-Responsive Core-Brush Nanocomposite for Enrichment of Glycoproteins. *ACS Appl. Mater. Interfaces* **2017**, *9*, 8985-8995.

(31) Kempe, M.; Mosbach, K. Direct Resolution of Naproxen on a Noncovalently Molecularly Imprinted Chiral Stationary-Phase. *J Chromatogr A* **1994**, *664*, 276-279.

(32) Hung, C. Y.; Huang, Y. T.; Huang, H. H.; Hwang, C. C. Synthesis and Molecular Recognition of Molecularly Imprinted Polymer with Ibuprofen as Template. *J. Chin. Chem. Soc.* **2006**, *53*, 1173-1180.

(33) Chen, D.-M.; Fu, Q.; Du, W.; Sun, S.-J.; Huang, P.; Chang, C. Preparation and Evaluation of Monolithic Molecularly Imprinted Stationary Phase for S-Naproxen. *J. Pharm. Anal.* **2011**, *1*, 26-31.

(34) Manesiotis, P.; Osmani, Q.; McLoughlin, P. An Enantio-Selective Chromatographic Stationary Phase for S-Ibuprofen Prepared by Stoichiometric Molecular Imprinting. *J. Mater. Chem.* **2012**, *22*, 11201-11207.

(35) Awino, J. K.; Zhao, Y. Protein-Mimetic, Molecularly Imprinted Nanoparticles for Selective Binding of Bile Salt Derivatives in Water. *J. Am. Chem. Soc.* **2013**, *135*, 12552-12555.

(36) Awino, J. K.; Zhao, Y. Polymeric Nanoparticle Receptors as Synthetic Antibodies for Nonsteroidal Anti-Inflammatory Drugs (Nsaids). *ACS Biomater. Sci. Eng.* **2015**, *1*, 425-430.

(37) Awino, J. K.; Gunasekara, R. W.; Zhao, Y. Sequence-Selective Binding of Oligopeptides in Water through Hydrophobic Coding. *J. Am. Chem. Soc.* **2017**, *139*, 2188-2191.

(38) Awino, J. K.; Gunasekara, R. W.; Zhao, Y. Selective Recognition of D-Aldohexoses in Water by Boronic Acid-Functionalized, Molecularly Imprinted Cross-Linked Micelles. *J. Am. Chem. Soc.* **2016**, *138*, 9759-9762.

(39) Gunasekara, R. W.; Zhao, Y. A General Method for Selective Recognition of Monosaccharides and Oligosaccharides in Water. *J. Am. Chem. Soc.* **2017**, *139*, 829-835.

(40) Wan, W.; Biyikal, M.; Wagner, R.; Sellergren, B.; Rurack, K. Fluorescent Sensory Microparticles That "Light-up" Consisting of a Silica Core and a Molecularly Imprinted Polymer (Mip) Shell. *Angew. Chem. Int. Ed.* **2013**, *52*, 7023-7027.

(41) Nowick, J. S.; Chen, J. S. Molecular Recognition in Aqueous Micellar Solution - Adenine Thymine Base-Pairing in Sds Micelles. *J. Am. Chem. Soc.* **1992**, *114*, 1107-1108.

(42) Nowick, J. S.; Chen, J. S.; Noronha, G. Molecular Recognition in Micelles - the Roles of Hydrogen-Bonding and Hydrophobicity in Adenine Thymine Base-Pairing in Sds Micelles. *J. Am. Chem. Soc.* **1993**, *115*, 7636-7644.

(43) Ariga, K.; Kunitake, T. Molecular Recognition at Air-Water and Related Interfaces: Complementary Hydrogen Bonding and Multisite Interaction. *Acc. Chem. Res.* **1998**, *31*, 371-378.

(44) A 1:1 FM/template ratio under such a condition translates to ~40% complexation if the binding constant is 5000 -1M. A 2:1 FM/template ratio translates to ~60% complexation.

(45) Zhang, H.; Fan, J.; Wang, J.; Zhang, S.; Dou, B.; Peng, X. An Off–on Cox-2-Specific Fluorescent Probe: Targeting the Golgi Apparatus of Cancer Cells. *J. Am. Chem. Soc.* **2013**, *135*, 11663-11669.

(46) Li, X.; Zhao, Y. Protection/Deprotection of Surface Activity and Its Applications in the Controlled Release of Liposomal Contents. *Langmuir* **2012**, *28*, 4152-4159.

(47) Fa, S.; Zhao, Y. Peptide-Binding Nanoparticle Materials with Tailored Recognition Sites for Basic Peptides. *Chem. Mater.* **2017**, *29*, 9284-9291.

(48) Fa, S.; Zhao, Y. Water-Soluble Nanoparticle Receptors Supramolecularly Coded for Acidic Peptides. *Chem. -Eur. J.* **2018**, *24*, 150-158.

(49) Kosower, E. M. Intramolecular Donor-Acceptor Systems .9. Photophysics of (Phenylamino)Naphthalenesulfonates - a Paradigm for Excited-State Intramolecular Charge-Transfer. *Acc. Chem. Res.* **1982**, *15*, 259-266.

(50) Chadha, G.; Zhao, Y. Properties of Surface-Cross-Linked Micelles Probed by Fluorescence Spectroscopy and Their Catalysis of Phosphate Ester Hydrolysis. *J. Colloid Interface Sci.* **2013**, *390*, 151-157.

(51) Skalka, N.; Krol, A.; Schlesinger, H.; Altstein, M. Monitoring of the Non-Steroid Anti-Inflammatory Drug Indomethacin: Development of Immunochemical Methods for Its Purification and Detection. *Anal. Bioanal. Chem.* **2011**, *400*, 3491-3504.

(52) Tanford, C.: *The Hydrophobic Effect: Formation of Micelles and Biological Membranes*; 2nd ed.; Krieger: Malabar, Fla., 1991.

(53) Awino, J. K.; Zhao, Y. Imprinted Micelles for Chiral Recognition in Water: Shape, Depth, and Number of Recognition Sites. *Org. Biomol. Chem.* **2017**, *15*, 4851-4858.

CHAPTER 5. SELECTIVE BINDING OF DOPAMINE AND ADRENALINE IN WATER BY FLUORESCENTLY FUNCTIONALIZED IMPRINTED MICELLES

Likun Duan[1], Yan Zhao[1]*

[1]Department of chemistry, Iowa State University, Ames, Iowa, 50011 United States

* Corresponding Authors

ABSTRACT. Catecholamines (CAs) such as dopamine and epinephrine played important roles in biology but their structural similarity makes it challenging to construct synthetic receptors with selective binding. A combination of covalent (boronate) and noncovalent (hydrogen-bonds) in molecularly imprinted cross-linked micelles was effective to distinguish these compounds and other related biological analogues. Micromolar binding affinities were observed and the binding was reported by fluorescent signals. An extra hydroxyl or methyl on the structure was readily detected, making these water-soluble nanoparticle receptors potentially useful in biological applications.

Introduction

Catecholamines (CAs) such as dopamine (DA, **1**), epinephrine (EP, **2**), and norepinephrine (NE, **3**) are neurotransmitters and/or hormones that regulate a plethora of biological processes including reward signalling, motor control, sleep, and stress.[1-3] Their biological significance has motivated many researchers to construct synthetic receptors, sensors, and fluorescent tracers that help the study of their biological activities.[4, 5] Receptors and molecular sensors can be built to form reversible covalent bonds for recognition, preferably with both the amino and catechol, through imine and

boronate ester formation, respectively.[6-8] Noncovalent interactions may also be used, including hydrogen-bonds, ion-pairs, and cation–π interactions, typically using a macrocyclic or tweezer framework.[9-15]

CAs are metabolized from tyrosine via intermediate 3,4-dihydroxyphenylalanine (i.e., *L*-DOPA, **4**). The latter can cross the blood–brain barrier and is used to increase the concentration of DA in the brain for patients with DA deficiency (e.g., Parkinson's disease).[1-3] Other naturally occurring analogues of CAs include tyrosine (**5**), 3-methoxytryamine (**6**), and tyramine (**7**).

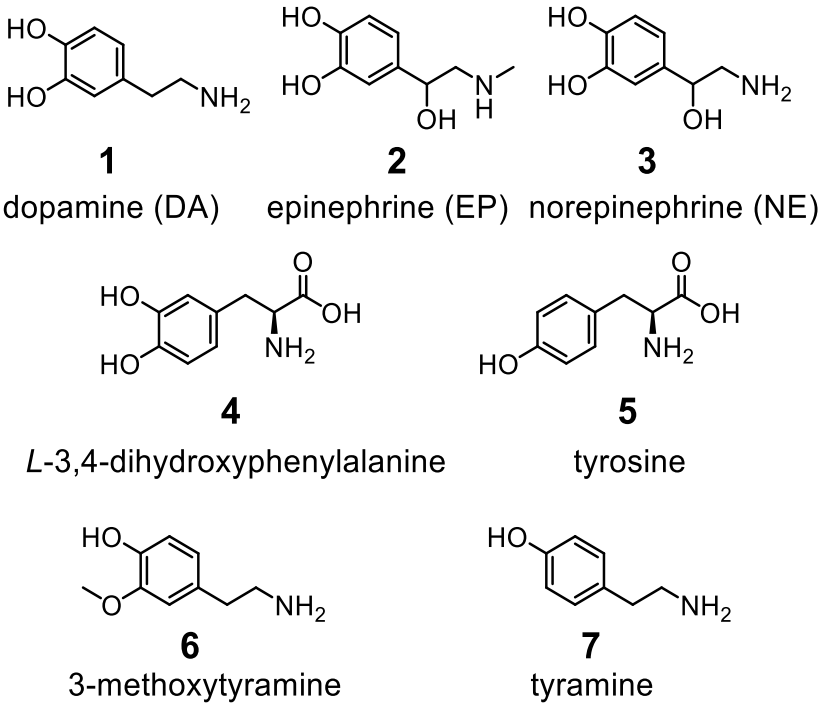

The structural similarity of CAs, their metabolic precursors, and other biogenic amines make it very challenging for a receptor to bind a particular CA selectively. Imine/iminium can be formed between an aldehyde and any one of **1**–**7**, although the reaction rates could differ. Because boronate ester can form between a boronic acid and **1**–**4**, using both imine and boronate would not be able to distinguish CAs. If noncovalent interactions are used for the

binding, a significant challenge comes from the aqueous environment, as water is an excellent hydrogen-bond donor and acceptor. With a large penalty paid for desolvation, most noncovalently based synthetic receptors either do not function in water or bind the compounds weakly.

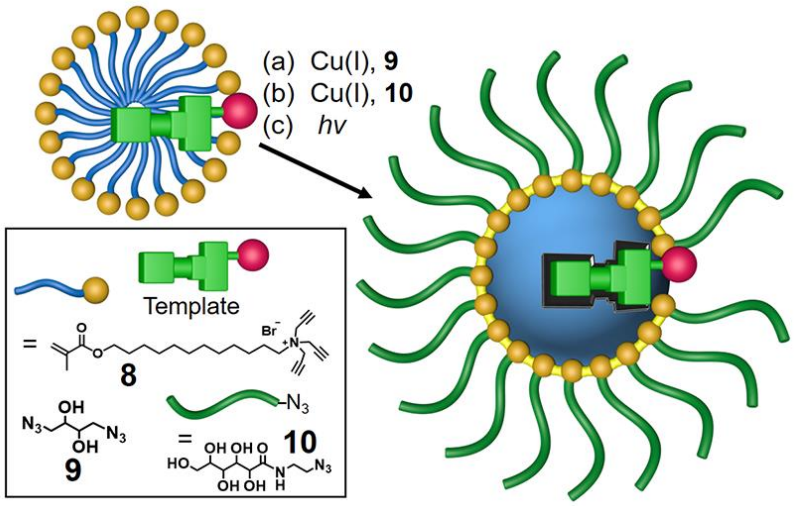

Scheme 1. Preparation of MINP through micellar imprinting.

In this work, we report a method to combine specific covalent and noncovalent interactions to build selective nanoparticle receptors for CAs in water, using DA and EP as examples. The combination not only afforded micromolar binding affinities, but also allowed us to distinguish DA and EP, even NE that differs from EP by a single methyl group.

To build the receptor, we employed micellar imprinting developed by our group, that utilized click chemistry-based surface cross-linking and free radical core-cross-linking for the templated polymerization (Scheme 1).[16] Although the concept of molecular imprinting has been known for decades,[17, 18] our method differed in several key aspects (Scheme 1). First, the key

imprinting step takes place in the surface-cross-linked micelle, when divinylbenzene (DVB) and the methacrylate of **8** undergo polymerization/cross-linking induced by 2,2-dimethoxy-2-phenylacetophenone (DMPA) under UV irradiation. It has been shown that the nano-confinement is key to the exceptional imprinting effect observed,[19] frequently with the imprinting factor exceeding 100.[20, 21] Second, the number of binding sites per nanoparticle can be simply controlled by the surfactant/template ratio, given that the cross-linked micelle contains approximately 50 surfactants.[16] Third, being cationically charged and decorated with a layer of sugar-derived surface ligand (**10**), the cross-linked micelles are soluble in water and selected organic solvents such as DMF, unlike most molecular imprinted polymers reported in the literature.[17, 18] Fourth, the resulting molecularly imprinted nanoparticles (MINPs) are ~5 nm in diameter according to dynamic light scattering (DLS) and transmission electron microscopy (TEM).[16, 20] The exceedingly high surface area of MINP and the location of the template near the surfactant/water interface—resulted from polar groups represented by the purpose sphere in Scheme 1—make the imprinted sites readily accessible. Lastly, covalent groups can be introduced in the imprinted site and modified in high yields through standard chemical reactions such as amidation and imine formation, due to the solubility of MINP and accessibility of the imprinted sites.[22, 23]

Preparation and characterization of MINPs are reported in the Supporting Information and followed previous procedures.[16] To make the MINP recognize CAs, we included two functional monomers (FMs) **11** and **12** in the formulation. Compound **11** was prepared by a six-step reaction from anthracene. It has several important features: a boronic acid with the ortho amino group to bind catechol via boronate formation, a methacrylamide for its covalent incorporation into the MINP, a fluorescent anthracene

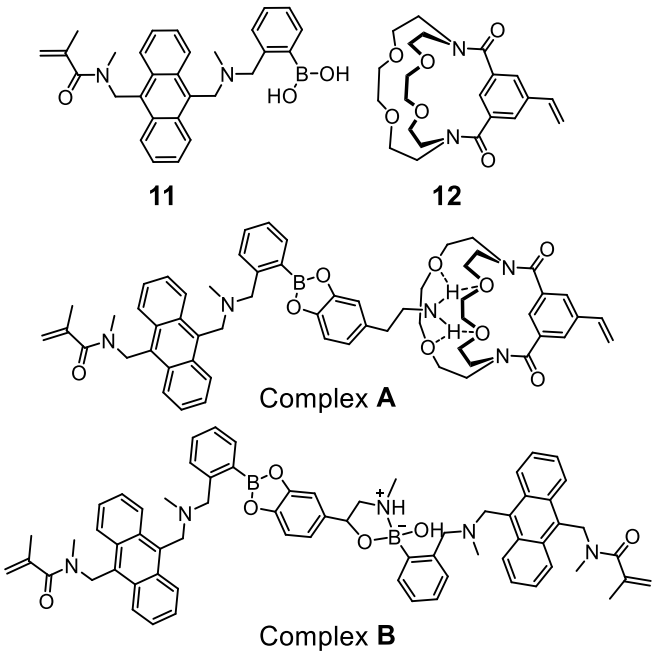

Figure 1. Structures of FM **11** and **12**, as well as the proposed complexes formed by DA (complex **A**) and EP (complex **B**).

to report the binding, and the amino group. FM **12** was first reported by us and was shown to be highly effective at binding amino/ammonium side chain of lysine in a micellar environment through hydrogen bonds.[20] Even though hydrogen-bonds are weak in water, they are known to be strengthened inside micelles[24, 25] and at the surfactant/water interface.[26]

Prior to the experiments, our postulation was that DA and EP differ in two aspects. EP has an extra hydroxyl next to the amino group and its amino group further functionalized with a methyl. Since **12** worked well for the amino side chain of lysine, it is expected to form a three-component complex (**A**) with DA and **11** (Fig. 1). The extra methyl of EP, on the other hand, reduces the number of potential hydrogen bonds

to be formed with **12**. Meanwhile, its extra β-hydroxyl makes it possible for EP to form a 1:2 complex (**B**) with FM **11**.

Table 1. Binding constants of MINPs prepared for DA and EP.[a]

Entry	Template	FM **11**	FM **12**	Guest	K_a ($\times 10^4$ M^{-1})	CRR[b]
1	DA	2 equiv	0 equiv	DA	1.9 ± 0.5	1
2	DA	2 equiv	0 equiv	EP	0.93 ± 0.06	0.49
3	DA	1 equiv	1 equiv	DA	3.8 ± 0.5	1
4	DA	1 equiv	1 equiv	EP	0.35 ± 0.14	0.09
5	DA	2 equiv	1 equiv	DA	3.1 ± 0.6	1
6	DA	2 equiv	1 equiv	EP	0.42 ± 0.13	0.14
7	EP	2 equiv	0 equiv	DA	0.51 ± 0.04	0.12
8	EP	2 equiv	0 equiv	EP	4.1 ± 0.25	1
9	EP	1 equiv	1 equiv	DA	0.61 ± 0.11	0.81
10	EP	1 equiv	1 equiv	EP	0.75 ± 0.24	1
11	EP	2 equiv	1 equiv	DA	1.0 ± 0.31	0.29
12	EP	2 equiv	1 equiv	EP	3.5 ± 0.51	1

[a] Binding constants were obtained from fluorescence titrations performed in duplicates in in 10 mM Tris buffer (pH = 9.0). [b] CRR is the cross-reactivity ratio, defined as the binding constant of a guest relative to that of the template for a particular MINP.

Our Binding data seems to support the above pictures. As shown in Table 1, we first prepared MINP(DA), with DA as the template and different ratios of FM/T for **11** and **12**. The binding constants were determined by fluorescence titrations (Figures S7–S32).

The amount of **11** was varied from 1 to 2 equivalents to the template, and the amount of **12** from 1 to 1 equivalent. As more FM **11** was used, the binding of DA by MINP(DA) first increased from 1.9 to 3.8 × 10^4 M^{-1} and then plateaued (within the experimental error) to 3.1 × 10^4 M^{-1} (entries 1, 3, and 5). Meanwhile, the binding for EP stayed relatively weak and reached the minimum at 1:1 **11**/**12** (entry 4). As a result, the strongest and most selective binding occurred at this ratio, as we had hypothesized. The selectivity is reflected in the cross-reactivity ratio (CRR), defined as the binding constant of a guest relative to that of the template for a particular MINP.

Table 2. Binding constants of MINP(DA).[a]

Entry	Template	Guest	K_a (× 10^4 M^{-1})	-Δ*G* (kcal/mol)	CRR[b]
1	**1** (DA)	**1** (DA)	3.8 ± 0.5	6.25	1
2	**1** (DA)	**2** (EP)	0.35 ± 0.14	4.83	0.09
3	**1** (DA)	**3** (NE)	0.72 ± 0.24	5.26	0.19
4	**1** (DA)	**4**	0.12 ± 0.04	4.20	0.03
5	**1** (DA)	**5**	0.08 ± 0.02	3.96	0.02
6	**1** (DA)	**6**	0.05 ± 0.01	3.68	0.01
7	**1** (DA)	**7**	0.20 ± 0.06	4.50	0.05

[a] The MINP was prepared at DA/**11**/**12** = 1:1:1. Binding constants were obtained from fluorescence titrations performed in duplicates in in 10 mM Tris buffer (pH = 9.0). [b] CRR is the cross-reactivity ratio, defined as the binding constant of a guest relative to that of the template for a particular MINP.

When the same experiments were done with MINP(EP), the optimal ratio was found 2:0 **11**/**12** (entries 7–8), where the binding for the template was the strongest and for the analogue was the weakest.

Table 2 shows the binding of MINP(DA) for guests **1**–**7**, with the MINP prepared at the optimal ratio of DA/**11**/**12** = 1:1:1. Consistent with successful molecular imprinting, the strongest binding was observed for the template (DA). The binding constant (3.8×10^4 M^{-1}) in the aqueous buffer (10 mM Tris) was much larger than what have been reported for previous receptors. The number corresponds to a binding free energy ($-\Delta G$) of 6.25 kcal/mol, which is substantial for a small water-soluble guest.

Table 3. Binding constants of MINP(EP).[a]

Entry	Template	Guest	K_a ($\times 10^4$ M^{-1})	$-\Delta G$ (kcal/mol)	CRR[b]
1	**2** (EP)	**1** (DA)	0.51 ± 0.04	5.06	0.12
2	**2** (EP)	**2** (EP)	4.1 ± 0.25	6.29	1.00
3	**2** (EP)	**3** (NE)	1.9 ± 0.25	5.84	0.46
4	**2** (EP)	**4**	0.07 ± 0.02	3.88	0.02
5	**2** (EP)	**5**	0.11 ± 0.01	4.15	0.03
6	**2** (EP)	**6**	0.03 ± 0.01	3.38	0.01
7	**2** (EP)	**7**	0.02 ± 0.01	3.14	0.005

[a] The MINP was prepared at DA/**11**/**12** = 1:2:0. Binding constants were obtained from fluorescence titrations performed in duplicates in in 10 mM Tris buffer (pH = 9.0). [b] CRR is the cross-reactivity ratio, defined as the binding constant of a guest relative to that of the template for a particular MINP.

Among the analogues, the one that showed the highest cross-reactivity was actually norepinephrine (NE, **3**), followed by epinephrine (EP, **2**). Their binding constants differed by a factor of 2. This trend is extremely telling, with regard to our binding model (Fig. 1). NE only differed from DA by an extra hydroxyl. Everything else was exactly the same as the template. Thus, it can engage the same covalent and noncovalent binding interactions as the template (DA) with MINP(DA). In this sense, the 5-fold difference in binding constant and nearly 1 kcal/mol difference in binding free energy were quite impressive, as they were derived from a single hydroxyl group.

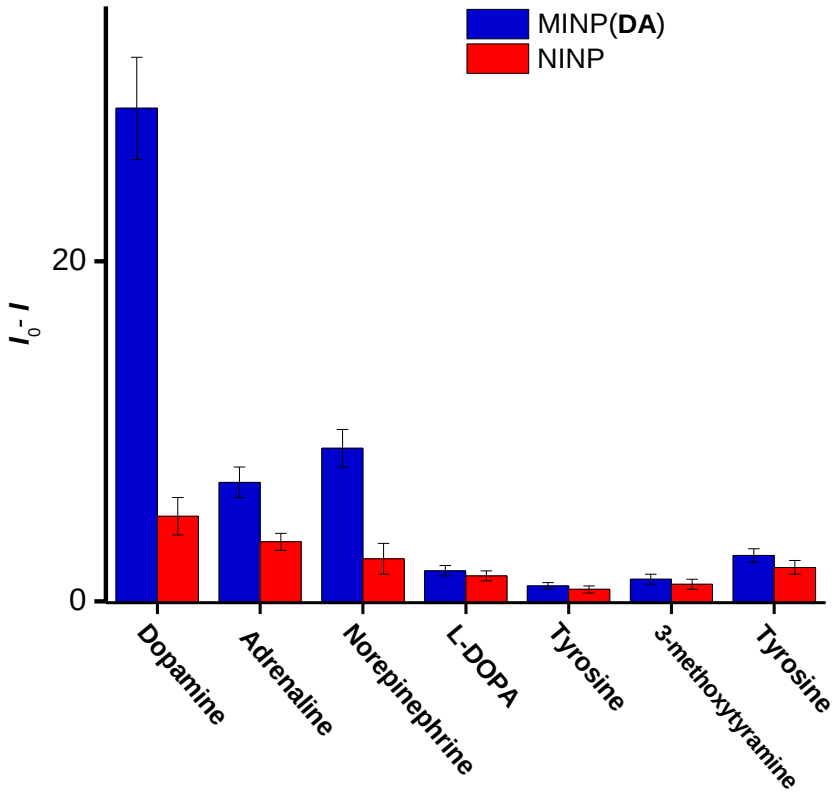

Figure 2. Change of intensity of MINP(DA) and NINP caused by **1**–**7** in 10 mM Tris buffer (pH = 9.0). [MINP] = 0.5 μM. [Guest] = 10 μM. λ_{ex} = 350 nm. The NINP was prepared with the same procedure as the MINP, except no template was used.

The extra methyl in EP (**2**) cost a further reduction of binding energy of $\Delta\Delta G$ = 0.43 kcal/mol with MINP(DA). The result is reasonable because the methylamino group would reduce the number of hydrogen bonds formed with the azacrown ring of FM **12** and introduce unwanted steric interactions in the binding. Note that the FM will turn into binding group inside the imprinted binding pocket.

Encouragingly, everything else including the CA precursors—i.e., *L*-DOPA (**4**) and

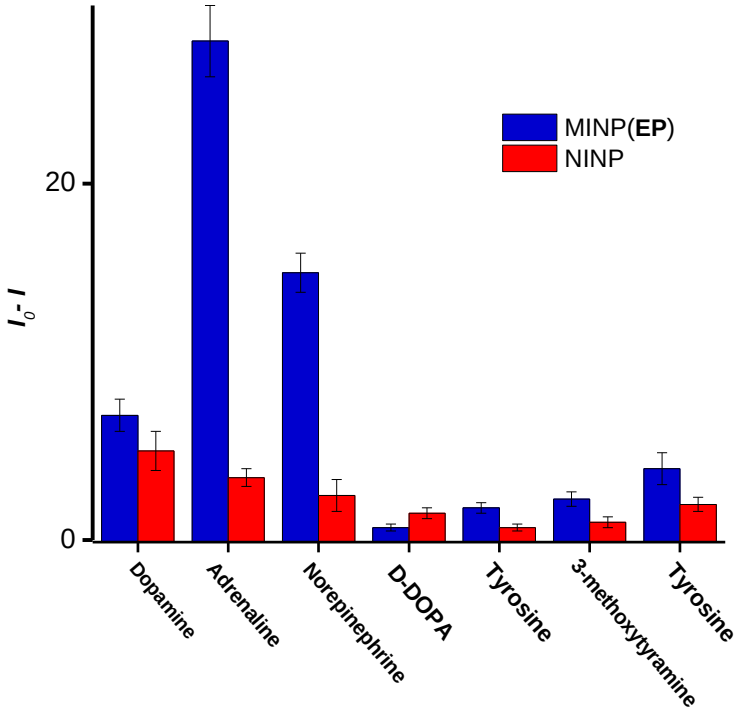

Figure 3. Change of intensity of MINP(EP) and NINP caused by **1**–**7** in 10 mM Tris buffer (pH = 9.0). [MINP] = 0.5 μM. [Guest] = 10 μM. λ_{ex} = 350 nm. The NINP was prepared with the same procedure as the MINP, except no template was used.

tyrosine (**5**)—bound very weakly. Structure-wise, an extra carboxylic acid (in **4**) was much less tolerated than an extra hydroxyl (in **3**). The importance of boronate formation was clear, as **6** and **7**, which were unable to form the boronate ester, showed much weaker binding even when a large portion of the structure of the template was maintained.

MINP(EP) showed very similar trends (Table 3), displaying the strongest binding for its own template. Notably, the most interfering analogue was norepinephrine (NE, **3**), with a CRR of 0.46 (entry 3). Notably, the difference in the binding free energy ($\Delta\Delta G$) was 0.45 kcal/mol, nearly identical to that observed for the two molecules when MINP(DA) was used as the receptor ($\Delta\Delta G$ = 0.43). It is possible that the "reproducibility" was simply coincidental. Otherwise, since two different binding interactions were used in MINP(DA) and MINP(EP) for the amino group, the identical $\Delta\Delta G$ = 0.43 could suggest that the methyl effect had a common origin (e.g., steric or hydrophobic in nature).

Since the binding pocket has a fluorescent group (i.e., anthracene) nearby, it is possible to use the MINPs as fluorescent sensors for these compounds Fig. 2 shows the change of emission intensity of 0.5 μM MINP(DA) upon the addition of 10 μM **1**–**7**. As expected, the targeted analyte (DA) gave the strongest quenching. As a comparison, we performed the same experiments with NINP, prepared with the same ratio of **11**/**12** = 1:1:1, without the template. As shown by the red columns, the nonimprinted micelles showed no noticeable selectivity.

We then added **1**–**7** to MINP(EP). Consistent with our binding data (Table 2), the fluorescently functionalized cross-linked micelle was able to sense its own template (EP, **2**) and the strongest interfering analyte was norepinephrine (NE, **3**). Selectivity, thus, could be predicted by the binding affinities.

In summary, we have used a combination of covalent and noncovalent binding groups to differentiate closely related biological guests in aqueous solution (CAs and their biogenic analogues). Our receptors easily detected the presence and absence of a single

hydroxyl or methyl, and transduced the binding into an easy-to-read fluorescent signal. MINPs can be prepared in less than two days once the FMs, cross-linkable surfactant, and cross-linkers are available. This work shows they have many of the "ideal" features illustrated in the Zimmerman review,[27] including "imprinting in water, simple preparation and purification, spectroscopic detection of binding, homogenous binding sites, and good processability". With easily modified surface and interior, as well as guest-sensitive fluorescent properties, these MINP have potential for many applications.

Acknowledgments

We thank NIGMS (R01GM113883) for financial support of this research

General Method

Routine ^{1}H and ^{13}C NMR spectra were recorded on a Bruker DRX-400, on a Bruker AV II 600 or on a Varian VXR-400 spectrometer. ESI-MS mass was recorded on Shimadzu LCMS-2010 mass spectrometer. Dynamic light scattering (DLS) data were recorded at 25 °C using PDDLS/ CoolBatch 90T with PD2000DLS instrument. Isothermal titration calorimetry (ITC) was performed using a MicroCal VP-ITC Microcalorimeter with Origin 7 software and VPViewer2000 (GE Healthcare, Northampton, MA).

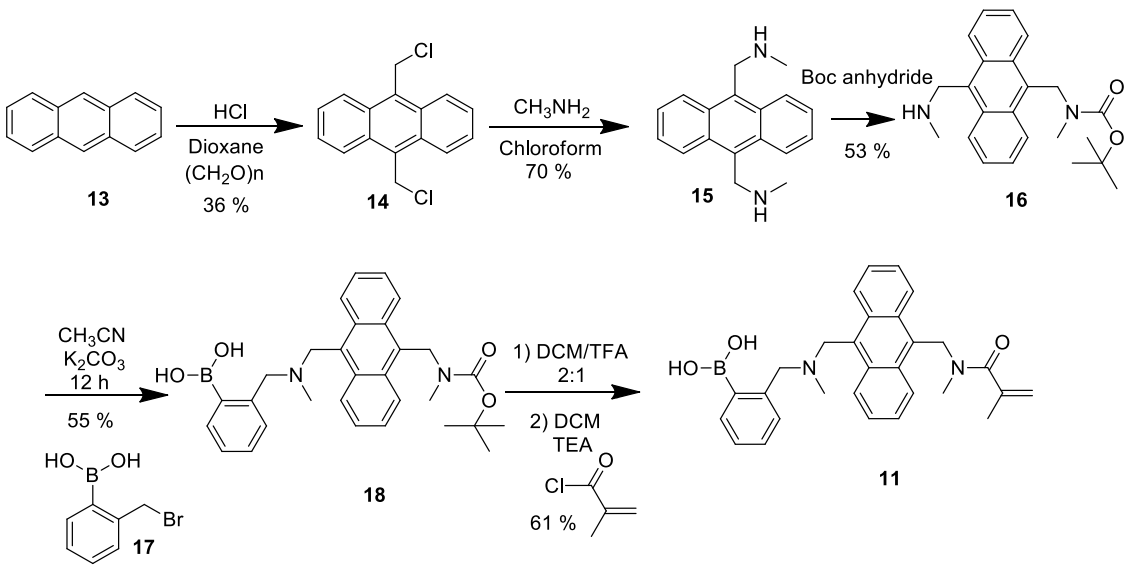

Scheme 1S: *syntheses of fluorescent functional monomer **11**.*

Syntheses

Compound 14-16 were synthesized following reported procedures. [1-3]

Compound 18A mixture of compound **16** (364 mg, 1 mmol), **17** (240 mg, 1.2 mmol) and potassium carbonate (152 mg, 1.2 mmol) in dry acetonitrile (50 mL) was heated to reflux under an argon atmosphere for 20 h. After the solid was filtered off, the filtrate was concentrated by rotary evaporation. The residual was then dissolved in dichloromethane, then washed three times by water. The organic layer was collected and dried by anhydrous sodium sulfate, and the solvent was then removed by rotaevaporation. The obtained crude product was further purified by column chromatography (CH_2Cl_2/MeOH, 20:1) to give a yellow powder (275 mg, 55%). 1H NMR (400 MHz, Chloroform-d) δ 8.42 (s, 2H), 8.11 (m, 3H), 7.57 – 7.20 (m, 7H), 5.51 (s, 2H), 4.48 (s, 2H), 4.06 (s, 2H), 2.47 (s, 3H), 2.24 (s, 3H), 1.57 (s, 9H). 13C NMR (151 MHz, CDCl3) δ 172.32, 141.25, 140.87, 135.99, 131.10, 130.90, 129.98,

127.88, 126.11, 125.96, 125.53, 125.49, 124.62, 83.24, 65.70, 58.38, 50.51, 42.15, 20.26, 17.42. HRMS (ESI/QTOF) m/z: [M + H]+ Calcd for C30H36BN2O4 499.2768; Found 499.2778

Compound 10. A solution of compound **18** (499 mg, 1 mmol) in 5 mL of anhydrous dichloromethane was added slowly to a 10 mL mixture of 50:50 dichloromethane and trifluoroacetic acid. After stirred at room temperature for 1 h, the mixture was concentrated by rotary evaporation. The residual was dissolved in anhydrous dichloromethane (10 mL), followed by the addition of triethylamine (0.3 mL) and methacryloyl chloride (0.2 mL, 2 mmol). The reaction mixture was stirred at room temperature for 12 h. The reaction solution was then extracted three times by water. The organic layer was collected and dried by anhydrous sodium sulfate, and the solvent was then removed by rotary evaporation. The obtained crude product was further purified by column chromatography over silica gel using 10:1 dichloromethane/methanol as the eluent to give a yellow powder (284 mg, 61%). ^{1}H NMR (600 MHz, $CDCl_3$) δ 8.36 (d, *J* = 8.4 Hz, 2H), 8.23–8.10 (m, 3H), 7.55–7.44 (m, 7H), 5.71 (d, *J* = 4.9 Hz, 2H), 5.19 (s, 1H), 5.04 (s, 1H), 4.52 (s, 2H), 4.00 (s, 2H), 2.60 (s, 3H), 2.25 (s, 3H), 2.01 (s, 3H). ^{13}C NMR (151 MHz, $CDCl_3$) δ 172.3, 141.3, 141.2, 140.9, 136.0, 131.1, 130.9, 130.0, 127.9, 126.1, 126.0, 125.5, 124.7, 115.5, 65.7, 58.4, 50.5, 42.2, 20.3, 17.4. HRMS (ESI/QTOF) m/z: $[M + H]^+$ Calcd for $C_{29}H_{32}BN_2O_3$ 467.2500; Found 467.2487.

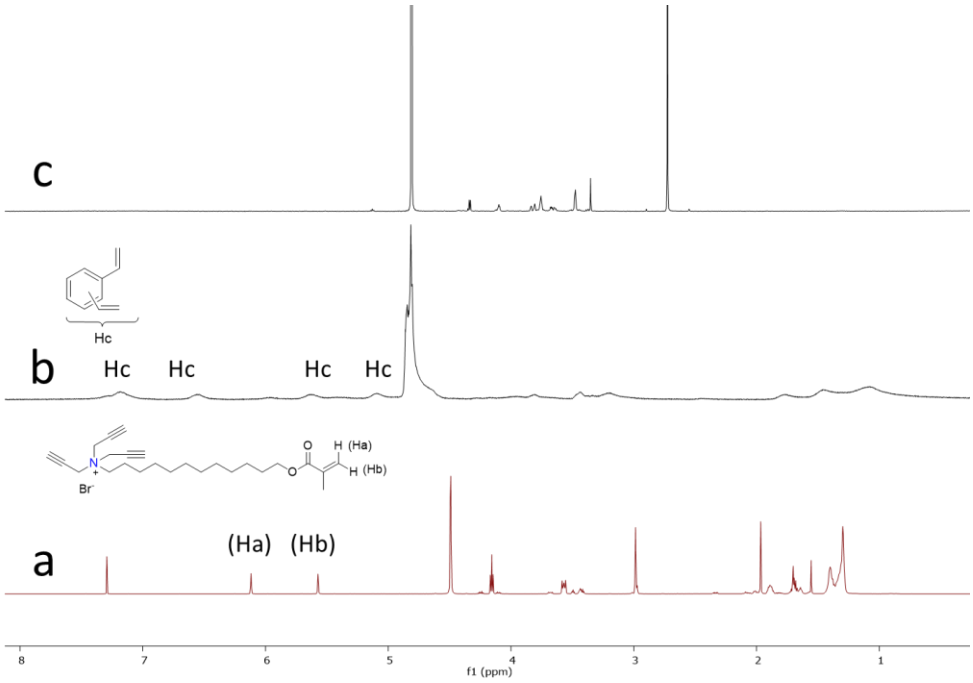

Figure S1. ^{1}H NMR spectra of (a) **8** in $CDCl_3$, (b) alkynyl-SCM in D_2O, and (c) MINP(DA) in D_2O.

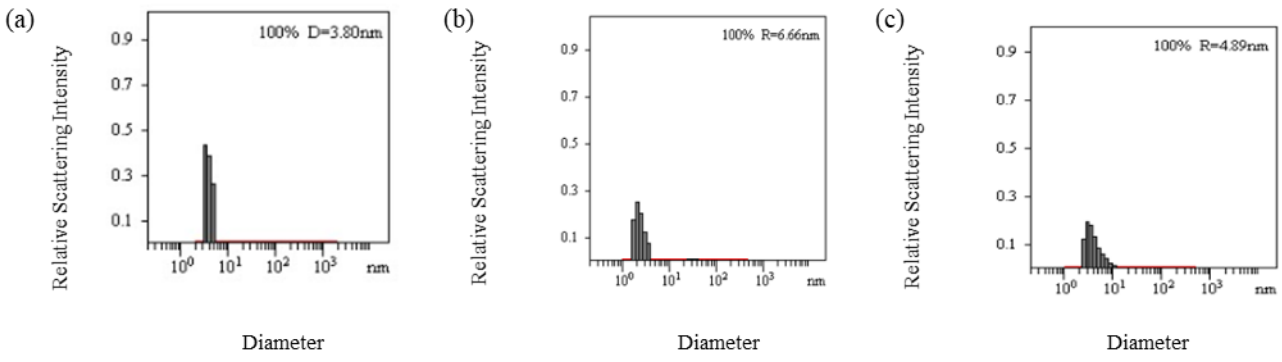

Figure S2. Distribution of the hydrodynamic diameters of the nanoparticles in water as determined by DLS for (a) alkynyl-SCM, (b) surface-functionalized SCM, and (c) MINP(DA) after purification.

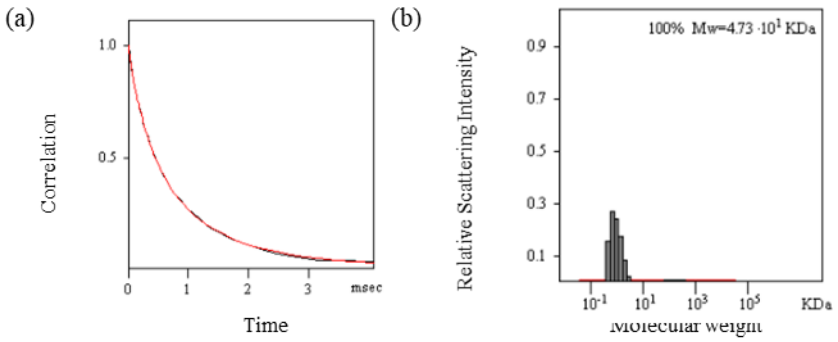

Figure S3. The correlation curve and the distribution of the molecular weight for MINP(DA) from the DLS. The PRECISION DECONVOLVE program assumes the intensity of scattering is proportional to the mass of the particle squared. If each unit of building block for the MINP(DA) is assumed to contain one molecule of compound **8** (MW = 465 g/mol), 1.2 molecules of compound **9** (MW = 172 g/mol), one molecule of DVB (MW = 130 g/mol), and 0.8 molecules of compound **10** (MW = 264 g/mol), the molecular weight of MINP(DA) translates to 47 [= 47300 / (465 + 1.2×172 + 130 + 0.8×264)] of such units.

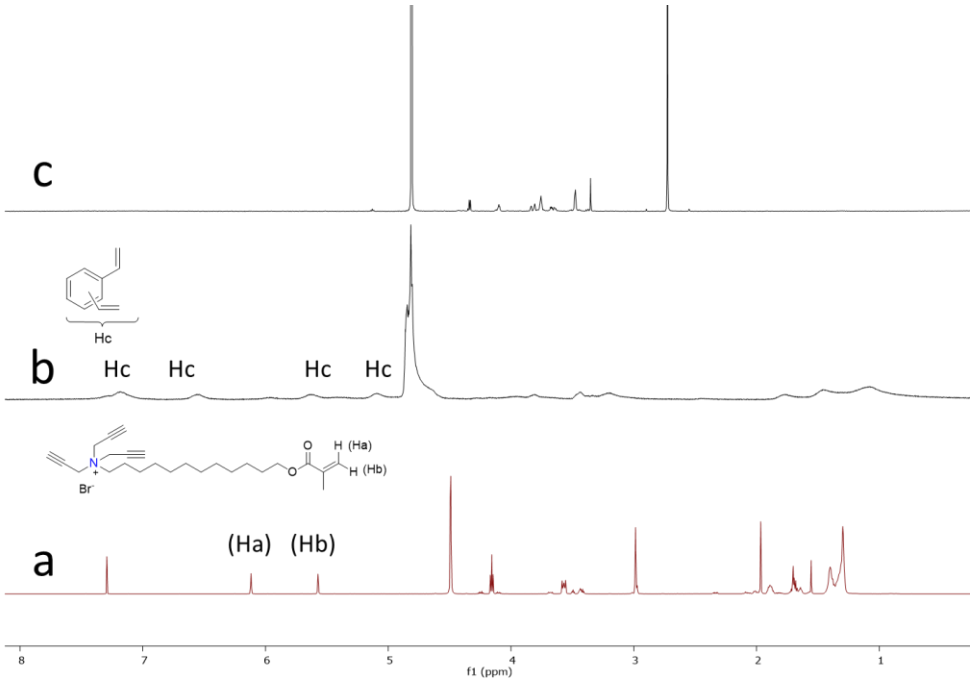

Figure S4. ^{1}H NMR spectra of (a) **8** in $CDCl_3$, (b) alkynyl-SCM in D_2O, and (c) MINP(EP) in D_2O.

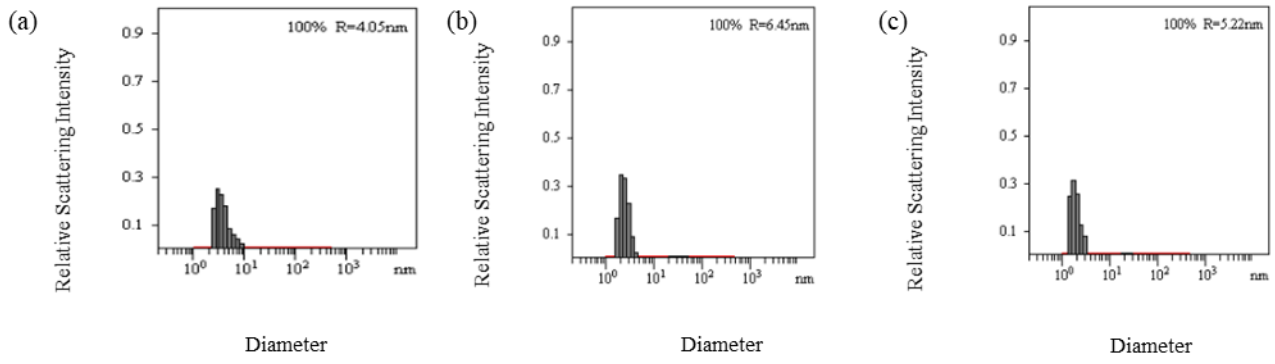

Figure S5. Distribution of the hydrodynamic diameters of the nanoparticles in water as determined by DLS for (a) alkynyl-SCM, (b) surface-functionalized SCM, and (c) MINP(EP) after purification.

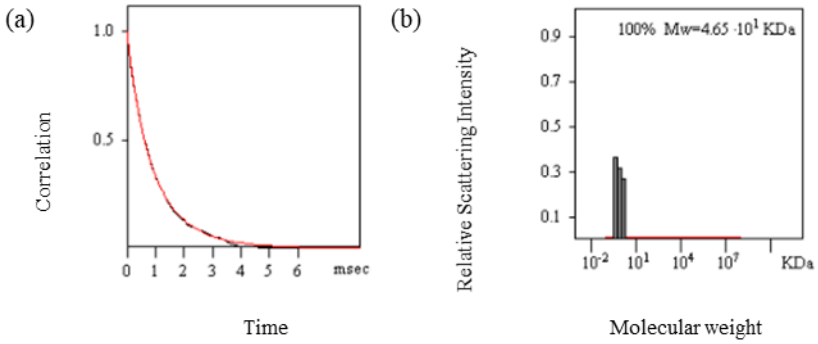

Figure S6. The correlation curve and the distribution of the molecular weight for MINP(EP) from the DLS. The PRECISION DECONVOLVE program assumes the intensity of scattering is proportional to the mass of the particle squared. If each unit of building block for the MINP(EP) is assumed to contain one molecule of compound **8** (MW = 465 g/mol), 1.2 molecules of compound **9** (MW = 172 g/mol), one molecule of DVB (MW = 130 g/mol), and 0.8 molecules of compound **10** (MW = 264 g/mol), the molecular weight of MINP1(8) translates to 46 [= 46500 / (465 + 1.2×172 + 130 + 0.8×264)] of such units.

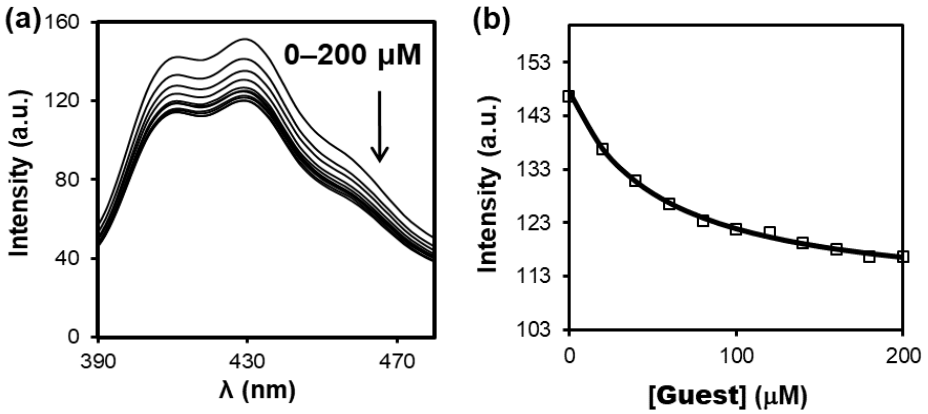

Figure S7. (a) Fluorescence emission spectra of MINP(DA) (2 equiv. FM **11** & 0 equiv. FM **12**) (λ_{ex} = 370 nm) upon addition of different concentrations of guest DA in 50 mM Tris buffer (pH 7.4). [MINP(DA)] = 2.0 μM. (b) Nonlinear least squares fitting of the emission intensity of MINP(DA) at 430 nm to a 1:1 binding isotherm. The data corresponds to entry 1 in Table 1.

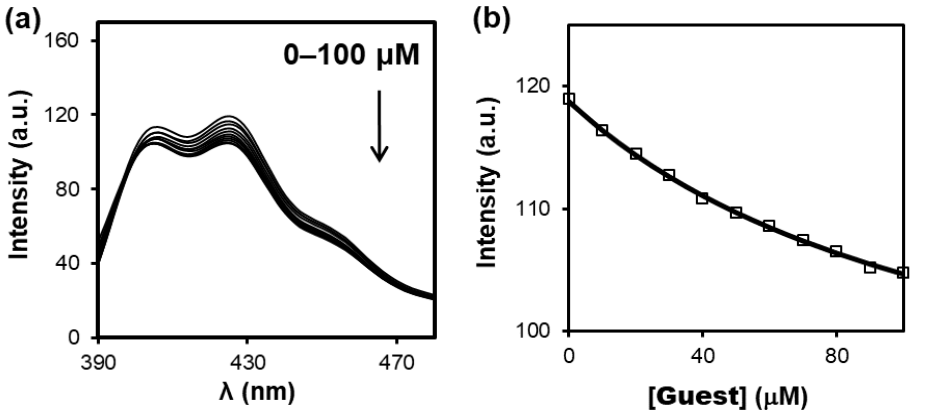

Figure S8. (a) Fluorescence emission spectra of MINP(DA) (2 equiv. FM **11** & 0 equiv. FM **12**) (λ_{ex} = 370 nm) upon addition of different concentrations of guest EP in 50 mM Tris buffer (pH 7.4). [MINP(DA)] = 2.0 μM. (b) Nonlinear least squares fitting of the emission intensity of MINP(DA) at 430 nm to a 1:1 binding isotherm. The data corresponds to entry 2 in Table 1.

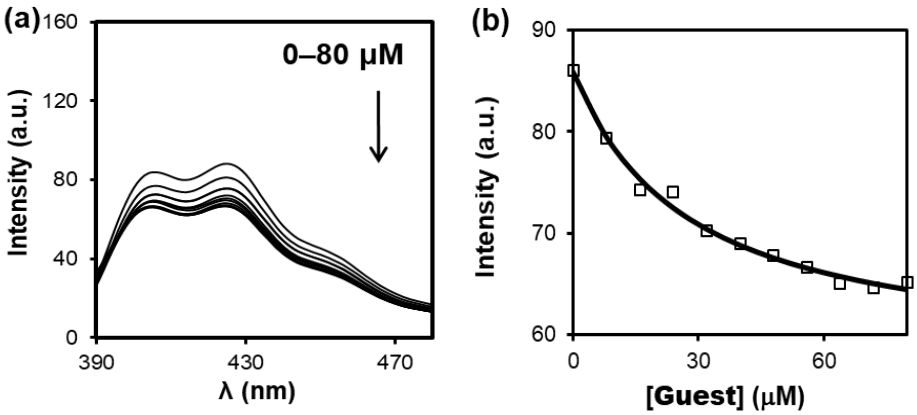

Figure S9. (a) Fluorescence emission spectra of MINP(DA) (1 equiv. FM **11** & 1 equiv. FM **12**) (λ_{ex} = 370 nm) upon addition of different concentrations of guest DA in 50 mM Tris buffer (pH 7.4). [MINP(DA)] = 2.0 μM. (b) Nonlinear least squares fitting of the emission intensity of MINP(DA) at 430 nm to a 1:1 binding isotherm. The data corresponds to entry 3 in Table 1 and entry 1 in Table 2.

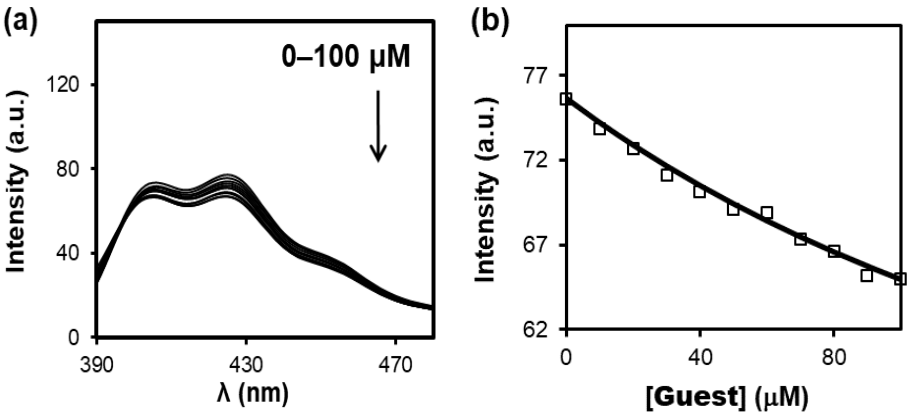

Figure S10. (a) Fluorescence emission spectra of MINP(DA) (1 equiv. FM **11** & 1 equiv. FM **12**) (λ_{ex} = 370 nm) upon addition of different concentrations of guest EP in 50 mM Tris buffer (pH 7.4). [MINP(DA)] = 2.0 μM. (b) Nonlinear least squares fitting of the emission intensity of MINP(DA) at 430 nm to a 1:1 binding isotherm. The data corresponds to entry 4 in Table 1 and entry 2 in Table 2.

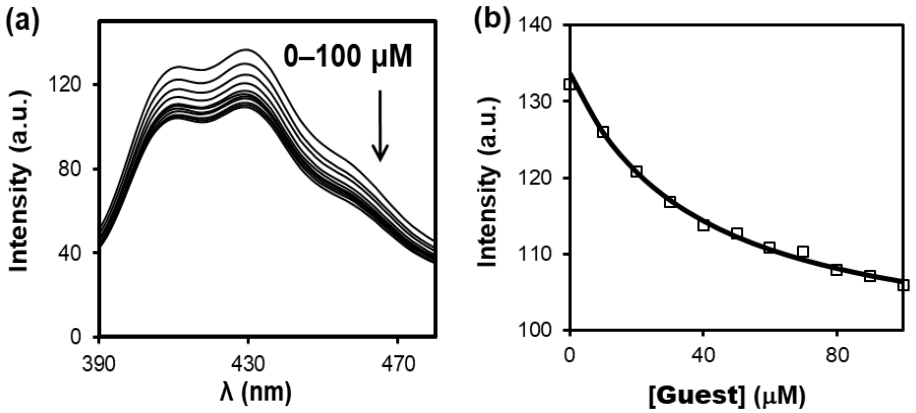

Figure S11. (a) Fluorescence emission spectra of MINP(DA) (2 equiv. FM **11** & 1 equiv. FM **12**) (λ_{ex} = 370 nm) upon addition of different concentrations of guest DA in 50 mM Tris buffer (pH 7.4). [MINP(DA)] = 2.0 μM. (b) Nonlinear least squares fitting of the emission intensity of MINP(DA) at 430 nm to a 1:1 binding isotherm. The data corresponds to entry 5 in Table 1.

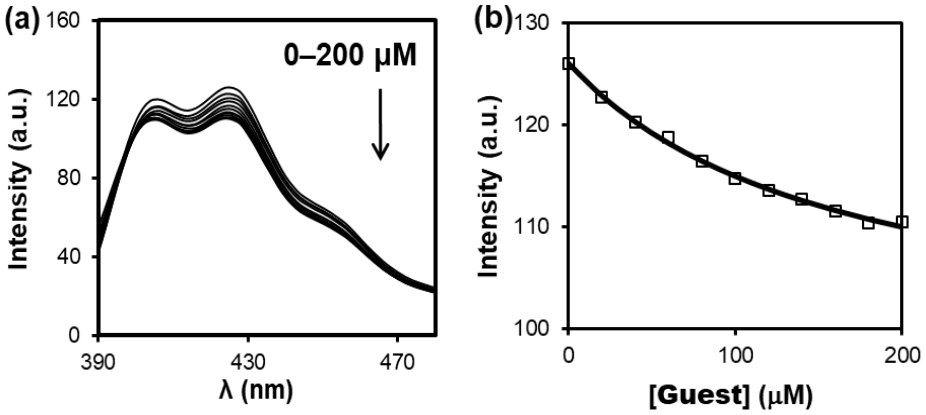

Figure S12. (a) Fluorescence emission spectra of MINP(DA) (2 equiv. FM **11** & 1 equiv. FM **12**) (λ_{ex} = 370 nm) upon addition of different concentrations of guest EP in 50 mM Tris buffer (pH 7.4). [MINP(DA)] = 2.0 μM. (b) Nonlinear least squares fitting of the emission intensity of MINP(DA) at 430 nm to a 1:1 binding isotherm. The data corresponds to entry 6 in Table 1.

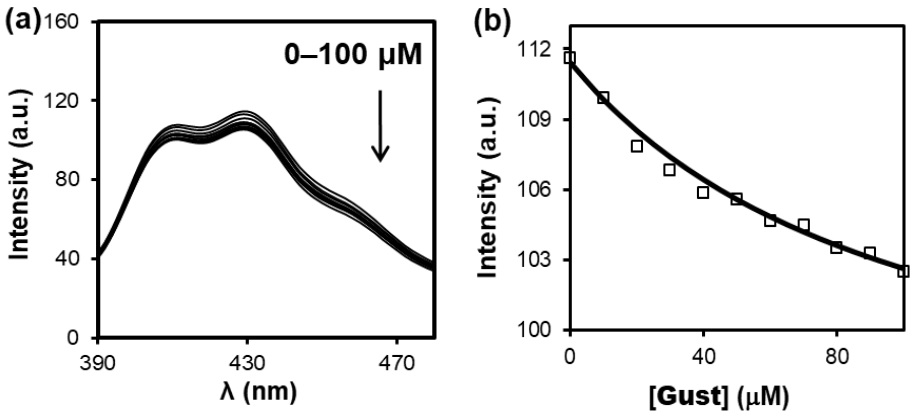

Figure S13. (a) Fluorescence emission spectra of MINP(EP) (2 equiv. FM **11** & 0 equiv. FM **12**) (λ_{ex} = 370 nm) upon addition of different concentrations of guest DA in 50 mM Tris buffer (pH 7.4). [MINP(EP)] = 2.0 μM. (b) Nonlinear least squares fitting of the emission intensity of MINP(EP) at 430 nm to a 1:1 binding isotherm. The data corresponds to entry 7 in Table 1 and entry 1 in Table 3.

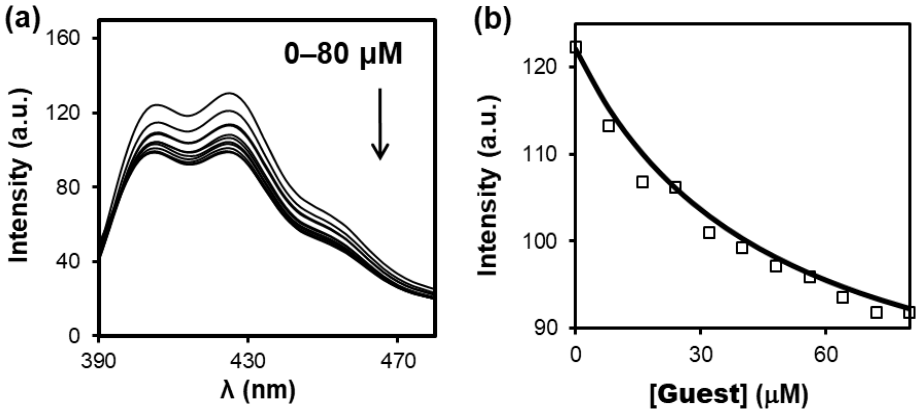

Figure S14. (a) Fluorescence emission spectra of MINP(EP) (2 equiv. FM **11** & 0 equiv. FM **12**) (λ_{ex} = 370 nm) upon addition of different concentrations of guest EP in 50 mM Tris buffer (pH 7.4). [MINP(EP)] = 2.0 μM. (b) Nonlinear least squares fitting of the emission intensity of MINP(EP) at 430 nm to a 1:1 binding isotherm. The data corresponds to entry 8 in Table 1 and entry 2 in Table 2.

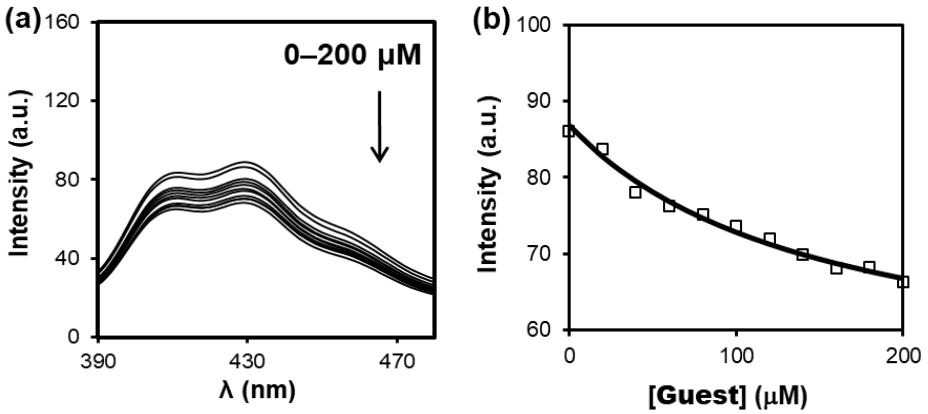

Figure S15. (a) Fluorescence emission spectra of MINP(EP) (1 equiv. FM **11** & 1 equiv. FM **12**) (λ_{ex} = 370 nm) upon addition of different concentrations of guest DA in 50 mM Tris buffer (pH 7.4). [MINP(EP)] = 2.0 μM. (b) Nonlinear least squares fitting of the emission intensity of MINP(EP) at 430 nm to a 1:1 binding isotherm. The data corresponds to entry 9 in Table 1.

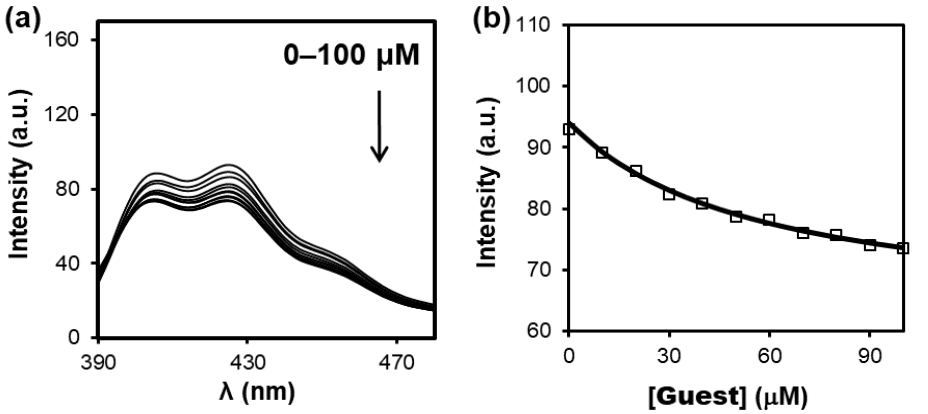

Figure S16. (a) Fluorescence emission spectra of MINP(EP) (1 equiv. FM **11** & 1 equiv. FM **12**) (λ_{ex} = 370 nm) upon addition of different concentrations of guest EP in 50 mM Tris buffer (pH 7.4). [MINP(EP)] = 2.0 μM. (b) Nonlinear least squares fitting of the emission intensity of MINP(EP) at 430 nm to a 1:1 binding isotherm. The data corresponds to entry 10 in Table 1.

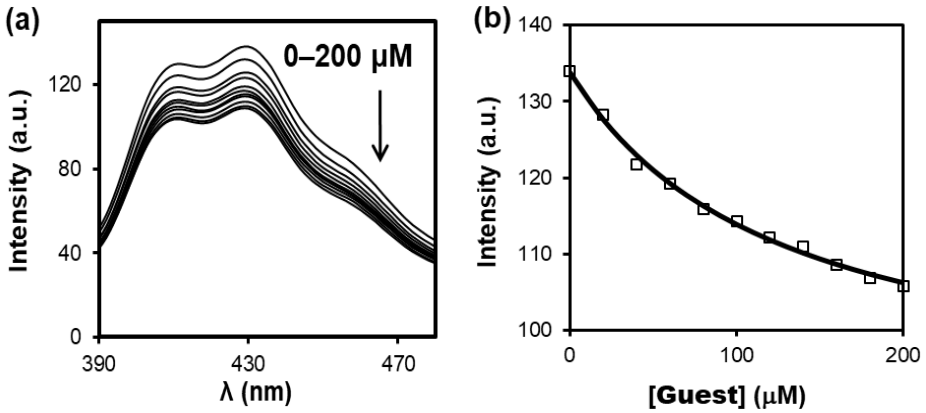

Figure S17. (a) Fluorescence emission spectra of MINP(EP) (2 equiv. FM **11** & 1 equiv. FM **12**) (λ_{ex} = 370 nm) upon addition of different concentrations of guest DA in 50 mM Tris buffer (pH 7.4). [MINP(EP)] = 2.0 μM. (b) Nonlinear least squares fitting of the emission intensity of MINP(EP) at 430 nm to a 1:1 binding isotherm. The data corresponds to entry 11 in Table 1.

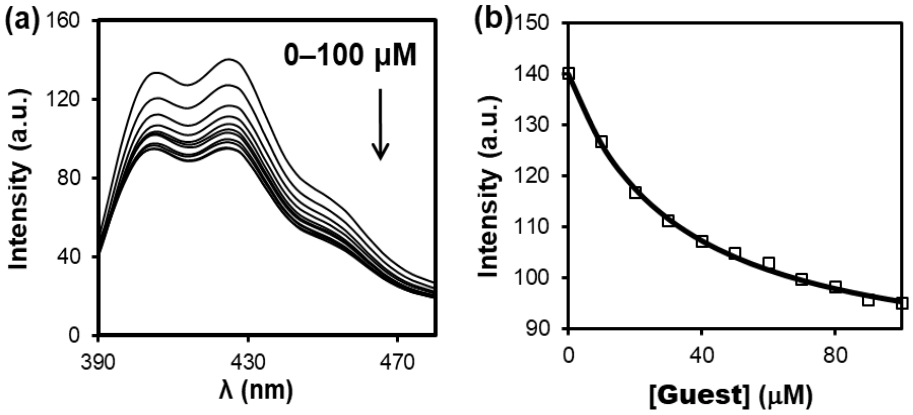

Figure S18. (a) Fluorescence emission spectra of MINP(EP) (2 equiv. FM **11** & 1 equiv. FM **12**) (λ_{ex} = 370 nm) upon addition of different concentrations of guest EP in 50 mM Tris buffer (pH 7.4). [MINP(EP)] = 2.0 μM. (b) Nonlinear least squares fitting of the emission intensity of MINP(EP) at 430 nm to a 1:1 binding isotherm. The data corresponds to entry 12 in Table 1.

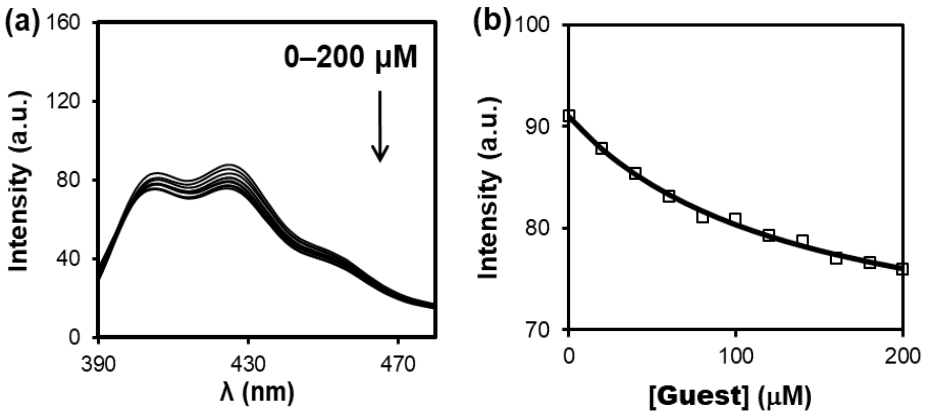

Figure S19. (a) Fluorescence emission spectra of MINP(DA) (1 equiv. FM **11** & 1 equiv. FM **12**) (λ_{ex} = 370 nm) upon addition of different concentrations of guest NE in 50 mM Tris buffer (pH 7.4). [MINP(DA)] = 2.0 μM. (b) Nonlinear least squares fitting of the emission intensity of MINP(DA) at 430 nm to a 1:1 binding isotherm. The data corresponds to entry 3 in Table 2.

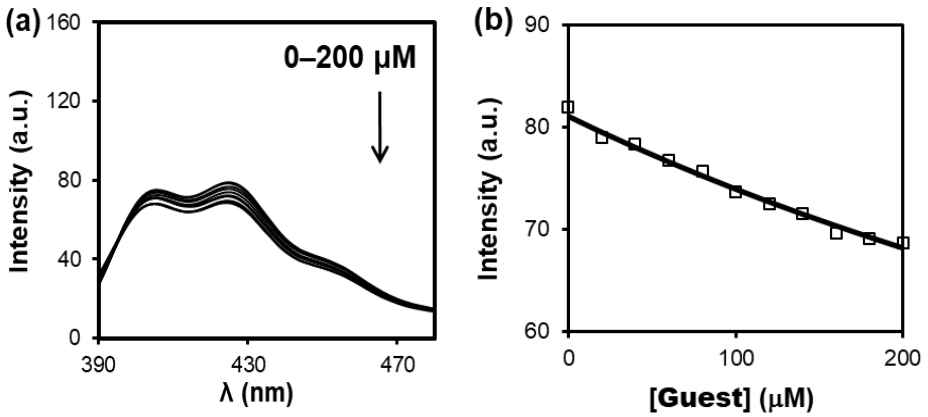

Figure S20. (a) Fluorescence emission spectra of MINP(DA) (1 equiv. FM **11** & 1 equiv. FM **12**) (λ_{ex} = 370 nm) upon addition of different concentrations of guest **4** in 50 mM Tris buffer (pH 7.4). [MINP(DA)] = 2.0 μM. (b) Nonlinear least squares fitting of the emission intensity of MINP(DA) at 430 nm to a 1:1 binding isotherm. The data corresponds to entry 4 in Table 2.

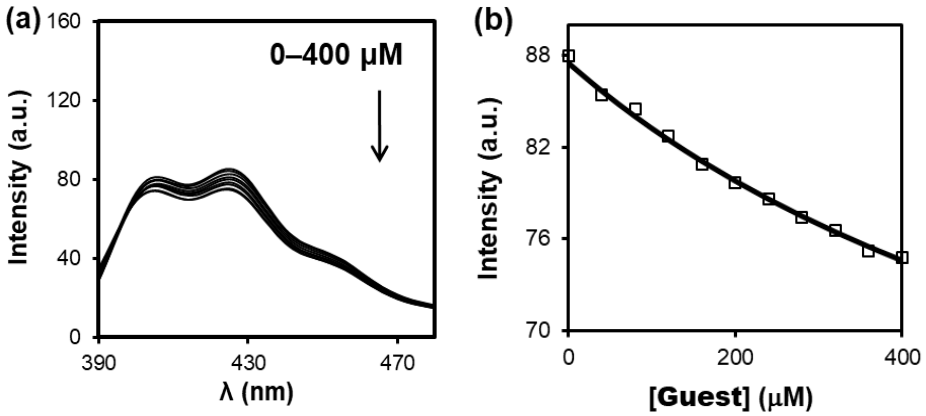

Figure S21. (a) Fluorescence emission spectra of MINP(DA) (1 equiv. FM **11** & 1 equiv. FM **12**) (λ_{ex} = 370 nm) upon addition of different concentrations of guest **5** in 50 mM Tris buffer (pH 7.4). [MINP(DA)] = 2.0 μM. (b) Nonlinear least squares fitting of the emission intensity of MINP(DA) at 430 nm to a 1:1 binding isotherm. The data corresponds to entry 5 in Table 2.

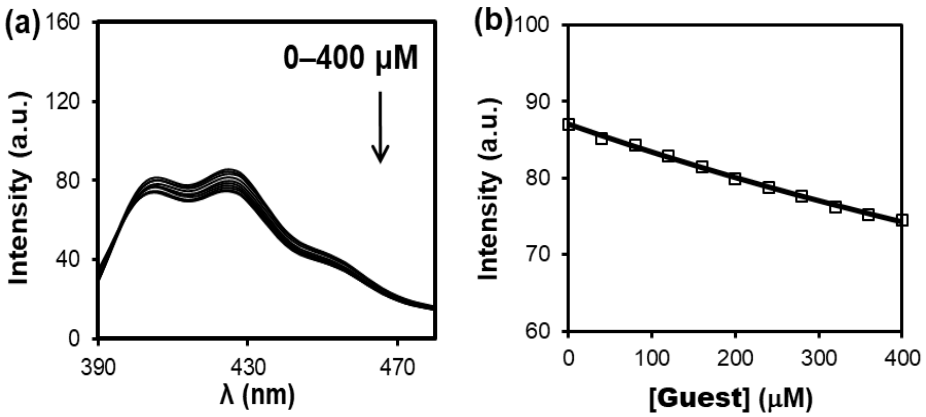

Figure S22. (a) Fluorescence emission spectra of MINP(DA) (1 equiv. FM **11** & 1 equiv. FM **12**) (λ_{ex} = 370 nm) upon addition of different concentrations of guest **6** in 50 mM Tris buffer (pH 7.4). [MINP(DA)] = 2.0 μM. (b) Nonlinear least squares fitting of the emission intensity of MINP(DA) at 430 nm to a 1:1 binding isotherm. The data corresponds to entry 6 in Table 2.

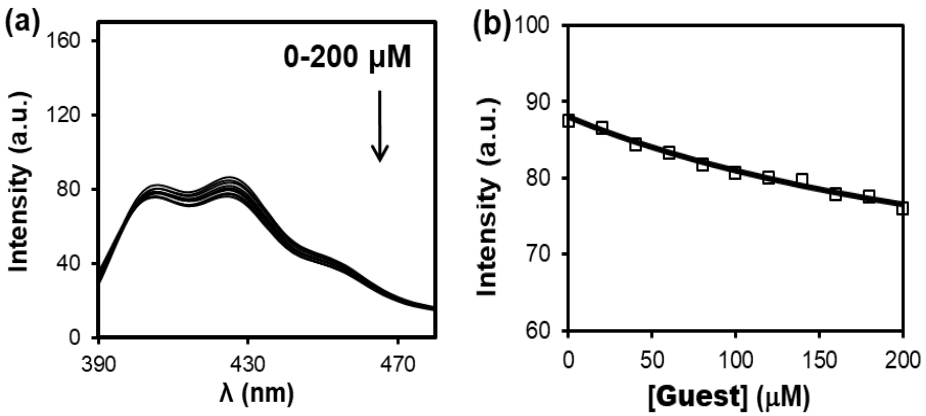

Figure S23. (a) Fluorescence emission spectra of MINP(DA) (1 equiv. FM **11** & 1 equiv. FM **12**) (λ_{ex} = 370 nm) upon addition of different concentrations of guest **7** in 50 mM Tris buffer (pH 7.4). [MINP(DA)] = 2.0 μM. (b) Nonlinear least squares fitting of the emission intensity of MINP(DA) at 430 nm to a 1:1 binding isotherm. The data corresponds to entry 7 in Table 2.

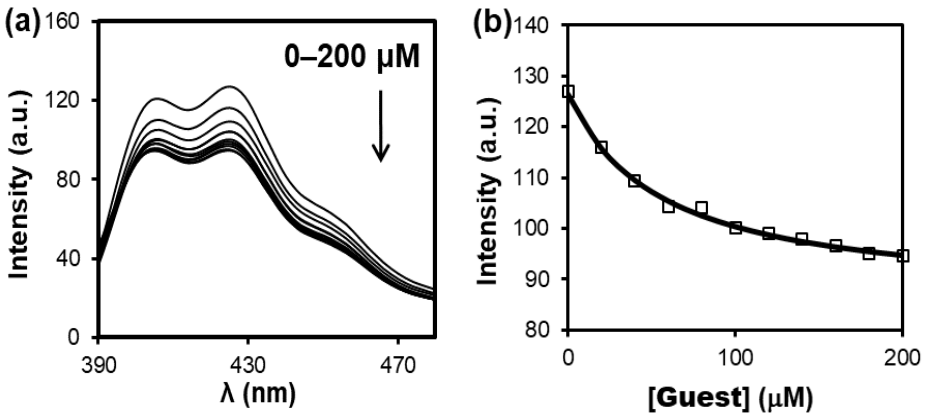

Figure S24. (a) Fluorescence emission spectra of MINP(EP) (2 equiv. FM **11** & 0 equiv. FM **12**) (λ_{ex} = 370 nm) upon addition of different concentrations of guest NE in 50 mM Tris buffer (pH 7.4). [MINP(EP)] = 2.0 μM. (b) Nonlinear least squares fitting of the emission intensity of MINP(EP) at 430 nm to a 1:1 binding isotherm. The data corresponds to entry 3 in Table 3.

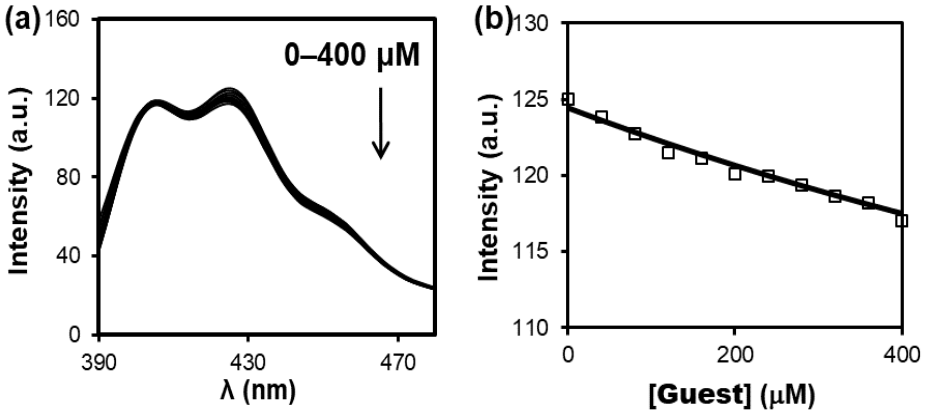

Figure S25. (a) Fluorescence emission spectra of MINP(EP) (2 equiv. FM **11** & 0 equiv. FM **12**) (λ_{ex} = 370 nm) upon addition of different concentrations of guest **4** in 50 mM Tris buffer (pH 7.4). [MINP(EP)] = 2.0 μM. (b) Nonlinear least squares fitting of the emission intensity of MINP(EP) at 430 nm to a 1:1 binding isotherm. The data corresponds to entry 4 in Table 3.

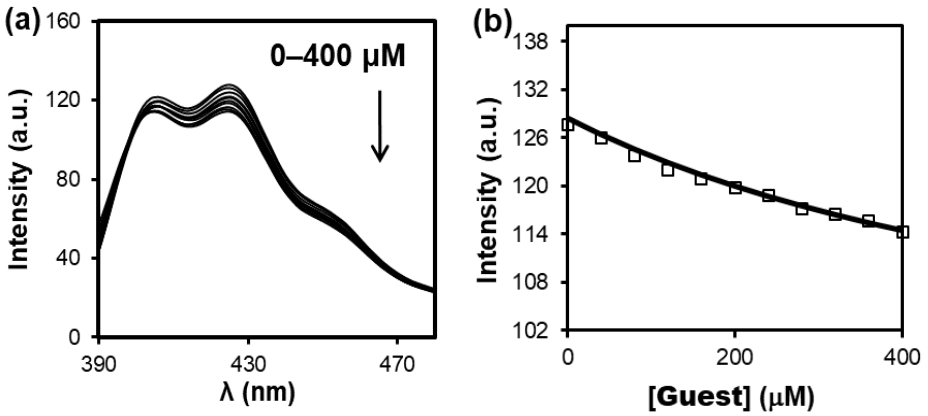

Figure S26. (a) Fluorescence emission spectra of MINP(EP) (2 equiv. FM **11** & 0 equiv. FM **12**) (λ_{ex} = 370 nm) upon addition of different concentrations of guest **5** in 50 mM Tris buffer (pH 7.4). [MINP(EP)] = 2.0 μM. (b) Nonlinear least squares fitting of the emission intensity of MINP(EP) at 430 nm to a 1:1 binding isotherm. The data corresponds to entry 5 in Table 3.

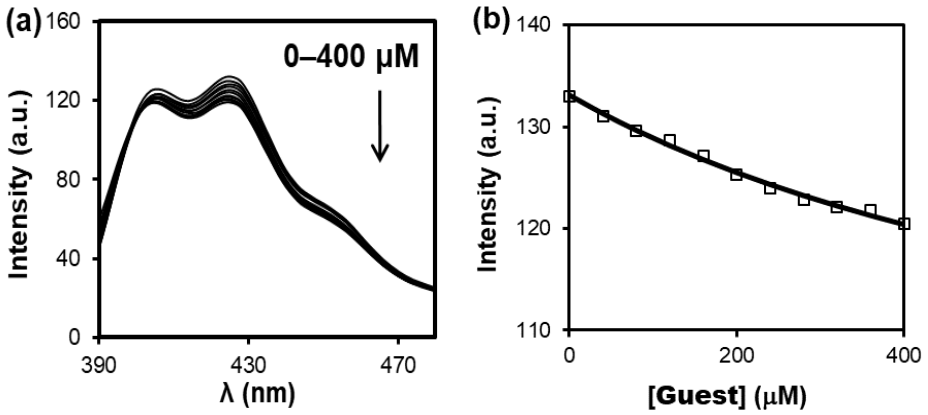

Figure S27. (a) Fluorescence emission spectra of MINP(EP) (2 equiv. FM **11** & 0 equiv. FM **12**) (λ_{ex} = 370 nm) upon addition of different concentrations of guest **6** in 50 mM Tris buffer (pH 7.4). [MINP(EP)] = 2.0 μM. (b) Nonlinear least squares fitting of the emission intensity of MINP(EP) at 430 nm to a 1:1 binding isotherm. The data corresponds to entry 6 in Table 3.

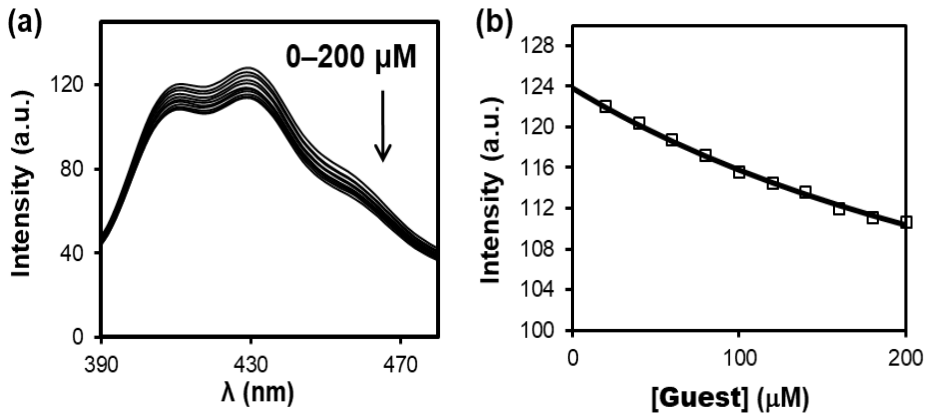

Figure S28. (a) Fluorescence emission spectra of MINP(EP) (2 equiv. FM **11** & 0 equiv. FM **12**) (λ_{ex} = 370 nm) upon addition of different concentrations of guest **7** in 50 mM Tris buffer (pH 7.4). [MINP(EP)] = 2.0 μM. (b) Nonlinear least squares fitting of the emission intensity of MINP(EP) at 430 nm to a 1:1 binding isotherm. The data corresponds to entry 7 in Table 3.

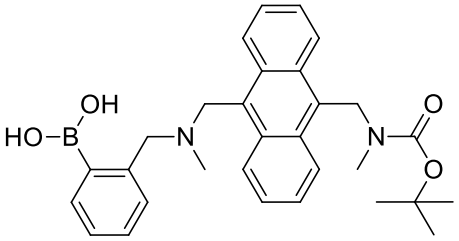

18

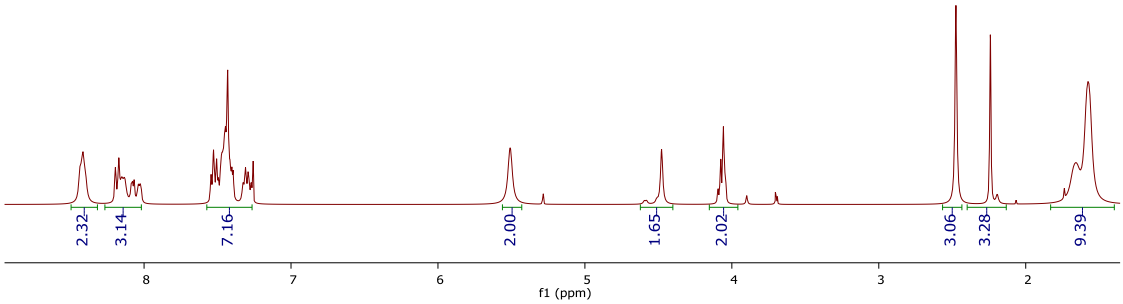

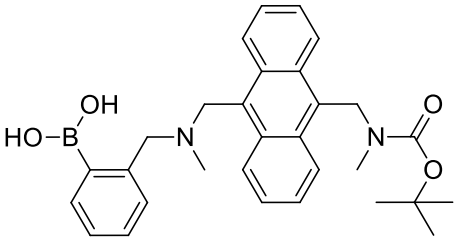

18

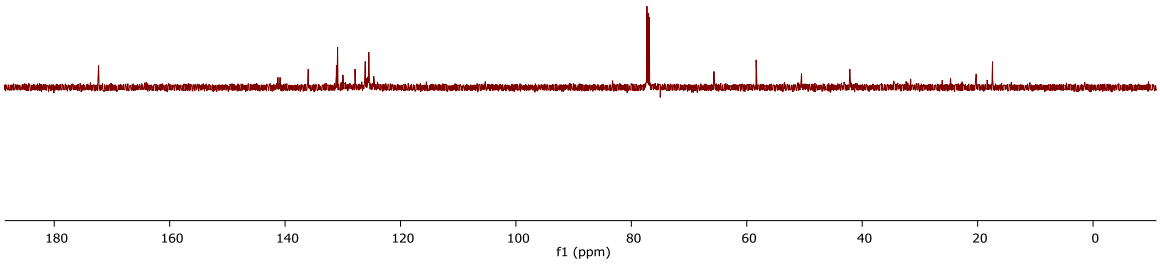

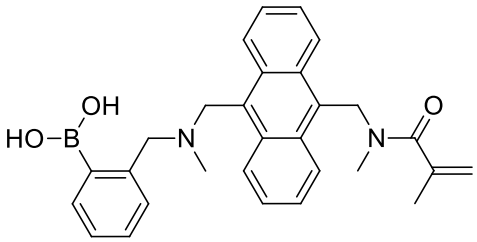

19

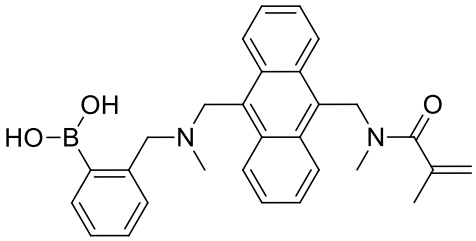

19

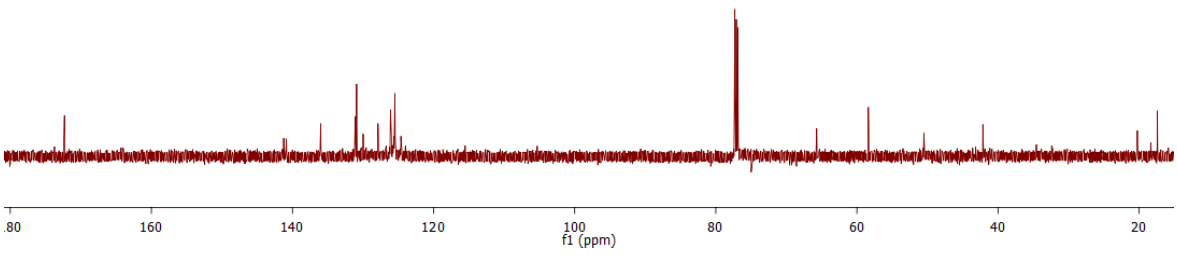

Notes and references

1. C. R. Lake and M. G. Ziegler, *The Catecholamines in psychiatric and neurologic disorders*, Butterworth, Boston, 1985.
2. H. Bönisch, U. Trendelenburg and N. Weiner, *Catecholamines*, Springer-Verlag, Berlin ; New York, 1988.
3. D. S. Goldstein, G. Eisenhofer and R. McCarty, eds., *Catecholamines: Bridging Basic Science with Clinical Medicine*, Academic Press, San Diego, 1997.
4. T. Pradhan, H. S. Jung, J. H. Jang, T. W. Kim, C. Kang and J. S. Kim, *Chem. Soc. Rev.*, 2014, **43**, 4684-4713.
5. J. A. Ribeiro, P. M. V. Fernandes, C. M. Pereira and F. Silva, *Talanta*, 2016, **160**, 653-679.
6. K. E. Secor and T. E. Glass, *Org. Lett.*, 2004, **6**, 3727-3730.
7. K. S. Hettie, X. Liu, K. D. Gillis and T. E. Glass, *ACS Chem. Neurosci.*, 2013, **4**, 918-923.
8. A. Chaicham, S. Sahasithiwat, T. Tuntulani and B. Tomapatanaget, *Chem. Commun.*, 2013, **49**, 9287-9289.
9. M. Herm, O. Molt and T. Schrader, *Chem.-Eur. J.*, 2002, **8**, 1485-1499.
10. O. Molt, D. Rübeling and T. Schrader, *J. Am. Chem. Soc.*, 2003, **125**, 12086-12087.
11. B. Escuder, A. E. Rowan, M. C. Feiters and R. J. M. Nolte, *Tetrahedron*, 2004, **60**, 291-300.
12. S. Kolusheva, O. Molt, M. Herm, T. Schrader and R. Jelinek, *J. Am. Chem. Soc.*, 2005, **127**, 10000-10001.
13. J. Kim, B. Raman and K. H. Ahn, *J. Org. Chem.*, 2006, **71**, 38-45.
14. F. Reviriego, M. I. Rodríguez-Franco, P. Navarro, E. García-España, M. Liu-González, B. Verdejo and A. Domènech, *J. Am. Chem. Soc.*, 2006, **128**, 16458-16459.
15. C. Givelet and B. Bibal, *Org. Biomol. Chem.*, 2011, **9**, 7457-7460.
16. J. K. Awino and Y. Zhao, *J. Am. Chem. Soc.*, 2013, **135**, 12552-12555.
17. G. Wulff, *Chem. Rev.*, 2001, **102**, 1-28.
18. K. Haupt and K. Mosbach, *Chem. Rev.*, 2000, **100**, 2495-2504.
19. K. Chen and Y. Zhao, *Org. Biomol. Chem.*, 2019, **17**, 8611-8617.
20. S. Fa and Y. Zhao, *Chem. Mater.*, 2019, **31**, 4889-4896.
21. L. Duan and Y. Zhao, *J. Org. Chem.*, 2019, **84**, 13457-13464.
22. J. K. Awino and Y. Zhao, *Chem.-Eur. J.*, 2015, **21**, 655-661.
23. X. Xing and Y. Zhao, *Org. Biomol. Chem.*, 2018, **16**, 2855-2859.
24. J. S. Nowick and J. S. Chen, *J. Am. Chem. Soc.*, 1992, **114**, 1107-1108.

25. J. S. Nowick, J. S. Chen and G. Noronha, *J. Am. Chem. Soc.*, 1993, **115**, 7636-7644.

26. K. Ariga and T. Kunitake, *Acc. Chem. Res.*, 1998, **31**, 371-378.

27. S. C. Zimmerman and N. G. Lemcoff, *Chem. Commun.*, 2004, 5-14.

28. Y. Qi, H. Xu, X. Li, B. Tu, Q. Pang, X. Lin, E. Ning and Q. Li, *Chem. Mater.*, 2018, **30**, 5478-5484.

29. E. Nakata, T. Nagase, S. Shinkai and I. Hamachi, *J. Am. Chem. Soc.*, 2004, **126**, 490-495.

30. W. Yang, H. Fan, X. Gao, S. Gao, V. V. R. Karnati, W. Ni, W. B. Hooks, J. Carson, B. Weston and B. Wang, *Chem. Biol.*, 2004, **11**, 439-448.

CHAPTER 6. GENERAL CONCLUSIONS

Although molecule recognition in water is challenging for many artificial receptors, this work demonstrates that molecularly imprinted nanoparticles (MINPs) could be used as receptors or sensors for a variety of bioactive molecules including alkaloids, nonsteroidal anti-inflammatory drug (NSAIDs), folic acid, and catecholamines in water. The preparation of MINP is extremely easy and convenient, complete in 2-3 days from readily available starting materials without harsh reaction conditions. Although the binding affinity might still be weak compared to those of natural antibodies, the rigid polymer matrix would enable MINP to work under adverse temperature and pH conditions, in which a protein easily denature. In addition, in comparison to other reported synthetic receptors, MINPs generally function much better in water with outstanding binding affinities and good selectivity toward similar structures. MINPs also represent a large improvement from traditional molecularly imprinted polymers, with their good water solubility, small size, and controllable numbers of the binding site. With a judicious selection of the cross-linkable surfactant and functional monomers, MINPs can be prepared for many other target molecules beyond bioactive drugs. Finally, installation of fluorescent functional monomers near the binding site converts MINP receptors into sensors, which can be very useful in biomedical research and diagnosis.